2013

FLUORINATED ARENE, IMIDE AND UNSATURATED PYRROLIDINONE BASED DONOR ACCEPTOR CONJUGATED POLYMERS: SYNTHESIS, STRUCTURE-PROPERTY AND DEVICE STUDIES

Arawwawala Don T. Liyanage
University of Kentucky, atliya2@uky.edu

FLUORINATED ARENE, IMIDE AND UNSATURATED PYRROLIDINONE
BASED DONOR ACCEPTOR CONJUGATED POLYMERS: SYNTHESIS,
STRUCTURE-PROPERTY AND DEVICE STUDIES

_____

DISSERTATION

_____

A dissertation submitted in partial fulfillment of the
requirements for the degree of Doctor of Philosophy in the
College of Arts and Science
At the University of Kentucky

By

Arawwawala Don Thilanga Liyanage

Director: Dr. Mark D. Watson, Professor of Chemistry

Lexington, Kentucky

2013

ABSTRACT OF DISSERTATION

FLUORINATED ARENE, IMIDE AND LACTAM-FUNCTIONALIZED DONOR ACCEPTOR CONJUGATED POLYMERS: SYNTHESIS, STRUCTURE-PROPERTY AND DEVICE STUDIES

After the discovery of doped polyacetylene, organic semiconductor materials are widely studied as high impending active components in consumer electronics. They have received substantial consideration due to their potential for structural tailoring, low cost, large area and mechanically flexible alternatives to common inorganic semiconductors. To acquire maximum use of these materials, it is essential to get a strong idea about their chemical and physical nature. Material chemist has an enormous role to play in this novel area, including development of efficient synthetic methodologies and control the molecular self-assembly and (opto)-electronic properties.

The body of this thesis mainly focuses on the substituent effects: how different substituents affect the (opto)-electronic properties of the donor-acceptor (D-A) conjugated polymers. The main priority goes to understand, how different alkyl substituent effect to the polymer solubility, crystallinity, thermal properties (eg: glass transition temperature) and morphological order. Three classes of D-A systems were extensively studied in this work. The second chapter mainly focuses on the synthesis and structure-property study of fluorinated arene (TFB) base polymers. Here we used commercially available 1,4-dibromo-2,3,5,6-tetrafluorobenzene (TFB) as the acceptor material and prepare several polymers using 3,3'-dialkyl(3,3'-R2T2) or 3,3'-dialkoxy bithiophene (3,3'-RO2T2) units as electron donors. A detail study was done using 3,3'-bithiophene donor units incorporating branched alkoxy-functionalities by systematic variation of branching position and chain length. The study allowed disentangling the branching effects on (i) aggregation tendency, intermolecular arrangement, (iii) solid state optical energy gaps, and (iv) electronic properties in an overall consistent picture, which might guide future polymer synthesis towards optimized materials for opto-electronic applications.

The third chapter mainly focused on the structure-property study of imide functionalized D-A polymers. Here we used thiophene-imide (TPD) as the acceptor moiety and prepare several D-A polymers by varying the donor units. When selecting the donor units, more priority goes to the fused ring systems. One main reason to use imide functionality is due to the, open position of the imide nitrogen, which provides an attaching position to alkyl substituent. Through this we can easily manipulate solubility and solid state packing arrangement. Also these imide acceptors have low-lying LUMOs

due to their electron deficient nature and this will allow tuning the optical energy gap by careful choice of donor materials with different electron donating ability.

The fourth chapter mainly contribute to the synthesis and structure property study of a completely novel electron acceptor moiety consist of a unsaturated pyrrolidinone unit known as Pechmann dye (PD) core. Pechmann dyes are closely related to the Indigo family. This can refer as 3-butenolide dimer connected via an alkene bridge, containing a benzene ring at the 5 and 5' positions of the lactone rings. We have prepared several D-A polymers using this PD system with benzodithiophene (BDT) as the donor unit. Different to common D-A polymers the HOMO and LUMO of the PD acceptor moiety are energetically located within the gap of the BDT, so that the electronic and optical properties (HOMO-LUMO transition) are dictated by the PD properties. The promising electronic properties, band gaps, high absorption coefficients and broad absorption suggest this new D-A polymers as an interesting donor material for organic solar cell (OSC) applications.

KEY WORDS: Organic semiconductor materials, Self assembly, (opto)-electronic properties, Donor-Acceptor conjugated polymers, Fluorinated arene, 3,3'-bithiophene donors, Thiophene-imide (TPD), Pechmann dye, benzodithiophene, organic solar cell.

Arawwawala Don Thilanga Liyanage

Student's Signature

08/12/2013

Date

FLUORINATED ARENE, IMIDE AND UNSATURATED PYRROLIDINONE BASED
DONOR ACCEPTOR CONJUGATED POLYMERS: SYNTHESIS, STRUCTURE-
PROPERTY AND DEVICE STUDIES

By

Arawwawala Don Thilanga Liyanage

Dr. Mark D. Watson

Director of Dissertation

Dr. Dong-Sheng Yang

Director of Graduate Studies

08/12/2013

Date

DEDICATED TO

My parents:
Mr. Arawwawala Don Vijitha Liyanage

Mrs. Chitra Renu De Silva

And

My wife and my best friend

Dilrukshi Chandima Hewage

ACKNOWLEDGMENTS

TABLE OF CONTENTS

iv

LIST OF TABLES

LIST OF FIGURES

Chapter 1: Organic semiconductors; A new frontier

Since the discovery of organic conducting polymers in 1977[1], this novel area of polymer research opens a new path to understand the fundamental chemistry and physics of π-bonded macromolecules. The concept of macromolecules was first proposed by Hermann Staudinger in 1920s and was awarded the Nobel Prize in Chemistry in 1953 for his discovery of macromolecules.[2] Since then many versions of polymeric materials were developed by scientists. From these polymeric materials, conducting polymers are among the most recent generations of polymers. Conducting polymers can be doped from insulator to metal, going into the field called organic electronics. The study of conducting polymers as organic semiconductor materials, have potential applications in the area of organic light-emitting diodes (OLEDs)[3], organic thin film transistors (OTFTs) also known as organic field effect transistors (OFETs),[4] photovoltaic devices (PVDs)[5], electro chromic devices (ECDs)[6], sensors[7] and radio-frequency identification (RF-ID)[8] tags. Conducting polymers have received extensive attention as alternatives to amorphous hydrogenated silicon OTFTs and PVDs , allowing structural tailoring and low cost, large area and mechanically flexible thin films.[9,10] Due to their lower charge-carrier mobility, organic semiconductors might never compete with inorganic semiconductors such as Si, Ge, and GaAs, in applications with high performance demands.[11] But organic semiconductors are technologically attractive due to their fundamental opto-electronic properties and processability at room temperature or moderate temperatures (solution processing) for potential applications in electronic and photonic devices with lower performance demands.[12]

Organic semiconductor materials can be mainly divided into two sub groups called organic conjugated small molecules and polymers. They have their own advantages and disadvantages. Organic conjugated small molecules such as acenes and heteroacenes have shown sufficiently high charge carrier mobilities due to their highly ordered packing arrangement, monodisperse nature, no end group contamination, well defined chemical structures and purification techniques. But drawbacks such as poor solubility, harsh processing methods and environmental and oxidative stability issues initially limited their use in real world applications. Many of these problems have been overcome by modifying the chemical structures.[13] Good film forming ability and easy solution processibility with control of molecular weight and solubilizing side chains made organic conjugated polymers additional promising candidates in this developing field. But these conjugated polymers suffer some limitations like, end group contaminations, wide polydispersity, fewer purification techniques and reproducibility issues, due to the batch to batch variation. In the race for higher performance OTFTs, the greater number of purification techniques and careful design of crystal packing seem to give small molecules the lead, but in the area of organic photo voltaics (OPVs) conjugated polymers have the lead over small molecules.

Application of organic semiconductor materials in consumer market mainly facing two major challenges: performance and life time, which still lag behind the traditional inorganic semiconductor materials such as Si, Ge, and GaAs. As an example, to compete with silicon-based inorganic semiconductor materials in PVDs, the organic semiconductor materials should demonstrate at least 10% power conversion efficiency (PCE) and 10-year life time.[14] Current state-of-the-art PVDs based on polymeric

semiconductor materials have reached PCE's closer to 8% and now 9% for proprietary materials,[15,16] but still far behind the ambient stability compared to inorganic semiconductor materials.

1.1 Ambient stability and electronic requirements

The ambient stability of organic semiconductor materials is very important for commercialization. Environmental vulnerability of these materials can be overcome by operating devices under inert conditions (e.g.: vacuum or encapsulation) but this could diminish or even eliminate the cost-savings of moving to organics. Stability of organic semiconductor materials can be divided into electrochemical stability which is intrinsic to particular materials and stability towards chemical reactions. In most cases the lower ambient stability is not due to the degradation of the ground-state semiconducting material as a result of chemical reaction, but arises due to the vulnerability of the radical anions or cations, generated during device operation, to atmospheric species like ozone, H_2O and O_2. Rational strategies to enhance the stability of these charged species (radical anions or cations) towards against atmospheric reactants are based on enhancing their kinetic and thermodynamic resistant to redox chemistry and/or trapping.[17-19]

Kinetic stability can be achieved by designing densely packed supramolecular architectures which oppose penetration of atmospheric species like H_2O and O_2,[20,21] while thermodynamic stability must be intrinsic to particular semiconductor material π systems.[17] To be an ambient stable p-type material, the highest occupied molecular orbital (HOMO) level should be deeper than -5.1 eV with respect to the vacuum level.[17] To be a stable n-type material against redox chemistry with H_2O and O_2, the lowest unoccupied molecular orbital (LUMO) should be below -3.7 eV and -4.9 eV with respect

to the vacuum level. But due to the over-potential in reaction between charge carriers and molecular O_2 ambient stability can be achieved with less negative LUMO energies. Considering over-potential of charge carriers and O_2 reduction of approximately 0.9 to 0.6 eV experimental and theoretical studies have shown that the ambient stable n-type materials should have a LUMO level lower than -4.0 to -4.3 eV with respect to vacuum.[17-19] In my thesis I mainly concentrated on p-type organic semiconductor materials so mainly focused on engineering HOMO energy levels.

1.2 Frontier molecular orbital engineering and design strategy of conjugated polymers

To control E_{HOMO} and E_{LUMO}, we are focusing on optical energy gap (E_g^{opt}) control. This is one of the many important factors in synthetic chemistry of functional π conjugated systems. Organic semiconductor materials with appropriate band structure are very important for device efficiency and device life time.[22] According to theoretical and experimental evidence E_g^{opt} of a π conjugated polymer basically depend on five contributors (figure 1.0). According to Ronacali's recent reviews [23,24] these five contributions are bond length alternation (BLA) ($E^{\delta r}$), energy associated to the twisting of the polymer backbone from its planarity (E^{θ}), the aromatic resonance energy of the aromatic units (E^{res}), the resonance and inductive electronic effects of attached substituent (E^{Sub}) and inter or intramolecular interactions in the solid state (E^{int}).[23,24] As synthetic chemist main priority goes to careful optimization of these five factors and tailors the E_{HOMO}, E_{LUMO} and E_g^{opt} depending on the desired application. The E_g^{opt} engineering is very important when we talk about organic photo voltaic (OPV) applications to obtain higher device efficiency. An ideal polymer donor for polymer solar cells (PSCs) should have broad and strong absorption in the visible and near IR region
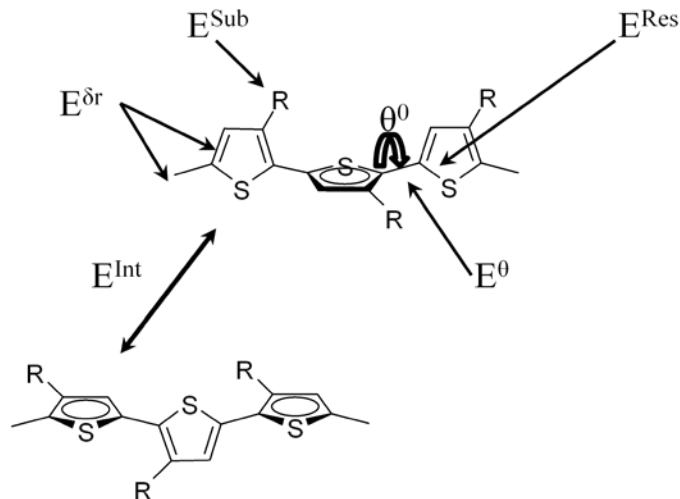
Figure 1.0: Contribution to band gap of conjugated polymers.[23,24]

(to harvest maximum solar flux) and suitable energy levels, well fitted with its fullerene

acceptor to achieve higher satisfactory open circuit voltage (V_{oc}) (This will discussed in

detail in OPV section). There are three major ways to efficiently tailor the E_g^{opt} or

broaden the absorption of donor polymer: (i) enlargement of the π system[25-27] (Above

mentioned E^{int} factor) (ii) transition from aromatic to quinoidal form (Above mentioned

$E^{\delta r}$ factor)[16,28] (iii) incorporation of donor-acceptor (D-A) functional units commonly

known as donor-acceptor approach (Above mentioned E^{sub} factor).[24] Both (i) and (ii)

have one major drawback of pulling up HOMO energy levels, lowering ambient stability

and decreasing V_{oc} when consider OPVs. Method (iii) overcomes this problem by

incorporating controlled sequences of electron donating (D) and electron accepting units

(A). Some D-A conjugated polymers have been reported with band gaps lower than 1.0

eV.[28-30] The D-A strategy is now widely used to design efficient polymer PVDs and

OTFTs. In these systems the E_{HOMO} is mainly governed by the donor unit, and the E_{LUMO}

is mainly governed by the acceptor unit. So both E_{HOMO} and E_{LUMO} energy levels and

hence E_g^{opt} can be well tuned. The introduction of this push-pull driving forces (D-A

strategy) facilitate electron delocalization via formation of quinoid structure (D-A $\rightleftharpoons$ D$^+$=A$^-$) over the conjugated backbone and reduce BLA significantly. Also this D-A strategy will not only tune E_g^{opt} of the material, it also manipulate the energies of the frontier molecular orbitals (FMO) or band edges relative to common electrode materials, which is very important for efficient charge injection and extraction. Figure 1.1 illustrates how this push-pull effect control the E_g^{opt} and FMO energy levels in a simpler way by using the concept of mixing of the molecular orbital's between the donor and acceptor in the D-A polymer. The E_{HOMO} of a resulted D-A polymer mainly depend on the E_{HOMO} of both donor and the acceptor, but more on the E_{HOMO} of donor. On the other hand the E_{LUMO} of the resulted D-A polymer depend on the E_{LUMO} of both donor and acceptor, but more on the E_{LUMO} of acceptor. So increasing the donor ability from donor "A" to donor "B" (higher E_{HOMO}), the resulting polymer E_{HOMO} and E_{LUMO} were both increased, but E_{HOMO} increased relatively more compared to E_{LUMO}, thereby decreasing the E_g^{opt} of the D-A polymer. Similarly, increasing the electron accepting ability of the acceptor monomer lowers the polymer E_{LUMO} more than E_{HOMO}. Again this will lower the E_g^{opt} of the D-A polymer. So this push-pull interaction effectively tune not only E_g^{opt} of the resulted polymer, but also the FMO energy levels of the polymers.[23,24] When considering the molecular designing of polymer semiconductors, it is very important to have reasonable solubility in common organic solvents to ensure solution-processability. It is most unfortunate if a polymer with otherwise ideal properties turns out to be insoluble and therefore unprocessable. The degree of solubility of a given polymer is governed by several factors, including the degree of polymerization (higher molecular weights, lower the solution processability), the nature (linear vs branch) and chain length of the pendant
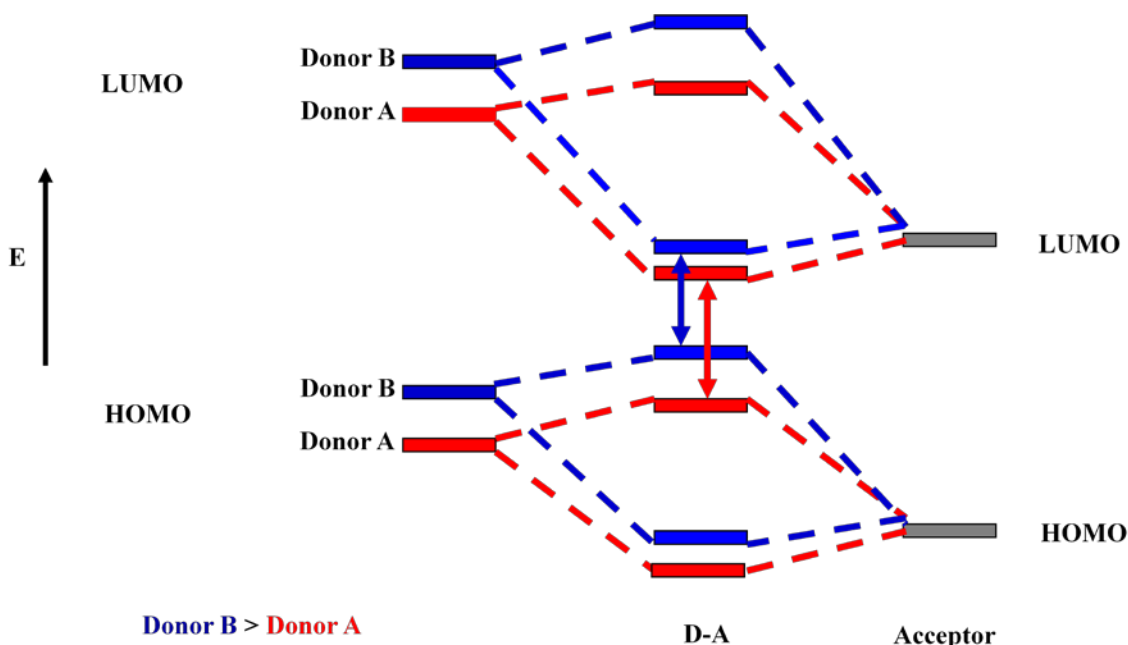
Figure 1.1: Diagram of FMO energy levels of donor (D) and acceptor (A) monomers to form molecular orbitals in D-A polymers.[24]

aliphatic chains, backbone rigidity,polymer regioregularity, and intermolecular interactions. Strong intermolecular π-π interactions are the most pronounced reason for lower solubility in polyaromatic conjugated polymers. Introducing aliphatic side chains which are covalently bonded to polymer main chain can improve solubility. Compared to linear side chains, branched aliphatic side chains are more effective in increasing solubility. From extended research and structure-property studies, now it is apparent that the choice of alkyl chains not only governs the solubility, but also ordering and morphology which is very important in the field of OPVs.[31,32]

1.3 Donor and acceptor building blocks

Inter and intra- molecular ordering of the conjugated polymers in solid-state films are very important for enhance device performance. So most of the times symmetric D and A units are usually selected to construct D-A polymers. In this section I'm going to explain briefly the rational selection strategies of donor and acceptor units.

1.3.1 Donor units

As stated earlier the donor units are electron-rich species often carrying electron donating substituents. Thiophene and benzene are the two most common basic donor units and the main building blocks to create new donor units in modern literature and in this whole thesis. Structural and electronic properties of benzene and thiophene are compared in figure 1.2.

Compared to benzene, thiophene is a five membered ring. Replacement of one "CH_2" unit by an "S" atom gives thiophene a less crowded environment and less steric congestion with adjacent neighboring groups. This can lower the backbone twisting due to the relatively less crowded nature of thiophene and increase the orbital overlap by enhancing effective conjugation length and co-planarity thereby decreasing the Eg^{opt}. The higher aromatic resonance stabilization energy (the aromatic resonance energy of benzene is 1.56 eV vs thiophene 1.26 eV[24]) of benzene lowers the delocalization of the electron cloud over the conjugated backbone, enhancing the BLA, relative to thiophene. But with thiophene the electron density can be more delocalized due to its less aromatic nature which can lower the BLA and increase the conjugation and co-planarity thereby lowering the Eg^{opt}. Due to this electron rich nature thiophene can raise the E_{HOMO} value and lower the Eg^{opt}. Effective comparison of these properties are shown in figure 1.2. The most commonly employed donor units are:

I. Bridged biphenyl units

II. Bridged bithiophene units

III. Thiophene-benzene fused units
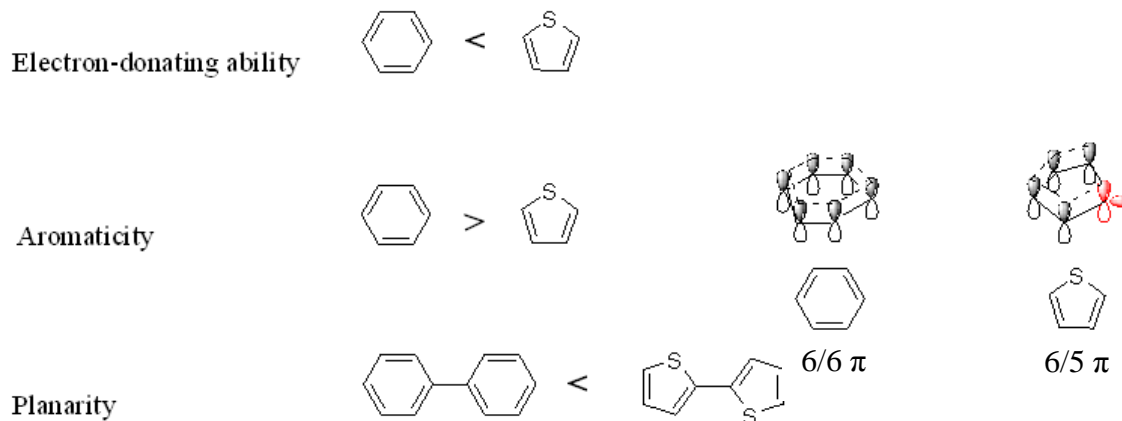
Figure 1.2: Comparison of properties of benzene and thiophene.[33]

In the biphenyl type donor molecules like fluorene, dibenzosilole and carbazole, the two benzene units are bridged by a carbon (C), silicon (Si) and nitrogen (N) atom respectively. Due to the presence of bridging atoms, these tri-cyclic systems are much more co-planar relative to their parent biphenyl unit. The bridging atom can influence the donor strength, considering that the carbazole unit have higher electron donating ability than dibenzosilole and fluorene due to the delocalization of N lone pair over the entire aromatic structure. Due to the electron-deficient nature (relative to thiophene) and higher aromatic stabilization energy of benzene, these units give rise to deeper E_{HOMO} in the polymers.[34-36]

2,2'-Bithiophene units bridged by C, Si and N atoms give rise to cyclopentadithiophene (CPDT), dithienosilole (DTS) and dithienopyrrole (DTP) respectively. Due to electron rich nature compare to the previously mentioned bridged biphenyl systems; these donor units can be ranked as strong donors (especially DTP unit).[37-39] The resulting D-A co-polymers have higher co-planarity (five membered thiophene rings introduce less steric hindrance) and relatively lower bandgaps. Various CPDT-based co-polymers give rise to good photovoltaic performance with average band gap around 1.45 eV and broad

absorption profiles.[37,40-42] Compared to CPDT units in similar polymers, the DTS unit can give better performance in OPVs. According to the literature, longer C-Si bonds relative to C-C bond in CPDT reduce the steric hindrance caused by pendent alkyl chains and give rise to better π-π stacking between polymer molecules. Also the interaction of the Si-C σ^*-orbital and the dithiophene S-C π^*-orbital lower the LUMO energy level, which give rise to lower band gap.[33,43,44]Compare to both CPDT and DTS, the co-polymers with DTP unit give rise to enhanced D-A orbital mixing which lower the band gaps and resulting wider absorption range (extended to 867 nm) due to the incorporation of N atom. [39] But the OPVs based on DTP units give lower performance due to the lower open circuit voltage (V_{oc}) (see OPV section) due to the high HOMO energy level resulting due to the electron-donating nitrogen atom.[39] The general rule is strong electron donors narrow band gap by raising E_{HOMO} and lowering E_{LUMO}.[34,35,37,39,42]

To obtain E_{HOMO} values that permit ambient device stability, it is better to use donor units with moderate electron donating ability. We can achieve this by using fused ring systems with both benzene and thiophene units. These systems are co-planar and rigid. Due to the presence of electron deficient benzene unit compare to the thiophene, able to keep E_{HOMO} level deep. Among this family of donors, IDT(indacenodithiophene) and BDT (benzodithiophene) units based co-polymers are more attractive for high efficiency OTFT and OPV devices.[45-48]

All the donor units discussed so far have the ability to carry at least 2 alkyl side chains. This can improve solubility in resulting co-polymers, which is crucial for solution processability in mild conditions. Also due to the co-planar geometries and rigid

structures of these systems suppress the rotational disorder along the polymer backbone by lowering the reorganization energy and enhance the intrinsic charge carrier mobility.

1.3.2 Acceptor units

An acceptor unit generally refers to π electron systems with electron-withdrawing substituents or the π systems containing electronegative heteroatoms. As examples we list arenes carrying cyano groups [49], or containing imine nitrogen (-C=N) such as in benzothiadiazole (BT),[38,50] thiazolothazole (TTz),[51-53] quinoxalin (QA),[54,55] thienopyrazine (TP),[56,57] bithiazole (BTz),[58-60] benzobisthiazole (BBTz),[61] benzotriazole (BTA),[62,63] s-tetrazine (STTz),[64,65] naphtho[1,2-c:5,6-c]bis[1,2,5]thiadiazole (NT),[66] thiadiazolo[3,4-c]pyridine or imide nitrogen (-CO-NR-CO-) such as in phthalimide(PH),[67] thieno[3,4-c]pyrrole-4,6-dione(TPD),[68-70] bithiophene-imide(BTI)[70] and naphthalene bisimide (NBI)[71] or lactam unit (-NR-CO-) in iisoindigo(II),[72,73] diketopyrrole [3,4-c]pyrrole-1,4-dione (DPP),[74,75] or carbonyl groups (C=O) such as in naptho[2,3-c]thiophene-4,9-dione (NTDO)[76] and ester substituted thieno[3,4-*b*]thiophene (TT)[77]. Electron accepting ability is determined by the relative position of LUMO energy level of the acceptor unit with respect to the vacuum level: lower the LUMO energy level, the stronger the electron accepting ability. So these acceptors can be broadly classified as strong acceptors, weak acceptors and medium acceptors depending on the relative electron withdrawing ability of the attach substituent or the presence of electronegative heteroatom's (e.g. fluorine).[33] Currently the most common strategy is to use already known acceptor molecule with chemically modified novel donor unit and prepare co-polymers and conduct structure-property studies.

1.4 General routes for synthesis of conjugated polymers

The synthesis of conjugated polymers most commonly relies on efficient carbon-carbon single bond formation between two unsaturated carbons in the aromatic units. Compared to electrochemical[78,79] or chemical oxidative polymerization,[80] transition-metal-catalyzed cross-coupling reactions provide a more controlled effective strategy for C sp^2-C sp^2 and C sp-C sp^2 bond formation.[81] The most commonly used transition-metal catalysts are nickel- or palladium- based complexes. The organometallic nucleophiles can be Grignard reagents(Kumada-Corriu)[82], Stannyl (Stille)[83], boron reagents (Suzuki-Miyaura)[84], or cuprates (Sonogashira)[85]. Also nickel-mediated Yamamoto dehalogenative coupling reactions can be used as an alternative pathway for carrying out homopolymerization of single monomers.[86] Classic reactions such as Wittig-Horner or Knoevenagel condensation can also be used in the synthesis of vinylene-containing conjugated polymers via C-C double bond formation.[87]

From all the above mentioned methods Stille coupling between stannanes and aryl halides to from C-C bonds has become the most versatile synthetic methodology for D-A co-polymers. The main advantages of this reaction are that it can tolerate different functional groups and operate under mild reaction conditions. Organo-tin and organo-halide monomers can be easily prepared generally without protecting groups. Stille polymerization is widely used in preparation of many varieties of different polymers, especially for thiophene-related polymers by taking advantage of highly electron rich thiophene monomers with electron-deficient halide and triflate monomers.[88,89]

1.4.1 Mechanism of the Stille coupling reaction

The general mechanism of Stille coupling is similar to many other transition-metal mediated coupling reactions, involving an oxidative addition step, a transmetallation step, and reductive elimination step, which yield the product and regenerates the catalyst. The Pd (0) species is the active catalyst. The Pd (II) precatalysts used in this reaction are reduced to Pd (0) by the organostannane monomers before entering the catalytic cycle. The first step in the catalytic cycle as shown in figure 1.3.
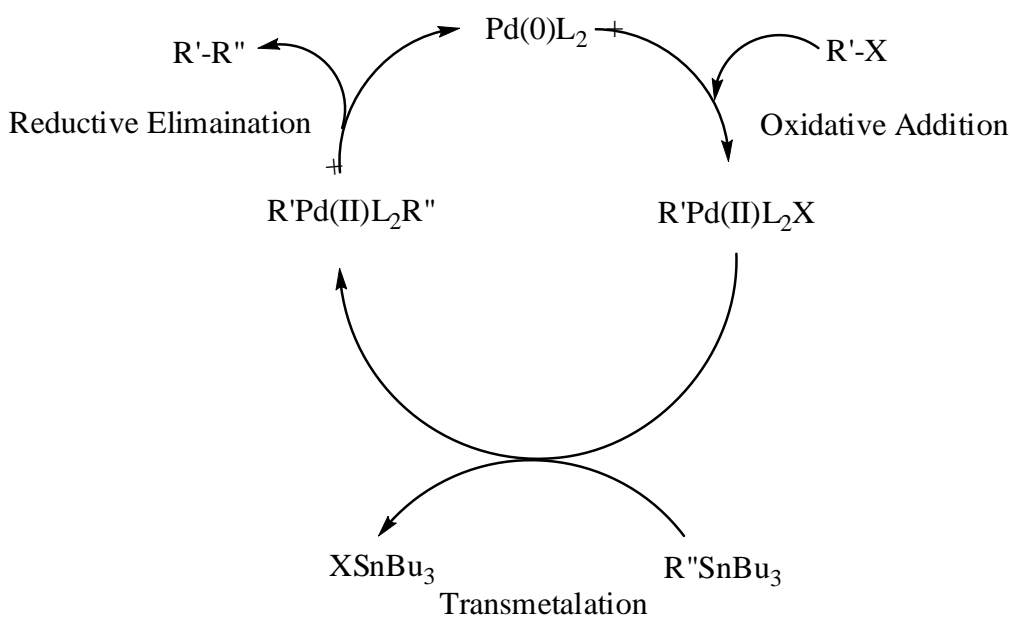
Figure 1.3: General mechanism of the Stille reaction.

is oxidative addition. Here the organohalide or triflate oxidatively adds to the Pd(0) active catalyst forming a Pd (II) intermediate [Pd(II)L_2R'X]. Here L, represent ligand; R' can be alkenyl, alkynyl or aryl group and finally X is Br, I, Cl (Halogen) or triflate (-OTf). Electron-donating ligands on Pd facilitate this oxidative addition step. The second major step is transmetallation generally regarded as the rate-determining step.[90]

Reductive elimination is the last step in the catalytic cycle which generates the coupled units and allows the palladium catalyst to re–enter to the catalytic cycle. All the polymers prepared in this work were prepared using Stille coupling reaction.

1.5 Electrochemistry of conjugated polymers

Voltammetric techniques are widely used by materials researchers to estimate FMO energy levels. Most commonly, a sweep technique, known as cyclic voltammetry (CV) is used to estimate E_{HOMO} and E_{LUMO}. This technique involves application of forward and reverse linear potential scans through a working electrode immersed in an electrolyte solution, also containing the redox active species of interest. If the material has accessible oxidations, an anodic wave appears in the forward positive scan, and a corresponding cathodic wave can be observed on the reverse scan, showing that the oxidation is reversible under the experimental conditions. The voltammetric instrument consists of a three electrode system. One of the three electrodes is working electrode, which potential is varied linearly with time. The second electrode is reference electrode. Here no current go through this reference electrode and potential remains constant throughout the experiment. The third electrode is counter electrode which conduct current via the electrolyte solution to the working electrode. In our group, to estimate FMO energy levels, we basically use pulse voltammetric technique known as differential-pulse voltammetry (DPV). Compared to CV, this DPV technique is more sensitive. DPV measures the current at a time when the difference between the faradaic current and the interfering charging current is large. Voltammetric methods evolved to measure the oxidation and reduction potentials of conjugated polymers typically involve deposition of the polymer material onto the working electrode. The onsets of oxidation and reduction

are used to estimate the E_{HOMO} and E_{LUMO}, respectively. The oxidation potential provides a relative estimate of the energy of HOMO which can consider as the ionization potential, the minimum energy required to remove an electron from an atom or molecule in the gas phase. According to these definitions it is clear that the energy values we obtain from this voltammetric technique are raw values because the HOMO/LUMO energies are scaled in vacuum, but our reduction/oxidation potentials are measured in thin films.

1.6 Wide angle x-ray diffraction (2D-WAXD) patterns of polymers

Supramolecular self-assembly is a very important aspect to obtain high device performance. Compared to inorganic semiconductors with long-range 3-dimensional order, organic semiconductor materials show comparatively lower device performance due to their weak Van der-Waals interactions and short range order. Also unlike inorganics, the electrons in organic materials are tightly bound to atoms lowering their free movement. Basically all these organics are insulators without any free charge Carriers. The supramolecular arrangements of all polymers reported here were investigated by 2D-WAXD from aligned fibers. Unlike small molecules, we cannot obtain single crystals from polymers. Powder diffraction patterns can be obtained, giving some information about the spacing between semi-regularly arranged molecules. To improve the utility of WAXD, scientists use polymer fibers, with polymer backbones aligned along the axis of the fiber. Here I have used home built mini-extruder to prepare polymer fibers. The polymer fibers obtained after passing through a die by mechanical force were mounted perpendicular to the incident X-ray beam and diffracted x-rays were collected by an area detector. Polymer fiber was mounted perpendicular to the incident X-ray beam, so diffraction maxima along the meridian (vertical axis) provide information
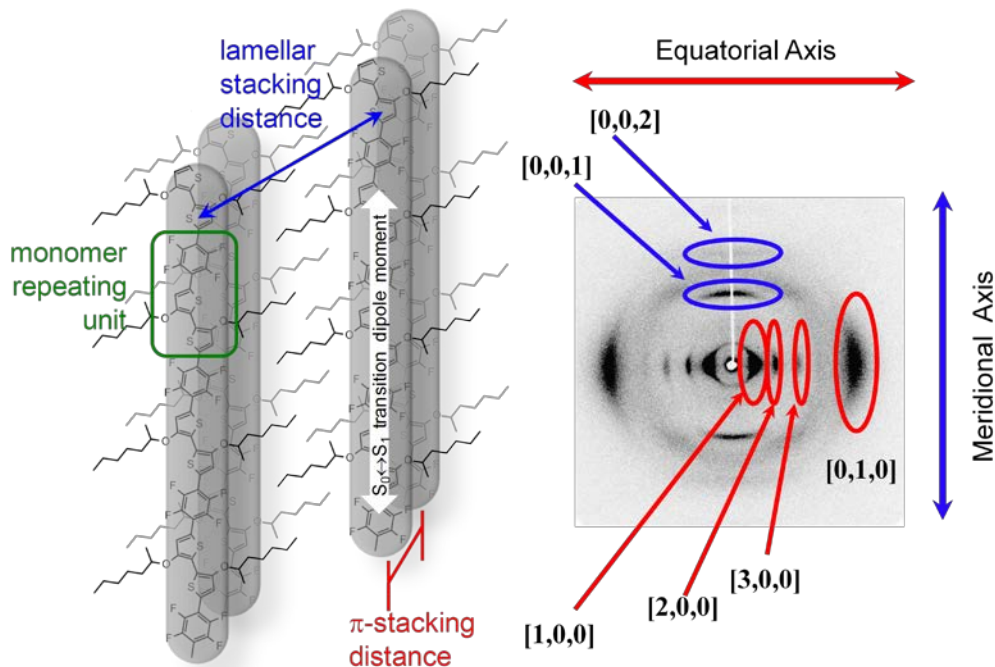
Figure 1.4: Schematic illustration of 2D WAXD pattern of an aligned fiber and lamellar packing of polymers within fibers. (The image was drawn by Dr. Johannes Gierschner Madrid Institute for Advanced Studies, IMDEA Nanoscience, Calle Faraday 9, Ciudad Universitaria de Cantoblanco, 28049, Madrid, Spain)

about repeating elements along the backbone and diffraction maxima along the equator (horizontal) reflect the lamellar spacing and π-stacking . But it is important to note that these values are upper limits, exceeding the actual stacking distance if the polymer backbones are tilted away along the normal stacking axis.

1.7 Organic thin film transistors (OTFTs) and Organic photovolataics (OPVs)

1.7.1 Organic vs inorganic transistors

TFTs are major building blocks in modern microelectronics. Silicon is the most common semiconductor material used in this industry. The difference of device performance between organic and inorganic semiconductors basically lies on bonding

properties, inter and intramolecular packing arrangements. In inorganic semiconductor materials, such as silicon, the atoms are held tightly with strong covalent interactions (100-400 kJ/mol)[91] and form highly ordered three-dimensional crystal lattice structure.[92] Due to the high degree of atomic orbital overlap, charge transport occur in highly delocalized band-like transport mechanism.[92] Compare to inorganic semiconductors, organic molecules are weakly bound together by van der Waals interactions (<5 kJ/mol), hydrogen bonding (10-65 kJ/mol) and π-π intermolecular interactions (0-50 kJ/mol).[91] So not like inorganic semiconductor materials organic semiconductor materials lack highly ordered three-dimensional crystal lattice structure and lower the atomic orbital overlap which lower the charge carrier transport.

1.7.2 Device structures of OTFTs

A transistor can be considered as an electron valve or switch, with the current flow between source and drain electrodes controlled by the degree of the electric field
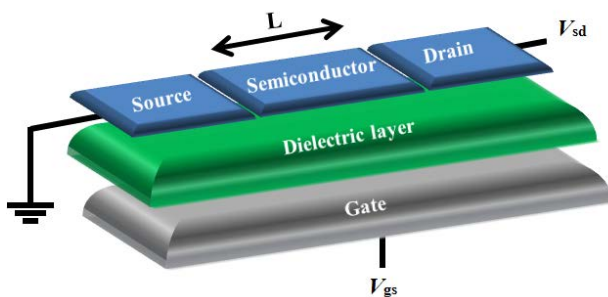
Figure 1.5: Schematic structure of an OTFT and applied voltages.

applied to the gate electrode. OTFTs also show same basic device architecture as their inorganic counterparts. As shown in figure 1.5 this device consists of three electrodes known as gate, source and drain, as well as dielectric insulating layer and organic semiconductor material. The channel length, or the distance between source and drain electrodes, is denoted as "L". The semiconducting layer can be vacuum sublimed, spin or

drop-cast in small molecules, but in polymers, this can be spin coated or drop-cast using suitable solvent system only. As dielectric layer, inorganic insulators such as SiO_2, Al_2O_3 and Si_3N_4 or polymeric insulators such as poly(methylmethacrylate)(PMMA) or poly(4-vinylphenol)(PVP) are commonly used.[4] The voltage applied between source and drain, or source-drain voltage, is denoted as V_{sd}. The voltage applied between source-gate is known as gate voltage and denoted as V_{gs}. Ideally when no gate voltage applied the conductance of the semiconductor layer should be zero because there are minimal mobile charge carriers present. So the device is in "off" state. When the gate voltage is applied, a higher concentration of mobile charges near the dielectric-semiconductor interface is induced and the transistor is in "on" state. Due to this origin of gate induced charging, these transistors commonly known as "field effect transitors".

1.7.3 Important parameters of organic semiconductor materials for OTFT application

The main priority of the research reported in this dissertation goes to the synthesis and structure property studies of the D-A polymeric materials. But it is very important to get an idea about the basic fundamental parameters we have to consider when we want to design an organic semiconductor material for effective device applications. In this paragraph, I'm briefly going to explain some important design rules in organic semiconductor materials developing for OTFT application. It is important to control the semiconductor FMO energy levels with respect to the corresponding electrodes work functions to obtain efficient charge injection and extraction. After charge injection, charge carriers have to migrate through intermolecular hopping between adjacent individual molecules. So closer π-π stacking and maximum orbital overlap is essential for

fast charge carrier transport. In following few paragraphs, I'm going to discuss some important design parameters of organic semiconductor materials for OTFT application.

1. Highly conjugated π-system with appropriate FMO energies

As discussed previously the FMO energy levels can determine whether the organic semiconductor material will undergo redox reactions with atmospheric species like O_2 and H_2O. The ambient stability of organic semiconductor material is very important to achieve very low "off" currents and higher mobility. Also the proper matching of the organic semiconductor FMO energies with electrodes are crucial, because the charge injection occurs from the source electrode to the organic semiconductor material which give rise to the charge accumulation in dielectric/semiconductor interface. So the relative energy difference between electrode and frontier molecular orbitals (E_{HOMO} for p-type material and E_{LUMO} for n-type material) of the organic semiconductor influences the effective charge injection and extraction. Simply stated the work function of the electrode should be comparable to the E_{HOMO} level for hole injection (p-type) or E_{LUMO} level for electron injection (n-type).[4]

2. Maximum π orbital overlap

The main pathway for charge carrier transport in organic semiconductor material is intermolecular hopping. Efficient π orbital overlap is critical for efficient charge carrier transport. Obtaining closer π stacking distance is critical for obtain efficient charge carrier transport.[91]

3. Better solubility and good film-forming properties

To obtain better films, polymer solubility is a critical factor. A good strategy to improve polymer solubility is to introduce branch aliphatic chains over linear aliphatic

chains. From extended research and structure property studies, it is apparent that the choice of alkyl chains not only govern the solubility properties, but can use as a tool to control polymer crystallinity and morphological order in thin film blends as discussed extensively in later paragraph.[31,93,94] Semiconductor films with large grain or domain dimensions and interconnectivity is better for efficient charge transfer.[95]

As mentioned earlier good solubility also important for solution based processing technology like ink jet printing etc. Solution processability is very important for polymers, because not like small molecules, polymers cannot process using vapor deposition techniques due to lower vapor pressure. Good strategy to obtain better solution processability is to use longer linear or bulky branched side chains. This will enhance solubility but have to empirically determine effects on order and order and π stacking for each new polymer.[4,96]

5. Purity and stability towards atmospheric species

Purity of semiconductor material is very important for efficient charge carrier transport in both inorganic and organic semiconductors. Impurities can trap charge-carriers and lower the charge carrier mobility. Also this can give rise to higher "off" currents and lower the current modulation. Long term stability is very important for commercialization of organic semiconductor material. Lower stability of organic semiconductor material may not be due to intrinsic factors, but due to extrinsic factors like atmospheric dopants reacting with charge-carriers as discussed above.[4,17]

1.7.4 Organic photovoltaic devices (OPVs)

The need of developing inexpensive renewable energy sources stimulates the scientific community to search for efficient, low cost, sustainable and environmentally

friendly (non-CO_2 releasing) energy sources like OPV devices. The organic, polymer based OPVs show the potential of obtaining cheap and easy methods to produce energy from light due to low cost solution processability (spin-coating, doctor blading, screen printing and inkjet printing).[5,97] Furthermore, organic semiconductor thin films (~100 nm) show high absorption coefficients in the range of $< 10^5$ cm^{-1} which makes them good chromophores for opto-electronic applications.[5]

1.7.5 Operation of OPVs

The energy conversion process in OPVs has four fundamental steps in the commonly accepted mechanism: a) absorption of light and generation of coulombically bound electron-hole pairs known as excitons. b) diffusion of exciton pair to donor-acceptor interface. c) dissociation of excitons to generate charges (holes and electrons) and d) charges transport to respective collection electrodes. [98] The electron-hole pair or exciton is strongly coulombically bound and does not separate in to free charge carriers before reaching the donor-acceptor interface due to low dielectric constant ($\varepsilon_r \sim 2\text{-}4$) of organic materials.[99] This binding energy is typically estimated to be 0.4-0.5 eV.[98] The energy difference between the LUMOs of the donor and acceptor phases provide the driving force for charge separation at the interface. Fullerenes are currently the most commonly employed organic acceptor materials used in OPVs.

By considering this, the ideal donor polymer should have its FMO energy levels according to figure 1.6 to obtain maximum charge separation on the interface. To obtain higher efficiency, photoinduced excitons have to reach the donor-acceptor interface within the lifetime of the exciton. The exciton diffusion lengths in organic semiconductors are usually around 10-20 nm. Blending conjugated polymers with

21

electron acceptors, such as fullerenes, is a very efficient way to break apart excitons into free charge carriers. Photophysical studies showed that photo induced charge transfer in such blends happens on a time scale of 45 fs. This is much faster compared to other competing relaxation processes such as fluorescence which occurs around ~1ns. To achieve efficient exciton dissociation within the exciton life time, material chemist design a new OPV architecture called bulk heterojunction (BHJ) model. Bulk heterojunction is a blend of donor and acceptor components in a bulk volume. Using this device architecture can obtain the donor-acceptor phase separation in a 10-20 nm scale.[98] Due to this nano
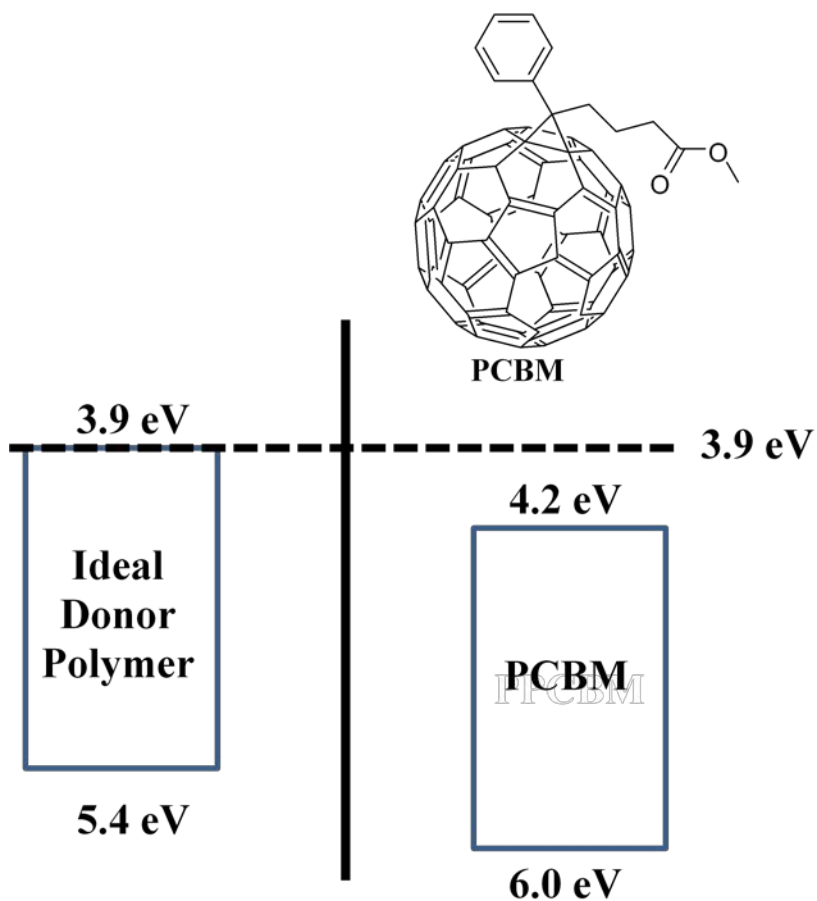
Figure 1.6: The ideal donor FMO energy values relative to the band structure of PCBM.[98]

scale interpenetrating network exciton can dissociate to the respected charges within the whole blend. The generated charges need to be transported to the appropriate electrode efficiently without recombination. The charge carriers need a driving force to reach to the desired electrodes. This driving force is determined by the energy difference between the HOMO level of the donor and the LUMO level of the acceptor which known as open circuit voltage (V_{oc}).[97]

As discussed earlier in BHJ solar cells the excitons produced anywhere in the channel can reach to the donor-acceptor interface within the exciton life time. These bulk heterojunction donor-acceptor phases need percolated pathways to transport holes and electrons to the desired electrode (anode/cathode). So the donor and acceptor phases should have nanoscale, bicontinuous and interpenetrating network. So bulk heterojunction devices are more sensitive to the nanoscale morphology in the blend.[99] Even if the electronic properties satisfy, the performance of BHJ solar cells still depends on the nanoscale molecular alignments of a donor and an acceptor. Control over the morphology of the blend films of the polymer and the fullerene derivative is a key step to achieve high efficiencies. The morphology is controlled not only by the backbone and side chains of the polymers but also by various device fabrication methods, such as the choice of solvents,[100,101] solvent additives,[42,102-104] and thermal[105-107] and solvent annealing.[108-111]

1.7.6 Important parameters of organic semiconductor materials for OPVapplication

Because of the wider band gaps in organic material, only a small portion of the incident solar light is absorbed. A material with a band gap of 1.1 eV (1100 nm), together with a broad absorption profile, has the potential to absorb 77% of the solar radiation on

earth.[5] But the majority of semiconducting polymers have band gaps around ~2 eV (620 nm), which limits the capability of harvesting of solar energy to maximum of 30%.[5] So we need better "solar spectrum" harvesting, low band-gap polymers for efficient power conversion.

The performance of OPV can characterized using a current-voltage curve depicted in figure 1.16. When no light is present the current flow is zero because there is no any exciton formation in the absence of light. In presence of light the OPV begins to generate excitons and dissociated excitons to free charge carriers generate electrical current. From the current-voltage (*I-V*) curve, we can obtain the maximum power point (MPP), on the *I-V* curve (I_{mpp} V_{mpp}) where the maximum power is produced. This is illustrated in the diagram as the area of the rectangle. The power conversion efficiency (η_e) of an OPV can be calculated using the following equation.[98,99]

$$\eta_e = \frac{V_{oc} \times I_{sc} \times FF}{P_{in}}$$

$$FF = \frac{I_{mpp} \times V_{mpp}}{I_{sc} \times V_{oc}}$$
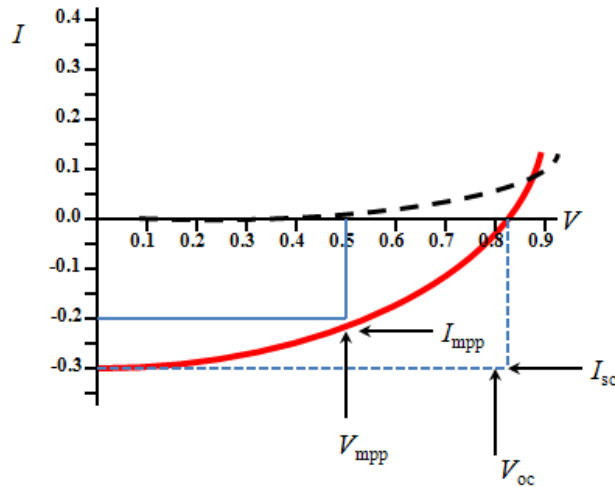
Figure 1.12: Example of current-voltage curve of polymer solar cell.[5]

24

As described below, V_{oc} is open circuit voltage, I_{sc} is short circuit current, FF is the fill factor and P_{in} is the energy of incident light. I_{mpp} and V_{mpp} are the current and voltage at the maximum power point. [5]

In following few paragraphs, I'm going to discuss some important parameters of OPV application.

1.Open-circuit voltage (V_{oc}):

This is the voltage across the photovoltaic cell when no current is flowing through the cell. As stated earlier this commonly determined by the difference of LUMO energy level of the acceptor and the HOMO energy level of the donor. The best strategy to increase the V_{oc} is to use donors which having deeper HOMO energy values. But this can increase the E_g^{opt} and lower the absorption of solar flux. So it is very important to keep a well balance in donor E_{HOMO} value and E_g^{opt}. For the acceptor these values are fixed because, currently, most frequently used acceptor is PCBM. Donor-acceptor strategy is a powerful tool to maintain this balance in an efficient way.

2.Short circuit current (I_{sc}):

This is the current which flow through the solar cell when there is no external resistant. This is highly depending on the charge carrier mobility of the organic semiconductor material. Due to lower mobility of the semiconductor material the active layer thickness is limited to few nanometers (~ 100 nm) because beyond a certain thickness charge carriers will not reach the electrodes before recombination.[97] Also higher absorbance of photon flux can increase the short circuit current by efficient formation of excitons. Therefore high mobility/low band gap materials are the general route for improving short circuit current.

3.Fill factor (FF):

This determined the fraction of charge carriers that actually reach to the electrodes. This is a competition between charge carrier recombination and transport. The distance a charge carrier can travel is a function of lifetime and mobility. So enhanced charge carrier mobility, well balanced mobility of electrons and holes, well controlled morphology with lower degree of defects can improve fill factor.[97]

4.Lifetime:

Another most important parameter of polymer OPV is operational life time. This is very important for commercialization aspects. As mentioned earlier 10% efficiency and 10-year life time is the minimum requirement to compete with current amorphous silicon based solar cells. The stability of the OPV is comparatively high compare to OTFTs because the active semiconductor layer is encapsulated between cathode and anode electrodes. But morphological degradation which may resulting due to elevated temperatures under solar irradiation can lower the life time of OPVs.[112]

1.8 Substituent effect in donor (D) acceptor (A) conjugated polymers.

One primary goal in this whole research period was to investigate the effect of substituents on polymer properties. How do different substituent's effect to the optical and electronic properties of the D-A co-polymers? From extended research and structure property studies, it is apparent that the choice of alkyl chains not only governs the solubility properties, but can be used as a tool to control polymer crystallinity and morphological order in thin film blends, which is an important issue in the field of organic solar cells (OSCs)[31,93,94,113]. The length of the side chains directly affects the solubility and interchain distances and order in the solution-deposited films.[114] Also the

electronic properties, surface tension and thermal properties (eg: glass transition temperature) can vary depending on the alkyl substituent.[115] Conjugated polymers carrying linear alkyl side chains either on donor or acceptor have attracted much attention in organic thin film transistor (OTFT) studies due to their relatively favorable charge transport properties.[46,67,116] Recent studies also demonstrated high charge carrier mobilities for polymers with branched alkyl chains.[117,118] This concept was successful also for OPVs, demonstrating higher photo conversion efficiencies (PCE) compared to their linear alkyl counterparts.[43-45,119]

The charge carrier mobility is not an intrinsic property of the material. It is highly dependent on the packing arrangement of the molecules or polymer chains both on local (amorphous vs. crystalline) and on macroscopic morphological (grain boundaries) length scales. The studies done on small molecules and mesogens clearly show that bulky substituent's can enhance solid state packing over the less bulky substituent. According to the work done by Anthony *et al* on rod shape materials, the bulky substituent's attached on the rod shape acene core, can lead to changing from a 1D, "slipped stack" arrangement to 2D, "bricklayer arrangement" with closer π stacking and relatively high charge carrier mobility.[13,120,121] Also the work done on disk-shape mesogens like triphenylenes have shown that bulkier thioether side chains show highly ordered helical columnar with higher charge carrier mobility over less bulky alkoxy substituents. Here the more bulky "S" atoms invoke fixed columnar arrangements by lowering the molecular rotation over "O" substituent linkage.[122,123] Also the work done on hexabenzocoronene showed that when attaching big bulky substituents to the pheriphery of the disk give rise to longer-range solid state order by forming nano ribbons. This also

proven by their uv-vis and X ray data.[124] From these studies it was clear that bulky substituent's give rise to long range order which is very important in device applications.

Recently considerable attention has been paid to the impact of polymer alkyl side chains (linear vs big bulky branch chains) on polymer:fullerene bulk heterojunction solar cell performance, in the area of open circuit voltage (V_{oc}) and short circuit current (J_{sc}) which are the two main parameters to obtain high efficiency solar cells. Although due to the presence of different attachment possibilities and different type of alkyl chains, it is very hard to get a clear idea how alkyl side chains influence the overall properties of the polymer:fullerene BHJ solar cells.[125-127] There are several literature works which used branch alkyl chains and obtain higher degree of morphological order and higher OTFT and OPV performance with stable HOMO energy values.[128-130] Morphological order and degree of crystallinity are the key players in obtaining high performance organic thin film devices. There are several literature works which used branch alkyl chains and obtain higher degree of morphological order and higher OTFT and OPV performance with stable HOMO energy values. Sagalman *et al*[128] have shown that Poly(3-alkylthiophenes) (P3ATs) incorporated with branch ethyl hexyl chains can obtain the similar crystalline order compare to its linear chain predecessor regio-regular poly(3-hexylthiophene) (rr-P3HT). Thompson *et al* has randomly introduced this 2-ethyl hexyl branch P3ATs to rr-P3HT. They also reported that the resulted random co-polymers show similar crystalline order and optical properties similar to rr-P3HT. Polymers with 25% 2-ethyl hexyl containing P3ATs showed higher V_{oc} and J_{sc} values compare to rr-P3HT with deeper HOMO values and relatively higher solar cell efficiency. Yang *et al* reported a study on napthodithiophene (NDT)-dithiophenebenzothiadiazole (DTBT) co-polymers varying

alkyl side chains on the NDT and DTBT units, by varying the length (octyl, dodecyl) and branching (2-ethylhexyl, 2-hexyldecyl) of the alkyl chains without changing the placement. Here the authors found pronounced influence of the alkyl side chains on the V_{oc} and J_{sc} of the resulting polymer: PCBM devices. Here authors stating that long and branched alkyl side chains give rise to larger V_{oc} values but lower J_{sc} values. [129] Biniek *et al* found an increased solar cell efficiency in presence of 2-ethyl hexyl chains over linear dodecyl chains in their study on side chain variation and site of attachment on benzo[1,2-b:4,5-b'] dithiophene-co-thieno[3,4-b]thiophene polymer. They observed higher V_{oc} and J_{sc} values in presence of branch alkyl chains. [32] Andersson *et al* also stated that branched side chains give rise to higher V_{oc} values compare to the linear alkyl chains in their study on carbozole-thiophene-quinoxaline-thiophene co-polymer.[126] Bronstein *et al* have studied the effect of side chain variation on OPV and OTFT performance on indacenothiophene-co-benzothiadiazole (IDT-BT) polymers. They found that higher mobilities can obtain in shorter bulky side chains and obtain higher OPV performance in presence of 2-ethyl hexyl side chains.[130] According to the recent study done by Frechet et al[131] have showed that by increasing the bulkiness closer to the polymer backbone enhance the exciton dissociation and improve the photocurrent which is important to obtain higher PCE. In an another study using furan containing diketopyrrolopyrrole (DPP) polymers, the same group has shown that linear alkyl groups can be used as the alternatives to the branched side chains by getting improve thin film nanostructural order and closer π staking which give rise to higher charge transport properties and higher OPV performance by enhanced fill factors (FF).[132] Higher V_{oc} and more deeper HOMO energy values can be achieve with increase backbone twisting but this will lower the J_{sc}. Bao *et*

al have systematically introduced backbone twisting and showed it is possible to obtain higher J_{sc} and V_{oc} with high solar cell performance values comparable to conjugated polymers with nearly planar backbones such as rr-P3HT.[133]According to these studies it is obvious that incorporation of branched alkyl side chains has gained growing attention by material chemist since it affects not only for the solubility but also the molecular packing and morphology, interaction between the polymer chains and frontier molecular orbital (FMO) energy levels.[45,130,134]

However, up to now detailed experimental and/or theoretical study to systematically investigate the impact of the side chains on the structural and optoelectronic properties and/or device performance are rare. This concerns the substituent position, as well as nature (e.g. alkyl, alkoxy) and type (linear vs. branched) of the substituents. So in this whole research period the prime goals were,

1. To systematically investigate how different substituents affect to the optical, electronic and solid state packing.

2. Manipulate good balance between solubility and solid state order via careful choice of side chains.

3. Try to achieve charge carrier mobility equal to or greater than that of amorphous silicon.

1.9 Summary of dissertation

As stated earlier the main focus of this dissertation is to get an idea of the structure property relationships of conjugated D-A co-polymers. The whole dissertation is consisting of five chapters including the introduction. Chapter 2 mainly focused on 2,3,5,6-tetrafluorobenzene (TFB) based D-A conjugated polymers. Here the main

priority goes to the substituent effects. How different substituent (linear or branch) and substituent type (alkyl or alkoxy) tethered to donor-co-monomer affects to the optical, electronic and solid state packing arrangement of the resulted TFB based D-A co-polymers. Also a detail study was done using 3,3'-dialkoxy bithiophene donor units incorporating branched alkoxy-functionalities by systematic variation of branching position and chain length. The study allowed disentangling the branching effects on (i) aggregation tendency, intermolecular arrangement, (iii) solid state optical energy gaps, and (iv) electronic properties in an overall consistent picture.

Chapter 3 mainly focuses on thiophene-imide (TPD) based D-A polymers. Here in addition to substituent effects, we planned to demonstrate how fused ring systems influence to the optical, electronic and solid state registry of these D-A co-polymers. Simillar to chapter 1, in chapter 3 also we incorporated dialkyl and dialkoxy bithiophene donors units. Here also we found that dialkyl bithiophene donors give rise to more stable E_{HOMO} values compare to the alkoxy substituent donors. As fused ring systems we used thienothiophene (TT), cyclopentadithiophene (CPDT) and indacenodithiophene (IDT).

Chapter 4 is mainly dedicated to a novel acceptor moiety, which was prepared by derivatizing a Pechmann dye core to the corresponding lactam functionality. This new acceptor unit was abbreviated as NPD. These polymers show well developed bimodal absorption profile almost extending to the near IR region. According to the electrical and optical properties these materials seem to be a promising candidates as the donor polymer in the BHJ solar cells with PCBM acceptor. From quantum mechanical calculations we found that these novel polymeric materials are different to common D-A polymers because the E_{HOMO} and E_{LUMO} of the NPD acceptor moiety are energetically located

31

within the gap of the BDT, so that the electronic and optical properties (HOMO-LUMO transition) are dictated by the NPD properties.

Chapter 5 briefly outlines some future potential of these 3 projects including some essential developments needed to obtain valuable data from these structures. Also in this chapter we introduce some novel acceptor material not commonly used in the organic electronic community. Finally the last chapter contains all the necessary experimental information on material synthesis, proof of purity by NMR and GCMS and material characterization techniques such as DSC and DPV etc.

Chapter 2: Influence of side chains on the properties of alternating donor-acceptor co-polymers tetrafluorobenzene acceptor units

2.1 Introduction

Thiophene related materials have played a prominent role in the organic semiconductor field due to their molecular geometry, rich electronic properties and the reactivity which open the way to a great structural versatility and freedom in control of electronic properties through derivation. At the early stage in the history of polythiophenes, unsubstituted polythiophene (PT) was prepared in the early 1980's through electrochemical polymerization techniques. This semiconductive (when doped) primarily 2,5-coupled polythiophene (figure 2.1) was found to be thermally and environmentally stable but insoluble.[135] To increase solubility, thiophenes with solubilizing alkyl chains at their 3-positions were polymerized to produce poly(3-alkyl thiophene)s (P3ATs).[136] Since 3-alkylthiophene has lower symmetry, coupling at the 2- and 5-positions leads to three possible regio-isomeric linkages: Head-to-Head (HH), Head-to-tail (HT), and tail-to-tail (TT). Initial chemical and electrochemical methods used for polymerization created random couplings which gave only 50-80 % HT linkages. The structural irregularity does not allow a high degree of order in the solid state, and caused twisted backbones and limited effective conjugation. Due to these reasons these regio-irregular rra-P3AT's give very poor conductivity. In 1992 regioregular P3ATs (rr-P3AT) were synthesized using a method developed by McCullough[136,137] and a similar method was published by Rieke.[138] The McCullough method, now known as Grignard metathesis (GRIM), produces rr-P3ATs with a HT regioregularity of 98-100 %. This gave rise to dramatic enhancement of the electrical properties of the P3AT's which is generally attributed to improved solid-state order as a

result of greater structural regularity. Until the last decade, this made rr-P3HT one of the

benchmark organic semiconductors, with OTFT charge-carrier mobility up to 0.1 cm^2/Vs.

But this benchmark polymer has several

Head-to-Head (HH)   **Head-to-tail (HT)**   **Tail-to-tail (TT)**

PT   **rra-PT**   **rr-PT**   **rs-PT**
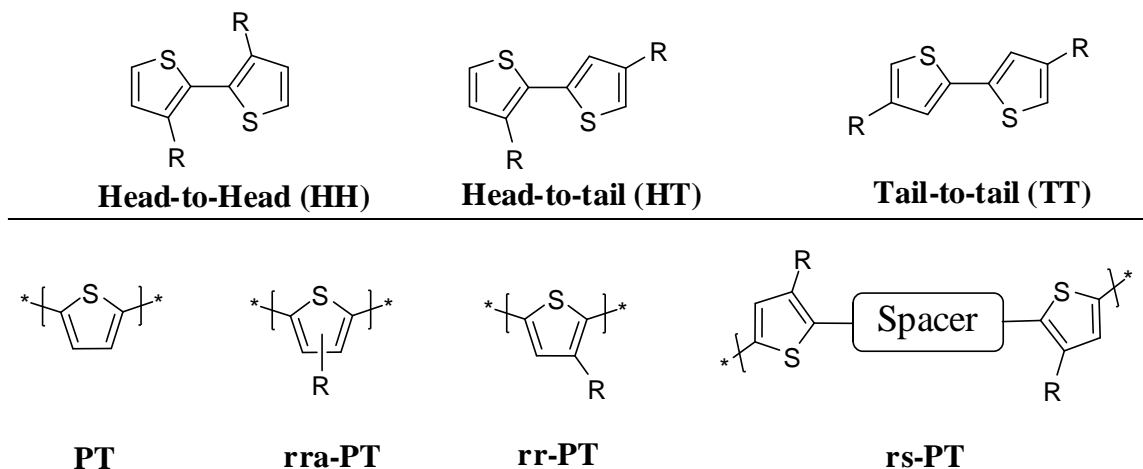
Figure 2.1: Top: Three regioisomeric types of 3-alkyl thiophene linkages. Bottom: Chemical structures of: unsubstituted 2,5-coupled polythiophene (PT); regioirregular polythiophene (rra-PT); regioregular HT P3AT, (rr-P3AT); regiosymmetric alternating polythiophene co-polymer (rs-PT).[136]

drawbacks like poor environmental stability.[139] The HOMO energy of rr-P3ATs (-4.8

eV) makes it susceptible to redox reactions with air. This results in doping, or production

of charge carriers. This is unacceptable for OTFs, where we want very low current except

when the device is switched on. It has also been proposed that high side chain

substitution frequency along the polymer backbone doesn't allow the side chains from

adjacent polymers to interdigitate (figure 2.2), which lowers the three-dimensional order.

The lack of interlayer registry gives rr-P3HT a two-dimensional smectic-like layer

arrangement.[139] To overcome these problems, non-alkylated conjugated spacers were

introduced into the polymer backbone between 3-alkyl thiophene units. This new design

became known as regiosymmetric polythiophene (rs-PT) depicted in figure 2.1. The
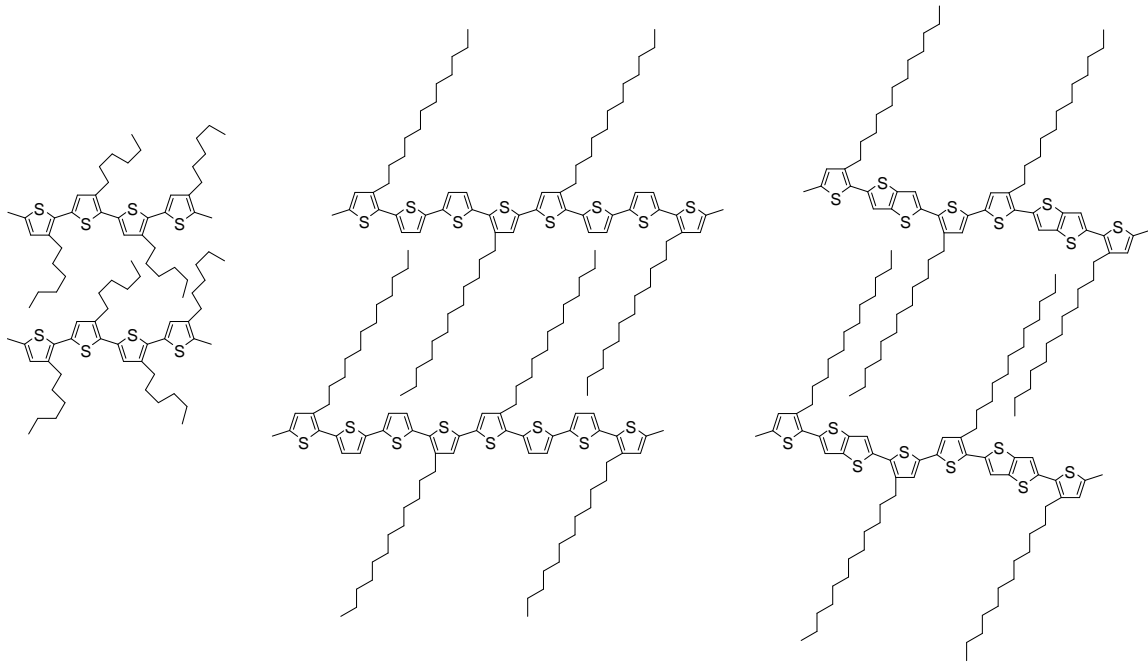
Figure 2.2: Illustration of side chain packing for (left) rr-P3HT, (middle) PQT, (right) PBTTT-C12.[139]

spacer units decrease side-chain substitution frequency along the polymer back bone, giving rise to long range three-dimensional order via interdigitation of side chains (figure 2.2). Using this idea a breakthrough arose in 2004 when Beng Ong in Xerox Research Centre of Canada reported a new polymer called poly(3,3'-dialkyl-quaterthiophene) abbreviated as PQT.[140] By introducing an unsubstituted bithiophene unit into the polymer backbone as spacer unit, they increase ionization potential (0.1 eV greater than for rr-P3HT) and enhanced solid state packing by interdigitation of side chains. The authors proposed that the polymer has long-range order overall, but rotationally disordered along the backbone due to the bithiophene linkage. So ionization potential is increased due to the rotational freedom along the backbone. The OFET devices fabricated from PQT showed mobilities of 0.14 cm^2/Vs and on/off ratio of over 10^7 under ambient condition.[140]

However, this publication and others following it do not report on the stability of devices after operating for extended periods of time in air. In 2006 Ian McCulloch from Merck Chemicals reported another series of polymers with a different conjugated "spacer".[22] The authors propose that the inserted thienothiophene units reduce the electron delocalization along the backbone and give rise to higher ionization potential. They have reported that the poly(2,5-bis(3-alkylthiophen-2-yl)thieno[3,2-b]thiophene)s (PBTTT) have an ionization potential 0.3 eV greater than rr P3HT.[141] The OTFT devices fabricated from PBTT showed mobilities of 0.6 cm^2/Vs and on/off ratio of over 10^7 under ambient condition. The initially good performance however very rapidly degrades in air. However, despite a lack of demonstrations of long-term OTFT operational stability in air, the fact that PQT and PBTTT OTFTs could give such impressive performance in air represented a major advance over P3HT and sparked a flurry of research activity from groups around the world. Various different rs-PTs have become the widely studied polymer semiconductors in the recent few years. Enhanced stability has been demonstrated for these rs-PTs but their device performance still degrades over time under ambient condition reducing their potential application in consumer electronics. So it is very important to develop new polymer semiconductors with long-term operational stability for large scale commercialization. The stability of the organic semiconductors largely depends on their frontier molecular orbital energy levels. As described in chapter 1, from recent studies it was clearly shown that D-A alternating conjugated polymers are the way to go for polymer-based ambient stable high performance organic semiconducting materials due to their favorable solid state interactions (inter or intra) and ability to carefully tune the FMO energy levels and optical energy gaps (Eg^{opt}).

1,2,4,5-Tetrafluorobenzene (TFB) units can serve as the non-alkylated spacer, also enhancing pi-stacking through intramolecular attractive interactions between TFB and thiophene units. [142] According to a publication from Nobert Koch, increased TFB loading (1%-15%) in polythiophenes give rise to higher ionization potentials.[143] Here they have introduced 1,4-dithienyl-2,3,5,6-tetrafluorobenzene (TFT) in several different loadings to poly(3-alkylthiophene) polymer and estimated ionization energy values by ultra-violet photoelectron spectroscopy (UPS).
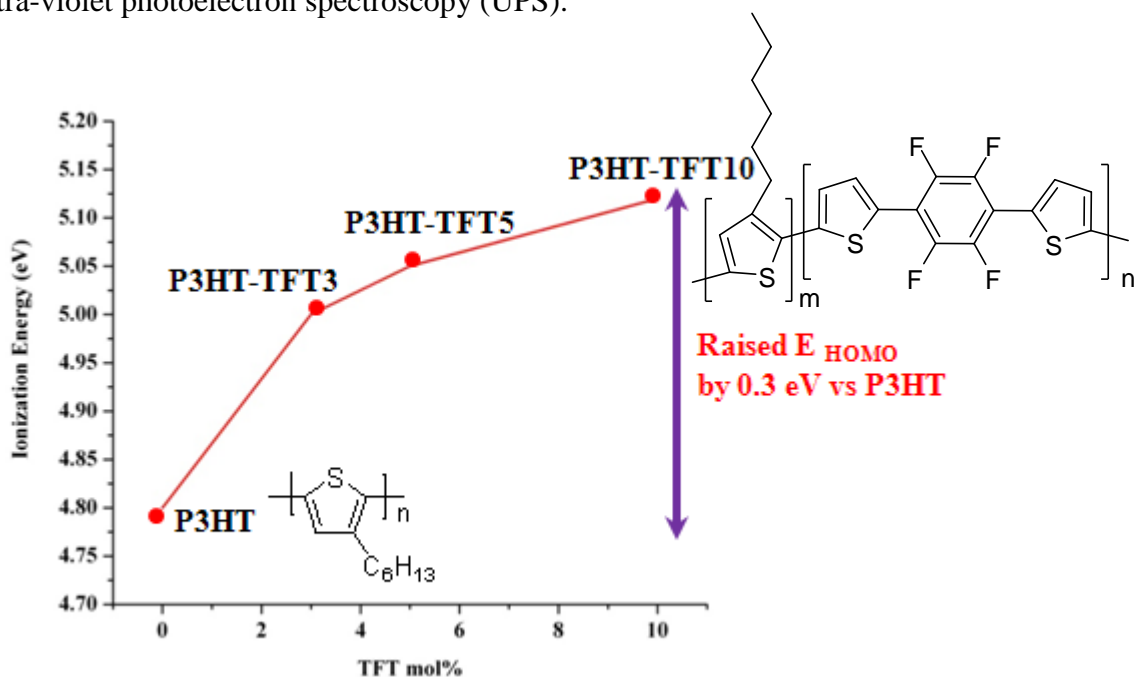
Figure 2.3: Poly(3-hexylthiophene) with different TFT loadings.[143]

The authors report a steady increase in ionization energy with increasing TFT loading, and that when TFT loading is 10% the ionization energy was increased by 0.3 eV relative to rrP3HT. But, since their synthetic method resulted in random spacing of the TFT units along the polymer backbone, when they increase TFT loading they also lower the solid state ordering of the polymer backbone, according to their uv-vis, DSC analysis and WAXD measurements. This could disrupt conjugation due to twisting of the backbone,

which could also increase ionization potential. So we cannot say that the enhanced ionization potential is directly related to the electronic properties of the TFB units.
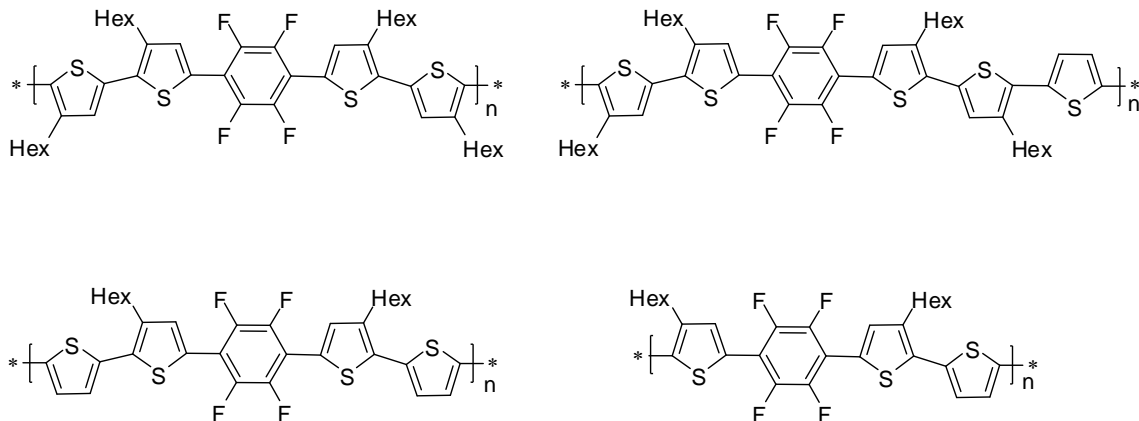
Figure 2.4: Published perfectly alternating TFB-oligothiophene co-polymers.[144]

Peter Skabara has synthesized several different rs-PT polymers with TFB as the non-alkylated spacer.[144] Unlike the polymers reported by Koch, these are not random co-polymers. These are perfectly alternating polymers as shown in figure 2.4. Also, the TFB loadings are much higher (17 – 25% of backbone rings) than those reported by Koch. In Koch's polymers, even a reported loading of 10% is really only 3.3%, because only one third of the rings in the TFT comonomer are TFB units. Skabara reported that incorporation of fluorinated units lower both LUMO and HOMO and also facilitated planarization of the backbone. But from his paper, it is very difficult to notice a general trend in how TFB loadings alter the HOMO or ionization potential.

A previous researcher from our group, Youngfeng Wang,[142] sought to employ the maximum TFB loading (33%) in rs-PTs without sacrificing solubility and backbone co-planarity.[142] Unlike most of the rs-PTs reported at that time, 3,3'-dialkyl bithiophene

(3,3'-R2T2) units with head-to-head (HH) linkages rather than tail-to-tail(TT) were employed. According to WAXD (wide angle X-ray diffraction) data and uv-vis study it was clearly obvious that the HH-linkage did not intrinsically preclude co-planarity in bithiophene repeating units, contrary to conventional wisdom.[142] Co-planarity is enhanced due to the intermolecular D-A interactions and intramolecular S-F interactions. At the same time, electrochemical measurements showed dramatic stabilization of the HOMO energy levels. According to the literature, there was already evidence showing HH linkages do not necessarily preclude the backbone conjugation. The study done by Barbarella et al, using two different thiophene oligomers with HH linkages clearly shown that the backbone co-planarity is a function of space-filling rather than the specific linkage. [145] Pomerantz[146] and Reynolds[147] also reported that co-planarity can exist in HH linkage containing sulphur -oxygen contacts.
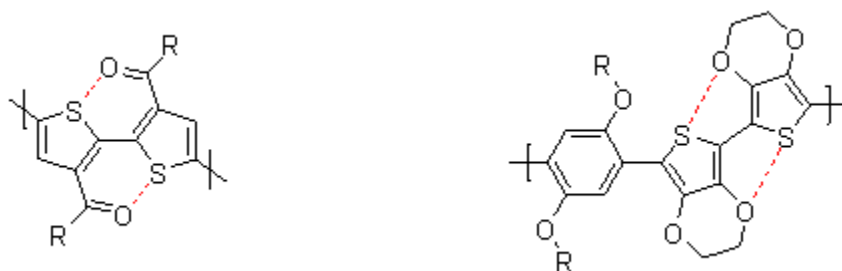
Figure 2.6: Polymers with HH linkage with sulphur-oxygen close contacts denoted by red dash lines.

From Wang's work and the work done by our other group members, and according to the literature it is clear that whether HH linkages preclude backbone co-planarity in a D-A co-polymer should highly depend on the acceptor space filling demand and favorable intramolecular interactions induce by the acceptor unit.[142,148,149] In Chapter 3, I will

further summarize some results from our group that point to this. (planarity in D-A polymers with 3,3'-R2T2 units depends on the acceptor)

Wang extended this work to include 3,3'-dialkoxy bithiophene (3,3'-RO2T2) units in place of 3,3'-R2T2 units. Not surprisingly, HOMO levels were greatly destabilized because of the enhanced electron-donating ability of the alkoxy side chains, and solubility was reduced due perhaps to greater planarization of the polymer backbone and enhanced intramolecular D-A intermolecular interactions.

So keeping these findings in mind, the project reported in this chapter focused on rs-PTs composed of TFB with both 3,3'-R2T2 and (primarily) 3,3'-RO2T2 units. The hypotheses to be tested include:

1. Further explore the idea that high loading of TFB in rs-PTs gives rise to higher ionization potentials and higher device stability.

2. Increasing alkyl side chain length in 3,3'-R2T2-based rs-PTs could improve upon their poor solubility and further enhance order and charge carrier mobility.

3. Incorporation of branched side chains in 3,3'-RO2T2 units could increase solubility without sacrificing long-range solid state order despite steric bulk in vicinity to the polymer backbone.

4. The position and size of branches in the side chains of 3,3'-RO2T2 units could not only tune solubility, but also FMO energy levels and optical properties.

2. 2 Synthesis of monomers and donor-acceptor polymers based on TFB unit
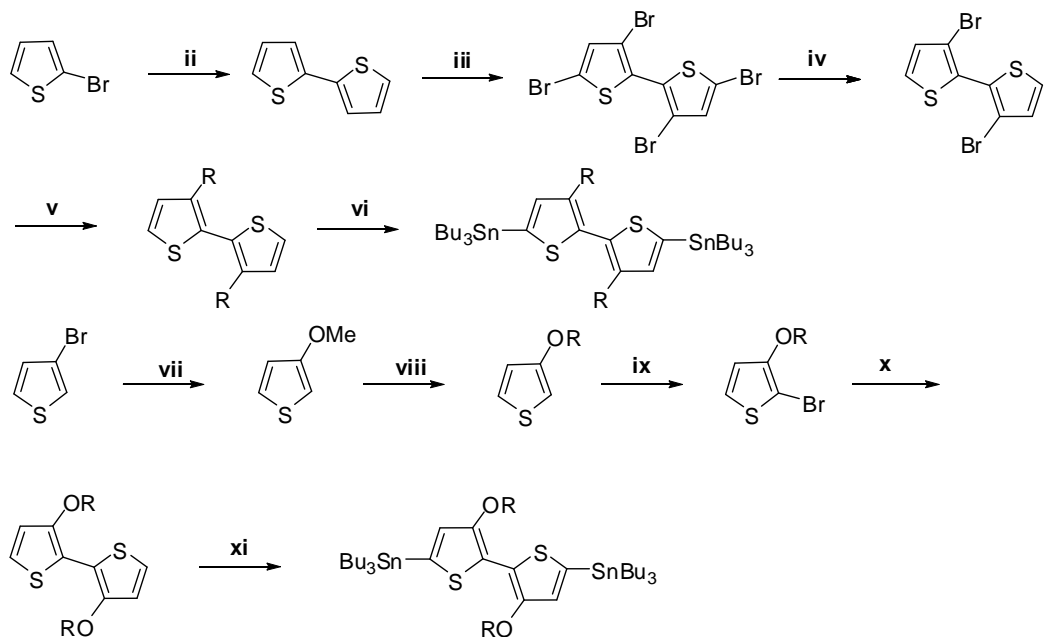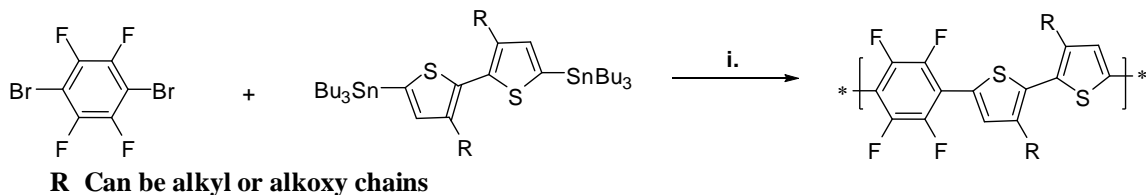
Alkyl Polymers
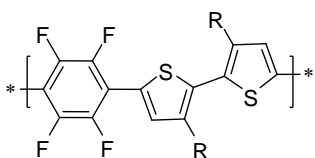
R: 2-P1 -C$_{12}$H$_{25}$

2-P2 -C$_{16}$H$_{33}$

2-P3 -C$_{18}$H$_{33}$

Alkoxy Polymers
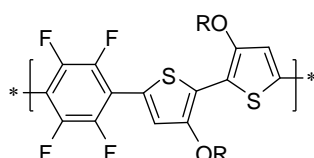
R: 2-P4 -O-C$_{16}$H$_{33}$

2-P5 -O-2-butyloctyl

2-P6 -O-1-methyltetradecyl

2-P7 -O-1-methylhexyl

2-P8 -O-1-ethylhexyl

2-P9 -O-1-propylhexyl

Figure 2.7: Synthesis scheme for polymers (top) and monomers (bottom). i. Pd$_2$(dba)$_3$, P (O-tolyl)$_3$, Anhydrous THF, 80 ^{0}C; ii. Mg, I$_2$, NiCl$_2$.dppp; iii. Br$_2$, HOAc, CHCl$_3$; iv. Zn,HOAc; v. RMgBr, NiCl$_2$.dppp; vi. a. n-BuLi, Anhydrous THF; b. Bu$_3$SnCl, -78 ^{0}C-rt; vii. NaOMe, CuBr, MeOH, DMF; viii. ROH, PTSA, Toluene; ix. NBS, DMF; x. Ni(COD)$_2$, COD, 2,2'-dipyridl, DMF, Toluene, 80 ^{0}C; xi. a. n-BuLi, THF; b. Bu$_3$SnCl, -78 ^{0}C-rt.

1,4-Dibromotetrafluorobenzene is commercially available and all the thiophene

monomers were synthesized using Kumada and Yamamato coupling. (for further details

Table 2.0: Properties of 3,3'-R2T2 vs 3,3'-RO2T2 TFB Polymers 2-P1- 2-P9

Polymer	yield (%)	M_n (KDa)[a] [PDI]	T_m[b] (°C)	λ_{max} (soln) (nm)	λ_{max} (film)[e] (nm)	$\Delta \lambda_{max}$ soln-film (nm)	λ_{onset}(film)[e] (nm)
2-P1	77	25 [1.82]	163.28	387[c]	490	103	562
2-P2	79	15 [1.57]	154.45	387[c]	490	103	566
2-P3	67	11 [1.47]	138.87	384[c]	490	106	566
2-P4	78	N/A[f]	366.18	490[d]	580/613	90/123	695
2-P5	74	13 [1.82]	353.32	510[d]	565/608	55/98	660
2-P6	68	10 [1.97]	339.64	510[d]	560/605	50/95	645
2-P7	70	N/A[f]	351.25	510[d]	545/595	35/85	645
2-P8	76	N/A[f]	346.34	510[d]	560/605	50/95	645
2-P9	79	N/A[f]	330.79	510[d]	560/603	50/93	645

[a] GPC vs polystyrene standards. [b] peak melting point from differential scanning calorimetry (10 °C/min). [c] 1×10^{-5} M in chlorobenzene. [d] 1×10^{-7} M in chloroform (values obtained from excitation profiles). [e] Pristine film spun-cast from 1 mg/ml chlorobenzene solution.[f] Polymer has poor solubility in THF at ambient temperature so could not obtain the molecular weight via GPC measurement

please refer to the experimental section). Two categories of bithiophene based donors

(alkyl and alkoxy) with different alkyl side chains were prepared to study the E_g^{opt} tuning,

FMO energy level manipulation , solubility improvement and self assembly control of

the resulted polymers. The synthetic schemes are summarized in figure 2.7. Purity of all

the monomers and polymers were checked by using ^{1}H NMR, ^{13}C NMR and ^{19}F NMR

and all these give satisfactory spectra. The structures of polymers and characterization

(yields, molecular weights, optical data and melting point temperatures are listed in table 2.0. Most of the yields are good to moderate. The relative molecular weights are moderately high for most of the polymers as determined by GPC (Gel Permeation Chromatography) using polystyrene standards.

2.3 Effect of 3,3'-R2T2 vs 3,3'-RO2T2 donor monomers on polymer optical, electronic and self assembly
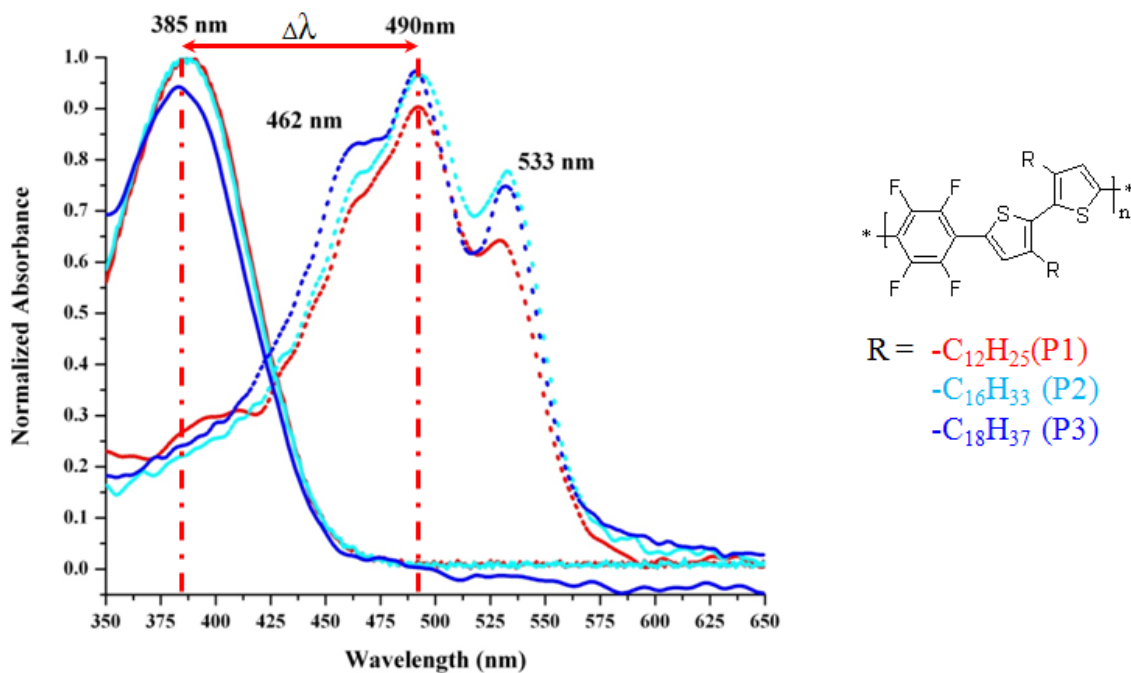
Figure 2.8: Normalized uv-vis spectra of TFB-based 3,3'-R2T2 polymers. Solution (Solid lines; 5 x 10^{-6} M in Chlorobenzene); as-cast films (dotted lines; spin coating (1mg/ml, Chlorobenzene) onto quartz plates) All measurements were done at room temperature.

In this section we are going to discuss the optical, electronic and solid state packing arrangement of the 3,3'-R2T2 and 3,3'-RO2T2 TFB based D-A co-polymers. More priority go to 3,3'-RO2T2 TFB based D-A co-polymers because we did a more detail study on them by changing the branching position and branching length of the alkoxy substituent closer to the polymer backbone and investigate optical, electronic and self assembly properties. All the 3,3'-R2T2-TFB co-polymers (**2-P1,2-P2** and **2-P3**) were

43

maroonish color in the solid state and yellow color in solution, and emit green fluorescence in solution under uv-irradiation. When going from solution to solid state all these three polymers showed significant red shift ($\Delta\lambda \sim 105$ nm) indicating extended conjugation and high co-planarity of the polymer back bone. The driving force for this observation may be intramolecular interactions between S-F[150] and intermolecular donor-acceptor interactions. Also from this observation it was clearly shown that HH-linkages do not preclude co-planarity of the polymer backbone and overall conjugation, as explained earlier. But when consider the solution measurements, all the three polymers show relatively narrow featureless absorption profiles due to lack of driving force for backbone co-planarity. The development of fine structure in solid state clearly indicates the rigidness of the resulted polymer backbone. This is due to the narrowing of the assessable population of states (vibrational and rotational energy levels). The basic nature of solution and solid state uv-vis profiles are similar in all the three polymers with same onset of absorption. This is obvious because all the three polymers share common polymer backbone and similar substituents. The only structural difference between the polymers is the length of the attached alkyl chains on bithiophene donor. Three distinct features are clearly visible in solid state measurements, shoulders at, (462 nm and 533 nm surrounding maxima near 496 nm) The low and high energy shoulders become more distinguished when going from shorter to longer linear alkyl chains ($-C_{12}H_{25}$ to $-C_{18}H_{37}$) indicating longer the alkyl chain the polymer backbone become highly ordered and rigid. According to the WAXD images depicted in figure 2.9 and the related data were in table 2.1, the polymer **2-P2** which has $-C_{16}H_{33}$ alkyl chains show very distinct diffraction

patterns on meridional direction compare to the polymer **2-P1** which has $-C_{12}H_{25}$ linear alkyl chains.
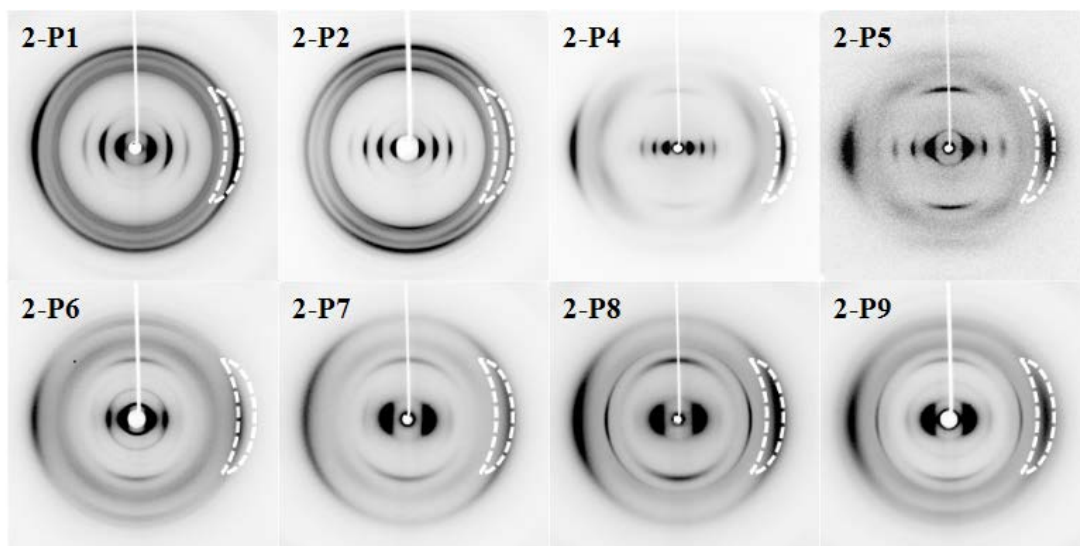
Figure 2.9: Fiber WAXD diffractograms for   3,3'-R2T2 and 3,3'-RO2T2 TFB co-polymers **2-P1**- **2-P9**.

This clearly indicate the longer alkyl chains resulted more ordered,crystalline, solid state arrangement compared to the relatively shorter chains. Unfortunately we did not have the WAXD diffractogram for polymer **2-P3**. Compare to **2-P1**, For   polymer **2-P2**, the diffraction patterns along the equatorial direction also show relatively narrow arcs and more distinct diffraction patterns indicating highly oriented repeating pattern of polymer backbones. The reason for these observations (well developed fine structure in uv and well distinguished diffraction patterns in WAXD) may be due to the higher interdigitation tendency of the longer linear alkyl chains, which may give rise to good inter-lock with adjacent polymer backbone's alkyl side chains. But from this measurements alone cannot determine if we have interdigitated alkyl chains or not.

When we compare the uv-vis profiles of these 3,3'-R2T2 polymers with 3,3'-RO2T2 polymer **2-P4** the resulted absorption profile is rather different and the polymer **2-P4** shows significant red shift both in solution and solid state measurements. Absorption profiles of D-A polymers highly rely on two factors; 1) electron donating

Table 2.1: Data collected from diffraction patterns in figures 2.9

Polymer	Lamellar spacing, L, L/2, L/3 (Å)	"d" π-spacing (Å)	Meridional Maxima (Å)
2-P1	21.12, 10.05, 6.72	3.68	N/A
2-P2	23.81, 12.18, 8.27, 6.22	3.69	N/A
2-P4	26.5, 14.5, 9.7	3.60	6.10
2-P5	19.0, 9.7, 6.6, 5.0	3.8	6.2, 3.8
2-P6	24.97, 12.1, 7.96	3.69	6.15
2-P7	16.04, 8.27	3.7	6.13
2-P8	16.36, 8.51, 5.06	3.74	6.17
2-P9	16.91, 8.72, 5.06	3.82	6.03

ability of the donor unit and electron withdrawing ability of the acceptor unit, 2) backbone conformation and arrangement. So one reason to the above observation is increasing electron donating ability of alkoxy chains compare to alkyl substituent. The alkoxy chains destabilize the HOMO energy level and lower the Eg ^{opt} (table 2.2). Also the small size of the oxygen atom, relative to the "CH$_2$" group in alkyl chain caused less

steric interactions, and/or the S-O intramolecular attractive interactions[146,147] promote backbone co-planarity. For this 2-P4 polymer both solution and solid state measurements have similar absorption profile. This may be due to the strong inter and intramolecular interactions both in solution and solid state or the polymer is highly disordered in solid state and there is no achievement of structural rigidity and order going from solution to the solid state. But according to the WAXD diffractogram (figure 2.9) this polymer seem to be highly ordered clearly indicating equatorial and meridional maxima relative to the previously mentioned 3,3'-R2T2 polymers with relatively shorter π stacking distance, most probably due to the higher D-A intermolecular interactions compared to the 3,3'-R2T2 polymers in the presence of strongly electron donating alkoxy substituents. This polymer has very poor solubility in common organic solvents like THF, toluene, chloroform etc and only moderate solubility in hot chlorinated solvents. Again this poor solubility may be due to the strong D-A intermolecular interactions which lower the penetrating ability of the solvent molecules. Also this polymer has less deeper E_{HOMO} value according to the DPV measurements indicating it will not lead to OTFTs with good ambient stability. As explained in chapter 1, ambient stability is very important for device applications. If we compare the E_{HOMO} values of our 3,3'-R2T2 polymers with this 3,3'-RO2T2 polymer, it clearly indicates that the 3,3'-R2T2 polymers give relatively deeper HOMO energy values in the range of ~ -5.90 eV. But this 3,3'-RO2T2 polymer has the E_{HOMO} -4.93 eV. As stated earlier the reason for this observation may be strong inter and intramolecular interations in the polymer **2-P4** compare to the 3,3'-R2T2 polymers, giving it highly co-planar backbone and enhancing the effective conjugation. Also

compare to alkyl linkages, alkoxy linkages are more electron donating which destabilize

the HOMO energy value and narrow Eg^{opt} of 1.78 eV compare to the Eg^{opt} values of 3,3'-

Table 2.2: Electrochemical and optical data for polymers

Polymer	$E_{ox}(V)$ [a]	$E_{HOMO}(eV)$ [b]	$E_{LUMO}(eV)$ [c]	$E_g^{opt}(eV)$ [d]
2-P1	1.07∓0.006	-5.87∓0.006	-3.66∓0.006	2.21
2-P2	1.15∓0.007	-5.95∓0.007	-3.76∓0.007	2.19
2-P4	0.13∓0.003	-4.93∓0.003	-3.15∓0.003	1.78
2-P5	0.5∓0.003	-5.3∓0.003	-3.42∓0.003	1.88
2-P6	0.14∓0.023	-4.94∓0.023	-3.02∓0.023	1.92
2-P7	0.25∓0.001	-5.05∓0.001	-3.13∓0.001	1.92
2-P8	0.28∓0.008	-5.08∓0.008	-3.16∓0.008	1.92
2-P9	0.30∓0.03	-5.1∓0.03	-3.18∓0.03	1.92

Experimental conditions: 0.1 M (n-Bu)$_4$N·PF$_6$ in anhydrous acetonitrile as supporting electrolyte, platinum disc as working electrode, platinum wire as counter electrode, silver wire as reference electrode and Fe/Fe$^+$ (-4.8 eV vs vacuum) as reference, scanning rate: 50 mV/s; All measurements conducted on solution-cast thin films under nitrogen. [a]Corrected E$_{ox}$ value respect to Fc/Fc$^+$. [b]E_{HOMO} = -[4.8+(E$_{ox}$-Fc/Fc$^+$)], E$_{ox}$ calculated using onset of DPV measurements (Oxidation peak). [c] E_{LUMO} = E_g^{opt} + E_{HOMO}. [d] E_g^{opt} Optical band gap estimated from the absorption edge of the film.

R2T2 polymers (table 2.2).The next question to arise is, how to stabilize the E$_{HOMO}$ level

of these 3,3'-RO2T2 polymer. So we decided to introduce a bulky branch chain closer to

the polymer backbone and investigate how this affects the overall optical-electronic and

solid state registry of the 3,3'-RO2T2 polymers. Compared to the linear alkoxy polymer 2-P4, this polymer show slight blue shifted absorption profile, both in solution and solid state measurements. The resulted polymer 2-P5 has Eg ^{opt} of 1.88 eV compared to its linear analogue 2-P4 which has Eg ^{opt} of 1.78 eV. This may be due to the backbone twisting caused by more bulky branched alkoxy chains. In other words, the dihedral angle (β in figure 2.11) between adjacent thiophene rings may increase and lower the orbital overlap. This decreased orbital overlap widens the HOMO-LUMO gap. This is the common argument in modern literature to explain similar observations, but we have another argument for this. There can be a rotation around the sigma bond between the thiophene sp^2-C and alkoxy "O". Here we become specifically interested in the dihedral angle, α , between alkyl side chain and thiophene plane. Depending on this dihedral angle, oxygen can work more as an electron donor via resonance or electron withdrawer via inductive effect and govern the electronic properties of the resulted polymer. Basically we are talking about Hammond parameters. Using the below cartoon (figure 2.11) this idea can be easily rationalized. For simplicity here we used 3-methoxy thiophene. When α is 90^0 the oxygen lone pairs are mostly out of conjugation with the thiophene π-system. So now inductive effect dominates over resonance, and oxygen behaves more as an electron withdrawer rather than donor. So this will stabilize the HOMO level. It is possible that steric repulsion between the bulkier side chains and the backbone favors this conformation. Calculations are underway in the group of Johannes Gierschner to support this idea. One of the past group member in our group, Tanmoy Dutta, in his recent publication has clearly shown that this argument is acceptable to explain differences in alkoxy-substituted poly(phenylene ethynylene)s. [151] But we cannot
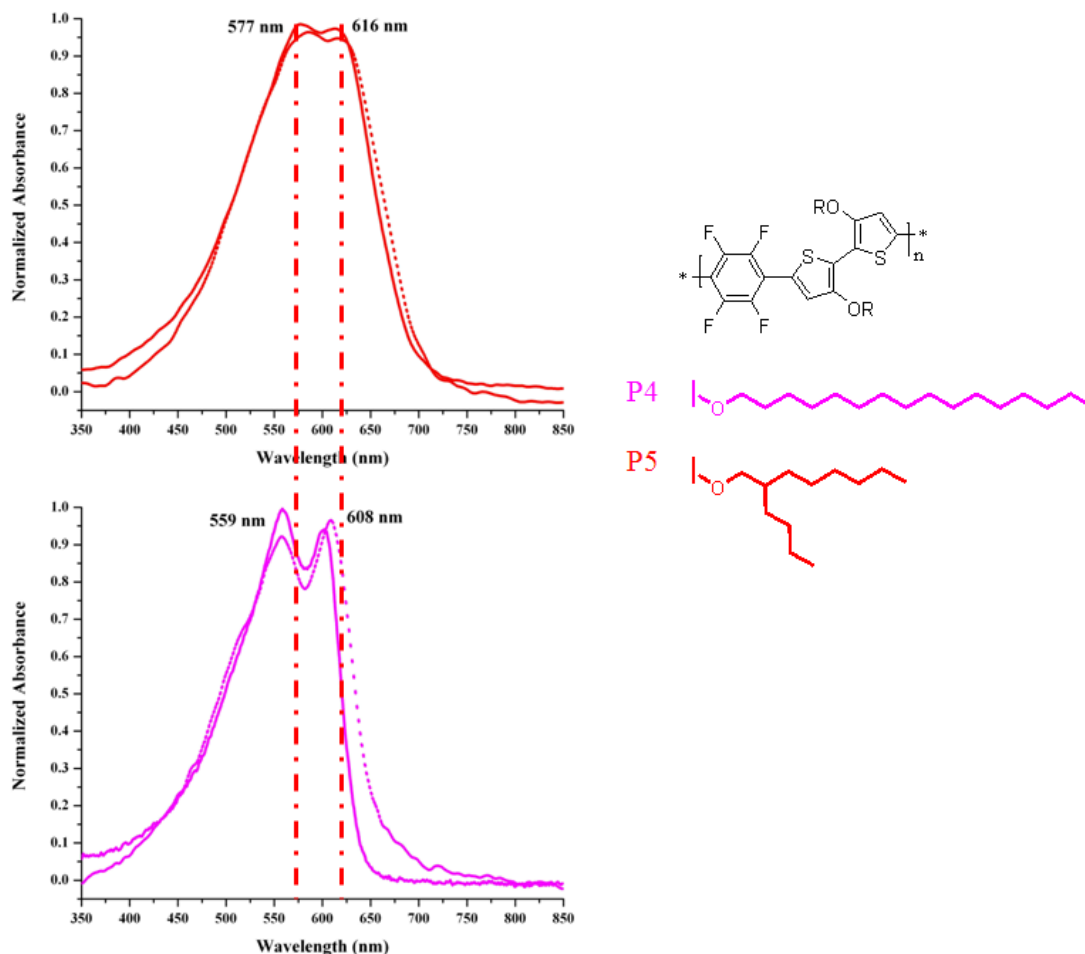
Figure 2.10: Normalized UV-vis spectra of 3,3'-RO2T2 TFB polymers 2-P4 and 2-P5. Solution (Solid lines; 1 x 10^{-5} M in chlorobenzene); as-cast films (dotted lines; spin coating (1mg/ml, chlorobenzene) onto quartz plates) All measurements were done at room temperature.

directly import that idea to our case due to structural and electronic differences. This 3,3'-RO2T2-TFB, butyl octyl branch polymer **2-P5** shows dramatically increased solubility in common organic solvents compare to the polymer **2-P4**. Polymer **2-P5** has reasonable solubility even in hexane at elevated temperatures (50 ^{0}C). The better solubility may be due to the highly disordered packing arrangement of this polymer due to the presence of
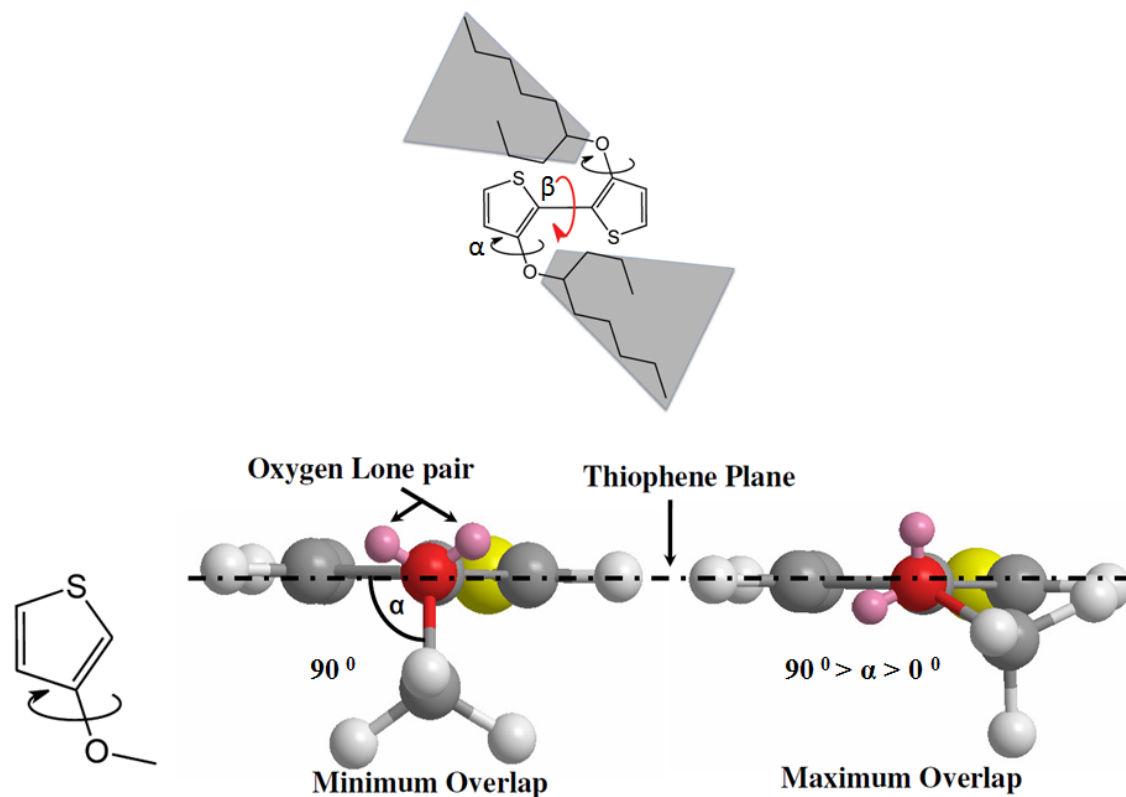
Figure 2.11: Dihedral angles between (top) 3,3'-bithiophene. (bottom) thiophene plane and oxygen lone pair in 3-methoxy thiophene

bulky branch chain. But when we investigate the WAXD diffractogram of this polymer **2-P5**, it seem to be this polymer is highly ordered compare to the linear alkoxy polymer **2-P4** clearly indicating off meridional diffraction patterns indicating 3-D solid state registry with relatively narrow sharp diffraction arcs compare to the polymer **2-P4**. The polymer **2-P4** has relatively closer π stacking distance compare to the polymer **2-P5** (table 2.1). If we carefully observe the solid state uv-vis profiles of polymer **2-P4** and **2-P5**, it is clearly obvious that polymer **2-P5** has well developed fine structure compare to the linear 3,3'-RO2T2-TFB polymer **2-P4** .This suggests more ordered rigid polymer backbone in polymer 2-P5 compare to the linear alkoxy polymer 2-P4, which is identical to what we observe in our WAXD diffractograms. The reason for difference in WAXD

may be that the crystallizable linear alkoxy side chains and polymer backbone compete with each other to obtain ordered packing arrangements, which may not be commensurate. Which will win depends on the relative strength of the intermolecular and intramolecular interactions of alkyl chains or polymer backbone. But with branched side chains, the more liquid like side chains should not compete with polymer backbone to obtain an ordered packing arrangement. The branched side chains may only work as space-filling spectators, leaving the ordered packing arrangement to be mainly governed by the polymer backbone via inter- or intra- molecular interactions. From these observations it is obvious that we can fine tune our E_{HOMO} values without much sacrificing the co-planarity of the polymer backbone and obtain higher solid state order by simply going from linear to branch alkoxy chains. For both of these 3,3'-RO2T2-TFB polymers, one common thing is obvious, that is, in these two polymers, the solution and solid state uv-vis absorption profiles are nearly the same suggesting similar molecular arrangements in both states. This kind of observation can be made if the polymers are highly disordered in the solid state so that there is little change in going from solution to the solid state. But from WAXD study we have clearly shown that both polymers **2-P4** and **2-P5** have highly ordered solid state registry with relatively close π stacking distances. So we cannot use this argument to explain the observed behavior. To explain this behavior we have done some computational and experimental study on this matter and detail explanation about this behavior will be explained in the end of this section.

As mentioned in chapter 1 from extended research and structure property studies, it is apparent that the choice of alkyl chains not only governs the solubility properties, but can use as a tool to control polymer crystallinity and morphological order in thin films.

[31,93,94] Up to now all the best OPV materials have branch alkyl chains. The top most materials have not only branch chains, they also have two chains attached to single atoms in condensed ring systems, which we can refer to as branching at zero position.[15,119] By influence of these observations and literature records, we decided to study the branching effect more in our particular polymer system. So we decided to change the branching position and branching length systematically and study how it affects the optical , electronic and solid state properties of our polymer system. From previous studies we have some idea about the behavior and properties of the TFB unit. This prior knowledge of acceptor was really helpful to get an idea, how this different substituents effect to the donor unit and finally to the whole polymer. So we further prepare 4 more 3,3'-RO2T2 polymers introducing branch side chains closer to the polymer backbone in sterically more congested 3,3' position in bithiophene unit. Now onwards, this branching position will be described as α position. Here we systematically varied the branching length at α position, from –methyl to propyl (polymers **2-P7**,**2-P8** and **2-P9**). These polymers show relatively better solubility compare to the polymer **2-P4** in common chlorinated solvents like chloroform, chlorobenzene and 1,2-dichlorobenzene, but they did not have better solubility in THF at ambient temperatures so could not obtain the molecular weights due to poor solubility. The above stated polymer **2-P5** has branching in the β position of the alkyl chain so we can state it as a β branch polymer. UV-Vis absorbance profiles of all the six dialkoxy bithiophene polymers are depicted in figure 2.12 for clear comparison. Again for all these six polymers we can observe both solution and solid state measurements have similar absorption profiles. More detailed study on this matter will be explained at the end of this section. According to our knowledge there is only one

publication which uses α-branched 3,3'-RO2T2 units, however preparing homopolymers.[152] Thus, this is the first report on donor-acceptor co-polymers based on α-branched 3,3'-RO2T2 units.
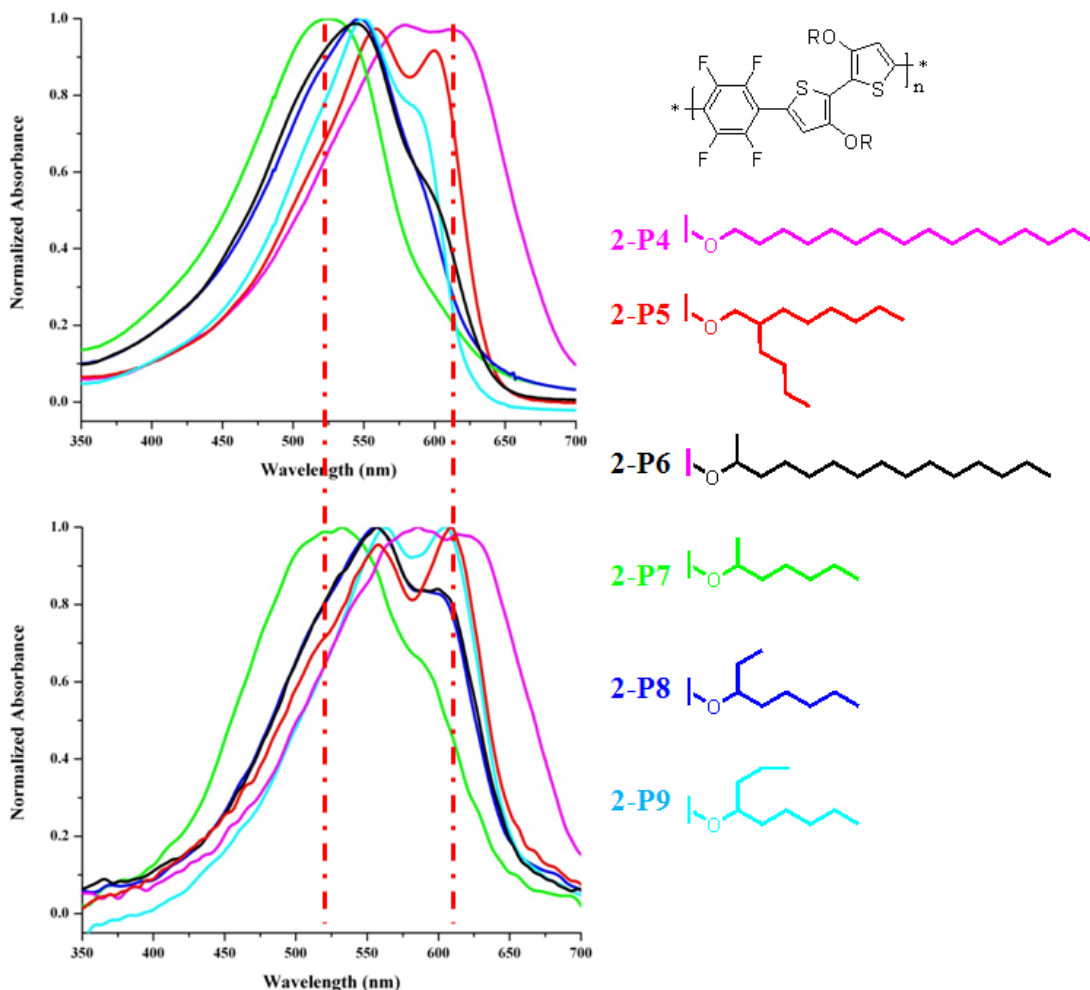
Figure 2.12: Normalized UV-vis spectra of 3,3'-RO2T2 TFB polymers 2-P4 to 2-P9. top: Solution (Solid lines; 1 x 10^{-6} M in Chloroform); bottom: as-cast films; spin coating (1mg/ml, Chlorobenzene) onto quartz plates) All measurements were done at room temperature.

If we think about the solid state uv-vis profiles of these α, β and linear 3,3'-RO2T2-TFB polymers, it seem to be the linear alkoxy polymer has the most red shifted absorption

profile and the α methyl polymer **2-P7** has the most blue shifted absorption profile. If we argue that steric bulk increase the twisting of the polymer backbone, then this α methyl polymer **2-P7** should have the most red shifted absorption profile in this α and β branch polymer series. But what we experimentally observed is when we increase the branching length the resulted absorption profiles become more red shifted with well development of fine structure, clearly indicating polymer backbones become more co-planar and highly rigid when increasing the branching length. From this observation we can clearly state that if we can provide enough space filling demand, still we can obtain relatively co-planar rigid polymer backbones in the presence of bulky branch chains. All these polymers show relatively long range order according to the WAXD diffractograms. Again, if we come to the solid state measurement, the blue shifted α methyl polymer **2-P7** does not show any well developed fine structure in its uv-vis profile but can see a shoulder development in low energy region. Both α branch polymers **2-P6** and **2-P8** have similar solid state absorption profiles. These two polymers indicate clear development of fine structure compare to the α methyl polymer **2-P7** but less distinct compare to the α-propyl branch polymer **2-P9** and β branch polymer **2-P5**. Compare to polymer **2-P9** the more bulky β branch polymer **2-P5** shows significant fine structure development compare to the all of these 3,3'-RO2T2-TFB polymers. These solid state uv-vis observations clearly correlate with the WAXD diffractograms of the polymers. In this 3,3'-RO2T2 polymer series the polymerswhich has β branch, **2-P5**, shows the most ordered solid state registry, clearly indicating off-meridional diffraction, as stated earlier indicating 3-D solid state order. According to the solid state uv-vis measurement this particular polymer showed well developed fine structure indicating polymer backbone is highly ordered and

rigid. If we compare WAXD diffractograms of the hexyl substituted α branch polymers (**2-P7,2-P8** and **2-P9**) the gradual change of the solid state registry become more prominent indicating increasing the branch increase the solid state packing order. It is clear that when going from **2-P7** to **2-P9** the diffraction pattern correspond to the π stacking and lamella spacing become narrower (not widely spaced) and well distinct clearly indicating highly oriented polymer backbone and alkyl substituent's. The polymer **2-P9** show well resolved diffraction patterns for lamellar spacing compare to the other two polymers **2-P7** and **2-P8**. The α methyl branch polymer **2-P7** show relatively less solid state order compare to all the other branch substituted polymers clearly proofing the observed solid state uv-vis profiles. For all these hexyl substituted α branch polymers (**2-P7,2-P8** and **2-P9**) the middle diffraction patterns are much broader compare to all the other polymers which we study in this chapter. This may be due to the less oriented alkyl substituent's closer to the polymer backbone. For all these 3 polymers (**2-P7**-**2-P9**) share the common substituent main chain length of six carbons. The polymer **2-P6** also has the α methyl substituent but the main alkyl chain is much longer compare to the **2-P7,2-P8** and **2-P9** polymers. This   α methyl polymer **2-P6** also showed very good solubility in common organic solvents like chloroform, THF, chlorobenzene etc. In this polymer we can clearly observe relatively more meridional diffraction maxima compared to the other α branch polymers 2-P7 to 2-P9 clearly indicating alkyl chains are relatively crystalline. The reason for this observation may be good interlock with adjacent polymer side chains as stated in the 3,3'-R2T2 polymers. Basically we can conclude all these 3,3'-RO2T2-TFB polymers have relatively close π-π stacking distances and solid state registry.

For all these polymers with hexyl side chains carrying an α branch (**2-P7**,**2-P8** and **2-P9**) the E_{HOMO} values are in ~ -5.1 eV range indicating again we were able to push the E_{HOMO} levels to relatively deeper values compare to the linear alkoxy polymer **2-P4**. Basically we can see monotonic increase of HOMO energy values by increasing of the side chain bulk (table 2.2). The reason for this behavior may be due to the different conformational arrangement of the polymer backbone. Uv-vis and WAXD data clearly indicate this bulky branch polymers are relatively more ordered so cannot say this monotonic increment of the HOMO energy values is due to the twisting of the polymer backbone due to the lower conjugation.

As stated earlier for all these 3,3'-RO2T2-TFB polymers the solution and solid state absorption profiles are similar. In solution measurements, the spectra showed significant spectral shifts for the different alkoxy substituents, although all constitutional factors which determine the spectral position, [33] i.e. nature and length of the conjugated backbone, substitution position as well as the substitution motif (alkoxy) are the same in all the cases. The polymer with the long linear side chains (**2-P4**) shows a strongly bathochromic (red) shifted, vibronically structured solution absorption spectrum with a maximum at around 580 nm, while the α-methyl- hexyl substituted polymer **2-P7** peaks at 520 nm, however unstructured and with a pronounced feature at the red edge; the solution uv-vis spectra of the other polymers are found in between these two extremes. The reason for this similarity in solution and solid state uv-vis absorption profiles may be due to the intramolecular effects such as different chain conformations, or intermolecular effects, such as (partial) aggregation, either through self-folding of the polymer chain or aggregation with other chains. In order to disentangle intra- and intermolecular effects we

first took a look at the chain conformation by means of DFT (density functional theory) quantum-chemical calculations which done by our collaborator Dr. Johannes Gierschner. Here they employ the BHandHLYP functional (6-311+G* basis set;Please ref SI) which was shown to reproduce well the intramolecular torsional potentials,[153-155]starting from a non-planar starting geometry of an ethyloxy-substituted monomer unit. According to the calculations the torsional angle θ_1 between the thiophene rings is essentially zero, thus favoring a co-planar anti-conformation (figure 2.13), and independent on length and branching of the alkoxy substituents. The co-planar conformation arises from S-O intramolecular interactions as reported earlier on similar substituted oligothiophenes.[155] The torsional angle θ_2 between the thiophene and the fluorinated benzene ring is 20º, so that in all, the conjugation is hardly disrupted along the polymer backbone. Finally, the torsion θ_3 between the alkoxy group and the thiophene ring shows some local minima, but the global minimum is at 0º (figure 2.13), and no impact of the chain conformation on the inter-thiophene bond torsion θ_1 is observed. If this computational study is true then our solution uv-vis profiles should be independent to the alkoxy substituent attached. But our experimental solution base uv-vis profiles instead vary with different alkoxy substituents. From the computational study we have to conclude that the observed difference in the solution spectra cannot be ascribed to an intramolecular effect. Therefore, following the hypothesis of chain aggregation at concentrations of 1×10^{-5} M we diluted further the solutions down to the concentrations of 1×10^{-7} M. At this concentrations however, absorption spectra cannot be measured due to limited sensitivity of the method. So we recorded photoluminescence excitation (PLE) spectra, where the
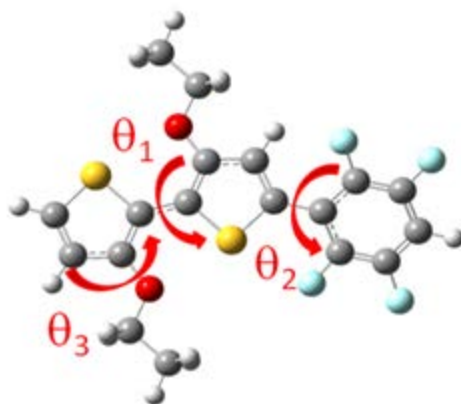
Figure 2.13: DFT-optimized ethyloxy-substituted monomer unit; relevant dihedral angles are indicated.

excitation wavelength is changed while the observed emission wavelength is kept constant. Although both, 'free' polymers and aggregates can principally contribute to the observed emission, the free chains are usually highly fluorescent while aggregates are not, thus allowing for photo selection of the non-aggregated species. Moreover, for all polymers the emission and excitation spectra turned out to be independent on the excitation and detection wavelength, respectively, indicating that the profiles are intrinsic to the same emitting species. The PLE spectra of the diluted solutions (1×10^{-7} M), depicted in figure: 2.14 are strikingly different from the absorption spectra of the 1×10^{-5} M solutions, showing a significant blue shift, suggesting that they arise from single chains (or less aggregated species). Moreover, the PLE spectra of the different polymers closely resemble each other as suggested by our computational study, thus indeed showing a very minor impact of α/β substitution on the single polymer molecules. A remarkable exception is polymer **2-P4**, being blue shifted both in PL (photoluminescence) and PLE. In fact, **2-P4** is the only unbranched polymer in the series, bearing a very long linear $-O-C_{16}H_{33}$ chain. The reason for this observation may be that the polymer length is less than the effective conjugation, due to premature precipitation
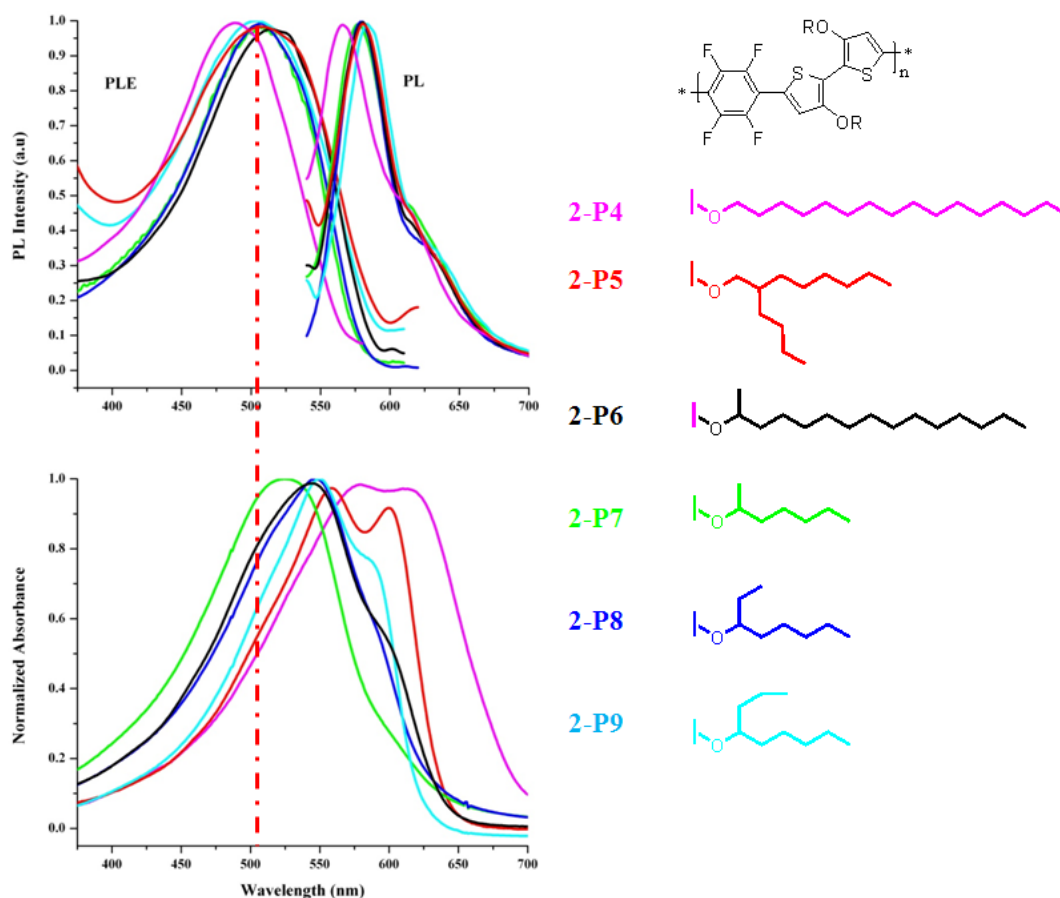
Figure 2.14: Normalized fluorescence (PL) and excitation spectra (PLE) of TFB polymers in Chloroform solution (1×10^{-7}M) at room temperature(top). Normalized absorption spectra of polymers in Chloroform solution (1×10^{-5} M) at room temperature (bottom).

during polymerization (The polymer has very poor solubility in THF, the polymerization media) or the resulted excitation and emission profiles only correspond to the low molecular weight oligomers which have better solubility and not represent the complete polymer sample (excitation and emission profiles are very sensitive to highly soluble fractions). The PLE spectra of all the polymers show structureless profiles, due to the torsional flexibility of the chain in the electronic ground state, which allows for efficient thermal population of low-frequency torsional modes.[155-158] Differently, the PL spectra

show some structured vibronic feature in long wavelength region due to the aggregated species which has lower quantum yield.[157,158] This dilution study suggests that our initial "solution" UV-Vis absorption measurements of the 3,3'-RO2T2 TFB polymers correspond to "pseudo-solutions" or highly aggregated species. In presence of strong D-A intermolecular interactions, due to the presence of strong electron donating alkoxy substituents may be the reason for this highly aggregated behavior in the solution state.

It's worth noting that aggregate formation in solution will determine not only to some extent the intermolecular arrangement in the film, but also the morphology, i.e. grain sizes and shapes, and thus sensitively influence the device characteristics, as investigated by several groups.[159-162] Aggregation of all polymers is correlated to substantial red shifts together with well visible fine structure (vibronic structure) development in the absorption spectra. The increase in vibronic structure can be attributed to a planarization of the molecular backbone. As explained earlier we can clearly observe the periodic development of fine structure when going from less branch to more branch versions from the long wavelength shoulder in solid state measurements clearly correlating with the WAXD diffractograms. So basically we are observing more ordered solid state arrangements in presence of bulky branch chains compare to less bulky versions.

2.4 Thermal analysis of polymers

Polymer melting points and thermal transitions were measured using endothermic maxima of 1 st order transitions detected by DSC (Mettler 822e , heating rate = 10 ^{0}C/ min, nitrogen purge). As stated earlier when we consider the TFB polymers it is clearly visible that all the TFB polymers with linear alkyl side chains undergo a small

endothermic transition in the 40-50 °C range, independent to the side chain length. This may be due to the thermal rearrangement of alkyl substituent in polymer backbone. More distinct, endotherms are seen above 100 °C, which we are assigning as the melting that increasing the length of the linear side chains lowers the melting point (figure 2.16). Due
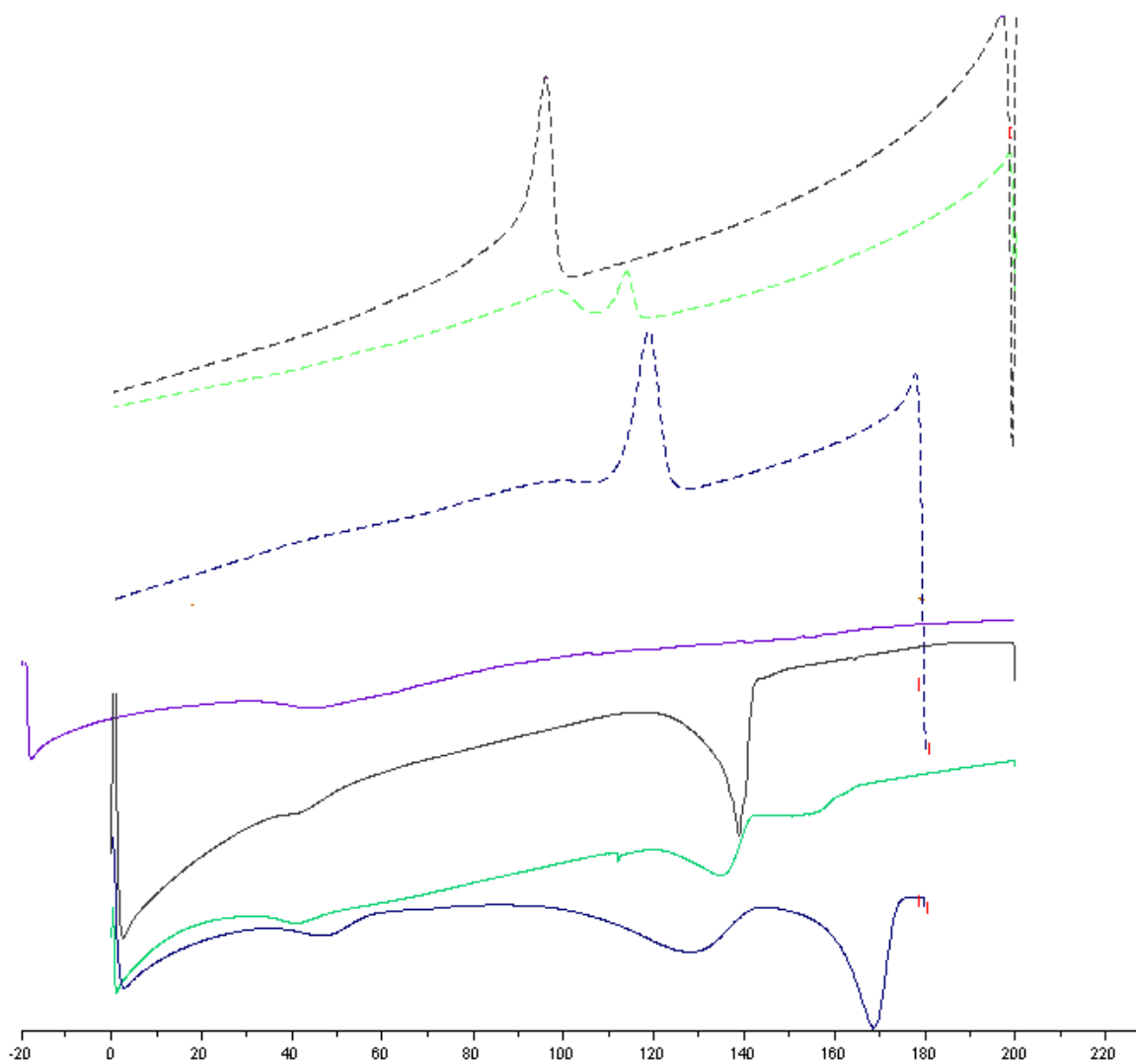
Figure 2.15: DSC thermograms of 3,3'-R2T2 TFB polymers. (First heating and cooling scans (10 ^{0}C/min) under N_2: blue-P1; green-P2 and black-P3; Solid lines represent the heating scans and dash line represent the cooling scans).

to the side chain melting, longer alkyl chains have more freedom or more entropy compare to the short side chains. Due to this, longer alkyl side-chains try to take apart polymer backbones and lower the melting point. Another possibility for this trend is that melted side chains work as a solvent and facilitate the backbone dissolving and lower the melting point. In literature also we can find some examples clearly indicating, increasing the length of the alkyl substituent lower the melting point.[141] All these linear alkyl TFB polymers show reversible thermal transitions. Compare to alkyl versions all the alkoxy polymers show higher melting temperatures well above 300 ^{0}C clearly indicating highly
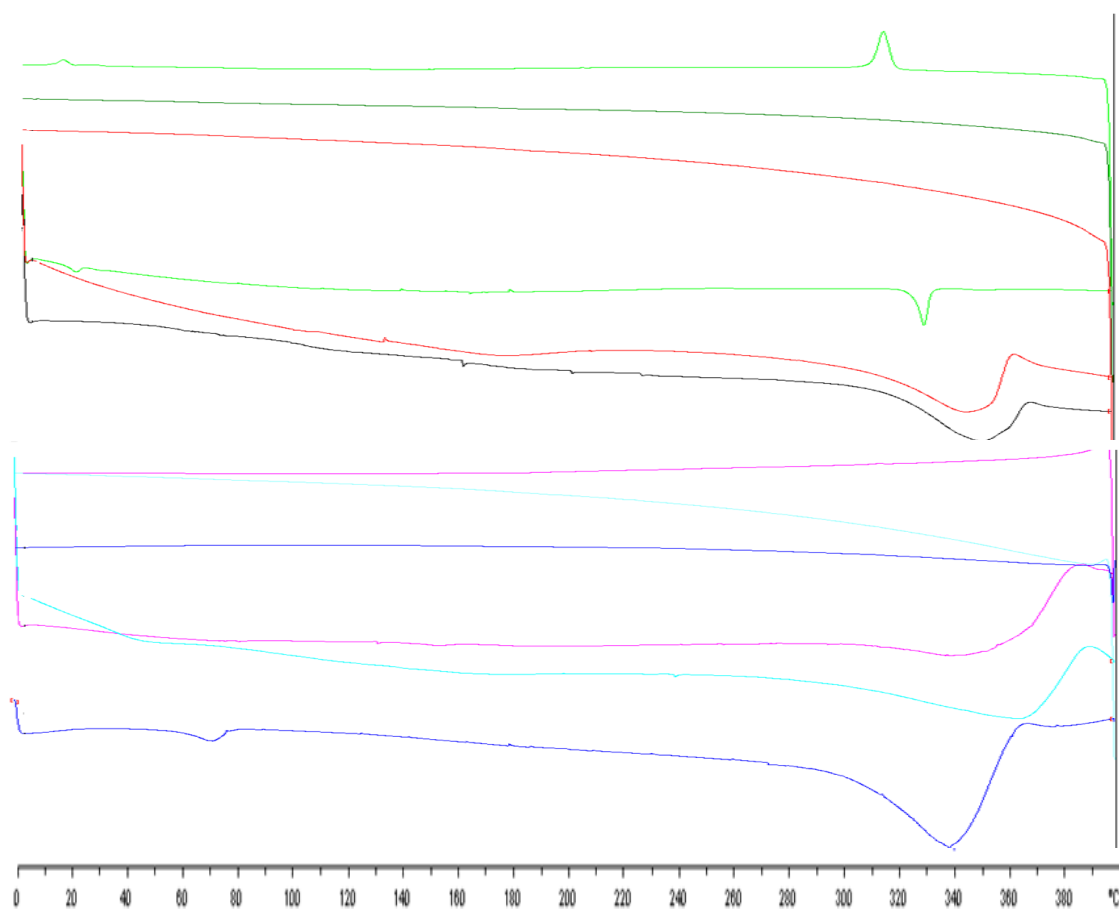
Figure 2.17: DSC thermograms of 3,3'-RO2T2 TFB polymers. (First heating and cooling scans (10 ^{0}C/min) under N_2: Cyan-P4; magenta-P5; Blue-P6; Black-P7; Red-P8 and

63

Green-P9; Solid lines represent the heating scans and dash line represent the cooling scans).

ordered solid state registry. Except polymer 2-P9 all the other polymers did not show any reversible thermal transitions. We do not have any reasonable explanation for this particular behavior. The irreversibility may be due to the loss of alkyl chains in higher temperatures indicated by thermogravimetric analysis (TGA).

2.5 TFB polymer device Study

One of the main target in this whole research period was to develop stable OTFTs with high charge-carrier mobility. After the structure property studies, device performance of the polymers reported here were investigated via an external collaboration with the Polyera Corporation, Skokie, Illinois. They use two different device architecture to obtain OTFT device performance.

a. Bottom gate device architecture

Here our collaborators used SiO_2 as dielectric layer and gold source and drain electrodes. OTFT device measurements were done in air. Further device details are unknown at the moment. In this device studies they checked both **2-P1** and **2-P2**. Both polymers obtain reasonable device performance with high on/off ratio with lower off currents in the range of picoamps. This clearly indicating this series of polymers at least show higher resistance to ambient doping compared to rr-P3HT, as might be expected from the higher oxidation potential. For **2-P1** they obtain 0.003 cm^2/Vs mobility with 7.0 x 10^4 $I_{on/off}$ ratio with -10 V threshold voltage (V_{th}). For 2-P2 they obtain 0.0004 cm^2/Vs mobility with 1.0 x 10^5 $I_{on/off}$ ratio with -10 to -15 V_{th}.

b. Top gate device architecture

Here our collaborators used a proprietary dielectric layer which is unknown at the moment. But obtained relatively better OFET device performance compare to previous device architecture. For 2-P2 they obtain 0.07 cm^2/Vs mobility with 1.0 x 10^6 $I_{on\text{-}off}$ ratio and 0 V, V_{th}. For 2-P1 they obtain 0.01 cm^2/Vs mobility with 5.0 x 10^5 $I_{on\text{-}off}$ ratio with 0 V, V_{th}. This difference of device performance depending on length of the side chains may mainly due to solubility difference and better film forming ability of 2-P2. On the other hand, it could be due to longer range order as explained earlier. Further justification cannot be done due to less amount of information available regarding to this device study.

2.6 Conclusions

From this study it was clearly shown that TFB co-polymers can obtain better ambient stability and high solid state registry with nearly co-planar polymer backbone, although we introduced substituent to the sterically more congested 3,3'-position in the bithiophene unit.

TFB polymers with linear alkyl chains showed much higher oxidation potentials (deep E_{HOMO}) compare to the more electron donating alkoxy substituted polymers. According to the device studies also it was obvious that these 3,3'-R2T2-based polymers show resistance to oxidative doping in ambient condition because their transistors show high current modulation ($I_{on}/I_{off}\sim10^5$ range) when measured in air. But we did not do any long term device stability study regarding to these polymers. Based on current device measurements, it is suggested that longer alkyl chains give better device performance.

This may be due to the good film forming ability (better solubility) and longer the alkyl chain it is easy to have good inter-lock with adjacent backbone side chains. So we can clearly proof our first hypothesis that the co-polymers with high loading of TFB give rise to higher ionization potentials and higher device stability. Also in 3,3'-R2T2-TFB polymers by increasing the alkyl substituent length we were able to obtain highly rigid and co-planar polymer backbone according to the uv-vis and WAXD measurements. Also according to the device results it clearly showing longer the linear alkyl chain better the charge carrier mobility. So from these observations we can state that we were able to proof our second hypothesis.

Compare to 3,3'-R2T2 units incorporation of 3,3'-RO2T2 units , destabilize the E_{HOMO} values of the resulted polymers. But when we incorporate the branch alkoxy chains we were able to improve the stability (deeper E_{HOMO} values) and solubility of the resulted polymers by improving the solid state packing arrangement. This was obvious if we compare the uv-vis and WAXD profiles of polymers 2-P4 and 2-P5. The branched alkoxy chains stabilize HOMO energy value relative to linear alkoxy chains. To get an idea about how branch chain effects to overall polymer properties we did a systematic study by introducing branching at α or β position with respect to "O" atom and changing the branching length of the alkyl chains. Combined optical, electronic and structural investigations allowed elucidating the effect of branching on the precise intermolecular arrangement, which sensitively tunes the electronic levels and optical properties through short- and long-range contributions. The study allowed to disentangle the branching effects on 1) aggregation tendency, intermolecular arrangement, 2) solid state optical bandgaps, and 3) electronic properties in an overall consistent picture, which might guide

future polymer synthesis towards optimized materials for (opto)-electronic applications.

From these observations we were able to proof our third and fourth hypothesis.

Chapter 3: Thiophene-Imide (TPD) and thiophene based alternating donor-acceptor co-polymers

3.1 Introduction

Arylene imides are one of the most studied classes of organic semiconductor materials due to their high electron affinity and charge transport properties.[163,164] Careful molecular functionalization together with proper device operational conditions

PDI **NDI** **Ph**

TPD **PMDI** **BTim**
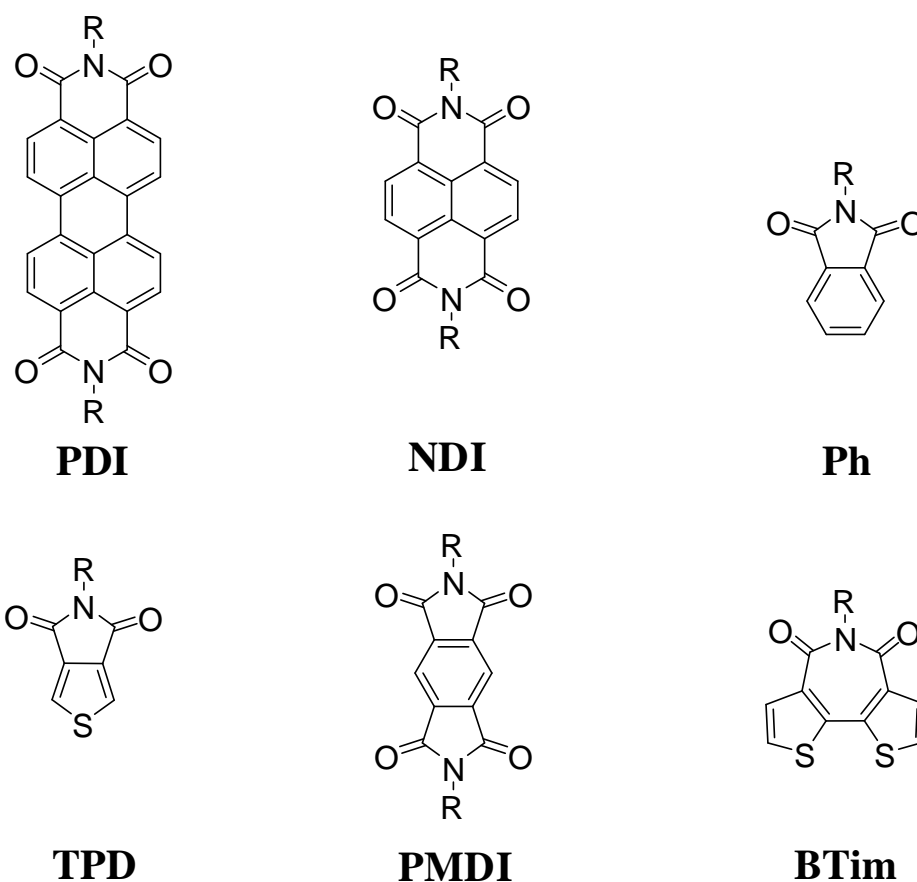
R- Alkyl or Aryl
Figure 3.0: General structures of commonly used imide functionalized acceptors

demonstrated that these materials can have ambient OTFT operations with high charge carrier mobility.[165-167] Impressive device performance was obtained for imide functionalized

small molecules with good ambient stability.[21,168] The time when we started this work there were very few imide-functionalized donor acceptor (D-A) polymers recorded in the literature, and our group was one of the pioneering group to incorporate imide functionalized arenes into D-A systems.[67,69,71,169,170] In organic chemistry, imide is a functional group consisting of two carbonyl groups attached to nitrogen (N). Due to the presence of strong electron withdrawing groups, dicarboxylic imides are usually introduced to the pi-systems to increase the electron affinity. Perylenediimides(PDI),[171-173] napthalene diimides (NDI),[71,174] pthalamides (PH),[67] thiopheneimides (TPD),[69] pyromellitic diimide (PMDI)[170] and bithiopheneimides (BTim)[175] (figure 3.0) are some of the commonly used imide functionalized acceptors in the literature. These are now widely studied electron accepting building blocks for D-A conjugated polymers.[15,176-178] Optical energy gaps (Eg^{opt}) of these materials can be finely tuned by careful attachment
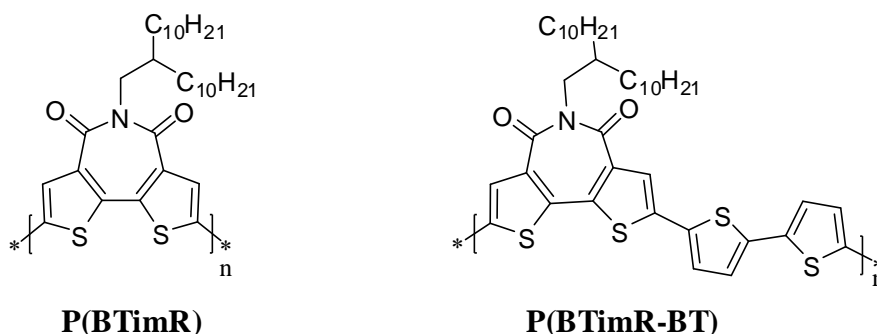
P(BTimR)   **P(BTimR-BT)**

Figure 3.1: Chemical structures of imide-functionalized bithiophene homopolymer P(BTimR) for n-type (left) and co-polymer P(BTimR-BT) for p-type (right) OTFT operation. [175]

of different substituent to the main arene core or by careful selection of donor units to incorporate with the imide units in polymers.[71,179] Another advantage of this imide functionality is the imide "N" creates an open position to attach side chains without disrupting the molecular backbone and allowing manipulating of solubility, morphology

and solid state packing. As mentioned earlier imide functionalized arylenes are some of the best n-type materials in organic electronic field with high charge carrier mobility.[168] Marks *et al* have shown that diluting loading of the imide-functionalized units within a polymer backbone can switch polarity from n-type to p-type (figure 3.1).[175] The co-polymer semiconductor material P(BTimR-BT) has a hole mobility of 0.01 cm^2/Vs but the homopolymer showed n-type behavior with electron mobility of 0.01 cm^2/Vs.

Imide functionalized materials have a long history as industrial dyes and pigments. The PDI precursor known as perylene-3,4,9,10-tetracarboxylic dianhydride (PTCDA) was one of the parent compound of this class of dyes which reported in 1912.[240] By simply modifying the PDI core by attaching different substituent to the imide "N" (the R groups) or on to the bay position (1,6,7,12 position) of the aromatic core, several different PDI dyes were manufactured with different chemical and physical properties. This ability to modify chemical and physical properties, depending on the attached substituent, is one of the driving force for PDI and other imide functionalized materials to thrive in the organic semiconductor field. Some examples of PDI derivative pigments are pigment red 179 and 178 and pigment 149 which are widely used in industry since 1950.[240] PDI-based pigments are very popular in automobile industry due to their high quality and durability.[180]

Horowitz *et al* first showed n-type behavior with electron mobilities of 10^{-5}cm^{2}V^{-1}s^{-1} can be obtained for *N,N'*-diphenyl substituted PDI based small molecules.[181] Malenfant *et al* recorded much higher electron mobility of 0.6 cm^{2}V^{-1}s^{-1} in *N,N'*-dioctyl substituted PDI but the ambient stability of this material was low.[182] Zhan et al first reported the PDI-based soluble D-A polymer with dithienothiophene donor units, which

demonstrated electron mobility of 1.3 x 10^{-2} $cm^2V^{-1}s^{-1}$.[176] Facchetti *et al* also reported a PDI-bithiophene D-A polymer with electron mobility of 2 x 10^{-3} $cm^2V^{-1}s^{-1}$.[183]

But due to poor solubility generally attributed to repeat units built from large aromatic cores along with difficulties in selective bromination and purification[184] of PDI, material chemists searched for a better alternative to the PDI core. This gave rise to the increased interest in the imide functionalized material, NDI. Selective bromination and purification of NDI materials are very easy compared to the PDI based materials[71]. NDI D-A copolymers are relatively more co-planar (conjugated) compared to the PDI polymers due to the less crowding in the NDI structure and the 2,6 bromination position respect to the PDI 1,7 bromination (sterically more congested bay region) position. Also the carbonyl "O" can potentially participate in attractive interactions with sulfur atoms of adjacent monomers.[146] The initial small molecule OTFT study on NDI give mobility of 10^{-4} $cm^2V^{-1}s^{-1}$.[185] Similar to the PDI case, improved device air stability was obtained when incorporating fluorinated alkyl chain on to the imide "N" on NDI, also yielding electron mobility of 0.57 $cm^2V^{-1}s^{-1}$. [186] Our group was the first to report using the NDI unit to prepare D-A conjugated polymers.[71,187]

In similar time period Faccheti *et al* have published more improve polymeric material based on NDI which give electron mobility of 0.85 $cm^2V^{-1}s^{-1}$. Recently our group has shown we can obtain ambipolar behavior using NDI based D-A polymers by careful choice of donors.[169] In our group another studied imide functionalized material was pthalamide (PH). Guo *et al* showed high hole mobilities can be obtained using PH based D-A polymers[67] and OPV PCE of 4.1% can be obtained. [188]

From above mentioned imide functionalized acceptors, in this particular work I

chose to continue the work of a prior group member, Xugang Guo, and further study the TPD unit as an acceptor unit within D-A co polymers. At the time I started this project there were very few literature reports of TPD based materials, the most recent being several years prior, and this unit was fairly novel within the organic semiconductor community. In earlier decades, Tour reported a few TPD based copolymers,[30] more recently followed by Nielson's 2004 report[189] of two TPD-based homopolymers, all without device studies. These homo polymers show maximum solution uv-vis absorption values in the range of 424 nm to 434 nm and the film absorption values in the range of 460 nm to 473 nm and efficient π stacking around 3.45-3.54 Å. Pomerantz reported ab initio calculations indicating that thiophene imide dimer is co-planar due to the favorable electrostatic oxygen-sulfur interactions.[146]

It is somewhat interesting to compare PH unit with this TPD unit. As explained in the introduction, thiophenes are more electron rich and its π electrons are more likely to delocalize along a D-A copolymer backbone compared to benzene π electrons due to the lower aromatic resonance energy. TPD D-A copolymers, as compared to PH analogues, may provide more delocalized π electron system with lower BLA. Also compared to PH unit, TPD unit has less steric interactions with adjacent donor unit, because compared to the PH benzene, now two C-H substituents are replaced by single "S" atom in thiophene. This should decrease steric interaction and increase the backbone planarity. So when we started this project the main goals to be tested include:

1. Ability to obtain   low Eg^{opt} conjugated D-A copolymers by careful choice of donor units combined with TPD acceptor units.

2. How 3,3'-R2T2 and 3,3'-RO2T2 units behave in this series of polymers.

3. Incorporation of branched side chains in 3,3'-RO2T2 units can improve FMO energy levels and solid state packing.

4. How fused ring systems effect the optical, electronic and solid state packing arrangement in TPD-based D-A copolymers.

Unfortunately, during this study several other groups also started to prepare polymers with the TPD unit and published in rapid succession. In recent literature it was demonstrated by others that TPD based D-A polymers can give state of the art OPV performance with PCE up to ~ 9.0% .[43,44,113,119,190]

3.2 Synthesis of monomers and polymers

TPD monomers were prepared similarly to publish procedure as depicted in figure 3.4.[189] First 3, 4-dibromothiophene was converted to 3,4-dicyanothiophene using Rosenmund-von Braun reaction and the resulting dicyano product was hydrolyzed using conc. HCl(aq). The resulting diacid was dehydrated to the corresponding anhydride by simply refluxing with acetic anhydride. The anhydride was condensed with different amines to obtain the corresponding imide functionality with different side chains. It is worth to note that in this step we obtained the open ring amic acid due to the 5 membered-5-membered ring strain so we closed the ring by increasing the reactivity of the open ring structure by simply converting it to acyl chloride in presence of $SOCl_2$ and obtain corresponding close ring product in high yield. Till this step it was fine to use the crude product for all the reactions. This close ring product can be easily purified using column chromatography and further purified by recrystallization. The imide group deactivates the thiophene ring towards electrophilic bromination, so have to use harsh

conditions to brominate the acceptor. The TPD co-polymers were prepared using different donor units by Stille coupling reaction (figure 3.2). After polymerization all the
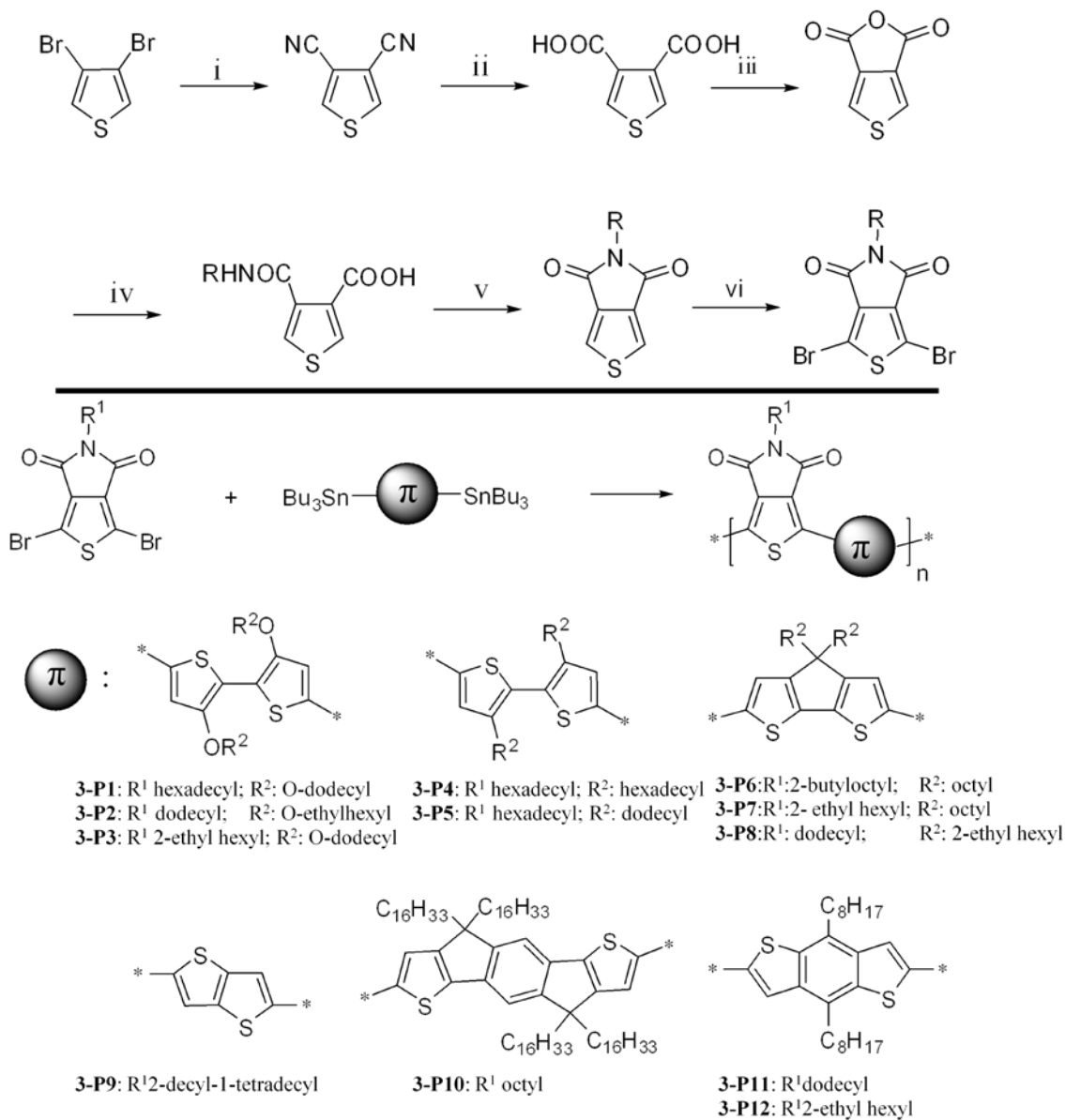
Figure 3.2: Synthesis scheme for monomers (top) and polymers (bottom). i. CuCN, Dry DMF, 170 ^{0}C; ii. 12N HCl, 55 ^{0}C; iii. Ac$_2$O, 140 ^{0}C; iv. RNH$_2$, AcOH, 130 ^{0}C; v. SOCl$_2$; vi. NBS, CF$_3$COOH, H$_2$SO$_4$, rt; vii. Pd$_2$(dba)$_3$, P (O-tolyl)$_3$, Anhydrous THF, 80 ^{0}C.

polymers were purified using sequential soxhlet extraction to remove low molecular weight oligomers. Due to the aggregation, reasonably

Table 3.0 Properties of TPD polymers 3-P1-3-P10

Polymer	yield (%)	M_n (KDa)[a] [PDI]	λ_{max}[b] (soln) (nm)	λ_{max} (film)[c] (nm)	$\Delta \lambda_{max}$ soln-film (nm)	λ_{onset}(film)[c] (nm)
3-P1	93	28 [1.32]	630	684	54	832
3-P2	79	21 [2.5]	738/684	751/684	13/0	823
3-P3	96	48 [1.6]	740/683	751/685	11/2	832
3-P4	85	14 [1.41]	452	546	92	691
3-P5	92	13 [1.54]	452	529	77	691
3-P6	89	33 [1.6]	643	691/643	48	744
3-P7	93	29 [2.68]	643	693/643	50	747
3-P8	83	16 [1.53]	653/601	682/620	29/19	727
3-P9	72	N/A[f]	637/596	643/596	6/0	694
3-P10	76	15[1.69]	603/558	603/558	0	645

[a] GPC vs polystyrene standards. [b] 1×10^{-5} M in cholorbenzene. [c] Pristine film spun-cast from 1 mg/ml cholorbenzene solution. [f] Polymer has poor solubility in THF at ambient temperature so could not obtain the molecular weight via GPC measurement

resolved ^{1}H NMR could only be obtained at elevated temperatures. (130 ^{0}C, $C_2D_2Cl_4$ as the NMR solvent). The characterization data (yields, relative molecular weights, optical data and thermal transitions are listed in table 3.0. Most of the yields are good to moderate. The relative molecular weights are high for most of the polymers as determined by GPC (Gel Permeation Chromatography) using polystyrene standards. As the donor units, I have incorporated 3,3'-R2T2 and 3,3'-RO2T2 units to get an idea about the substituent effects and to investigate tunability of the properties, similar to the previously discussed TFB polymers (Chapter 2). The purpose of incorporating fused ring systems is to investigate how these ring systems effect to the overall properties of the

polymers (optical, electronic properties and solid state packing arrangement). In literature it has been reported that introducing fused aromatic systems like those employed here can give rise to more stable HOMO energy values due to the localization of the electron density.[141,191,192] Also the fused ring systems can lower the reorganization energy and increase the electron transfer rates. More co-planar conjugated backbones can be obtained by lowering the rotational degree of freedom and enhancing the intermolecular π-π stacking.

3.3 Optical, electronic properties and self assembly of TPD co-polymers

The optical properties of TPD polymers were investigated using uv-vis absorption measurements (figure 3.4 and 3.6) and their absorption data are listed in table 3.0. All of the polymers show wide absorption profiles indicating these polymers may be interesting candidates for OPV applications. As seen in Chapter 2, it is again obvious when going from 3,3'-R2T2 to 3,3'-RO2T2 donors there is a significant red shift in both solution and thin film measurements (approximately~200 nm) similar to previously described TFB co-polymers. This clearly indicates the effect of increasing electron density of donor units. Also the presence of intramolecular S-O interactions in 3,3'-RO2T2 donors cause backbone to be more co-planar compare to the 3,3'-R2T2 donors which has more steric crowding due to the "CH$_2$" hydrogens. Addition to these reasons, 3,3'-RO2T2 donors can easily form intramolecular charge transfer complex with the adjacent acceptor unit and give rise to more rigid co-planar backbone by lowering the BLA.
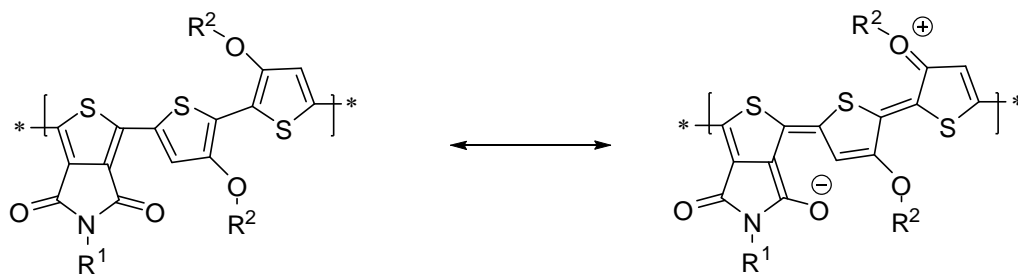
Figure 3.3: Intramolecular charge transfer of TPD donor-acceptor polymers

TPD co-polymers with 3,3'-R2T2 donors do not show any significant fine structure development when going from solution to the solid state. But they show significant red shift indicating the polymer backbone become more co planar. The reason to this behavior may be due to the easy delocalizability of π electrons due to the lower aromatic resonance energy of thiophene compare to the fluorinated arene in TFB co-polymers and lower the BLA. Here the polymer backbones tend to become more co-planar and conjugated by lowering the degree of rotational freedom. When we compare the film absorption profiles of polymer **3-P4** and **3-P5**, **3-P4** show more rigid backbone with development of fine structure compare to polymer **3-P5**. In TFB polymers also we observe the same trend. Again the reason may be good inter-lock with adjacent backbone side chains when increasing the length of the alkyl substituent, when going from $-C_{12}H_{25}$ to $-C_{16}H_{33}$. The 3,3'-RO2T2 -TPD polymers **3-P1**,**3-P2** and **3-P3** the solid state absorption measurements, show similar overall absorption width expanding from ~350 nm to 800 nm range. In **3-P1** polymer, which has the linear alkoxy chain on bithiophene donor, show clear red shift (~54nm) when going from solution to the solid state with less developed fine structure. The solid state measurements of **3-P1** polymer show distinct
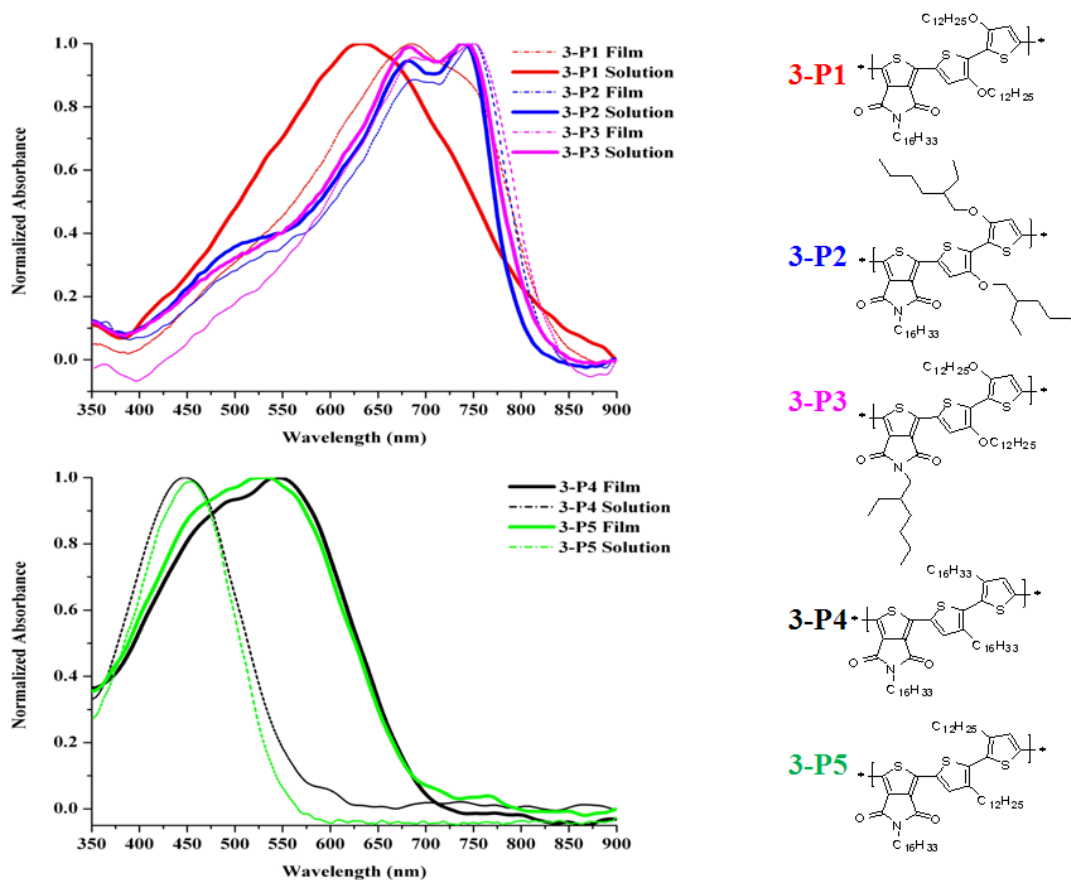
Figure 3.4: Normalized uv-vis spectra of TPD co-polymers 3-P1-3-P5. Solution (thick solid lines; 1 x 10^{-5} M in chlorobenzene); as-cast films (short dash dot; spin coating (1mg/ml, chlorobenzene) onto quartz plates) All measurements were done at room temperature.

maxima at 684 nm and shoulder at 740 nm wavelength. But in polymers **3-P2** and **3-P3** when we introduce the branch 2-ethylhexyl chains either on donor or acceptor the solution spectra are red shifted with little change on going from solution to the solid state absorption measurement, compare to the longer linear alkoxy chain polymer **3-P1**. Simillar effect we observe in TFB co-polymers when we incorporate branch alkoxy chain on to the 3,3'-RO2T2 unit. Both these polymers (**3-P2** and **3-P3**) show well developed fine structure in both solution and film absorption measurements and **3-P2** show slight blue shifted absorption edge compare to the polymers **3-P1** and **3-P3** which has similar

absorption edge. To obtain a clear explanation about the observed behavior, we used the WAXD images of the corresponding polymers. According to the WAXD images all the 3 polymers show solid state order. In polymer **3-P1** we can clearly see sharp diffraction maxima for lamellar spacing and π stacking. For both polymers **3-P2** and **3-P3** we cannot observe sharp diffraction maxima for lamella spacing. The middle small ring in the diffractogram clearly indicate the alkyl chains and the backbone not properly oriented in polymers **3-P2** and **3-P3** even in extrusion. This may be due to the to the relatively high alkyl chain bulk created by the 2-ethyl hexyl branch chains which lower the solid state packing with adjacent polymer backbones. Compare to polymers **3-P2** and **3-P3**, the polymer **3-P1** has linear alkyl chains and they can have good inter-lock with adjacent backbone side chains. This may be the reason for clear diffraction maxima correspond to the lamella spacing in polymer **3-P1**. All the three polymers indicate meridional diffraction maxima. Overall the long linear alkoxy polymer **3-P1** show more solid state order relative to the polymers **3-P2** and **3-P3** which have branch side chains in either donor or acceptor, although they show more fine structure development in solid state absorption measurements. Another reason for this well develop fine structure may be, we were not measuring the actual solution, but measuring highly aggregated polymers in "pseudo-solution" as discuss in chapter 2. So this may be the reason that in polymers **3-P2** and **3-P3** have similar solution and solid state absorption profiles. These aggregates may have similar intermolecular and conformational order similar to the solid state packing arrangement of the polymers. But all these three polymers show better solubility in common organic solvents like THF, chloroform and chlorobenzene at ambient

conditions. The different chain conformations in the solution phase, may be the reason, that we did not observe similar effect in the solution absorption profile of linear alkoxy
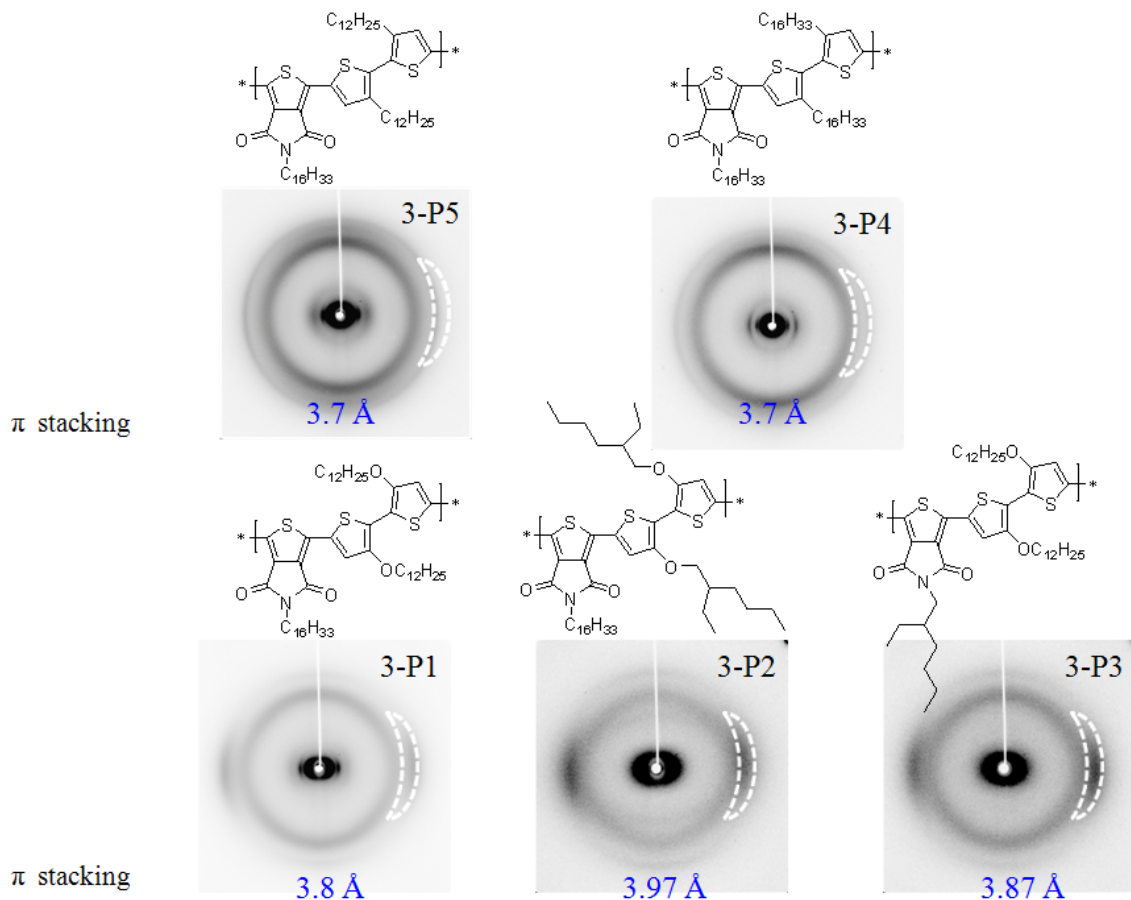
Figure 3.5: Fiber WAXD diffractograms of TPD polymers 3-P1-3-P5 without annealing polymer **3-P1**, which shows blue shifted unstructured solution absorption profile compare to the polymer **3-P2** and **3-P3**. To get a clear idea about this observation we have to do DFT quantum mechanical calculations. As stated earlier, if we think about the solid state absorption profile of the 2-ethylhexyl branch polymers, when the branch is on the donor unit (polymer **3-P2**) we could see slight blue shift in the absorption edge ($\Delta\lambda \sim$ 9 nm) compare to the other 2 polymers which has linear alkoxy chain on donor unit (polymer **3-P1** and **3-P3**). The reason may be steric crowding introduced by the branch alkoxy

chains (polymer **3-P2**) over linear alkoxy chains which can twist the polymer backbone and lower the effective conjugation length. The polymer **3-P3** also has the 2-ethyl hexyl chain but it is on the imide "N" and it was much farther away from the polymer backbone. So it doesn't have any significant effect on the backbone effective conjugation and show similar absorption edge compare to the polymer **3-P1** which has linear alkyl chains on both donor and the acceptor. Electrochemical measurements also well matched with corresponding absorption profiles of the polymers. Both the linear alkyl 3,3'-R2T2 polymers (polymers **3-P4** and **3-P5**) show relatively shallow E_{HOMO} values (-5.59 eV) compare to the 3,3'-RO2T2 polymers **3-P1**,**3-P2** and **3-P3** which shows HOMO energy values of -4.84 eV, -5.021 eV and -4.918 eV respectively. (table 3.0) The E_{HOMO} energy levels mainly depend on the electron donating ability of the donor. If the donor has higher electron donating ability the resulted polymer E_{HOMO} become less deep compare to the zero energy vacuum level. As stated in Chapter 1 to be ambient stable the organic semiconductor materials should have much deeper E_{HOMO} values compare to the -5.1 eV with respect to the vacuum energy level. But similar to the TFB polymers when we introduce branch chains to the donor unit we were able to stabilize the E_{HOMO} of the polymer **3-P2** by 0.18 eV with respect to the polymer **3-P1** carrying linear alkoxy side chains on the donor unit. Polymers, **3-P1** and **3-P3** show similar E_{HOMO} value although the polymer 3-P3 has 2-ethyl hexyl chain on the imide "N". As stated in Chapter 1, HOMO energy of a D-A polymer is highly depends on the donor unit. In this particular acceptor the substituent attached to it may have very minor effect to the resulted polymer E_{HOMO} energy value. So the resulted minor difference of the E_{HOMO} energy values of the

polymer **3-P1** and **3-P3** most probably due to the different conformation and packing arrangement in the solid state.

Not like TFB polymers, in TPD polymers we can easily attached fused ring systems to polymer backbone without sacrificing the solubility and solid state packing due to the attachment of alkyl chains on to the imide "N". Fused ring systems work as valuable donor units in D-A systems due to their structural rigidness (which lower the backbone twisting) and lower the reorganization energy which enhanced the charge carrier mobility. Also by incorporating highly aromatic resonance stabilized unit such as benzene (ex: benzodithiophene (BDT)) we can easily obtain more stable E_{HOMO} values as depicted in literature. Compare to alkoxy versions of TPD polymers **3-P1**, **3-P2** and **3-P3** when we introduced fused ring systems, the resulted uv-vis profiles show blue shift due to the less electron donating ability of the donors. But compare to the linear alkyl 3.3'-R2T2 polymers **3-P4** and **3-P5**, all the fused ring polymers except **3-P10**, show red shifted absorption profiles indicating more structural rigidity of the polymer backbone due to the low degree of rotational freedom. The TPD-cyclopentadithiophene (CPDT) polymers **3-P6** and **3-P7**, with branched chains on "N" (**3-P6**: 2-butyloctyl; **3-P7**: 2-ethylhexyl),give similar solution and solid state uv-vis absorption profiles. Both these polymers have similar molecular weights so we can have a fair comparison of their properties. The solution absorption profiles are structureless indicating less or no aggregation effect. Higher solubility due to the branch chains may be one reason for this observation. As similar to other branch chain versions again the solid state absorption profiles show well developed fine structure in long wavelength region indicating high backbone rigidity and co-planarity. Compare to these two polymers (**3-P6** and **3-P7**), the
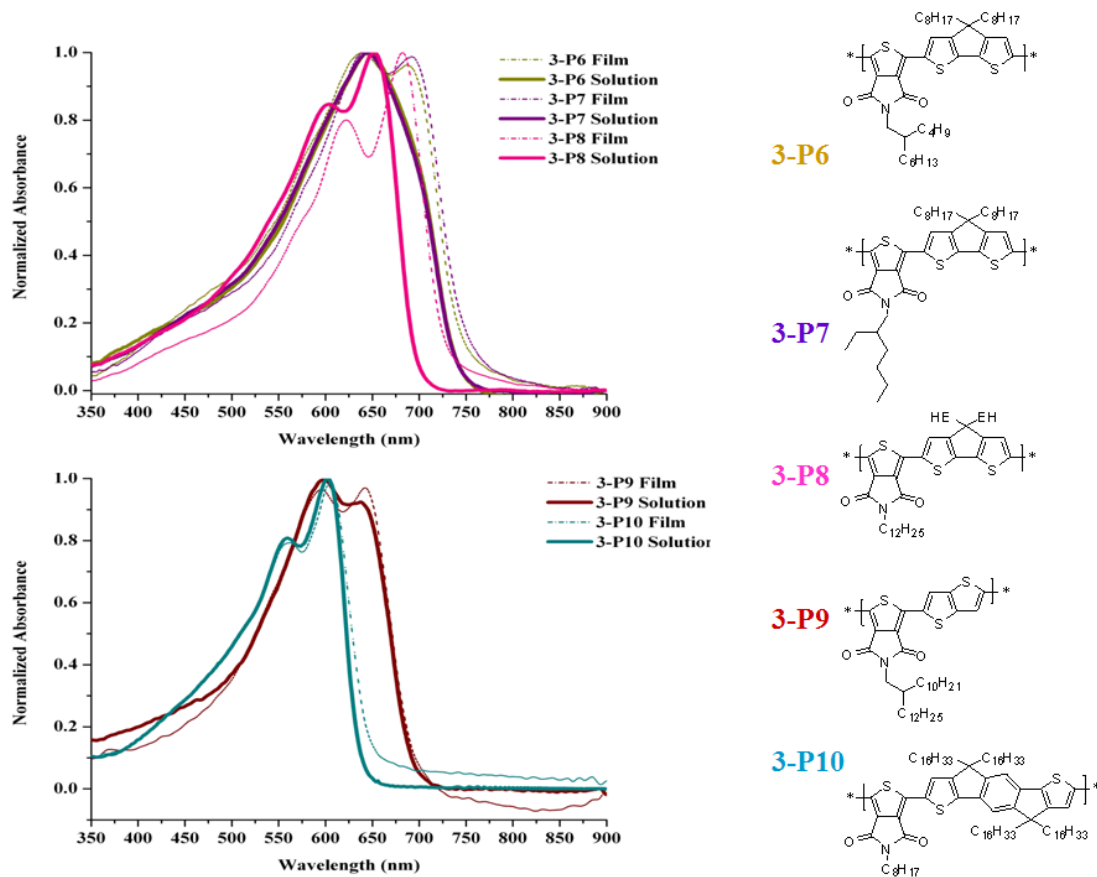
Figure 3.6: Normalized uv-vis spectra of TPD co-polymers 3-P6-3-P10. Solution (thick solid lines; 1 x 10^{-5} M in chlorobenzene); as-cast films (short dash dot; spin coating (1mg/ml, chlorobenzene) onto quartz plates) All measurements were done at room temperature.

third TPD-CPDT polymer **3-P8** shows fine structure development in both solution and solid state. In this polymer the imide "N" has the linear alkyl chain and the CPDT unit has 2-ethylhexyl branch unit different to **3-P6** and **3-P7**. This polymer show very minor blue shift compare to other two polymers **3-P6** and **3-P7** in solid state absorption profile. The reason for this observation may be the low molecular weight of **3-P8** which did not reach to the effective conjugation length or due to the bulky branch on CPDT unit lower the solid state packing arrangement of the polymer backbone and lower the conjugation. Compare to all the three TPD-CPDT polymers, the TPD polymers with thienothiophene

(TT) and indacenothiophene (IDT) show blue shift in both solid and solution measurements with identical solution and solid state absorption profile. The TPD-TT polymer has bad solubility in THF which is the reaction medium of the polymerization. So the observed blue shift may be due to the low molecular weight of the polymer which did not reach to it's effective conjugation length. The TPD-IDT polymer also has lower molecular weight compare to other TPD polymers. However, if the lower molecular weight was not the actual cause for the blue shift, then the reason for the resulted optical behavior may be due to their fused ring structures. Compare to CPDT the TT has less overall conjugation length and this may be another reason for observed blue shift around ~ 40 nm in solid state optical measurements. But the IDT donor unit has higher conjugation length compare to both CPDT and TT units, but this has the most blue shifted absorption profiles in both solid and solution state. The reason for this observation may be high orthogonal side chain density of the IDT unit which disrupt the close packing arrangement of the adjacent polymer backbone and lower the solid state order and co-planarity To shed some light on these observations it is a good idea to compare the electrochemical and WAXD data of these resulted fused ring polymers. It is clearly obvious that the TPD-IDT polymer is highly amorphous and doesn't show any solid state registry in WAXD images. As stated earlier the high orthogonal side chain density on the polymer backbone disrupt the close solid state packing of the adjacent polymer units. So polymer backbone and alkyl chains not at all well ordered in this polymer even in the extrusion. This clearly indicate by the ring like diffraction patterns in the WAXD diffractograms. This observation is well matched with the uv-vis profile of this polymer. The TPD-IDT polymer was the most blue shifted polymer among this series and it shows
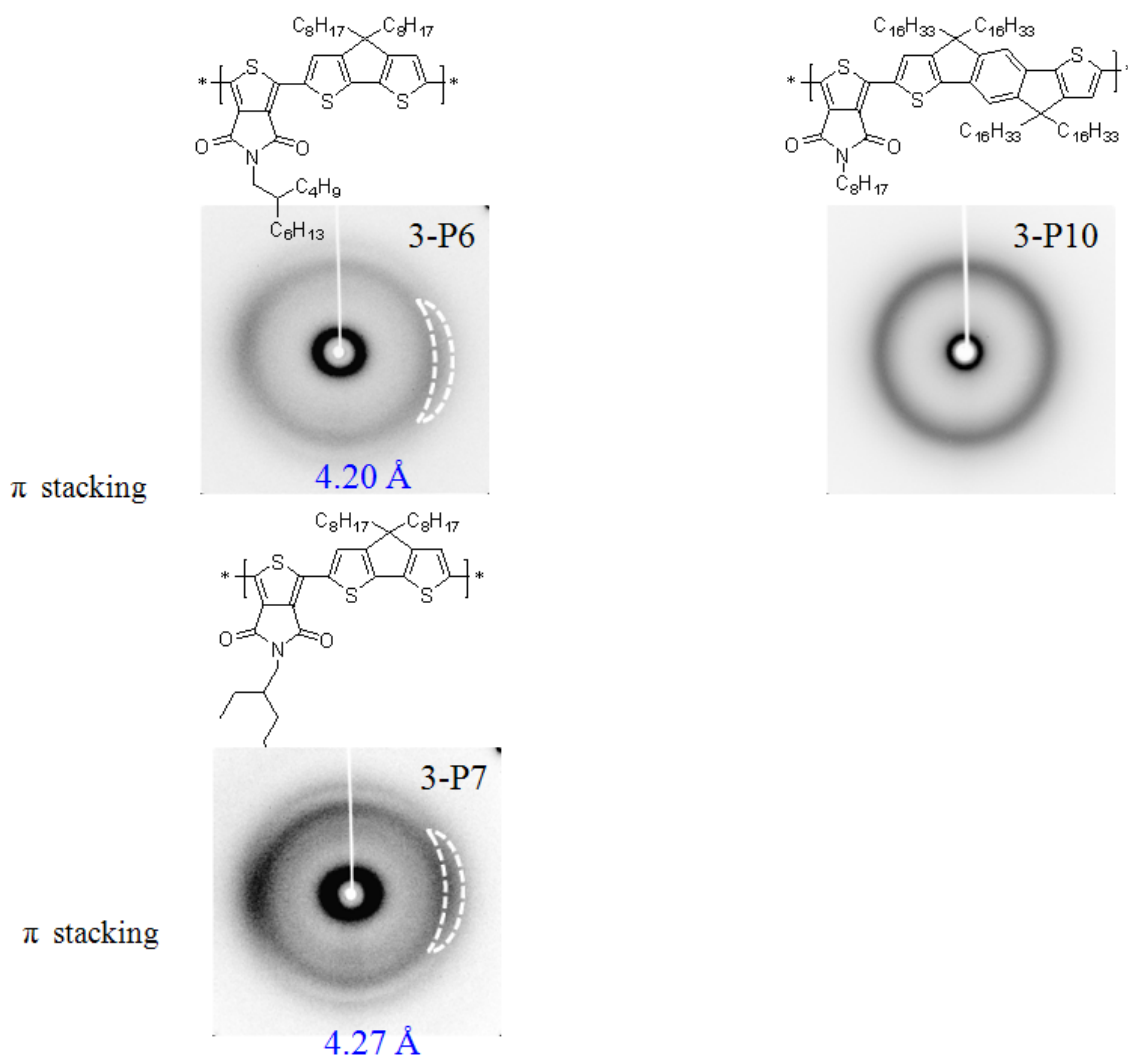
Figure 3.7: Fiber WAXD diffractograms of TPD polymers without annealing

similar absorption profile both in the solution and solid state indicating there is no any driving force to obtain more ordered packing arrangement due to the highly amorphous nature of the polymer. The development of fine structure may be due to the different conformational order in the polymer backbone and alkyl substituents. The TPD-CPTD polymers also do not show well distinguished solid state registry according to the WAXD images. They also have less dense orthogonal side chains on the CPDT donor compare to the IDT unit. The TPD-CPDT polymer **3-P6** also show more amorphous nature with very weak diffraction correspond to the π stacking. Again the more bulkier

2-butyl octyl side chains on the imide "N" and the orthogonal linear alkyl chains on the

CPDT unit may lower the close pack arrangement of the polymer backbones. This is

Table 3.1: Electrochemical and optical data for polymers

Polymer	$E_{ox}(V)$ [a]	$E_{HOMO}(eV)$ [b]	$E_{LUMO}(eV)$ [c]	$E_g^{opt}(eV)$ [d]
3-P1	0.042 ∓ 0	-4.84 ∓ 0	-3.35 ∓ 0	1.49
3-P2	0.221 ∓ 0	-5.021 ∓ 0	-3.51 ∓ 0	1.51
3-P3	0.118 ∓ 0.013	-4.918 ∓ 0.013	-3.43 ∓ 0.013	1.49
3-P4	0.790 ∓ 0.008	-5.59 ∓ 0.008	-3.80 ∓ 0.008	1.79
3-P6	0.529 ∓ 0.011	-5.33 ∓ 0.011	-3.66 ∓ 0.011	1.67
3-P7	0.571 ∓ 0.012	-5.37 ∓ 0.012	-3.71 ∓ 0.012	1.66
3-P8	0.551 ∓ 0.023	-5.35 ∓ 0.023	-3.58 ∓ 0.023	1.77
3-P9	1.06 ∓ 0.007	-5.86 ∓ 0.007	-4.07 ∓ 0.007	1.79
3-P10	0.751 ∓ 0	-5.55 ∓ 0.0	-3.63 ∓ 0.0	1.92

Experimental conditions: 0.1 M $(n\text{-Bu})_4N\cdot PF_6$ in anhydrous acetonitrile as supporting electrolyte, platinum disc as working electrode, platinum wire as counter electrode, silver wire as reference electrode and Fe/Fe^+ (-4.8 eV vs vacuum) as reference, scanning rate: 50 mV/s; All measurements conducted on solution-cast thin films under nitrogen. [a]Corrected E_{ox} value respect to Fc/Fc^+. [b]$E_{HOMO} = -[4.8+(E_{ox}-Fc/Fc^+)]$, E_{ox} calculated using onset of DPV measurements (Oxidation peak). [c]$E_{LUMO} = E_g^{opt} + E_{HOMO}$. [d]$E_g^{opt}$ Optical band gap estimated from the absorption edge of the film.

clearly indicated by the increase π stacking distance of the polymer. The middle ring of

the diffractogram clearly indicate alkyl chains and polymer backbone not properly

oriented. Unfortunately we do not have the WAXD images for polymer 3-P8 to get an

idea about its solid state packing behavior. The polymer **3-P7** has relatively more ordered nature compare to the polymer **3-P6** according to the WAXD image, but both show similar solution and solid state absorption profiles in the uv-vis study.

If we think about the electrochemistry measurements of this TPD fused ring polymers it shows both TPD-TT polymer (**3-P9**) and the TPD-IDT polymer (**3-P10**) show the deeper E_{HOMO} energy values compare to the rest of the series. So it clearly indicates both these polymers have lower conjugation length or the disruption of the conjugation length, relative to other polymers. According to the WAXD image the TPD-IDT polymer shows, it is highly amorphous. So this polymer doesn't have well ordered solid state registry and this will lower the relative conjugation length of the polymer by resulting a more shallow E_{HOMO} value. As stated above we could not get a WAXD image for the polymer, TPD-TT ,so cannot say this polymer is amorphous or not. But this polymer show very poor solubility in the reaction medium. (THF) So the main reason for the observed more deeper E_{HOMO} may be due to the lower molecular weight of the polymer, which lowers the effective conjugation length. All the 3, TPD-CPDT polymers show similar E_{HOMO} values. Compare to these fused ring polymers and 3,3'-R2T2 polymers all the 3,3'-RO2T2 polymers show less shallow E_{HOMO} values mainly due to the increase electron donating ability of the alkoxy chains and favorable inter and intra molecular interactions which caused polymer backbone to be more co-planar.

3.4 Effect of acceptor units on polymer optical properties and self-assembly

For all the previous discussions we used one particular acceptor unit with several different donor units and compare the differences of opto-electronic properties of the resulted donor-acceptor polymers. Polymer properties can vary depending on the

acceptor unit. So to get an idea how different acceptor units effect to the polymer optical properties and self assembly here we are trying to compare three different acceptor units with two common donor units. It is important to note that opto-electronic properties of the resulted polymers are a function of the FMO energy levels resulted due to the hybridization of the donor and acceptor molecular orbitals and it require computational calculations to obtain a qualitative picture. But we can obtain some rough idea about the behavior of different polymer systems by comparing their uv-vis, WAXD and electrochemical data concerning relative geometry, sterics and relative packing arrangement. First we will consider the polymers obtain from 3,3'-R2T2 unit. It is clear that TPD-3,3'-R2T2 polymers show red shifted absorption profile compare to PH and TFB; 3,3'-R2T2 co-polymers. Compared to PH and TFB, TPD has less steric interactions with donor unit due to the five membered thiophene ring. Also due to the less aromatic nature of the thiophene ring, the π electrons can be easily delocalized over the polymer backbone by lowering the BLA. TFB polymer show red shift compare to PH, but it is blue shifted compare to the corresponding TPD co-polymer. Here TFB has more driving force to obtain more planar rigid backbone due to the S-F intramolecular interactions, although, both PH and TFB has benzene ring as the acceptor unit. But in PH it doesn't have this favorable intramolecular interactions compare to the TFB unit to obtain more planar ordered polymer backbone. Compare to all these three polymers this TFB co-polymer show well developed fine structure in solid state absorption profile clearly indicating more driving force to obtain more rigid polymer backbone. These observations clearly demonstrated in WAXD diffractograms. As stated earlier due to enhance inter and intramolecular interactions the TFB polymer backbone is highly rigid

Figure 3.8: Normalized UV-vis spectra of dialkyl bithiophene polymers. Solution (blue line; 1 x 10^{-5} M in chlorobenzene); as-cast films(red line; spin coating (1mg/ml, chlorobenzene) onto quartz plates) All measurements were done at room temperature

and show long range solid state order. But the PH polymer doesn't show any solid state order and the polymer seem to be highly amorphous. Twisting the polymer backbone due to the steric effects and high side chain density on the polymer backbone lower the solid state packing with adjacent polymer backbone may be the reason for this observation. TPD 3,3'-R2T2 co-polymer also not show well distinguish solid state order

although it shows more red shifted absorption profiles in the uv-vis absorption measurement. Again the reason for this observation may be the high side chain density on the polymer backbone (both donor and acceptor unit has alkyl substituents) which lower the solid state packing arrangement with adjacent polymer backbones. But both this TPD and TFB 3,3'-R2T2 co-polymers show similar π stacking distances.

When we compare these 03 acceptors with 3,3'-RO2T2 donors the results are completely different. Again the TPD polymer show red shift compare to all the other 03 polymers. But now the PH polymer is less blue shifted compare to TPD and it is red shifted relative to TFB polymer. The reason for this observation may be intramolecular charge transfer which give rise to low BLA and more co-planar polymer backbone in TPD and PH units as stated earlier. This will overcome the steric problem associate with PH benzene. Also now, there is this S-O intramolecular interaction which help the backbone to be co-planar. The parent polymer poly(3,3'-dialkoxy-2,2'-bithiophene) has a optical energy gap of 1.6 eV. According to the donor acceptor concept the resulted polymers should have lower band gaps but the insertion of PH did not alter the optical energy gap and have very little effect on it. But compare to parent polymer, the TPD co-polymer narrower the optical energy gap. The TFB polymer blue shifted compare to all the other 3 polymers but show long range solid state registry compare to all the other 2 polymers according to the WAXD data. In TFB-3,3'-RO2T2 co-polymer has more driving force to obtain relatively highly ordered solid state packing arrangement due to the intramolecular S-F and S-O interactions. Not like 3,3'-R2T2 case here both TPD and PH polymers also show long range solid state order according to the WAXD images. So
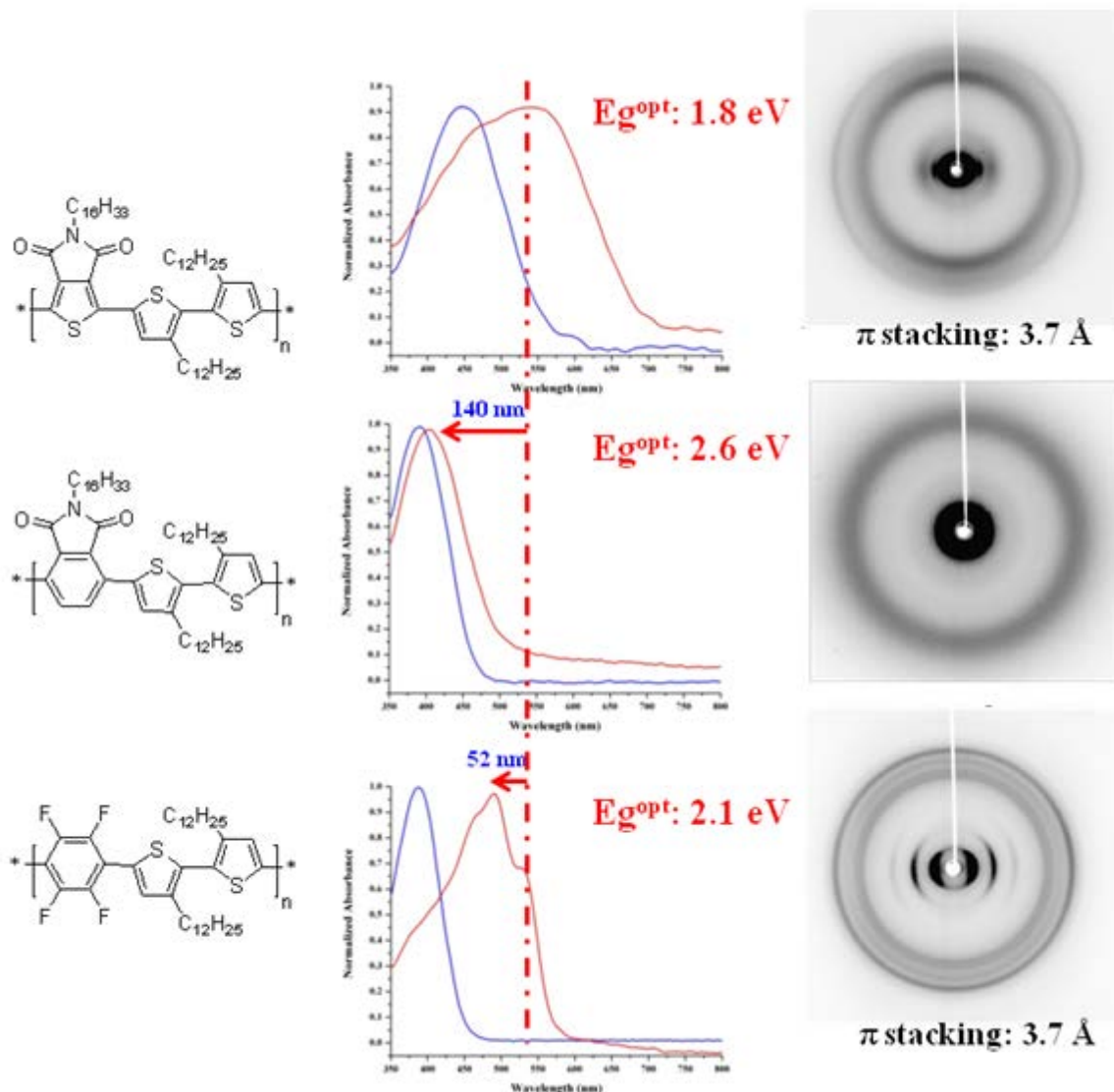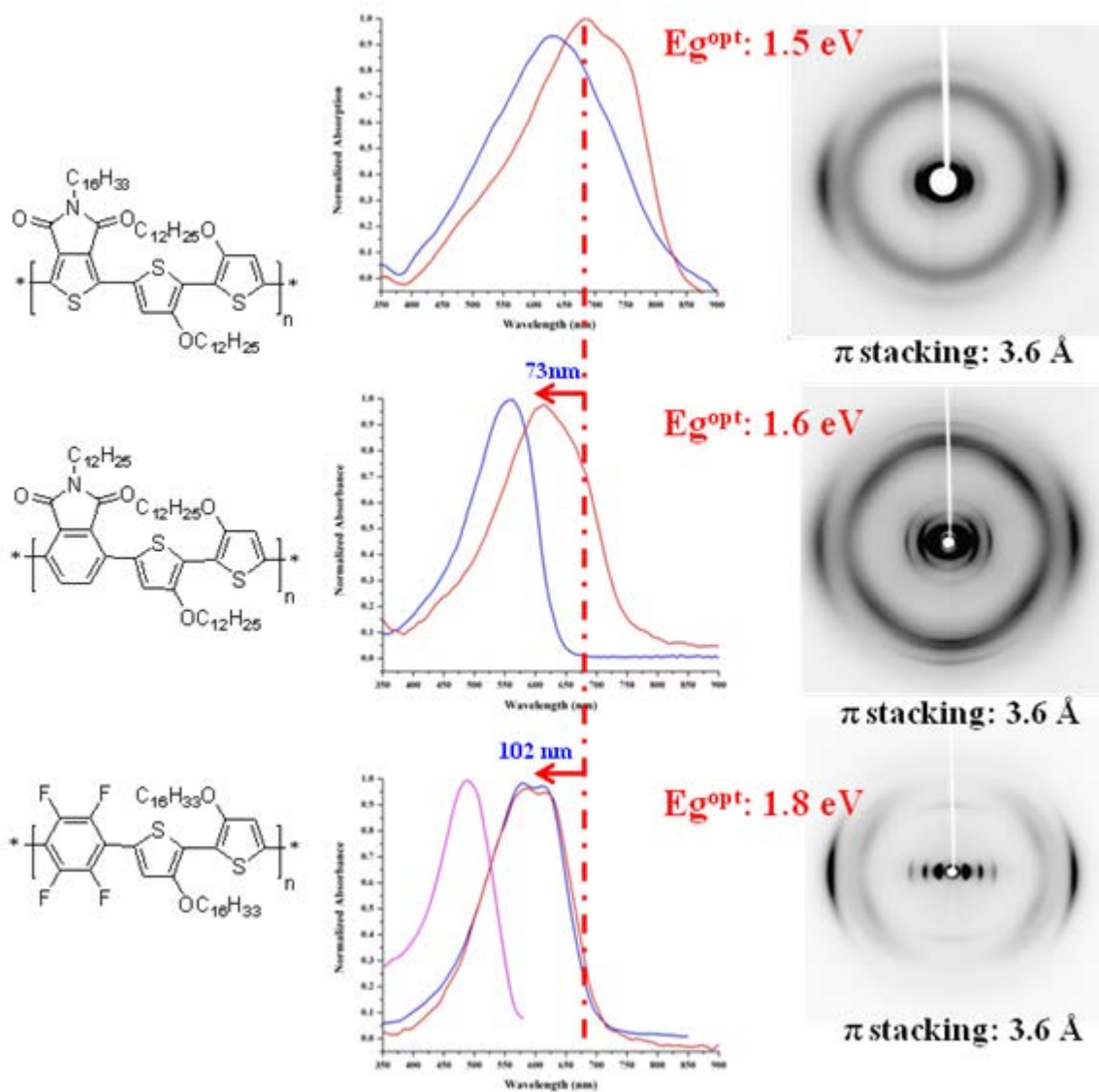
Figure 3.9: Normalized UV-vis spectra of dialkoxy bithiophene polymers. Solution (blue line; 1 x 10^{-5} M in chlorobenzene); as-cast films(red line; spin coating (1mg/ml, chlorobenzene) onto quartz plates) All measurements were done at room temperature

from these observations it is clear that the polymer properties not only govern by donor they also highly depend on the acceptor.

3.5 Device study of TPD polymers: OTFT study

Hole Mobility = 2.23×10^{-3} cm^2/Vs
$I_{on}/I_{off} = 10^5$
$Vt = 6.0$ V

Hole Mobility = 1.81×10^{-3} cm^2/Vs
$I_{on}/I_{off} = 10^4$
$Vt = -0.3$ V

Hole Mobility = 1.89×10^{-6} cm^2/Vs
$I_{on}/I_{off} = 10^2$
$Vt = -28.9$ V

Hole Mobility = 2.31×10^{-6} cm^2/Vs
$I_{on}/I_{off} = 10^2$
$Vt = -28.2$ V

Hole Mobility = 1.25×10^{-3} cm^2/Vs

$I_{on}/I_{off} = 10^2$

$V_t = 10.3$ V

Hole Mobility = 2.58×10^{-4} cm^2/Vs

$I_{on}/I_{off} = 10^4$

$V_t = -3.4$ V
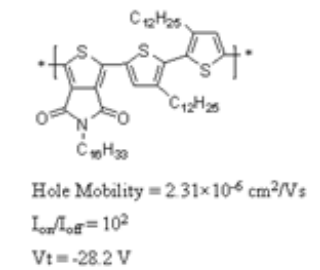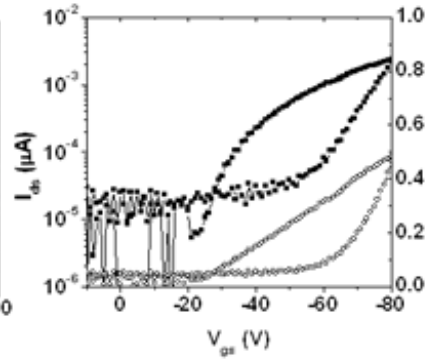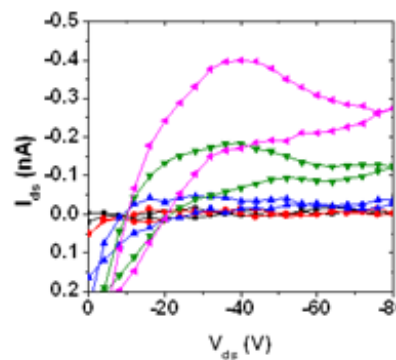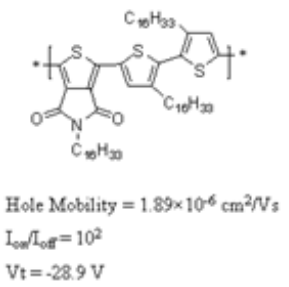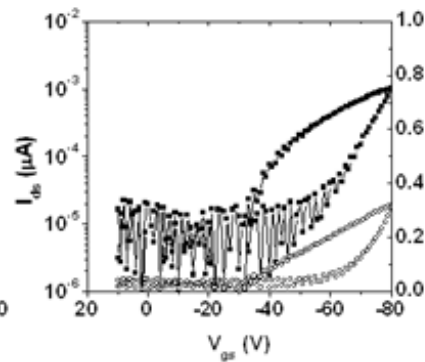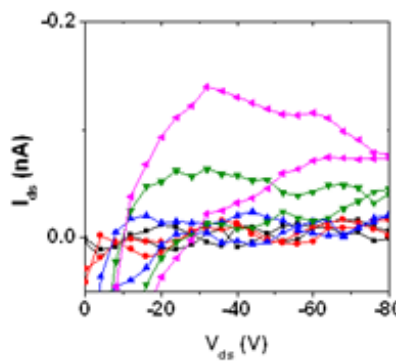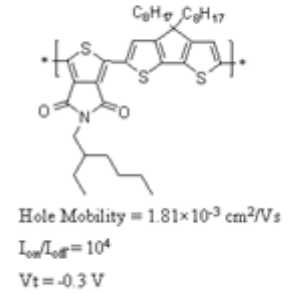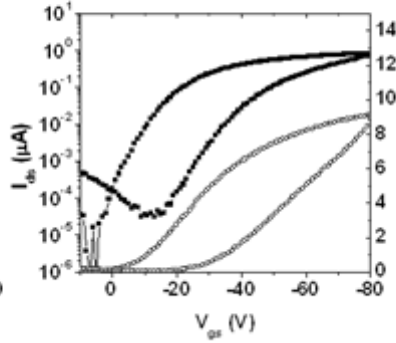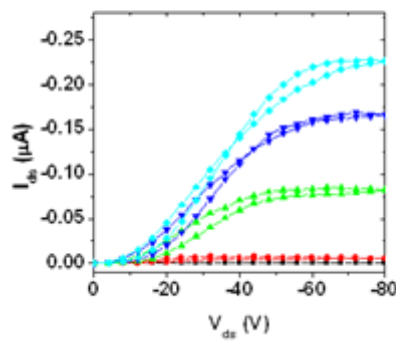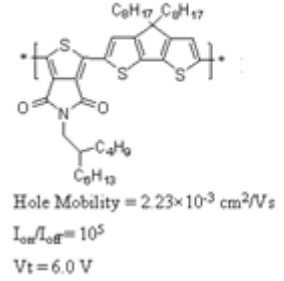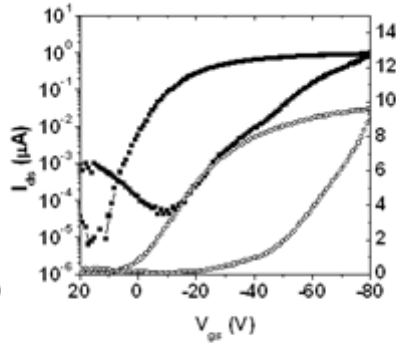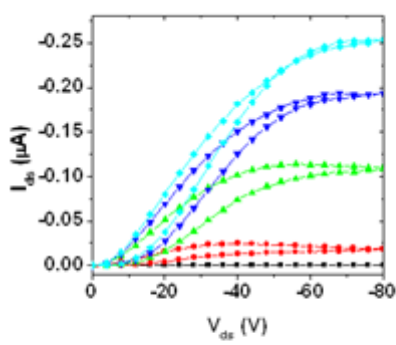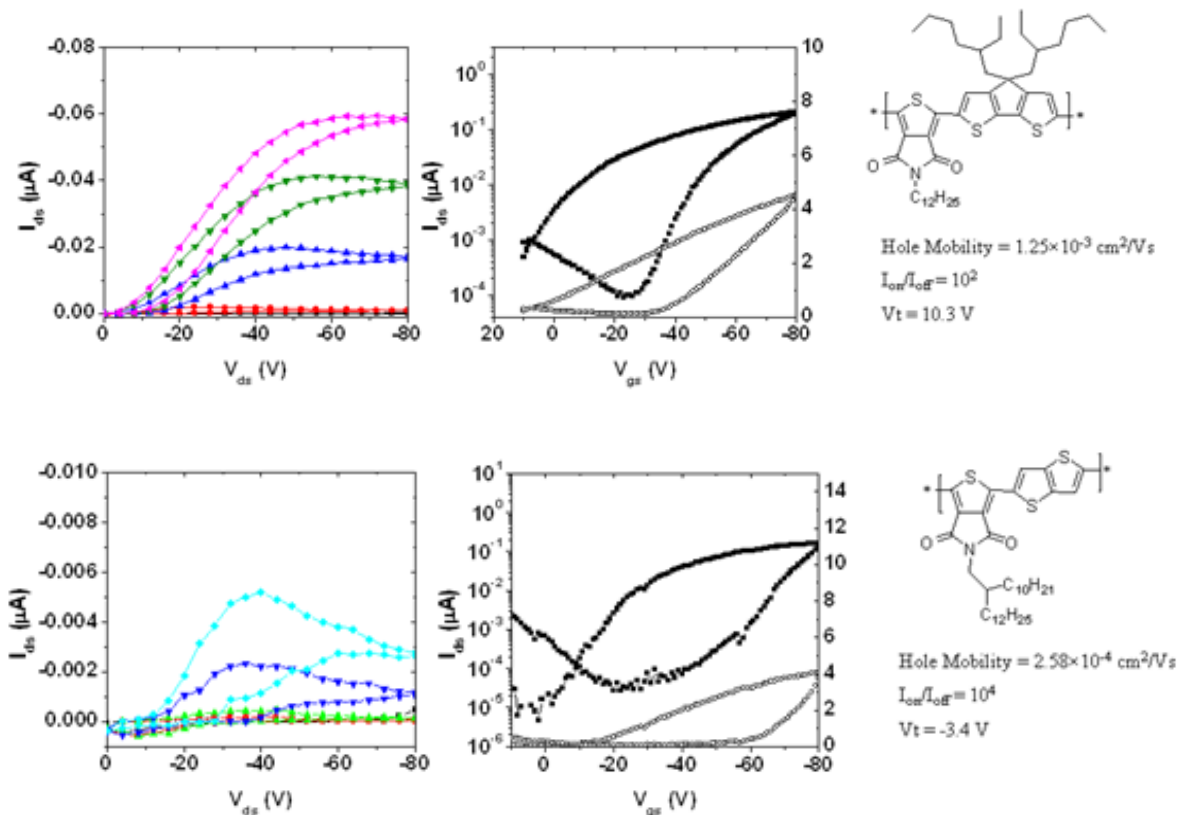
properties. According to the collaborator the OTFTs were fabricated using most basic, standard device architecture: bottom-gate/bottom-contact geometry. All the materials gave moderate device performance, mobilities in the range of 10^{-3}-10^{-4} cm^2/Vs. The polymers with branch alkyl chains give better hole mobilities. The reason for this behavior may be good film forming property due to the better solubility. The TPD-TT polymer give moderate device performance most probably due to the bad solubility in device processing conditions.

3.6 Conclusions

A series of thiophene-imide (TPD) based polymers were prepared and study their opto-electronic properties. All these polymers exhibited higher molecular weights and better solubility except **3-P9** in common organic solvents like THF, toluene, chloroform and cholorbenzene etc. Different substituent and fused ring effects to the polymer

93

backbone were extensively studied using uv-vis measurements and WAXD data incorporated with electrochemical measurements. Not like TFB co-polymers all the TPD co-polymers show less pronounced solid state registry according to the WAXD diffractograms. The high alkyl substituent density on the polymer backbone (both on donor and acceptor unit) lower the solid state packing arrangement with adjacent polymers is the main reason for low solid state registry in this class of polymers. But all these polymers show relatively low Eg^{opt} values compare to the previously explained TFB co-polymers. It was obvious that by careful choice of donor units we can obtain lower Eg^{opt} and relatively broader absorption profiles compare to the TFB co-polymers.

Again we observe 3,3'-R2T2 incorporated polymers give relatively more shallow E_{HOMO} values compare to the 3,3'-RO2T2 incorporated polymers. But by introducing branch alkoxy substituents, we were able to fine tune the E_{HOMO} similar to the TFB co-polymers discussed in chapter 2. The fused ring systems give rise to shallow E_{HOMO} values but they lack the solid state registry due to the grafted alkyl chains on the fused ring system which lower the close solid state packing. But these fused ring systems incorporate with alkyl substituent's are very important to enhance the polymer solubility. This is clearly obvious if we think about the polymer TPD-TT (**3-P9**) which shows very poor solubility.

Compare to TPD 3,3'-R2T2 co-polymers, the fused ring polymers give more red shifted absorption profile. But they show blue shifted absorption profiles compare to the TPD 3,3'-RO2T2 co-polymers. Depending on the intrinsic character of the fused ring system polymer opto-electronic properties are hugely varies. In this study we used CPDT, TT and IDT as the fused ring donor units. Preliminary device study of these polymers

94

show moderate device performance with charge carrier mobility around 10^{-3} to 10^{-6} cm^2/Vs range.

Chapter 4: Alternating donor-acceptor co-polymers built from unsaturated pyrrolidinone acceptors

4.1 Introduction

Chemically modified traditional dyes, pigments and their derivatives such as phthalocyanines, perylene bisimides, naphthalene bisimides, merocyanines, and diketopyrrolopyrroles have attracted considerable attention, in the past few decades as organic semiconductor materials both as polymers and small molecules.[71,174,176,193-197] Higher absorptivity and broder absorption profile in the visible and near infrared (NIR) spectral region, lower band gaps and higher environmental stability make them promising candidates for OPV's as a renewable energy source in future, due to their low cost, light weight, and solution processability.[74,198-205] In recent years PSC materials have witness great success with overall PCE reaching the range of 9%.[119] The Eg^{opt}, E_{HOMO} and E_{LUMO} of conjugated polymers are amongst the most important parameters for determining the performances of the PSC with respect to the common acceptor PCBM.[98] The photon flux density of the solar spectrum is highest in the wavelength range from red (uv-vis) to near IR, so conjugated polymers need to absorb in this range to obtain the maximum photovoltaic effect. So it is very important to develop conjugated polymers with wider absorption range as well as high absorption coefficients to obtain maximum use of the solar flux.[206] So it is very important to design novel materials with low band gap between 1.2 eV to 1.9 eV with proper FMO energy levels to obtain optimize V_{oc} and efficient charge separation.[56]

Similar to "imide" functionalized materials, acceptors based on unsaturated pyrrolidinone units are gaining increasing attention in the organic electronic community due to their broad absorption characteristic and high charge carrier mobility in OTFT and

OPV studies. Among them Diketopyrrolopyrrole (DPP)[207,208] is prominent material due to its excellent electron-accepting ability which give rise to deeper HOMO energy values and low band gap polymers (figure 4.0). DPP is a fused bicyclic 8π electron system containing two lactam units. DPP based polymers blended with PCBM give rise to moderate solar cells efficiency. OPV performance of 5.28% were achieved for DPP-based polymer solar cells [198] and 4.4% [209] for the DPP-based small molecule alternatives. Similarly (E)-1H,10H-[3,30]biindolylidene-2,20-dione also known as iso-indigo (II) is a structural isomer of the well known pigment known as indigo (figure 4.0).[72,73,210,211] Unlike
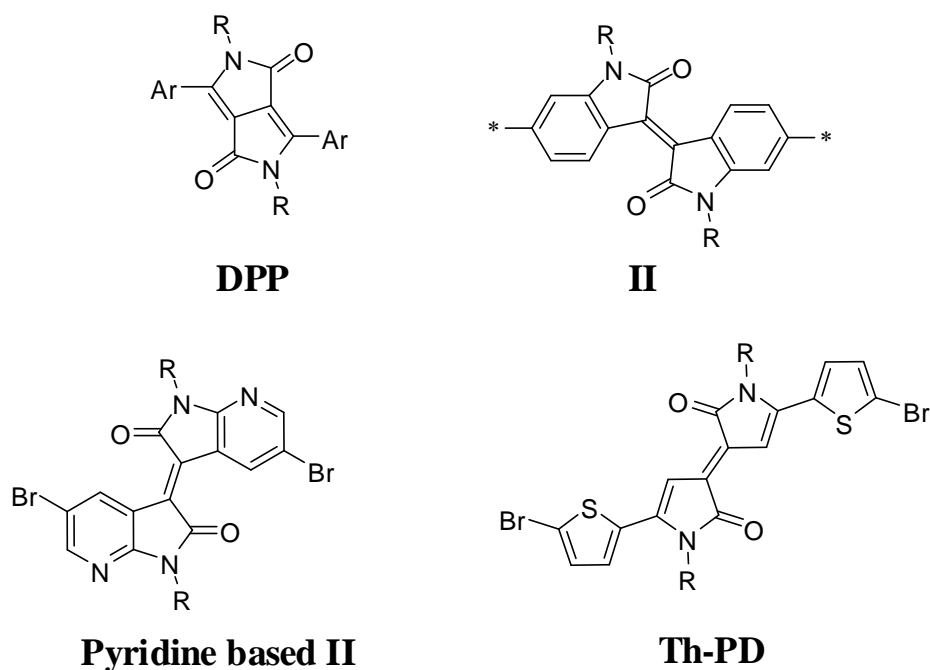
Figure 4.0: Popular and proposed organic semiconductor building blocks similar to NPD core.

blue colored indigo, the II has reddish brown color with absorption maxima around 365 nm and 490 nm in DMSO according to the literature. [210] Due to the extended conjugation length in II unit it can absorb and harvest more solar flux compare to most of the known acceptor materials. Reynolds *et al* first used this II unit to prepare D-A-D or A-D-A type

small molecules. They obtain OPV performance of 1.76% with a V_{oc} of 0.74 V.[73] They also incorporate this unit to prepare some D-A conjugated polymers.[211] Andersson et al also used this II unit to prepare D-A polymers and obtain OPV performance of 6.3%.[72]

This chapter introduces the first example of a novel suite of donor acceptor conjugated polymers built from pyrrolidinone derivatives of a known dye molecule the "Pechmann dye"(PD). The PD core has several similarities of the building blocks like DPP and II. (figure 4.0) The first PD was accidently prepared by Hans von Pechmann in 1882, when he was planning to prepare 1,4-napthoquinone from β-benzoylacrylic acid. von Pechmann was unable to propose a structure for this new compound.[48] After several debates on mechanism and structure, in the early 20th century Bogert and coworkers proposed it as a bifunctional lactone and referred it as "Pechmann Dye".[212,213] Since then this has demonstrated as a 3-butenolide dimer connected via an alkene bridge and containing a benzene ring at the 5 and 5' positions of the lactone rings. (figure 4.1)
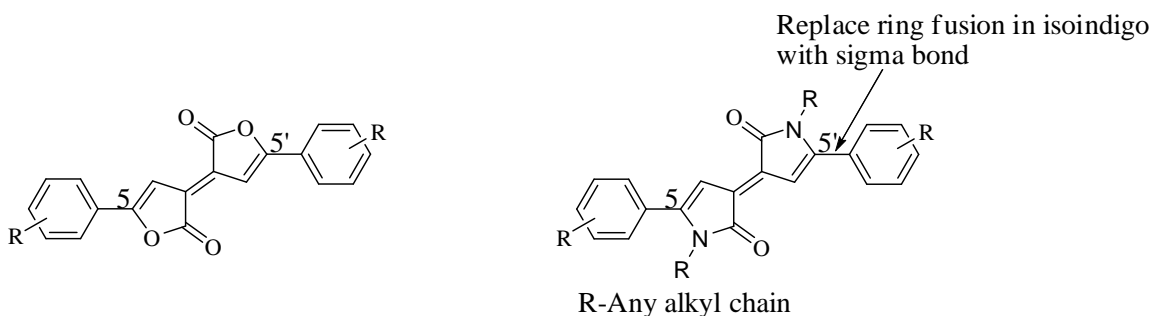
Figure 4.1: General Structure of Pechmann dye (left) and novel amidated acceptor monomer (right)

This so called PD is used as a red pigment. Due to its lower solubility most probably due to the strong intermolecular π-π interactions lower it use as a common dye molecule. In this study we used this PD core and functionalized it to a lactam to improve the solubility. We thought this unit may be an interesting acceptor unit for D-A conjugated

polymers. Up to now all the good organic semiconductor materials are derived from popular organic dye molecules as mentioned in the introduction section. Also this amidated Pechmann dye derivative has two electron withdrawing carbonyl groups to improve its electron withdrawing ability as the acceptor material similar to the DPP and II units. The open position of "N" gives ability to attach two alkyl chains to improve solubility which is very important in solution processing. This novel amidated Pechmann dye unit, now onwards abbreviated as NPD is closely related to the II unit. The main difference is in NPD, the fused phenyl ring in II is replaced by a sigma bond (figure 4.1). So the phenyl rings in NPD has more degree of freedom compare to II acceptor unit. Also compare to II unit the NPD unit has more extended conjugation. This is obvious if we compare the solid state colors of brominated II monomer unit and NPD monomer unit. Brominated II unit has deep red color,[210,211] compare to brominated NPD unit which has deep blue color with absorption maxima around 310 nm and 563 nm in 1×10^{-5} M chloroform solution (figure 4.4). According to this observation it seems to be the attached alkyl chains on "N" not disrupt the conjugation in NPD monomer unit. Also the brominated NPD monomer has similar uv-vis absorption profiles independent to the alkyl side chain attached on the "N" (figure 4.4). Sullevian *et al* [214] has prepared unbrominated thiophene (Th-PD) substituted pechmann dye derivatives without converting them to lactams and study their optical and electronic properties. According to them, these materials show thermal stability up to 250 ^{0}C. The 3-alkyl substituted Th-PD shows HOMO value of -5.31 eV and LUMO of -3.66 eV. According to the uv-vis profile unalkylated Th-PD shows λ max of 570 nm with absorption edge of 2.02 eV ($CHCl_3$: 1×10^{-7}M).[214] Here this unit shows relatively weak absorption band around 300 nm and

broad absorption band extending from 400 to 600 nm with 2 prominent shoulders.[214] If we compare our "N" substituted brominated NPD monomers with this literature recorded unit, it is obvious the absorption profiles (figure 4.4) are completely different. In our case we observe more prominent, relatively narrow absorption band around 300 nm range and broad featureless absorption profile extending from 400-700 nm range with λ max of 561 nm and absorption edge at 1.88 eV. It is not fair to do a direct comparison with this literature recorded unbrominated Th-PD lactone unit with our brominated NPD lactam unit (bromine can slightly red shift the absorption profile) due to their structural and substitutional differences because our NPD unit is a lactam with alkyl substitution on "N" which can cause steric crowding with adjacent units. The same group did some further study on this Th-PD system. In this study they convert this lactone to lactam and attached $-C_{12}H_{25}$ alkyl chain on to the lactam "N" .[215] The obtain uv-vis profile is somewhat similar to the uv-vis profile we got for our brominated NPD monomer. Now they also obtain more prominent bimodal absorption bands at ~333 nm and 613 nm range with onset of absorption at 1.75 eV.[215] The reason for the blue shift of our monomer absorption profile with respect to the literature recorded values may be due to the steric effects caused by six membered phenyl rings over the five membered thiophene rings or strong intramolecular charge transfer in presence of more electron rich thiophene over benzene which has higher aromatic stabilization energy respect to the thiophene.[215] But we can conclude our NPD monomer is not significantly twisted by introducing phenyl rings instead of attaching thiophene in the 5,5' position of the 3-butenolide dimer connected via an alkene bridge. [214] According to the X-ray crystal structure study done by Trotter *et al* has shown the actual PD core with phenyl rings is co-planar.[216] But after

introducing alkyl chains on to the "N" can cause some steric crowding with the adjacent phenyl rings.

From these observations we can conclude this novel NPD unit as a possible novel acceptor moiety for donor-acceptor (D-A) material within the organic semiconductor field with cross-conjugated electron withdrawing carbonyl groups. Already this moiety itself exhibits a donor-acceptor-donor (D-A-D) motif and can expect large effective intermolecular overlaps and efficient charge transfer in the solid state.[217] These type of "quadrupolar" molecules have received great attention due to their high two photon absorption cross sections which can change its quadrupolar moment upon photo excitation.[218-220] Also amidation of the lactone ring with aryl- or alkyl amines allows the manipulation of solubility, packing and morphology. In all, we can state the NPD unit is an attractive candidate for electron-accepting co-monomer in novel series of donor-acceptor polymers which was not sufficiently appreciated yet. Thus, the present work we have combined the NPD as an acceptor unit with BDT, CPDT and IDT donor unit as a new D-A co-polymer family. So in this project our main priorities are,

1. How replacing the ring fusion in II unit by sigma bond, effect to the optical and electronic properties of NPD unit.

2. How different donor units and substituent's effect to the optical and electronic properties of the NPD based co-polymers.

3. Investigate these novel co-polymers have suitable properties for OPV applications.

4.2 Synthesis of monomers and donor-acceptor polymers based on PD unit
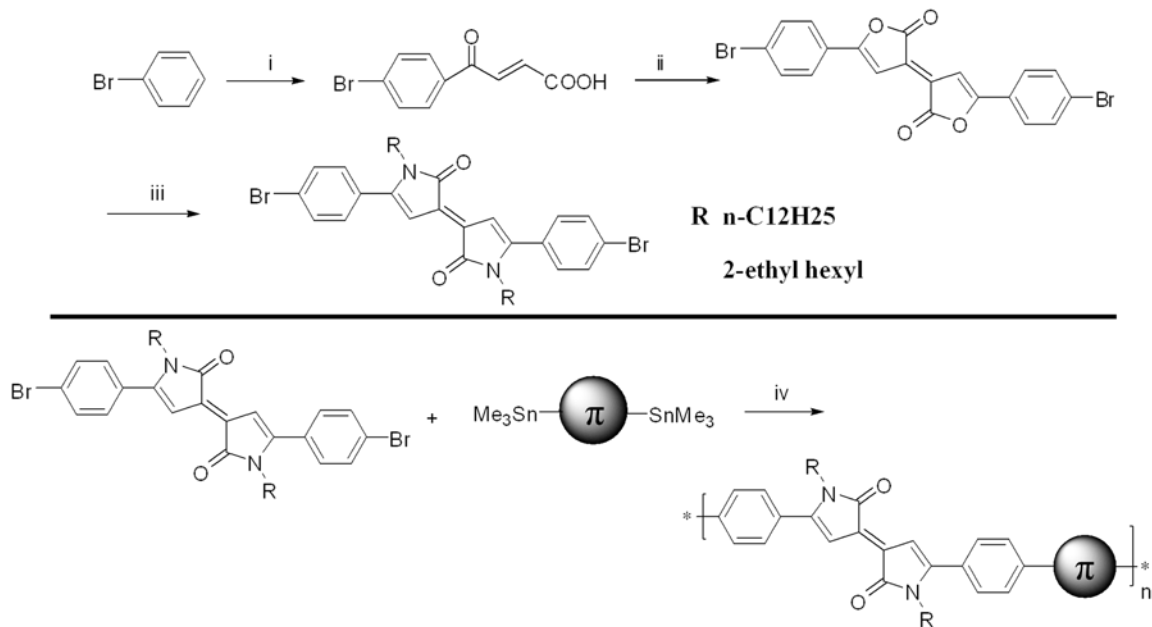
Figure 4.2: Synthesis scheme for monomers (top) and polymers (bottom). i. maleic anhydride, anhydrous AlCl$_3$, Dry DCM,rt;90% ii. Cat CuCl/NH$_4$Cl, AC$_2$O, 140 ^{0}C;65% iii.R-NH$_2$, glacial AcOH, 140 ^{0}C, 3hrs.;10-20% iv. Pd$_2$(dba)$_3$, P (O-tolyl)$_3$, Anhydrous THF, 80 ^{0}C.

Friedel-Crafts acylation of bromobenzene with maleic anhydride afforded the yellow colored (2E)-4-(4-bromophenyl)-4-oxo-2-butenoic acid in high yield (~ 90%) without further purification. Maroonish red Pechmann dye core was prepared according to the procedure proposed by Bergmann in presence of catalytic amount of NH$_4$Cl and anhydrous CuCl in 65% yield after recrystallizing the crude in the presence of glacial acetic acid.[221] Then the Pechmann dye core was converted to a lactam derivative in the presence of corresponding alkyl amine in glacial acetic acid under N$_2$ atmosphere. Corresponding brominated monomers then polymerize with different donors. The synthesized polymers are depicted in figure 4.3. Details on synthesis and characterization can found in experimental section.
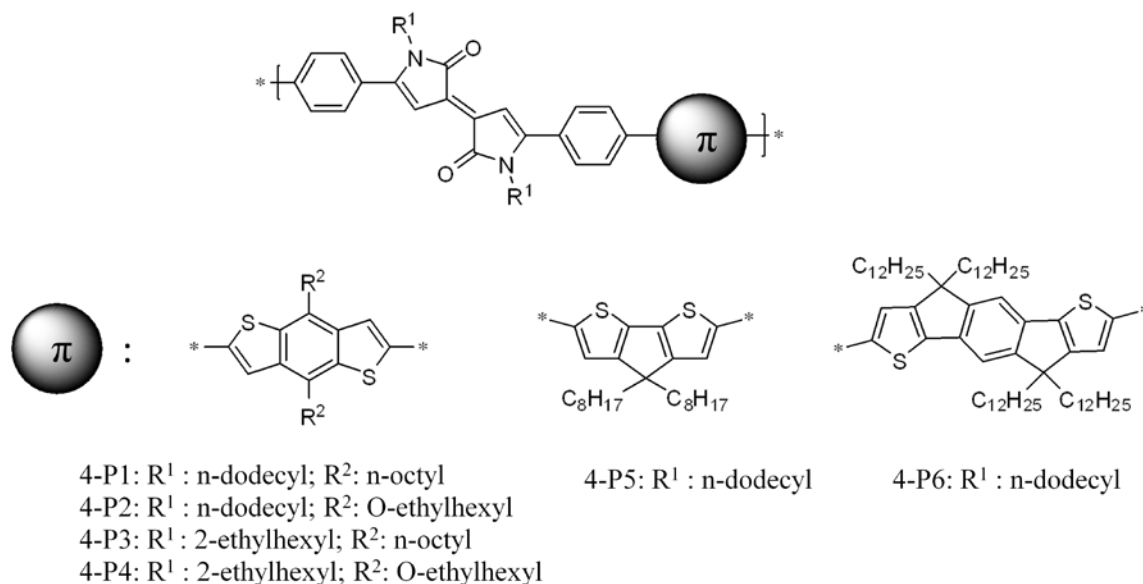
Figure 4.3: NPD-thiophene co-polymers

For all these polymers the molecular weight (Mn) could not measure due to the poor solubility in THF at room temperature. This may be due to the highly aggregating tendency of the corresponding NPD-co-polymers due to the strong π-π intermolecular interactions. Polymers have solubility in chlorinated solvent like hot chloroform (50 ^{0}C) and chlorobenzene and 1,2-dichlorobenzene at ambient temperatures. But in future studies it is very important to graft more bulky branch chains on NPD "N" to obtain better solubility compare to these polymers.

4.3 Optical, electronic properties and self assembly of NPD co-polymers

The optical properties of NPD polymers were investigated using uv-vis absorption measurements of chloroform solutions and spin cast films (figure 4.4) and their absorption data are listed in table 4.0. In solution, all the polymers exhibited two distinct absorption bands with maxima at about 620-660 nm (A$_1$) and 376-419 nm (A$_2$) range,

polymers **4-P1** to **4-P4** the short wavelength absorption band hardly differs in their position upon changing the alkyl-substitution in the D and A units. In any case, pre-bands

Table 4.0: Properties of PD Polymers 4-P1- 4-P6

Polymer	yield (%)	Td^a (°C)	λ_{max}^b (soln) (nm)	λ_{max} (film)^c (nm)	$\Delta \lambda_{max}$ soln-film (nm)	λ_{onset}(film)^c (nm)
4-P1	83	341.05	615/376	630/386	15/10	776
4-P2	84	324.89	623/378	657/390	41/13	810
4-P3	82	357.35	616/377	623/378	07/01	756
4-P4	82	327.31	619/377	628/377	09/00	756
4-P5	74	372.68	653/419	658/421	5/2	775
4-P6	48	350.05	635/421	640/420	5/1	745

^{a}Td 5% weight loss temperature according to the TGA under N_2. ^{b} $1x10^{-5}$ M in cholorform. ^{b} Pristine film spun-cast from 1 mg/ml cholorbenzene solution.

at around 740 nm are observed for the n-dodecyl substituted polymers (**4-P1**, **4-P2**), indicating some aggregated polymers (as can be seen from comparison with the absorption spectra of the spin-coated films, see figure 4.4), which points to decreased solubility compared to the n-ethylhexyl counterparts (**4-P3** and **4-P4**). In order to understand the electronic and optical properties of the new co-polymer system our collaborator Dr. Johannes Gierschner performed some (time-dependent) density functional theory (TD)DFT calculations on the NPD-BDT donor unit. For the frontier molecular orbital (MO) correlation diagram of the monomer with the NPD and BDT moieties, see figure 4.5. [The geometries were optimized without symmetry constrictions employing the B3LYP functional and 6-311G* basis set as described in the Gaussian09
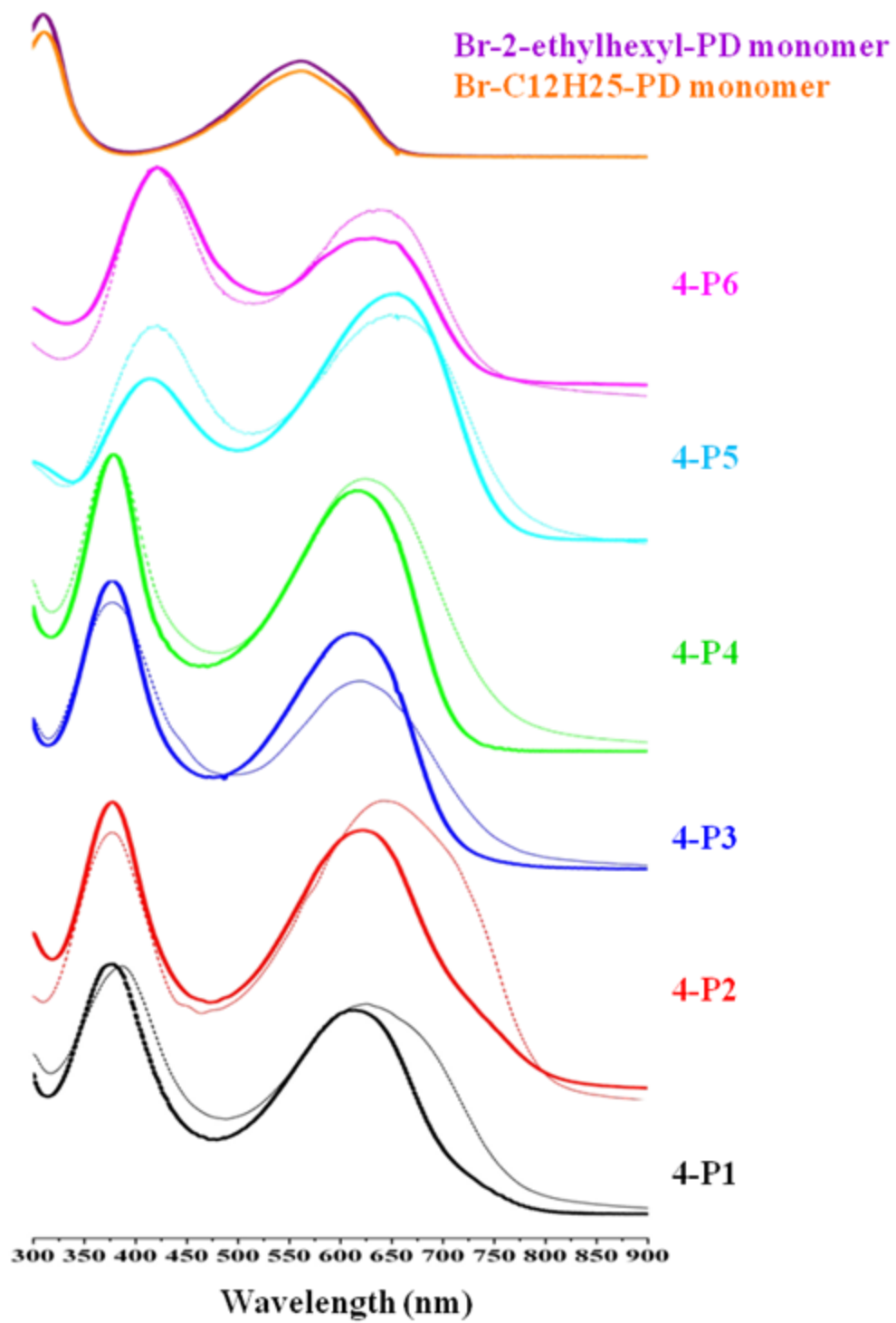
Figure 4.4: Normalized UV-vis spectra of NPD brominated monomers (top) and co-polymers. Solution (Solid lines; 1 x 10^{-5} M in CHCl$_3$); as-cast films (dotted lines; spin

coating (1mg/ml, chlorobenzene) onto quartz plates) All measurements were done at room temperature.

program package (Frisch, M. J.; et al, Gaussian 09, Revision A.02, Gaussian, Inc., Wallingford CT, 2009). The MOs toplogies were plotted with Molekel (P. Flükiger,H. P. Lüthi, S. Portmann, J. Weber, MOLEKEL, Version 4.3;Swiss National Computing Centre CSCS, Manno, Switzerland, 2000, http://www.cscs.ch/molkel/). The electronic situation in the NPD is distinctively different to the majority of the D-A co-polymers. The latter are characterized by an energy gain of both, the highest occupied and lowest occupied MOs (HOMO, LUMO) of A against D, so that the HOMO is located mainly on D and the LUMO mainly on A. In the NPD unit, however, both HOMO and LUMO are located almost exclusively on the NPD unit. This is due to the fact that (i) the frontier MOs of NPD are located within the gap of BDT, (ii) the LUMO offset is too large ($\Delta LUMO_{D-A}$ = 1.76 eV) to form a common LUMO, and (iii) a common HOMO cannot be formed due to symmetry reasons. Thus, the A_1 band, which corresponds to the transition from the ground to the first excited state and is mainly described by an HOMO to LUMO excitation is a localized intra- NPD unit π-π^* type transition, different to common D-A polymers where the first excited state exhibits typically substantial charge transfer (CT) character due to localized LUMOs;[222,223] or as recently reported, due to localized HOMOs.[151] Differently, the A_2 band of the NPD, mainly described by a HOMO to LUMO+1 excitation, exhibits strong charge transfer (CT) character due to the particular electronic configuration in the NPD. The bimodal absorption profile is kind of characterizing to the NPD co-polymers. This kind of bimodal absorption profiles can be observed in D-A polymeric systems incorporate with fluorine units.[224,225] But to get a more detail idea about the electronic properties, we have to do the (TD) DFT

calculations on higher oligomers of the NPD-BDT system. But according to these calculations it seems to be this NPD co-polymers are not behaving like traditional D-A polymers. Compare to the
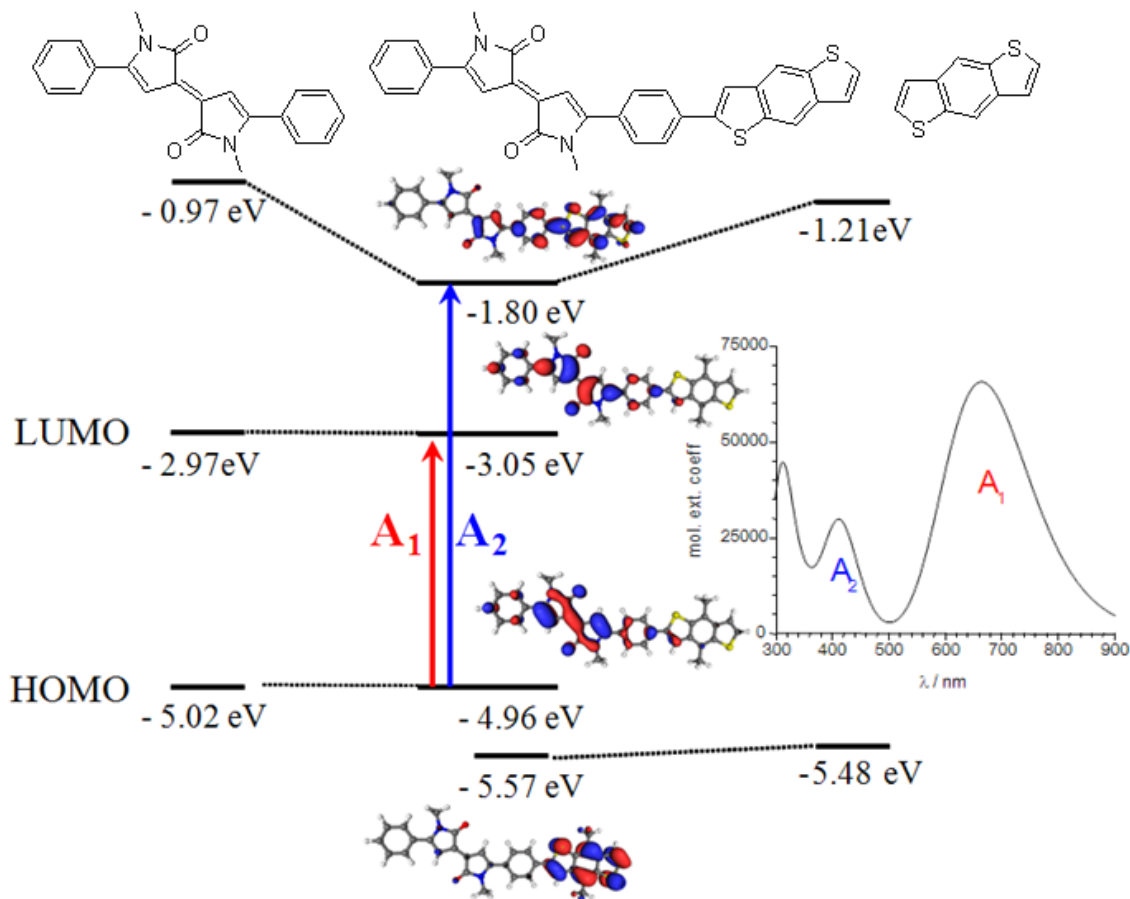
Figure 4.5: DFT calculated MO correlation diagram for the NPD-BDT co-monomer; the TD-DFT calculated absorption spectrum is shown as an inset.

NPD-BDT co-polymers, corresponding II-BDT co-polymers do not show this type of significant bimodal absorption profile. But in the study done by Andersson *et al* using II-BDT co-polymers show bimodal absorption profile but the short wave length absorption band is not very distinct compare to our NPD-BDT polymers.[226] Several other groups also worked on this same system, (II-BDT co-polymers) but in their study the short

wavelength absorption band is less distinct compare to the study done by Andersson et al.[210,211,227,228]

Both Chunyue Pan *et al*[227] and Zhang *et al*[210] have prepared the same II-BDT polymer with 2-ethyl hexyl branch side chains on II unit and 2-ethyl hexyloxy side chains on BDT. This system is somewhat similar to our polymer **4-P4**. According to the Chunyue Pan *et al* and Zhang *et al* this II-BDT polymer has similar absorption profiles for both solution and film measurements. Not only these two groups, all the other groups which work on this II unit with different donor systems (fused or non fused donor units) also observe this similar trend in their uv-vis absorption profiles.[72,211,227,228] In our study also all the polymers with NPD units give similar absorption profiles both in solution and solid phase. According to the literature the reason for this behavior may be due to the aggregation or weak π-π stacking in the solid phase. But according to the previous study done on TFB co-polymers (chapter 2) we can state that this behavior is most probably due to the high aggregation tendency in these big π units through intermolecular interactions. Again if we compare our polymer **4-P4** with literature recorded polymer II-BDT with 2-ethyl hexyloxy chains, it is clear that the II-BDT co-polymers have red shifted absorption profiles compare to the NPD-BDT unit. The shift of λ_{max} in long wavelength absorption band is approximately 54 nm. If we compare the onset of absorption in these polymers our NPD-BDT polymer, **4-P4** show 756 nm (Eg^{opt}~1.64 eV), the II-BDT, 2-ethylhexyloxy polymer recorded by Chunyue Pan *et al* shows 782 nm (Eg^{opt}~1.58 eV) and the polymer synthesized by Zhang *et al* shows 763 nm (Eg^{opt}~1.62 eV). The molecular weight of the polymer recorded by Chunyue Pan *at al* is 11 kDa (PDI= 2.2) and it gives PCE of 0.9%. The polymer recorded by Zhang *et al* has molecular

weight of 22 kDa (PDI=1.5) with a PCE of 1.91%. Both these polymers show relatively high molecular weights. The reason for the blue shift in our polymer **4-P4** compare to the literature recorded II-BDT, 2-ethylhexyloxy polymer may be due to the low molecular weight (the polymer did not reach to its effective conjugation length) due to the poor solubility in the reaction medium. Another reason for this observed blue shift may be due to the replacing of the ring fusion in II unit with a sigma bond in NDT unit. Now our resulted NPD unit, phenyl rings have more degree of freedom, so it cause backbone twisting to reduce the steric crowding with adjacent 2-ethylhexyl chains by lowering the effective conjugation. Another reason for this observed blue shift may be due to the presence of unsubstituted phenyl ring in the NPD unit which can lower the delocalization of electron density due to the higher aromatic resonance stabilization energy.

Another interesting feature in this NPD co-polymer series is that when going from NPD monomer to the polymer (see figure 4.4), we cannot see much shifting in the resulted polymer absorption profile. The resulted red shift is in the ~ 70-50 nm range. But in traditional D-A polymers normally we can observe huge red shift ~ 200 nm or more when going from monomers to polymers. Again the reason for this observation may be due to the localization of both HOMO and LUMO on the NPD unit according to the DFT calculations. So this NPD co-polymer system not behaving likes traditional D-A polymers which we discussed in earlier chapters and recorded in the literature.

All the NPD-BDT polymers show broad absorption profiles extend to 800 nm. with higher absorption coefficient in ~ 10^4 $mol^{-1}.cm^{-1}.L$ range. Relatively strong interactions are observed for **4-P2** which shows a solid-state shift ($\Delta\lambda$ onset~ 54 nm) compared to **4-P4**, which shares the same donor motif. A similar effect, although much

less pronounced, can be observed comparing the **4-P1** and **4-P3** polymers. As observed before by us and others this shows once more the subtle impact of the side-chains on the solid state organization, which has to be carefully engineered to optimize the polymer layers for device application. In this respect, the N-functionalization with long linear alky chains (**4-P1**, **4-P2**) certainly helps in the crystallization of the polymers. This is clearly obvious in the WAXD measurements of the polymer **4-P1** and **4-P2** clearly indicating meridional and lamellar diffraction arcs. As mentioned earlier to further gain some idea

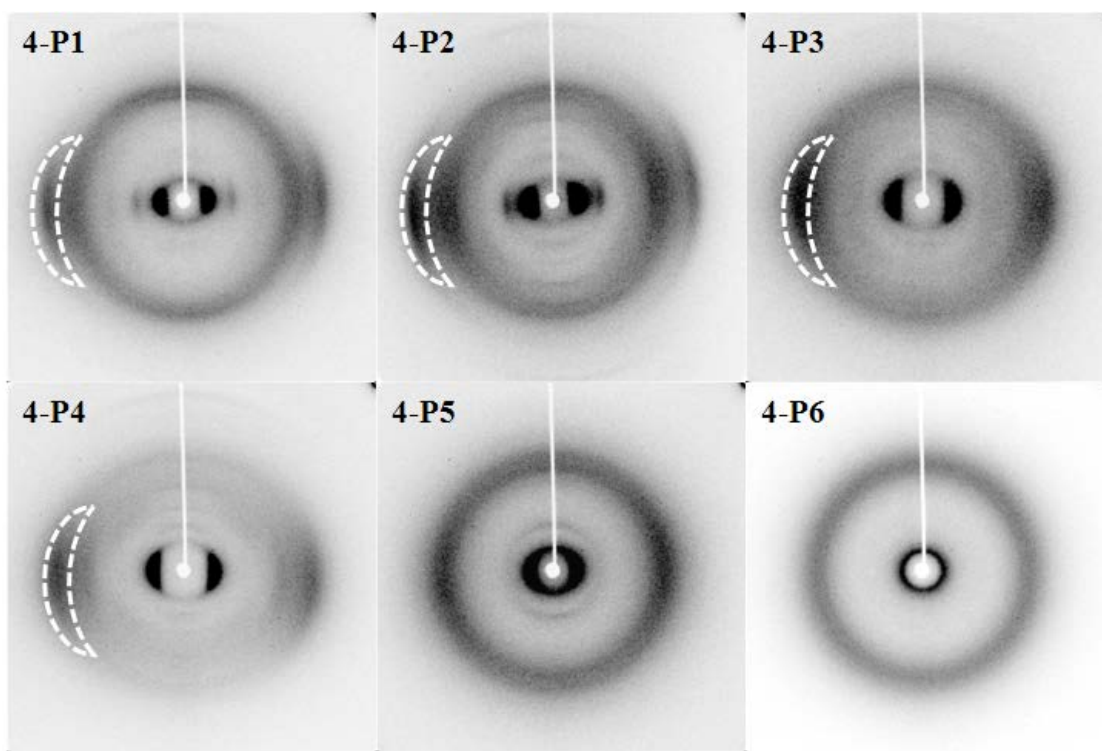**Figure 4.6**: Fiber WAXD diffractograms from polymers **4-P1** to **4-P6** (not annealed)

about how different fused ring systems behave in this novel system, we further prepared another 2 polymers using n-dodecyl substituted NPD as acceptor unit and using CPDT and IDT as the donor units. Both these 2 polymers show red shifted λ max in solid state measurements compare to NPD-BDT polymers **4-P1**, **4-P3** and **4-P4**. Both this NPD-

CPDT and NPD-IDT polymers show similar λ max values both in solution and solid state measurements. The reason for these observations may be due to the aggregation of polymer chains in presence of intermolecular interactions or there is no any distinct order in solid state compare to the solution phase. To get an idea about solid state registry we obtain the WAXD data of these polymers. Except polymer **4-P5** and **4-P6**, all the other NPD polymers show some solid state registry. NPD polymers of **4-P1**,**4-P2** and **4-P4** show more pronounced solid state packing compare to all the other polymers. Again similar to TPD-IDT polymer (chapter 3) NPD-IDT polymer does not show any solid state registry. This is due to the presence of high orthogonal side chain density which distrupt the close packing of polymer backbones and lower the solid state registry. In this series of polymers both acceptor unit and donor unit has alkyl substituents, so in presence of high alkyl side chain density, it is very difficult to obtain enough space filling for adjacent polymer backbones to obtain closer π stacking and long range solid state order. This is clearly obvious in uv-vis profiles, clearly indicating there is no any difference between solution and solid state absorption profiles, indicating highly disordered solid state. The polymer **4-P5** also show more amorphous nature although it shows weak meridional arc. Again this polymer also has similar uv-vis profiles in both solution and solid state, clearly indicating the solid state is highly disordered. All the X ray fibers were extruded at 90 ^{0}C and did not do any thermal treatment other than that. Compare to all the six polymers NPD-alkoxy BDT polymers show more ordered solid state arrangement. The reason to this behavior may be due to the intramolecular charge transfer as explained in the TPD polymers in chapter 3. So due to this backbone become more co-planar and rigid. The polymers with linear alkyl chain on NPD "N" show closer π stacking compare to the

branch alkyl version of NPD. The literature on II-BDT co-polymers not mentioning anything about the solid state registry of these polymers. So we cannot compare this group of polymers with our NPD polymers effectively regarding the solid state packing arrangement.

Table 4.1: Data collected from diffraction patterns in figures 4.6

Polymer	Lamellar spacing, L, L/2, L/3 (Å)	"d" π-spacing (Å)	Meridional Maxima (Å)
4-P1	18.44, 9.62, 4.34	3.56	4.40
4-P2	18.29, 9.8, 4.5	3.50	10.52,7.32, 4.39
4-P3	14.51	3.95	-
4-P4	14.48, 4.83	3.78	10.43, 7.46, 4.25
4-P5	19.41	4.35	11.11
4-P6	-	-	-

4.4 Electrochemistry of polymers

Differential Pulse Voltammetry (DPV) measurements were obtained using

Table 4.2: Electrochemical and optical data for polymers

Polymer	E_{ox} (V) [a]	E_{HOMO} (eV) [b]	E_{LUMO} (eV) [c]	$E_g{}^{opt}$ (eV) [d]
4-P1	0.593∓0.087	-5.393∓0.087	-3.79∓0.087	1.60
4-P2	0.513∓0.005	-5.313∓0.005	-3.78∓0.005	1.53
4-P3	0.590∓0.002	-5.390∓0.002	-3.75∓0.002	1.64
4-P4	0.503∓0.040	-5.303∓0.040	-3.66∓0.040	1.64
4-P5	0.583∓0.006	-5.383∓0.006	-3.78∓0.006	1.60
4-P6	1.510∓0.022	-6.31∓0.022	-4.65∓0.022	1.66

Experimental conditions: 0.1 M (n-Bu)$_4$N.PF$_6$ in anhydrous acetonitrile as supporting electrolyte, platinum disc as working electrode, platinum wire as counter electrode, silver wire as reference electrode and Fe/Fe$^+$ (-4.8 eV vs vacuum) as reference, scanning rate: 50 mV/s; All measurements conducted on solution-cast thin films under nitrogen. [a]Corrected E$_{ox}$ value respect to Fc/Fc$^+$. [b]E_{HOMO} = -[4.8+(E$_{ox}$-Fc/Fc$^+$)], E$_{ox}$ calculated using onset of DPV measurements (Oxidation peak). [c] E_{LUMO} = E_g^{opt} + E_{HOMO}. [d] E_g^{opt} Optical band gap estimated from the absorption edge of the film.

polymer films cast on a Pt button electrode to get an idea about FMO energy levels. All

the measurements were carried under N$_2$ atmosphere using 0.1 M (n-Bu)$_4$N.PF$_6$ as the

supporting electrolyte in anhydrous acetronitrile solution. All the results are summarized

in table 4.2. As estimated from the oxidation potentials, the HOMO energies of **4-P1**, **4-P3** (5.39 eV) are somewhat stabilized against the **4-P2**, **4-P4** counterparts (5.30 eV). But

this difference is relatively low (~ 0.08-0.087 eV). According to the DFT calculation

done by our collaborator the HOMO energy is localized on the acceptor. So changing

from alkyl BDT to alkoxy BDT cannot have substantial effect on the resulted polymer

HOMOs. Sometimes the difference may be due to the different packing arrangement.

Both **4-P3** and **4-P4** show similar solid state packing arrangement according to the

WAXD profiles compare to the polymers **4-P1** and **4-P3**. But to get clear idea we have to

do some DFT calculations using higher oligomers. The low lying HOMO levels of all the

polymers makes them less vulnerable against air oxidation and suggests higher V_{oc}

values in OPV operation. Both linear dodecyl NPD-CPDT (**4-P5**) and NPD-IDT(**4-P6**)

polymers also showed very stable HOMO values. From all these six polymers the

polymer **4-P6** shows the deepest HOMO energy value. This may be due to the highly

twisting of the polymer backbone due to the high orthogonal side chain density. Again

this polymer does not show any solid state registry in WAXD measurements but showed

broad absorption profile in uv-vis measurement. Again if we compare the previously

mentioned II-BDT polymers with our NDP polymer **4-P4**, the polymer **4-P4** show deeper

HOMO values. (-5.30 eV). The HOMO values recorded for II-BDT with 2-ethyl hexyl

side chains are in the rage of -5.11 eV (Chunyue Pan *et al*) and -5.20 eV (Zhang *et al*). As

mentioned earlier this difference may be due to the twisting of the polymer backbone due

to the more rotational freedom of phenyl ring in the presence of steric crowding due to

the adjacent alkyl chain attached to the "N" or due to the lower electron delocalization in
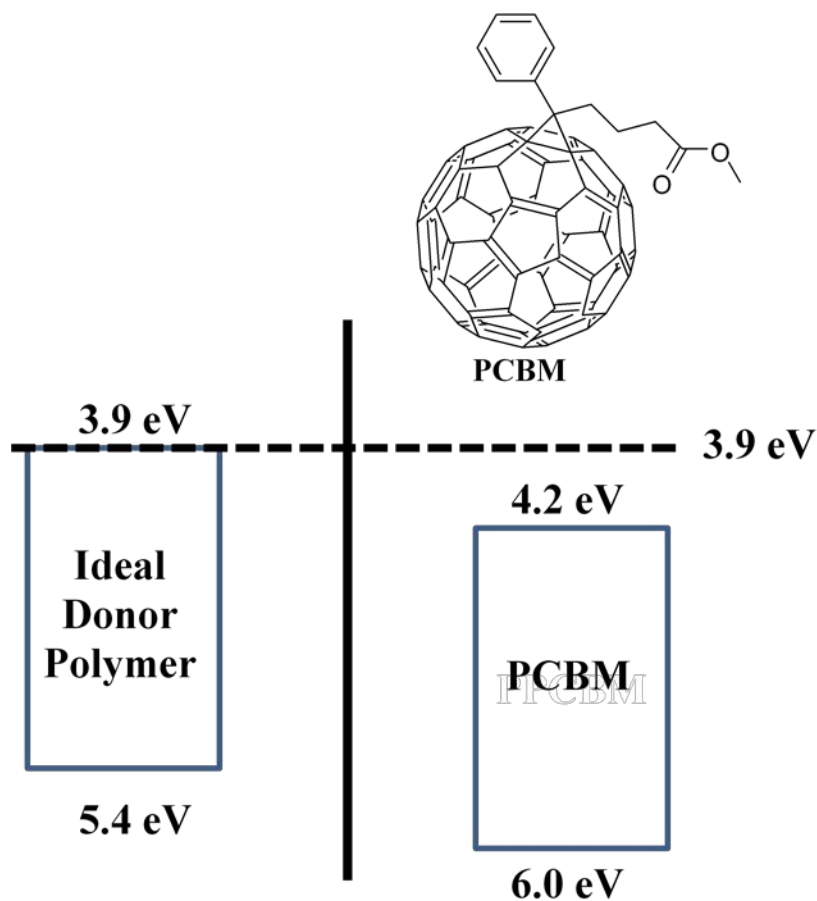
presence of phenyl ring on the NPD unit.

Figure 4.7: FMO energy levels of the ideal donor polymer with respect to PCBM[5]

According to the device engineers the ideal polymeric material should have following

energy levels with respect to the common acceptor PCBM to get the idealistic PCE value

of 10%.[47] So the ideal polymer should have a HOMO around ~ -5.4 eV with respect to the vacuum level and Eg^{opt} around 1.5 eV. If we think about our novel polymer system they exactly show electronic properties similar to this ideal polymer with broad absorption profile. So we can conclude this novel polymer material may be a good candidate as the donor material for bulk-heterojunction solar cells. But still we did not do any device measurements using these polymer systems.

4.5 Thermal analysis of polymers

Thermogravimetric analyses (TGA) indicate that all polymers are stable up to about ~300 ^{0}C (table 4.0). Except polymers **4-P2** and **4-P4** all the other 4 polymers show mainly single weight lose. But the polymers **4-P2** and **4-P4** show two prominent weight loses. Here the first low temperature weight lost may be due to the elimination of alkoxy ethyl hexyl chains grafted on BDT unit and the high temperature second weight lost may be due to the elimination of lactam alkyl chain on NPD unit. All the polymers did not show any melting transition up to 300 ^{0}C in differential scanning calorimetry study (DSC);. However, **4-P1** and **4-P2** showed an irreversible exothermic transition around 167 ^{0}C and 163 ^{0}C respectively which might be due to segmental motion of the linear alkyl chains. Differently, **4-P3** ,**4-P4**, **4-P5** and **4-P6** did not show any transitions during the heating scans. None of the polymers show any transitions in the cooling scans.

4.6 Conclusions

Here we have showed the synthesis and structure property study a suite of novel donor-acceptor (D-A) conjugated polymers using a novel acceptor moiety derived from a Pechmann dye core (PD) as an acceptor and BDT, CPDT and IDT as donors, synthesized by Stille coupling reaction. All polymers except **4-P6** have LUMO levels comprised in

the -3.74 eV To -3.79 eV range and HOMO levels comprised in the -5.30 eV to -5.39eV range, with solid state band gaps around ~ 1.6 eV. Different to common D-A polymers the HOMO and LUMO of the NPD acceptor moiety are energetically located within the gap of the BDT, so that the electronic and optical properties (HOMO-LUMO transition) are dictated by the NPD unit. The promising electronic properties, band gaps, high absorption coefficients and broad absorption suggest the new D-A polymers as an interesting donor material for OPV applications. Future work will focus on oligomer studies. Compare to well-known acceptor material II, this NPD unit give relatively blue shifted absorption profiles. The reason for this observation may be introducing more rotational freedom to the NPD unit by replacing the ring fusion by a sigma bond. So according to the experimental evidence it seem to be II unit is more coplanar compare to our NPD unit. Electrochemical data also shows II polymers have less deeper E_{HOMO} values compare to the corresponding NPD polymers suggesting more co-planarity and extended conjugation in the polymer. But if we think about monomer alone the absorption profile of the II monomer is more blue shifted relative to the NPD monomer. So sometimes the observed blue shift in the polymer measurements may be due to the low molecular weight of the resulted NPD polymers due to their poor solubility in THF which was the reaction medium. So in future studies on this system, it is very important to attached more bulky alkyl side chains to obtain better solubility. In this preliminary study on this novel acceptor, it seems to be, this unit can be a promising candidate for OPV study according its opto-electronic properties.

Chapter 5: Outlook and future plans

Still there are more potential areas to explore in these three projects, which I have discussed in this dissertation. Up to now we were able to improve optical, electronic and solid state packing arrangement of these D-A co-polymers by careful choice of donor and acceptor unit. Basically in this chapter more priority goes to the improvement of fluorinated arene (TFB) based polymers and modified unsaturated pyrrolidinone based NPD polymers. Currently we are not interested to work on thiophene imide (TPD) based D-A polymers because this is one of the most popular acceptor material in the organic electronic field at the moment.

5.1 Fluorinated-arene based D-A co-polymers

From this study it was obvious that TFB polymers with linear alkyl chains have much higher oxidation potentials. According to the device studies also it was obvious that these polymers show resistance to oxidative doping by ambient air because their transistors show high current modulation. ($\sim 10^5$ range) when measured in air. But we did not do any long term device stability study regarding to these polymers. Based on current device measurements, it is suggested that longer alkyl chains give better device performance. This may be due to the good film forming ability (better solubility) and longer the alkyl chain it is easy to have good inter-lock with adjacent backbone side chains. Up to now I have prepared only polymers with linear alkyl chains. So it will be interesting to see how branched alkyl chains affect the structure-property studies of this series of polymers. So my future plan is to prepare this below series of polymers (figure 5.0) and study their structure-property relations. The side chains with n =1,2,3… are commercially available as bromides or alcohols. The polymer with n = 1 was previously prepared by Yongfeng Wang in our group using oxidative polymerization technique using anhydrous $FeCl_3$ but not studied extensively.
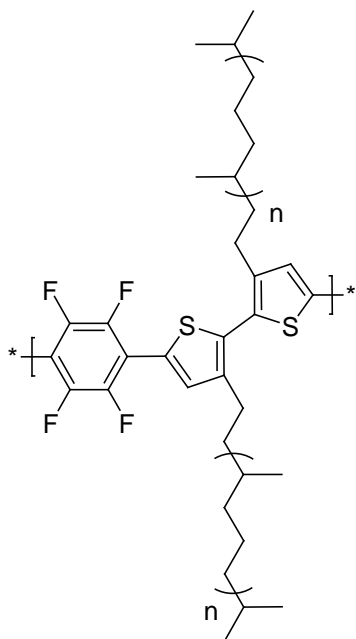
Figure 5.0: Proposed chemical structure of the branch 3,3'-R2T2 TFB co-polymers

Incorporation of alkoxy side chains, destabilize the HOMO energy value. This was clearly obvious when we compare linear alkoxy polymer 2-P4 with the alkyl-substituted polymers. But we were able to engineer the FMO energies, relative conjugation, solubility and solid state order by incoperating steric bulk closer to the polymer backbone. So to obtain clear idea about how branched alkoxy chains alter the FMO energy values it's better to synthesize the above series of polymers by changing branching length and branching position (figure: 5.1). Here R and R' denote alkyl side chains with different number of carbon atoms. As discussed in chapter 2, I have already prepared several polymers having α branch chains with six carbons long main chain and varying the branching length. But this polymers were not soluble in THF so could not obtain the molecular weights. It may be a good idea to do a similar study using more lengthy chain with carbon 12 or more. Then we can easily obtain better solubility. Also we can study the branching effect on the β position by selectively varying the branching position and length of the substituents. From these studies we can obtain more detail view on how branching effect to the optical, electronic and solid state registry in the D-A co-polymers.
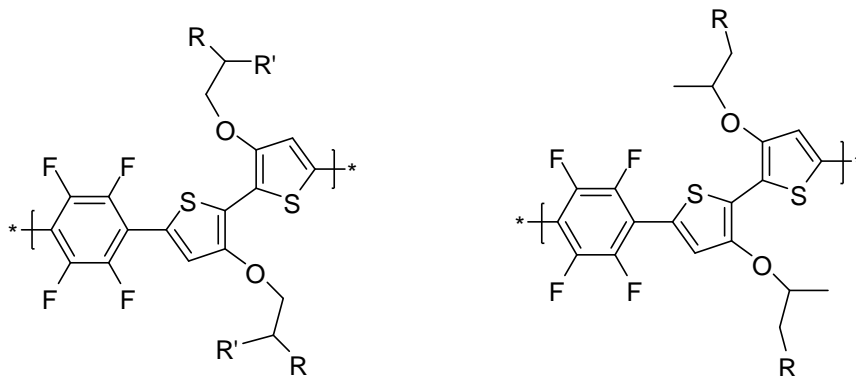
Figure 5.1: Proposed chemical structure of the α and β branch 3,3'-RO2T2 TFB co-polymers.

5.2 Unsaturated pyrrolidinone based D-A co-polymers

This is a completely new molecule in organic electronic field based on Pechmann dye
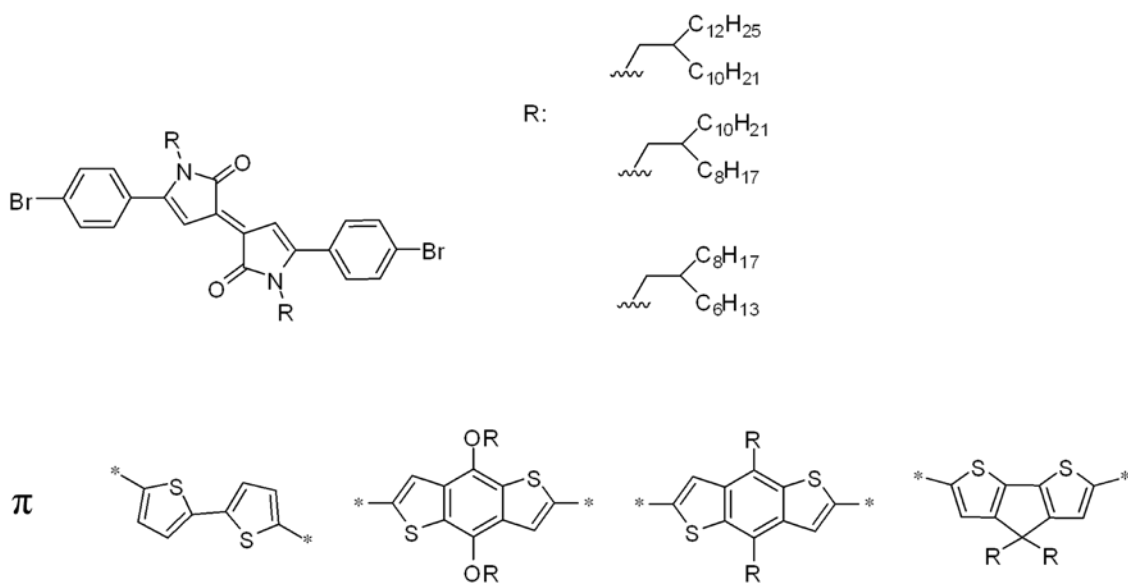

Figure 5.2: Proposed chemical structures of unsaturated pyrrolidinone derivatives based co-polymers.

derivative as discussed in chapter 4. During my research career I have prepared only six polymers using this unit. So there is more room to explore on this novel material. It's a good idea to incorporate bulky branch chains to improve solubility. Some of the commonly used branch

substituent in organic electronic field is depicted in figure 5.3. It is better to prepare some more D-A co-polymers using this novel system to get a broad idea about their structure property studies. Also using this material we can prepare some oligomers and study their properties for organic semiconductor based applications. If we think about the oligomer study we can prepare two types of oligomers based on general structure D-A-D or A-D-A. Actually this Pechmann dye derivative itself has D-A-D nature and can state it as a "push-pull-chromophore" .

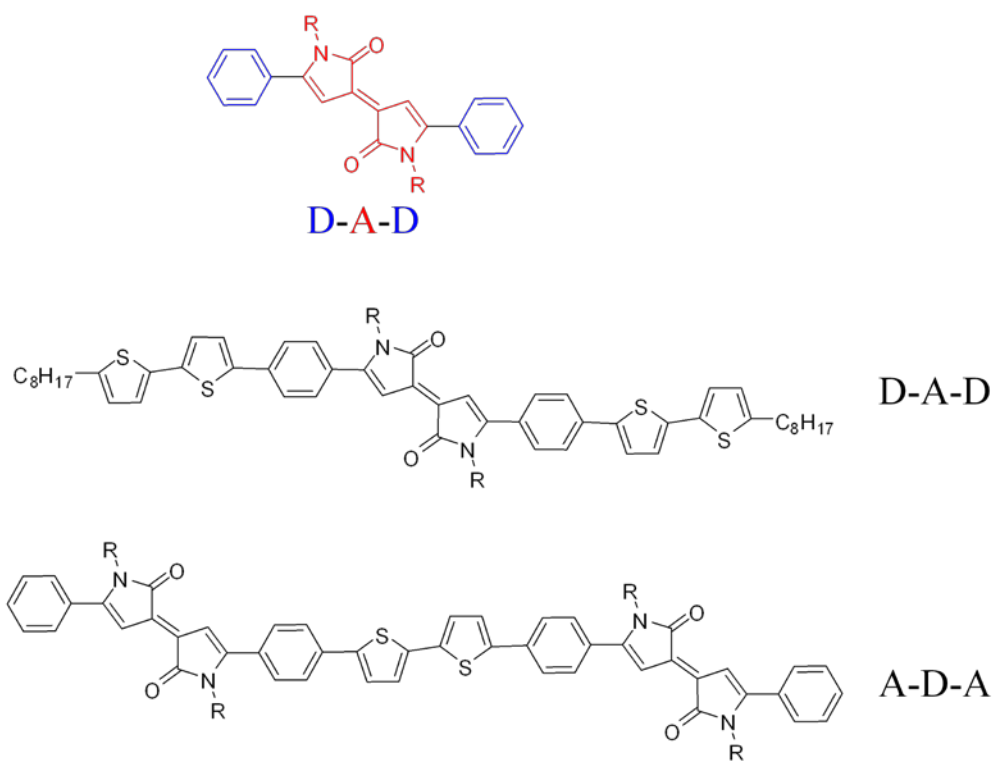**Figure 5.3**: General structure of donor-acceptor-donor nature in Pechmann dye derivative. (top) and proposed D-A-D and A-D-A oligomer architecture.

Compare to polymers, oligomers have several advantages, such as monodisperse nature, well defined structure, easy purification methods, higher solubility, no-end group contamination and can easily obtain reproducible results. Reynolds *at al* has used this D-A-D and A-D-A strategy to

prepare some oligomers using isoindigo unit which is structurally simillar to our Pechmann dye

derivative which was extensively discussed in chapter 4. Another modification we can do to this

Pechmann dye derivative is to replace phenyl ring with a thiophene moiety and prepare D-A

polymers using that system. Sullivan *et al* has done some study on this system. As discussed in

chapter 4 this unit is relatively more co-planar compare to the benzene containing NPD unit.

Another interesting structure we can propose is iso-indigo unit with pyridine moiety (figure 5.4).

According to the literature incorporating pyridine moiety can stabilize resulting HOMO energy

value by 0.1 eV unit. This effect is similar to incorporation of "F" substituents to the aromatic

core which also has the ability to stabilize the resulting HOMO energy by 0.1 eV unit.

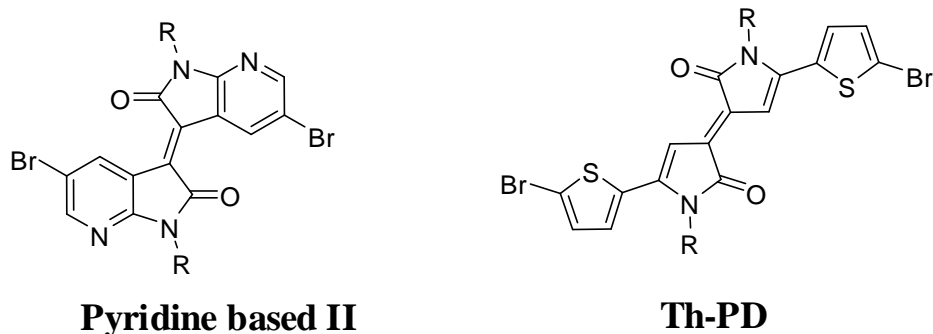**Pyridine based II**   **Th-PD**

Figure 5.4: General structures of pyridine base iso-indigo unit and thiophene based Pechmann
dye derivative (Th-Pd) as the acceptor moiety for D-A polymers.

So it is obvious we can modify these Pechmann dye derivatives and iso-indigo units to prepare

novel organic semiconductor materials as conjugated polymers or oligomer study.

Chapter 6: Experimental section and spectra

6.1 Materials and method

Diethyl ether, Acetonitrile, Tetrahydrofuran (THF) and Toluene were distilled from appropriate drying agents and stored over molecular sieves under argon or nitrogen. 2-heptanol, 3-octanone, 4-nonanol, 2-pentadecanone ,1-hexadecanol, 2-butyloctanol were purchased from VWR chemicals and used without further purification. Unless otherwise stated all other materials were used as purchased. 3-methoxythiophene was prepared according to the literature procedure.[1] All manipulations and reactions were carried under nitrogen using standard Schlenk techniques. ^{1}H, ^{13}C and ^{19}F spectra were recorded using Varion INOVA 400 MHz spectrometer (purchased under the CRIF Program of the National Science Foundation, grant CHE-9974810). Chemical shifts were recorded relative to the referenced residual protio-solvent signals. GC-MS data were collected from an Agilent technologies 6890N GC with 5973 MSD using two different temperature programs (70 ^{o}C →275 ^{o}C, Helium 1.0 mL/min or 70 ^{o}C→ 350 ^{o}C, Helium 2.0 mL/min) depending on the analyte. Polymer relative molecular weights were measured using a Waters 600 E HPLC system, driven by waters Empower Software and equipped with two linear mixed-bed GPC columns (American Polymer Standards Corporation, AM Gel Linear/15) in series. Polymer elutants were measured using both refractive index and photodiode array detectors and the system was calibrated with 11 narrow PDI polystyrene samples in the range 580 to 2 x 10^{6} Da with THF at a flow rate of 1mL/min. Endothermic maxima of 1 st order transitions detected by differential scanning calorimetry (Mettler 822^{e} , heating rate = 10 ^{o}C / min, nitrogen purge). TGA curves were recorded on a TA Instrument Model No. TGA Q500. UV-Vis absorption data were

measured using Varion Cary 1 UV-Visible spectrophotometer. Differential pulse voltammetry (DPV) measurements were carried under nitrogen atmosphere using a BAS-100 A voltammetric analyzer with 0.1 M tetra-*n*-butylammonium hexafluorophosphate in anhydrous acetonitrile as supporting electrolyte. Fc/ Fc$^+$ was used as external reference for all the measurements. As electrodes, used Platinum disk working electrode, a platinum wire counter electrode and silver wire reference electrode. Scan rate was 50 mV/S. All DPV measurements were done under inert conditions. Polymer films were produced by drop casting from chlorobenzene solutions (1 mg/ml). WAXD data of polymers were collected on Bruker-Nonius X8 Proteum using an area detector and extruded, oriented fibers, mounted perpendicular to the incoming beam.

5.2 Synthesis section of chapter 2

Compound 2.0:^{2} To an oven dried 250 ml vacuum flask, Mg was added (8.5g, 35.5 mmol) followed by a small piece of iodine crystal. Then added 200 ml of dry ether followed by drop wise addition of 2-bromothiophene (48.08 g, 295.5 mmol) at 0 ^{o}C. The reaction mixture was refluxed for 2 hours. After cooling to room temperature the resulted Grignard reagent was added to another portion of 2-bromothiophene (39.76 g, 244.6 mmol) in 165 ml of dry ether containing 5% NiCl$_2$.dppp (1.34 g, 2.46 mmol) at 0 ^{o}C. After stirring overnight at room temperature, the reaction mixture was treated with saturated NH$_4$Cl .Aqueous layer was extracted with ether three times. The ether layer was extracted by deionized water three times and dried over MgSO$_4$ and filtered. The solvent

was removed by rotary evaporation and crude product was purified via column of silica gel with hexane as the elutent to give **2.0** as white solid (88%). ^{1}H NMR (400 MHz, CDCl$_3$): δ 7.21 (d, 2H), 7.18 (d, 2H), 7.02 (dd, 2H). ^{13}C NMR (100 MHz, CDCl$_3$): δ 137.6, 127.97, 124.55, 123.97.

Compound 2.1:[2,3]   To compound **2.0** (20.00 g, 0.12 mol) in a 2-neck round bottom flask fitted with a reflux condenser was added   glacial acetic acid (72 ml) and chloroform (160 ml) and cool down to 0 ^{o}C. To this mixture Br$_2$ (22 ml, 3.65 equiv) was added drop wise. During the addition of   Br$_2$(l) the reaction mixture became a green color semi-solid. After complete addition   the reaction mixture wad stirred 5 hours at room temperature and then refluxed for an additional 12 hours. After cooling to room temperature added 10% KOH (180 ml) and extracted 2 times using 2 portions of chloroform (360 ml x 2). Organic layer was dried over MgSO$_4$ and filtered. The solvent was removed by rotary evaporation and crude product was purified by recrystallization using EtOH as the solvent. Obtain pale yellow-white crystals (71%). ^{1}H NMR (400 MHz, CDCl$_3$): δ 7.03 (s, 2H). ^{13}C NMR (100 MHz, CDCl$_3$): δ 132.89, 129.45, 114.73, 112.03.

Compound 2.2:   n-Butyl lithium (2.5 M in hexane) (9.6 ml, 0.024 mol) was added dropwise at -78 ^{o}C to a solution of compound **2.1** (5.96 g, 0.012 mol) in dry ether (150 ml). The reaction mixture turned to green color. Then warm down to 0 ^{o}C. The reaction mixture immediately turned to brown color. Continue stirring for additional 6 hours at 0 ^{o}C. Then the reaction mixture was treated with saturated NH$_4$Cl and extracted with ether. The ether layer was dried over MgSO$_4$ and filtered. The solvent was removed by rotary evaporation and crude product was purified via column of silica gel with hexane as the elutent to give **2.2** as a pale yellow color solid (73%). ^{1}H NMR (400 MHz, CDCl$_3$): δ

7.38 (d, 2H), 7.06 (d, 2H). ^{13}C NMR (100 MHz, CDCl$_3$): δ 131.02, 129.09, 127.73, 112.85.

Compound 2.3b:[2] Grignard reagent was freshly prepared using *n*-hexadecyl bromide (2.74 g, 3eq) and Mg (0.216g, 3eq) in dry ether. This freshly prepared hexadecylmagnesiumbromide was added drop wise to a suspension of compound **2.3**(1.0 g, 0.003 mol) and NiCl$_2$. dppp (0.0813 g, 0.05 eq) in dry ether (35 ml) at room temperature. The reaction mixture was stirred overnight at room temperature. The reaction mixture was treated with saturated NH$_4$Cl and extracted with ether. The ether layer was extracted by deionized water three times and dried over MgSO$_4$ and filtered. The solvent was removed by rotary evaporation and crude product was purified via column of silica gel with hexane as elutent to give compound **2.3b** as a white color solid (54%). ^{1}H NMR (400 MHz, CDCl$_3$): δ 7.26(d, 2H), 6.94 (d, 2H), 2.46 (t, 4H), 1.52 (t, 4H), 1.22 (m, 52H), 0.86(t, 6H).

Compound 2.3a:[2] This was prepared and isolated following the same procedure as compound **2.3b** but using dodecylbromide as the alkyl bromide. After purification via column of silica gel with hexane as elutent to give compound **2.3a** as a white color solid (80 %) ^{1}H NMR (400 MHz, CDCl$_3$): δ 7.26(s, 2H), 6.94 (d, 2H), 2.47 (t, 4H), 1.51(m, 4H), 1.23(m, 36H), 0.87 (t, 6H). ^{13}C NMR (100 MHz, CDCl$_3$): δ 142.56, 128.93, 128.74, 125.43, 32.15, 30.94, 29.91, 29.89, 29.79, 29.67, 29.65, 29.59, 29.00, 22.92, 14.35.

Compound 2.3c:[2] was prepared and isolated following the same procedure as compound **2.3b** using octadecylbromide as the alkyl bromide. After purification via column of silica gel with hexane as elutent to give compound **2.3c** as a white color solid. (80%) ^{1}H NMR (400 MHz, CDCl$_3$): δ 7.23(d,2H), 6.91(d,2H), 2.44(t,4H), 1.50(m, 4H),

1.20(m,60H), 0.83(t,6H). ^{13}C NMR (100 MHz, CDCl$_3$): δ 142.54, 128.9, 128.72, 125.40, 32.13, 30.91, 29.91, 29.76, 29.62, 29.57, 28.98, 22.9, 14.33 (Note: Some peaks in ^{13}C NMR spectrum were overlaped)

Compound 2.4b: [2 2 4] n-Butyl lithium (1.92 ml, 2.5 M in hexane) was added dropwise at -78 °C to a solution of compound **2.3b** (1.0g, 0.0016 mol) in dry THF (20 ml). Then stirred 1 hour at -78 °C, followed by 1 hour at room temperature. Then again cool down to -78 °C and tributyltin chloride (1.56 g, 0.0016 mol) was added as one portion. The reaction mixture was stirred for additional 2 hours at room temperature. Then the resulted reaction mixture was diluted with hexane and washed with water. (30 ml x 2). Dried over MgSO$_4$ and filtered. After solvent was removed by rotary evaporation the crude was purified by column chromatography. (alumina, 95:5 hexane: triethylammine) to give monomer **2.4b** as a pale yellow oil (85%). ^{1}H NMR (400 MHz, CDCl$_3$): δ 6.95(s, 2H), 2.52(t, 4H), 1.57(m, 56), 1.24(m, 24), 1.07(m,12H), 0.86(m, 24).

Compound 2.4a:[4] This was prepared and isolated following the same procedure as compound **2.3b**. (85%) ^{1}H NMR (400 MHz, CDCl$_3$): δ 6.96(s, 2H), 2.52(t,4H), 1.56(m, 16H), 1.22(m, 48H), 1.09(m, 12H), 0.86(m, 24H). ^{13}C NMR (100 MHz, CDCl$_3$): δ 142.78, 137.31, 136.31, 135.38, 32.17, 31.23, 29.96, 29.94, 29.91, 29.89, 29.80, 29.74, 29.62, 29.21, 28.98, 27.49, 22.93, 14.35, 13.92, 11.01.

Compound 2.4c:[4] This was prepared and isolated following the same procedure as compound **2.4b**.(92%) δ 6.96(s, 2H), 2.52(t,4H), 1.56(m, 16H), 1.22(m, 72H), 1.07(m, 12H), 0.86(m, 24H).

Compound a: A solution of 3-octanone (10 g, 70 mmol) in 50 ml of dry dichloromethane and 50 ml of dry methanol was cool down to 0 $^{\circ}$C. To this added NaBH$_4$ (2.65 g, 70 mmol) as several portions. After complete addition warm down to room temperature and stirred for an additional 5 hours. After 5 hours, cool down to 0 $^{\circ}$C and added 100 ml of water. Extracted with dichloromethane (3 x 100 ml). The combined organic layers were dried over anhydrous MgSO$_4$, and concentrated under reduced pressure. The resulted crude colorless oil was used without further purification. (9.89 g, 98%). ^{1}H NMR (400MHz, CDCl3) δ: 0.86 (t,3H), 1.16 (broad d, 4H), 1.26 (broad m, 3H), 1.40 (broad m, 7H), 3.76 (broad m,1H) ^{13}C NMR (100MHz, CDCl3) δ: 14.25, 22.79, 23.65, 25.92, 29.49, 32.01, 39.56, 68.36 (**Note:** some peaks in[13]C NMR spectrum overlap).
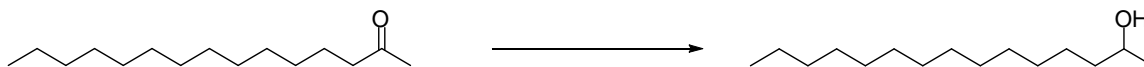
Compound b: This was prepared and isolated as colorless oil using the same procedure as Compound **a** but using commercially available 2-pentadecanone. (87 %).^{1}H NMR (400MHz, CDCl3) δ: 0.86 (t, 3H), 1.16 (d, 3H), 1.26 (broad m, 23H), 1.41 (m, 2H), 3.78 (m, 1H). ^{13}C NMR (100MHz, CDCl3) δ: 14.31, 22.88, 23.66, 25.97, 29.55, 29.84, 32.11, 39.57, 68.39(**Note:** some peaks in[13]C NMR spectrum overlap).
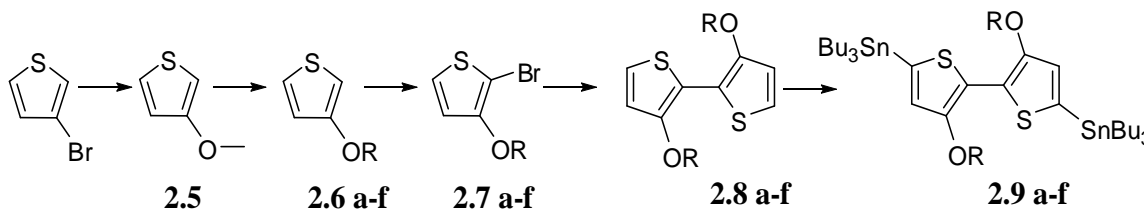
Compound 2.5:[1] To a 250 ml oven dried vacuum flask, was added sodium methoxide (32.42 g, 600 mmol), anhydrous MeOH (60 mL) and DMF (100 mL). To this reaction

suspension, 3-bromothiophene (37.48 mL, 400 mmol) and copper bromide (5.76 g, 40 mmol) were successively added. Then the reaction mixture was refluxed at 120 °C for 2 h. After cooling to r.t., the reaction was filtered and washed with DCM (3 x 100 mL). The filtrate was washed with H_2O (2 x 200 mL), brine (2 x 200 mL) and dried over $MgSO_4$. After removal of the solvent, the crude product was purified via column using DCM/hexane (1/4) as the eluent. Colorless oil (very volatile) was obtained as pure product (54%). ^{1}H NMR (400 MHz , $CDCl_3$): δ 7.20 (dd, 1H); 6.75 (dd, 1H); 6.28 (dd, 1H); 3.80 (s, 3H). ^{13}C NMR (100 MHz, $CDCl_3$): δ 159.08; 124.98; 119.39; 96.73; 57.54.

R=2.6a-α-methyl hexyl
    2.6b-α-ethyl hexyl
    2.6c-α-propyl hexyl
    2.6d-α-methyl tetradecyl
    2.6e-*n*-hexadecyl
    2.6f-2-butyloctyl
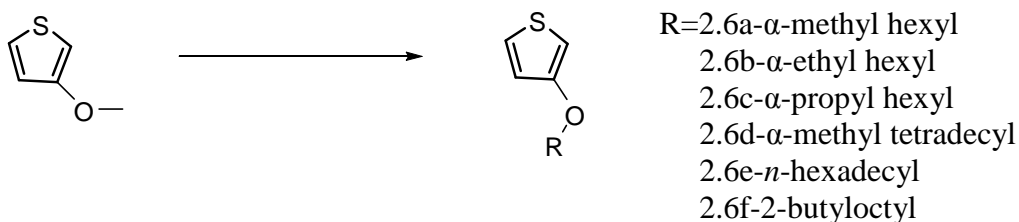
Compound 2.6a:[1] To an oven dried 250 ml vacuum flask was added 3-methoxythiophene (4.92 g, 40.5 mmol), 2-heptanol (10.0 g, 86.1 mmol), p-toluenesulfonic acid monohydrate (0.82 g, 0.1 eq, 4.31 mmol) and 50 ml of bulk toluene. The reaction mixture was heated in a 130 ºC oil bath overnight. After dichloromethane/water extraction, the organic layer was dried over $MgSO_4$. After solvent evaporation, the residue was purified by column chromatography (silica gel 3:1 hexane:dichloromethane) to obtain compound **2.6a** as a colorless liquid. (6.9 g, 81 %)^{1}H NMR (400MHz, CDCl3) δ: 0.86 (t, 3H), 1.28 (m, 7H), 1.52 (broad m, 2H), 1.68 (m, 2H), 4.17 (m, 1H), 6.19(dd,1H), 6.70(dd.1H),7.12(dd,1H). ^{13}C NMR (100MHz, CDCl3) δ: 14.18,19.83,22.83,25.33,31.97,36.52,76.67,98.48,120.34,124.46,156.95. GC-MS: m/z: 196 ($C_{11}H_{18}SO^+$), 100 (100%: $C_4H_4SO^+$)

Compound 2.6b:[1] This was prepared and isolated as a colorless liquid using the same procedure as compound **2.6a** but using already synthesized compound **a** as the alcohol. (74 %).^{1}H NMR (400MHz, CDCl3) δ: 0.91 (t, 3H), 0.98 (t, 3H), 1.33 (broad m, 6H), 1.71 (broad m, 4H), 4.03 (m, 1H), 6.23(dd,1H), 6.77(dd.1H),7.14(dd,1H). ^{13}C NMR (100MHz, CDCl$_3$) δ:9.73, 14.21, 22.80, 25.29,26.62,32.11,33.47,81.84,98.45,120.41,124.32,157.50. GC-MS: m/z: 212 (C$_{12}$H$_{20}$OS$^+$), 100 (100%: C$_4$H$_4$SO$^+$).

Compound 2.6c:[1] This was prepared and isolated as a colorless liquid using the same procedure as compound **2.6a** but using 4-nonanol as the alcohol. (37 %).^{1}H NMR (400MHz, CDCl3) δ: 0.86 (t, 3H), 0.91 (t, 3H), 1.39 (b, 6H), 1.61 (m, 6H), 4.04 (m, 1H), 6.19(dd,1H),   6.72(dd,1H),   7.12   (dd,1H).   ^{13}C   NMR   (100MHz,   CDCl3) δ:14.29,18.81,22.77,25.22,32.10,,33.99,36.23, 80.45 , 98.18 , 120.32,124.22,157.39. GC-MS: m/z: 226 (C$_{13}$H$_{22}$OS$^+$), 100 (100%: C$_4$H$_4$SO$^+$).
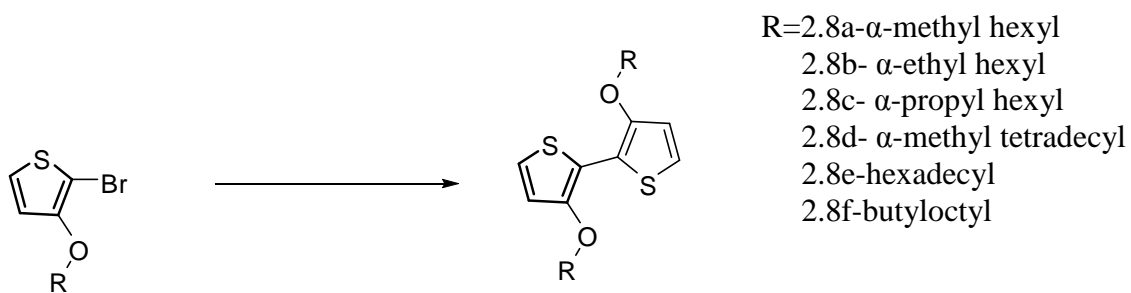
Compound 2.6d:[1]This was prepared and isolated as a colorless liquid using the same procedure as compound **2.6a** but using already synthesized compound **b** as the alcohol. (84%).^{1}H NMR (400MHz, CDCl3) δ: 0.86 (t, 3H), 1.23(m, 24H), 1.53 (m, 1H), 1.69 (m, 1H), 4.16 (m, 1H), 6.19(dd,1H), 6.70(dd,1H), 7.12(dd,1H),. ^{13}C NMR (100MHz, CDCl3) δ: 14.34,19.94,22.92, 25.73,29.88,32.15,36.62,76.62,98.32,120.43,124.42,156.93. GC-MS: m/z: 310 (C$_{19}$H$_{34}$OS$^+$) , 100 (100%: C$_4$H$_4$SO$^+$).

Compound 2.6e:[1]This was prepared and isolated as a colorless solid using the same procedure as compound 2.6a but using 1-hexadecanol as the alcohol. (65%).^{1}H NMR (400MHz,CDCl$_3$):δ   0.86(t,3H),1.21(m,24H),1.42(m,2H),1.75(m,2H),3.92(m,2H),6.21 (dd,1H),6.74(dd,1H),7.15(dd,1H).^{13}CNMR(100MHz,CDCl$_3$):δ.14.21,22.79,26.28,   29.83

,32.16,70.49,97.00, 119.80,124.70, 158.20. (**Note:** some peaks in[13]C NMR spectrum overlap).GC-MS: m/z: 324 ($C_{20}H_{36}OS^+$) , 100 (100%: $C_4H_4SO^+$).

Compound 2.6f:[1]This was prepared and isolated as a pale yellow liquid using the same procedure as compound **2.6a** but using 2-butyl octanol as the alcohol.(85%)^{1}H NMR (400 MHz, CDCl$_3$): δ0.88(q,7.31H),1.28(broad m,17H),1.75(broad m,1H), 3.82(m,2H),6.21(dd,2H),6.76(dd,1H),7.15(dd,1H).^{13}CNMR(100MHz,CDCl$_3$):δ14.33, 22.91,23.29,27.05,29.29,29.91,31.26,31.57,32.09,38.11,73.36,96.93,119.86,124.72, 158.56 (**Note:** some peaks in[13]C NMR spectrum overlap). GC-MS: m/z: 268 ($C_{16}H_{28}OS^+$) , 100 (100%: $C_4H_4SO^+$).

R=2.7a-α-methyl hexyl
2.7b- α-ethyl hexyl
2.7c- α-propyl hexyl
2.7d- α-methyl tetradecyl
2.7e-hexadecyl
2.7f-butyloctyl
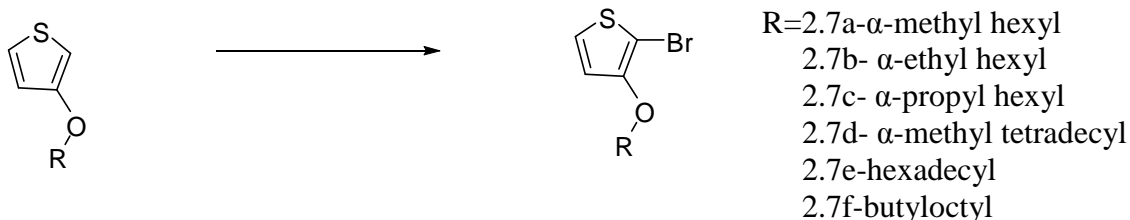
Compound 2.7a:[4] NBS (3.22 g, 18.105 mmol) was added in one portion to compound **2.6a** (3.59 g, 18.105 mmol) in 46 ml of anhydrous DMF at 0 ºC and the whole was warmed to room temperature and stirred overnight under dark conditions. The reaction mixture was diluted with ether (50 ml) and washed with water (2 x 20 ml). The organic layer was dried over MgSO$_4$, concentrated under reduced pressure, and the residue subjected to column chromatography (silica gel,hexane) to give compound **2.7a** as a pale yellow liquid (4.61 g, 92 %). Note: This compound was highly unstable when concentrated. So every time did not remove all the solvents and used as soon as possible for the next step. Dilute compound can store in refrigerator without any degradation for

future use. ^{1}H NMR (400MHz, CDCl$_3$) δ: 0.88 (t, 3H), 1.28 (m, 6H), 1.52 (broad m,4H),1.71(m,2H),4.19(m,1H),6.69(d,1H),7.14(d,1H).^{13}CNMR(100MHz,CDCl$_3$)δ:14.43, 20.50 ,22.71, 25.08 ,31.97,36.55,78.93,93.54,119.21,124.18,153.88.

Compound 2.7b:[4] This was prepared and isolated as a colorless liquid using the same procedure as compound **2.7a** but using compound **2.6b**. (96 %). Note: This compound is highly unstable when concentrated. So every time did not remove all the solvents and used as soon as possible for the next step. Dilute compound can store in refrigerator without any degradation for future use. ^{1}H NMR (400MHz, CDCl3) δ: 0.92 (t,3H),1.0(t,3H),1.34(broadm,4H),1.45(broadm,2H),1.66(broadm,4H),4.06(m,1H) ,6.70 (d,1H),7.13(d,1H).^{13}CNMR(100MHz,CDCl3)δ:9.65,14.41,22.94,25.26,27.17,32.16, 33.82,84.14,93.34,119.20,124.38,154.48. GC-MS: m/z: 292 ($C_{12}H_{19}OSBr^+$) , 180 (100%: $C_4H_3SOBr^+$).

Compound 2.7c:[4] This was prepared and isolated as a colorless liquid using the same procedure as compound **2.7a** but using compound **2.6c.** (98%) Note: This compound is highly unstable when concentrated. So every time did not remove all the solvents and used as soon as possible for the next step. Dilute compound can store in refrigerator without any degradation for future use.^{1}H NMR (400MHz, CDCl3) δ: 0.87 (t, 3H),0.92(t,3H),1.29(m,6H),1.42(m,4H),1.60(m,4H)4.08(m,1H),6.69(d,1H),   7.14(d,1H). ^{13}CNMR(100MHz,CDCl3)δ:14.36,18.63,22.89,25.06,32.08,34.25,36.56,82.96,93.12, 119.00,124.35,154.47. (**Note:** some peaks in[13]C NMR spectrum overlap).GC-MS: m/z: 306 ($C_{13}H_{21}OSBr^+$) , 180 (100%: $C_4H_3SOBr^+$).
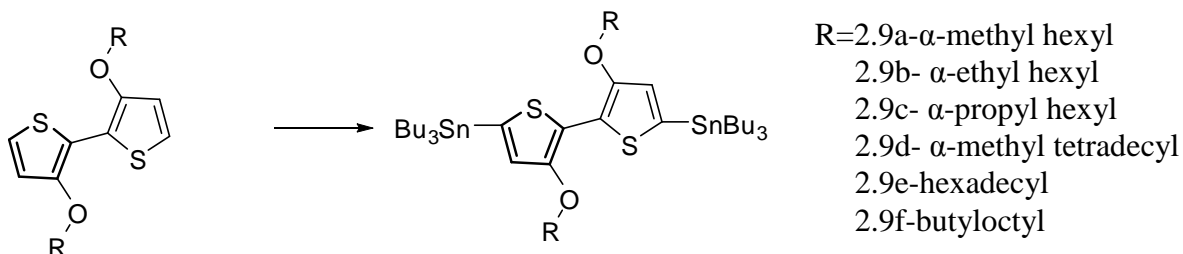
Compound 2.7d: This was prepared and isolated as a colorless liquid using the same procedure as compound **2.7a** but using compound 2.6d**.** (89%) Note: This compound is

highly unstable when concentrated. So every time did not remove all the solvents and used as soon as possible for the next step. Dilute compound can store in refrigerator without any degradation for future use.^{1}H NMR (400MHz, CDCl3) δ: 0.86 (t, 3H), 1.23(m,25H),1.53(m,1H),1.70(m,1H),4.19(m,1H),6.67(d,1H),7.14(d,1H).^{13}CNMR (100MHz,CDCl3)δ:14.34,20.40,22.92,25.64,29.89 ,32.16,36.80,79.08, 93.83,119.31 ,124.17,153.88. (**Note:** some peaks in[13]C NMR spectrum overlap). GC-MS: m/z: 389 ($C_{19}H_{33}OSBr^+$) , 180 (100%: $C_4H_3SOBr^+$).

Compound 2.7e:[4]This was prepared and isolated as a colorless solid using the same procedure as compound **2.7a** but using compound compound **2.6e**.(82%) ^{1}H NMR (400 MHz,CDCl$_3$):δ7.16(d,1H),6.73(d,1H),4.01(t,2H),1.73(m,2H),1.43(m,2H),1.24(m,24H) ,0.87(t,3H).^{13}CNMR(100MHz,CDCl$_3$):δ14.36,22.93,26.04,32.16,56.68,72.47,75.00, 91.79 , 117.72 , 124.31,154.76. (**Note:** some peaks in[13]C NMR spectrum overlap). GC-MS: m/z: 403 ($C_{20}H_{35}OSBr^+$) , 180 (100%: $C_4H_3SOBr^+$).

Compound 2.7f:[4] This was prepared and isolated as a yellow liquid using the same procedure as compound **2.7a** but using compound **2.6e.** Note: This compound is highly unstable when concentrated. So every time did not remove all the solvents and used as soon as possible for the next step. Dilute compound can store in refrigerator without any degradation for future use.(80%)^{1}HNMR(400MHz,CDCl$_3$): δ0.87(broadq,6H),1.27 (broadm,17H),1.44(broadm,2H),1.73(m,1H),3.88(m,2H),6.73(d,1H),7.15(d,1H). ^{13}CNMR(100MHz,CDCl$_3$):14.33,22.87,23.27,26.99,29.24,29.89,31.06,31.37,32.03,38.37 ,75.32,91.86,117.77,124.13,154.94.GC-MS:m/z:348 ($C_{16}H_{27}OSBr^+$) , 180 (100%: $C_4H_3SOBr^+$).

R=2.8a-α-methyl hexyl
2.8b- α-ethyl hexyl
2.8c- α-propyl hexyl
2.8d- α-methyl tetradecyl
2.8e-hexadecyl
2.8f-butyloctyl

Compound 2.8a:[4] A mixture of bis(1,5-cyclooctadienyl)nickel (0) (2 g, 7.3 mmol) 2,2'-dipyridyl (1.14 g, 7.3 mmol), 1,5-cyclooctadiene (0.6 ml, 4.87 mmol) and 25 ml anhydrous DMF was stirred at 80 ºC for 1 hour under argon. To this purple black solution, compound **2.7a** (1.35 g, 4.87 mmol) in 30 ml anhydrous toluene was added drop wise at room temperature. The resulting reaction mixture was stirred at 80 ºC overnight. The reaction mixture was diluted with ether and washed with 10 % HCl, brine and organic layer was dried over $MgSO_4$. After concentration under reduced pressure, the residue was subjected to gradient column chromatography (silica gel, 1:0 → 3:1 hexane:DCM) to give compound **2.8a** as a pale yellow liquid.(0.57 g, 59 %). ^{1}H NMR (400MHz, CDCl3) δ: 0.89 (Broad t, 6H), 1.33 (m, 14H), 1.47 (broad m, 4H), 1.64 (m, 2H), 1.85 (m, 2H), 4.35(m,2H),6.79(d,2H),7.06(d,2H). ^{13}C NMR (100MHz, CDCl3) δ: 14.28,22.83,25.50,32.09,36.93,78.32,115.50,116.83,150.99. GC-MS: m/z: 394 $(C_{22}H_{34}O_2S_2^+)$, 198 (100% : $C_8H_6S_2O_2^+$).

Compound 2.8b:[4] This was prepared and isolated as a pale yellow liquid using the same procedure as compound **2.8a** but using compound **2.7b**. (85 %).^{1}H NMR (400MHz, CDCl3) δ: 0.88 (t, 6H), 0.99 (t, 6H), 1.30 (broad m, 8H), 1.44 (m, 4H), 1.65 (m, 2H), 1.75(m,6H), 4.18(m,2H), 6.79(d,2H), 7.03(d,2H). ^{13}C NMR (100MHz, CDCl3) δ:

9.82,14.31,22.61,25.21, 27.05 ,32.00 ,33.73,83.09,114.88,116.20,121.44,151.38. GC-MS: m/z: 422 ($C_{24}H_{38}O_2S_2^+$) , 198 (100%: $C_8H_6S_2O_2^+$).

Compound 2.8c: This was prepared and isolated as a pale yellow liquid using the same procedure as compound **2.8a** but using compound **2.7c**. (68 %).^{1}H NMR (400MHz, CDCl$_3$) δ: 0.86 (t, 6H), 0.91 (t, 6H), 1.27 (m, 8H), 1.45 (m, 8H), 1.65 (m, 4H), 1.74(m,4H), 4.22(m,2H), 6.78(d,2H), 7.02(d,2H). ^{13}C NMR (100MHz, CDCl$_3$) δ: 14.46,18.92,22.82,25.42, 32.18, 34.53 ,36.79,81.96,114.83,116.43,121.55,151.37.

Compound 2.8d: This was prepared and isolated as a colorless solid using the same procedure as compound **2.8a** but using compound **2.7d**. After column further purify by recrystalization using ethanol (32 %).^{1}H NMR (400MHz, CDCl3) δ: 0.83 (t, 6H), 1.21(m, 50H),1.59(m,2H),1.80(m,2H),4.29(m,2H),6.76(d,2H),7.0(d,2H).^{13}CNMR (100MHz,CDCl3) δ: 14.29,20.38,22.92, 25.82,29.83,32.22,36.89,78.41,115.52,116.89, 121.72,151.01(**Note:** some peaks in[13]C NMR spectrum overlap). GC-MS: m/z: 489, 207 (100%)

Compound 2.8e: This was prepared and isolated as a colorless solid using the same procedure as compound **2.8a** but using compound **2.7e**. (65%)^{1}H NMR (400 MHz, CDCl$_3$):   δ0.86(t,6H),1.24(m,48H),1.50(broadm,4H),   1.82(m,4H),4.07(m,4H), 6.82(d,2H)7.04(d,2H).^{13}CNMR(100MHz,CDCl$_3$):δ14.28,22.72,26.23,29.84,32.20, 72.11, 114.27,116.31,121.72,152.15. (**Note:** some peaks in[13]C NMR spectrum overlap). GC-MS: m/z: 646 ($C_{40}H_{70}O_2S_2^+$) , 646 (100%).

Compound 2.8f: This was prepared and isolated as a colorless solid using the same procedure as compound **2.8a** but using compound **2.7f**.(70%)^{1}H NMR (400 MHz, CDCl$_3$):   δ0.87(broad   q,12H),1.28(broad   m,25H),1.45(broad   m,4H),

1.57(m,4H),1.82(m,2H),3.99(m,4H),6.84(d,2H),7.06(d,1H).^{13}CNMR (100MHz,CDCl$_3$)

:14.33,22.91,23.29,27.05,29.29,29.91,31.26,31.57,32.09,38.11,73.36,96.93,119.86

,124.72,158.56. GC-MS: m/z: 534 (C$_{32}$H$_{54}$O$_2$S$_2$$^+$) , 198 (100%: C$_8H_6S_2O_2$$^+$).

R=2.9a-α-methyl hexyl
2.9b- α-ethyl hexyl
2.9c- α-propyl hexyl
2.9d- α-methyl tetradecyl
2.9e-hexadecyl
2.9f-butyloctyl

Compound 2.9a:[4] **n**-Butyl lithium (1.70 ml 2.5 M in hexane, 4.26 mmol) was added

dropwise at -78 ºC to compound **2.8a** (0.56 g, 1.42 mmol) in 20 ml of dry THF and the

whole was stirred at -78 ºC for 1 hour, followed by 1 hour at room temperature. After

cooling to -78 ºC, tributyltin chloride (1.15 ml g, 1.42 mmol) was added in one portion

and the whole was warmed to room temperature and stirred for additional 2 hours. The

reaction mixture was diluted with hexane (50 mL) and washed with water (2 x 20 ml) and

brine, dried over MgSO$_4$. After concentration by rotary evaporation, the residue was

purified by column chromatography (alumina, 95:5 hexane:triethyl amine) to give

compound **2.9a** as a colorless liquid (0.94 g, 68 %). ^{1}H NMR (400MHz, CDCl3) δ: 0.79

(m, 17H), 0.88 (m, 31H), 1.07 (m, 12H), 1.29(m,13H), 1.57(m, 9H),

1.83(m,2H),4.34(m,2H),6.77(s,2H).^{13}CNMR(100MHz,CDCl$_3$)δ:9.15,10.99,13.82,20.42,

2.93, 25.55 ,27.53,29.66, 32.18,37.09,78.01,121.70,124.63,132.34,152.81 (**Note:** some

peaks in^{13}C NMR spectrum overlap).

Compound 2.9b:[4] This was prepared and isolated as a pale yellow liquid using the same

procedure as compound **2.9a** but using compound **2.8b**. (69 %).^{1}H NMR (400MHz,

CDCl3) δ: 0.85 (broad m, 6H), 0.94 (t, 6H), 1.04 (t, 12H), 1.31 (broad m, 22H), 1.54 (m,

8H),1.70(m,8H),4.14(m,2H),6.72(s,2H).^{13}CNMR(100MHz,CDCl$_3$)δ:

9.87,10.94,13.92,14.28,22.84, 25.38,27.02,27.50,39.23,32.26,33.76,82.72, 120.94,124.12, 132.04,152.94 (**Note:** some peaks in[13]C NMR spectrum overlap).

Compound 2.9c:[4] This was prepared and isolated as a pale yellow liquid using the same procedure as compound **2.9a** but using compound **2.8c.** (75 %). ^{1}H NMR (400MHz, CDCl3) δ: 0.89 (broad m, 30H), 1.07 (t, 12H), 1.34 (m, 24H), 1.57 (m, 16H), 1.64 (m, 4H),1.74(m,4H),4.23(m,2H),6.76(s,2H),.^{13}CNMR(100MHz,CDCl3)δ:10.96,13.92, 18.91 ,22.85,25.36,27.49, 29.22,32.26,34.43,36.71,81.60,120.88,124.09,132. 01 , 153.14 (**Note:** some peaks in[13]C NMR spectrum overlap).

Compound 2.9d:[4] This was prepared and isolated as a pale yellow liquid using the same procedure as compound **2.9a** but using compound **2.8d**. (75%).^{1}H NMR (400 MHz, CDCl$_3$): δ. 0.89(t,3H), 1.06(t,12H),1.26(broadm,55H) , 1.58(broad m,16H), 1.81(broad m,2H),4.35(broad m,2H),6.78(s,2H).^{13}CNMR(100MHz,CDCl$_3$): 10.97,13.93, 14.33,20.37,22.92,25.87,27.48,29.21,29.94,32.15,37.10,77.95,121.66,124.80, 132.31, 152.71. (**Note:** some peaks in[13]C NMR spectrum overlap).

Compound 2.9e:[4] This was prepared and isolated as a pale yellow liquid using the same procedure as compound **2.9a** but using compound **2.8e**. (85%). ^{1}H NMR (400 MHz,CDCl$_3$):δ0.88(q,24H),1.08(t,12H),1.34(broadm,61H),1.56(m,16H),1.84(m,4H),4.09 (m, 4H),6.81(s,2H).^{13}CNMR(100MHz,CDCl$_3$):10.97,13.93,14.36,22.93,26.47, 27.49 ,29.20, 29.96, 32.17,72.23,120.49,123.94,132.64,153.91(**Note:** some peaks in[13]C NMR spectrum overlap).

Compound 2.9f:[4] This was prepared and isolated as a pale yellow liquid using the same procedure as compound **2.9a** but using compound **2.8f.** (85%)^{1}H NMR (400 MHz,CDCl$_3$):0.87,(Broadm,30H),1.07(t,12H),1.31(m,50H),1.55(m,8H),.79(m,2H),

3.99(m,4H) ,6.80(s,2H).^{13}CNMR(100MHz,CDCl$_3$):10.94,13.91,14.40,22.96, 23.37,27.26, 27.50, 29.21 ,29.46,30.04,31.35,31.64,32.20,38.81,74.22,119.88,123.29,132.42,154.12. (**Note:** some peaks in^{13}C NMR spectrum overlap).

General Procedure for Stille Polymerization:

To an air free flask containing the two monomers (0.2 mmol each) was added a mixture of Pd$_2$(dba)$_3$ and tri(o-tolyl)-phosphine (1:8 molar ratio between Pd$_2$(dba)$_3$ and tri(o-tolyl)-phosphine: 0.03% Pd loading) under inert atmosphere. After 3 pump/purge cycles of reduced pressure and refilling with N$_2$, anhydrous, degassed THF (4 ml) was added via syringe and the vessel was sealed and its contents stirred vigorously in an 80 °C bath for 48 hours. After cooling to room temperature, the reaction mixture was dripped into 100 ml vigorously stirred methanol solution containing 5 ml of 12 N HCl. After stirred for 4 hours, the solid was collected by centrifugation. The solid polymer was dried and subjected to sequential soxhlet extraction. Unless until stated the common sequential solvents were methanol, acetone, hexane and chloroform. After soxhlet extraction polymer solution was concentrated and reprecipitated using 100 ml methanol and collected by centrifugation. Then dried it under reduced pressure.
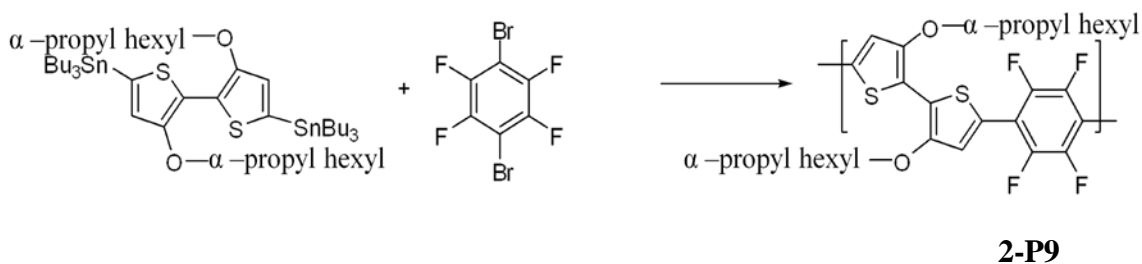

2-P1
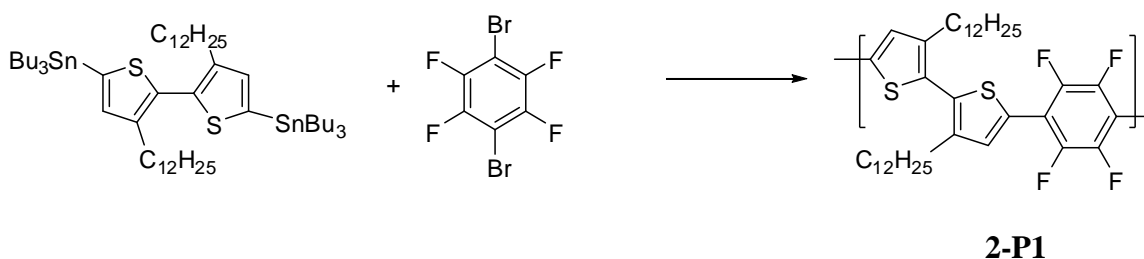
2-P1: Yield 79%. This was prepared following the general procedure for polymerization and purified by sequential soxhlet extraction using methanol, acetone, hexane and chloroform as the solvents. After dried in vacuum polymer **2-P1** obtained as maroonnish-

red solid Mn: 25 kDa, PDI: 1.82, ^{1}H NMR (C$_2$D$_2$Cl$_4$, 90 ºC, 400 MHz, ppm) δ: 7.61 (s, 2H); 2.68 (t, 4H); 1.68 (m, 4H); 1.29 (br,m, 36H), 0.91 (t, 6H). ^{19}F NMR (C$_2$D$_2$Cl$_4$, 90 ºC, 376 MHz) δ (ppm): -141.83 (broad singlet, 4F), -141.982 (broad singlet, 0.5 F).
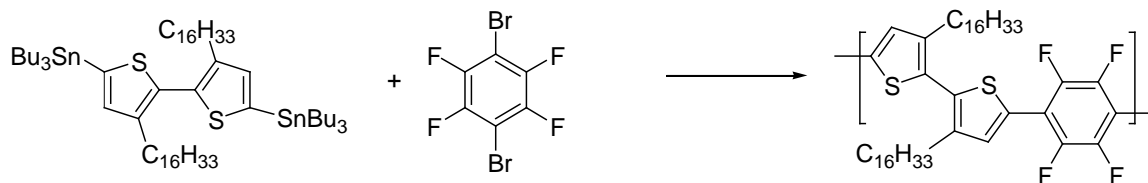
2-P2

2-P2: Yield 77%. This was prepared following the general procedure for polymerization and purified by sequential soxhlet extraction using methanol, acetone, hexane and chloroform as the solvents. After dried in vacuum polymer **2-P2** obtained as maroonnish-red solid. Mn: 15 kDa, PDI: 1.57, ^{1}H NMR (CD$_2$Cl$_4$, 90 ºC, 400 MHz, ppm) δ: 7.63 (S, 2H); 2.708 (t, 4H); 1.704 (t, 4H); 1.312 (m, 52H), 0.927 (t, 6H).^{19}F NMR (CD$_2$Cl$_4$, 90 ºC, 376 MHz, ppm) δ: -140.98 (4F) , -141.130 (0.83F).
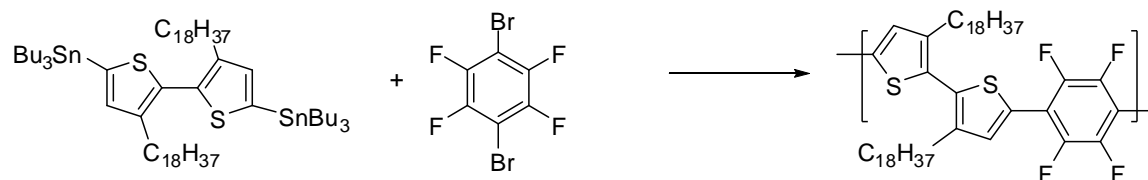

2-P3

2-P3: Yield 67%. This was prepared following the general procedure for polymerization and purified by sequential soxhlet extraction using methanol, acetone, hexane and chloroform as the solvents. After dried in vacuum polymer **2-P3** obtained as maroonnish-red solid Mn: 11 kDa, PDI: 1.47, ^{1}H NMR (C$_2$D$_2$Cl$_4$, 90 ºC, 400 MHz, ppm) δ: 7.61 (s, 2H); 2.68 (t, 4H); 1.68 (m, 4H); 1.29 (br,m, 58H), 0.91 (t, 6H). ^{19}F NMR (C$_2$D$_2$Cl$_4$, 90 ºC, 376 MHz) δ (ppm): -141.01 (broad singlet, 4F)

2-P4
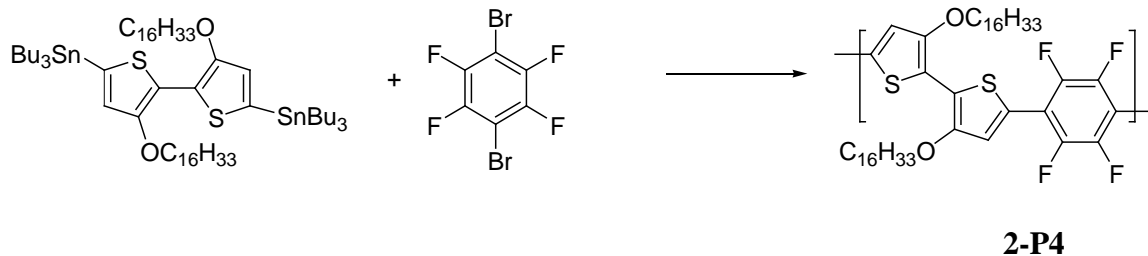
2-P4: Yield 78%. This was prepared following the general procedure for polymerization and purified by sequential soxhlet extraction using methanol, acetone, hexane, chloroform and chlorobenzene as the solvents. After dried in vacuum polymer **2-P4** obtained as deep blue solid. Molecular weight was not available due to the low solubility in THF. ^{1}H NMR (400 MHz, C$_2$D$_2$Cl$_4$, 90 ºC): δ 0.95(b,6H),1.34(broad m,53H), 2.0(b,4H), 4.28(m, 3.5H), 7.49 (broad singlet, 1.09H), ^{19}F NMR (C$_2$D$_2$Cl$_4$, 90 ºC, 376 MHz) δ (ppm): -141.73.

2-P5
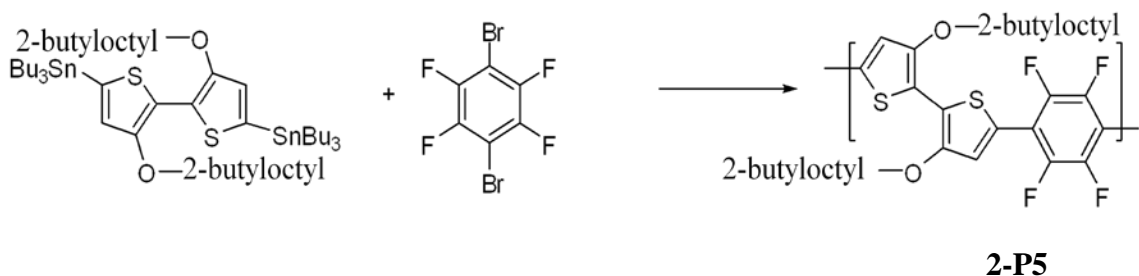
2-P5: Yield 74%. This was prepared following the general procedure for polymerization. Due to very easy solubility in soxhlet extraction only used methanol and acetone. Then purified polymer using pentane recrystallization. After dried in vacuum polymer **2-P5** obtained as purple solid. Mn: 13 kDa, PDI: 1.82 (Note: Due to the presence of low molecular weight part Mn is low. It was difficult to remove low molecular weight oligomers due to very easy solubility.) ^{1}H NMR (C$_2$D$_2$Cl$_4$, 90 ºC, 400 MHz, ppm): 7.51 (s, 1.34H); 4.20 (s, 3.27H); 2.02 (m, 1.78H); 1.43 (broad m, 35.25H), 0.96 (broad, 12H). ^{19}F NMR (C$_2$D$_2$Cl$_4$, 90 ºC, 376 MHz) (ppm): -141.80.

2-P6
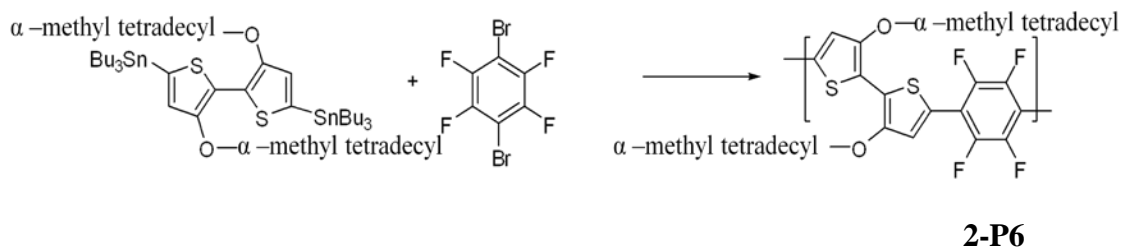
2-P6: Yield 68%. This was prepared following the general procedure for polymerization and purified by sequential soxhlet extraction using methanol, acetone, pentane (4 hrs) and hexane as the solvents. After dried in vacuum polymer **2-P6** obtained as deep blue solid. Mn~ 10 kDa, PDI: 1.97(Note: Due to the presence of low molecular weight part Mn is low. It was difficult to remove low molecular weight oligomers due to very easy solubility.) ^{1}H NMR (400 MHz, $C_2D_2Cl_4$, 90 °C): δ 0.91(b,6H), 1.31 (broad m,54H), 4.52(m, 2H), 7.45 (broad singlet, 1.58H), ^{19}F NMR ($C_2D_2Cl_4$, 90 °C, 376 MHz) δ (ppm): -141.80.

2-P7
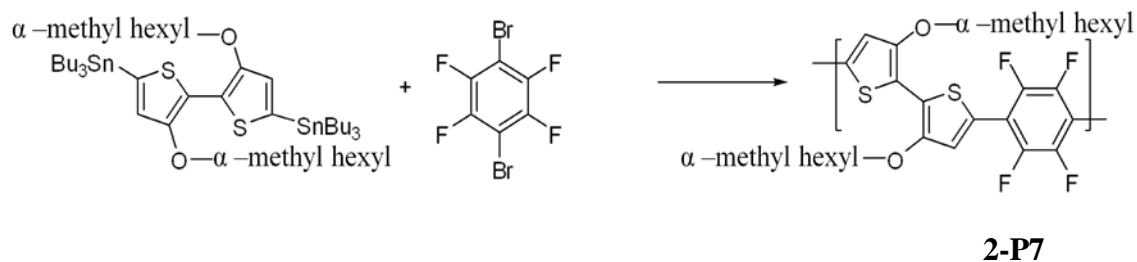
2-P7: Yield 70%. This was prepared following the general procedure for polymerization and purified by sequential soxhlet extraction using methanol, acetone, hexane and chloroform as the solvents. After dried in vacuum polymer **2-P7** obtained as deep blue solid. Molecular weight was not available due to the low solubility in THF. ^{1}H NMR (400 MHz, $C_2D_2Cl_4$, 90°C):δ 0.94(b,6H),1.42(broad m,20H),1.74(m,1.76H), 1.93(m,1.54H), 4.50(broad,1.2H), 7.43(broad s,1.48H) ^{19}F NMR ($C_2D_2Cl_4$, 90 °C, 376 MHz) δ (ppm): -142.08.

2-P8
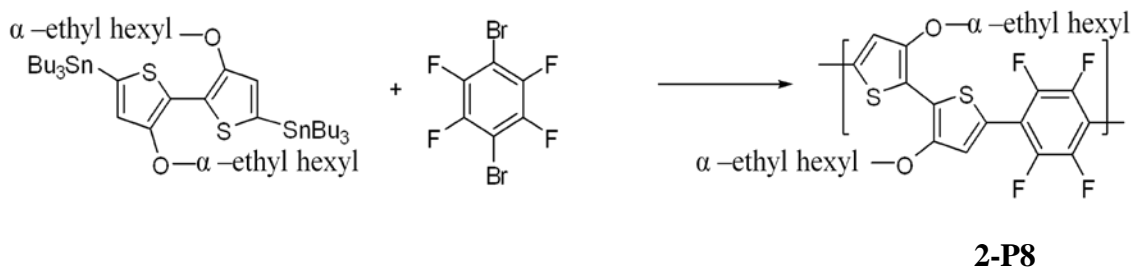
2-P8: Yield 76%. This was prepared following the general procedure for polymerization and purified by sequential soxhlet extraction using methanol, acetone, hexane and chloroform as the solvents. After dried in vacuum polymer **2-P8** obtained as deep blue solid. Molecular weight was not available due to the low solubility in THF. ^{1}H NMR (400 MHz, C$_2$D$_2$Cl$_4$, 90 °C): δ 0.94(b,6H), 1.11(b,5.53H), 1.40 (broad m,14H), 1.89 (broad m, 6.69H), 4.36(m, 1.26H), 7.44 (broad singlet, 1.69H), ^{19}F NMR (C$_2$D$_2$Cl$_4$, 90 °C, 376 MHz) δ (ppm): -142.6.

2-P9

2-P9: Yield 79%. This was prepared following the general procedure for polymerization and purified by sequential soxhlet extraction using methanol, acetone, hexane and chloroform as the solvents. After dried in vacuum polymer **2-P9** obtained as deep blue solid. Molecular weight was not available due to the low solubility in THF. ^{1}H NMR (400 MHz, C$_2$D$_2$Cl$_4$, 90 °C): δ 0.96(b,11.72H),1.42 (broad m,16.34H), 1.92 (broad m, 7.38H), 4.44(m, 1.86H), 7.47 (broad sinqlet, 1.61H), ^{19}F NMR (C$_2$D$_2$Cl$_4$, 90 °C, 376 MHz) δ (ppm): -142.09.

141

DFT Calculations details:
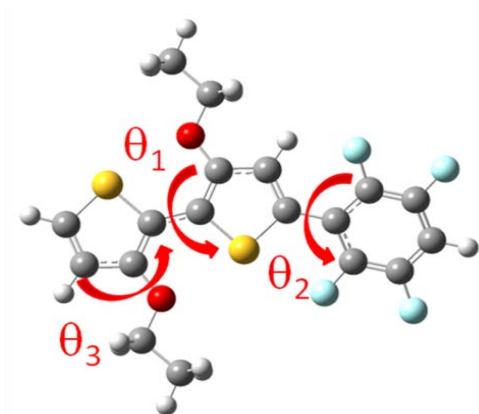
Ground state geometries of the monomer repetition units were optimized employing density functional theory (DFT) within the Gaussian09 package,[R1] employing the BHandHLYP functional (6-311+G* basis set) was used. No symmetry restrictions were imposed and the calculations were started from various non-planar geometries.

[R1] Gaussian 09, Revision A.02, M. J. Frisch, G. W. Trucks, H. B. Schlegel, G. E. Scuseria, M. A. Robb, J. R. Cheeseman, G. Scalmani, V. Barone, B. Mennucci, G. A. Petersson, H. Nakatsuji, M. Caricato, X. Li, H. P. Hratchian, A. F. Izmaylov, J. Bloino, G. Zheng, J. L. Sonnenberg, M. Hada, M. Ehara, K. Toyota, R. Fukuda, J. Hasegawa, M. Ishida, T. Nakajima, Y. Honda, O. Kitao, H. Nakai, T. Vreven, J. A. Montgomery, Jr., J. E. Peralta, F. Ogliaro, M. Bearpark, J. J. Heyd, E. Brothers, K. N. Kudin, V. N. Staroverov, R. Kobayashi, J. Normand, K. Raghavachari, A. Rendell, J. C. Burant, S. S. Iyengar, J. Tomasi, M. Cossi, N. Rega, J. M. Millam, M. Klene, J. E. Knox, J. B. Cross, V. Bakken, C. Adamo, J. Jaramillo, R. Gomperts, R. E. Stratmann, O. Yazyev, A. J. Austin, R. Cammi, C. Pomelli, J. W. Ochterski, R. L. Martin, K. Morokuma, V. G. Zakrzewski, G. A. Voth, P. Salvador, J. J. Dannenberg, S. Dapprich, A. D. Daniels, O.

Farkas, J. B. Foresman, J. V. Ortiz, J. Cioslowski, and D. J. Fox, Gaussian, Inc., Wallingford CT, 2009.

6.3 Synthesis section of chapter 3
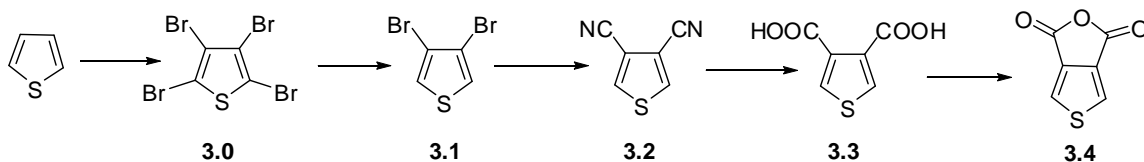
Compound 3.0:[5] A solution of thiophene (39.41 g, 0.47 mol) in chloroform (19 ml) was cooled to 0 ^{o}C. Then added liquid bromine dropwised using an additional funnel. Refluxed for 4 hours at 70°C. Cool down to room temperature and added Solution of KOH in ethanol (KOH (51.7 g) in 282 ml of ethanol). Filtered the product using water and extracted using chloroform. Organic layer was dried over $MgSO_4$ and filtered. The solvent was removed by rotary evaporation and crude product was purified by recrystallization using ethanol: chloroform 3:1 mixture as the solvent to obtained white color needle like crystals (92%). ^{13}C NMR (100 MHz, CDCl$_3$): δ 117.17, 110.49.

Compound 3.1:[5] To an acetic acid/ water mixture(1:2, 10 ml) compound **3.0** (5 g, 0.013 mol) was added and subjected to 3 pump/purge cylces of argon. Quickly added powdered zinc (2.76 g, 3.2 equiv) and refluxed at 110 ^{0}C for overnight. After cooling down to room temperature the reaction mixture was filtered and filterate was extracted with diethyl ether. Organic layer was dried over $MgSO_4$ and filtered. The solvent was removed by rotary evaporation and crude product was used without further purification. (Slightly yellow color oil)(72%). ^{1}H NMR (400 MHz, CDCl$_3$): δ 7.29 (s,2H). ^{13}C NMR (100 MHz, CDCl$_3$): δ 123.94, 114.07.

Compound 3.2:[5] To an air free flask added compound **3.1** (7.12 g, 0.03 mol) followed by cuprous cyanide (8.06 g, 3 equiv) and dry DMF (17 ml). Then degassed 15 minutes and

refluxed at 165 $^{\circ}$C overnight. After cooling to room temperature added a mixture of anhydrous FeCl$_3$ in 1.7 M HCl solution (30 g of FeCl3 in 52.5 ml of 1.7 M HCl solution) Stirred again at 70 $^{\circ}$C for 30 minutes. After cooling to room temperature added DCM (100 ml). Aqueous layer was extracted with DCM (40 ml x 4). Combine organic layers were washed using 5% HCl, H$_2$O and saturated NaHCO$_3$ and again with water. Organic layer was dried over MgSO$_4$ and filtered. The solvent was removed by rotary evaporation and brown color crude product purified using sublimation. (110 ^{0}C, 0.6 mmHg)(72%). ^{1}H NMR (400 MHz, CDCl$_3$): δ 8.05 (s,2H). ^{13}C NMR (100 MHz, CDCl$_3$): δ 137.16, 113.31, 111.93.

Compound 3.3:[5] To a air free flask added copound **3.2** (1.98 g, 0.015 mol) followed by KOH (8.42 g, 10 equiv) powder. To this mixture added 100 % ethylene glycol (32 ml). Refluxed at 200 ^{0}C overnight. After cooling down to room temperature the reaction mixture was poured into water and washed several times using diethyl ether. Then acidified using conc. HCl and extracted using diethyl ether. Organic layer was dried over MgSO$_4$ and filtered. The solvent was removed by rotary evaporation and crude product was purified by recrystallization using water to obtain white color crystals.(27%). ^{1}H NMR (400 MHz, D$_2$O): δ 8.30 (s, 2H). ^{13}C NMR (100 MHz, D$_2$O): δ 170.24, 140.44, 134.50.

Compound 3.4:[5] To compound **3.3** (0.84 g, 0.005 mol) added acetic anhydride (21 ml) and stirred at 140 $^{\circ}$C overnight. After cooling down to room temperature yellow color reaction solution was concentrated to a pale brown solid which was recrystallized by toluene to obtain pale yellow color crystals.(73%). ^{1}H NMR (400 MHz, CDCl$_3$): δ 8.07(s,2H). ^{13}C NMR (100 MHz, CDCl$_3$): δ 156.54, 135.42, 129.50.
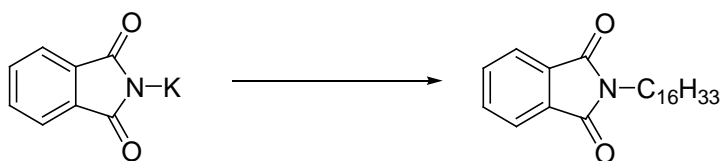
3.5

Compound 3.5:[4] Potassium phthalimide (3.0 g, 0.0162 mol) was added to a solution of hexadecylbromide (4.5 ml, 0.0147 mol) in Dry DMF(18 ml). This was refluxed at 90 °C overnight. After cooling down to room temperature, resulted white color suspension was extracted by water/ DCM. The organic layer was dried over $MgSO_4$ and filtered. After solvent was removed by rotary evaporation the crude was purified using column of silica gel with DCM (1:3) as eluent to give white color solid(92%).^{1}H NMR (400 MHz, CDCl3): δ 7.81(dd, 2H), 7.68(dd, 2H), 3.65(t, 2H), 1.64(m, 2H), 1.27(m,26H), 0.85(t,3H).). ^{13}C NMR (100 MHz, $CDCl_3$): δ 182.52, 168.16, 133.53, 131.88, 122.85, 37.78, 31.61, 29.37, 29.30, 29.26, 29.17, 29.04, 28.89, 28.29, 26.56, 22.38, 13.81.
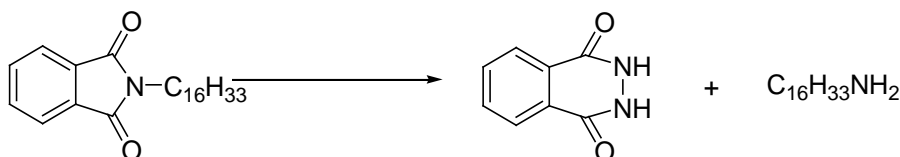
3.6

Compound 3.6:[4] Hydrazine hydrate (hydrazine, 51%)(1.04 ml, 3 equiv) was added to compound **3.5** (2.04 g, 0.0055 mol) in bulk methanol (26 ml). Then refluxed at 95 °C for 6 hours. After cooling down to room temperature, diluted with DCM (25 ml) and washed with 10 % KOH (15 ml x 2). Aqueous layer again extracted with DCM (25 ml x 3). The organic layer was dried over $MgSO_4$ and filtered. After solvent was removed by rotary evaporation white color solid was obtained. Used this crude product for future synthesis without further purification. (97%)

3.4 **3.7** **3.8**
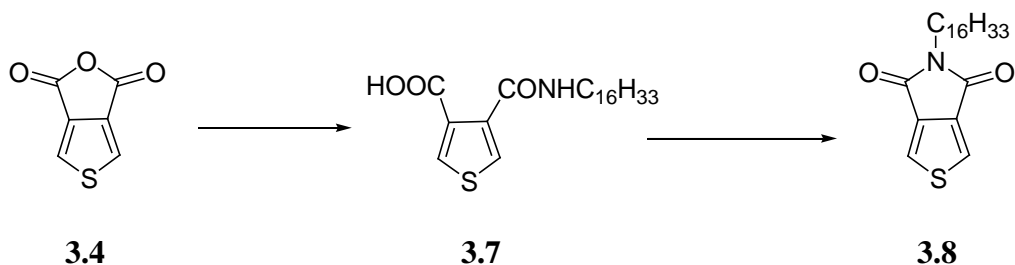
Compound 3.7:[5] To a solution of compound **3.4** (0.54, 0.0035 mol) in bulk toluene (55 ml) compound **3.6** (0.896 g, 1.06 equiv) was added and refluxed 24 hours at 110 ^{o}C. After cooling down to room temperature crude product was collected by filteration. Filterate was washed with 5% HCl and extracted with ether. The organic layer was dried over MgSO$_4$ and filtered. After solvent was removed by rotary evaporation white color solid was obtained by recrystallization using toluene as the solvent.(94%)

Compound 3.8:[5] To compound **3.7** (1.26 g, 0.0032 mol) thionyl chloride (70 ml) was added and refluxed at 80 ^{o}C for 3 hours. Then cool down to room temperature and concentrated to obtain pale yellow crystals. Recrystallization using hexane gave white color crystals.(84%). ^{1}H NMR (400 MHz, CDCl$_3$): δ 7.76(s,2H), 3.57(t,2H), 1.60(m, 2H), 1.26(m, 26H), 0.84(t, 3H). ^{13}C NMR (100 MHz, CDCl$_3$): δ 162.5, 136.5, 125.64, 38.71, 32.11, 29.88, 29.77, 29.70, 29.55, 29.40, 28.67, 27.07, 22.89,14.32.

3.9
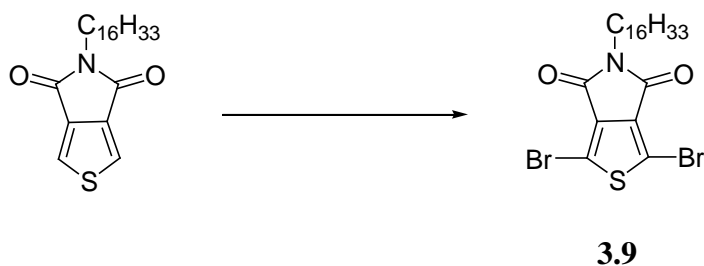
Compound 3.9:[5] To an air free flask compound **3.8** (0.32 g, 0.000843 mol) was added followed by conc. H$_2$SO$_4$ (1.26 ml) and trifluoroacetic acid (4.215 ml). To this reaction mixture NBS (0.6 g, 4 equiv) was added as one portion. Refluxed at 55 ^{o}C overnight.

After cooling down to room temperature brown color solution was poured in to ice cooled water (50 ml) and then extracted with DCM. The organic layer was dried over $MgSO_4$ and filtered. After solvent was removed by rotary evaporation crude product was purified using column of silica gel with hexane/ DCM (7:3) as the eluent to give white color solid. This was further purified by recrystallization using ethanol(51%). ^{1}H NMR (400 MHz, CDCl3): δ 3.57(t, 2H), 1.59(m,2H), 1.25(m,26), 0.85(t,3H). ^{13}C NMR (100 MHz,CDCl$_3$):δ160.60,135.02,113.12,39.05,32.14,29.90,29.87,29.83,29.78,29.65,29.57 ,29.36, 28.46, 22.91,14.34.
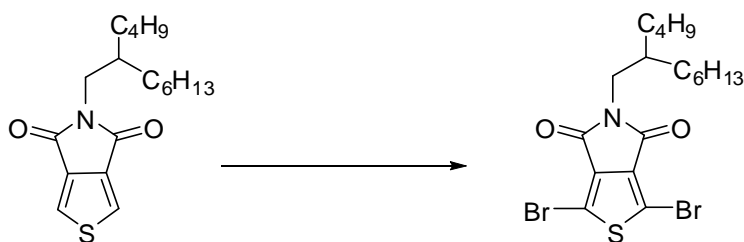
3.10

Compound 3.10:[5] This was prepared similar to compound **3.9**. (63%) ^{1}H NMR (400 MHz, CDCl3): δ 3.46-3.44(d,2H),1.78(m,1H),1.22(m,16H),0.85(m,6H) ^{13}C NMR (100 MHz, CDCl$_3$): δ160.87,134.94,113.13,43.27,37.07,32.05, 29.82,28.69, 26.48 ,23.19 ,14.33,14.31
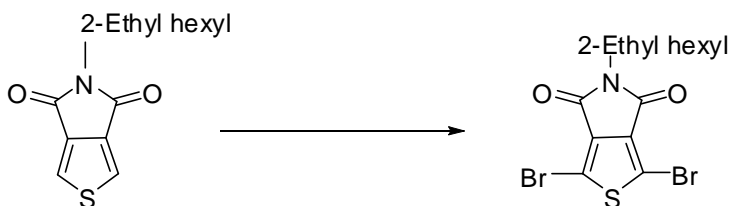
3.11

Compound 3.11:[5] This was prepared similar to compound **3.9**. (53%) ^{1}H NMR (400 MHz, CDCl3): δ 3.46-3.44(d,2H),1.73(m,1H),1.26(m,8H),0.86(m,6H)

3.12   **3.13**   **3.14**   **3.15**
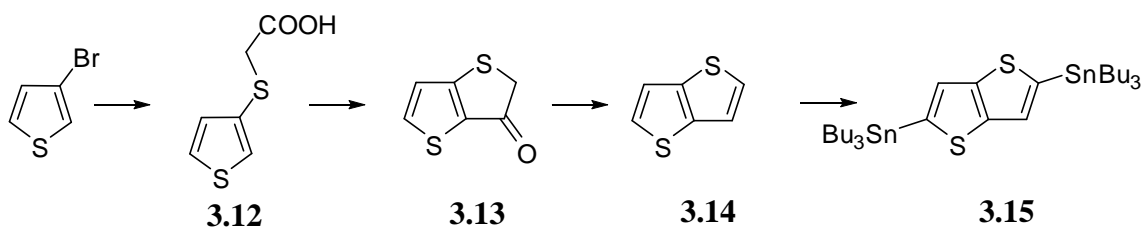
Compound 3.12:[6] To an ether solution (75 ml) of 3-bromothiophene (25 g, 153 mmol) which was kept in -78 °C, n-BuLi (2.5 M in hexane) (65 ml, 162 mmol) was slowly added dropwise. Then the reaction mixture was stirred at -78 °C for 30 min. Then added sulfur (5.19 g, 162 mmol) as one portion. The yellow color reaction mixture was stirred for an additional 1 hour at -78 °C. To this reaction mixture then added a solution of potassium bromoacetate in a mixture of THF/H$_2$O (3:4; v/v) in a period of 1 hour.(The bromoacetate was prepared by adding a solution of K$_2$CO$_3$ (23.04 g) in 83 ml of H$_2$O to a solution of bromoacetic acid (23.16 g) in 62.5 ml of THF) The resulted white suspension was stirred for additional 2 hour at 55 ^{0}C. After that cool down to room temperature and diluted with H$_2$O until a clear solution formed. The organic phase was separated and the aqueous phase was acidified using 2 N HCl and extracted it using ether (3 x 200 ml). Combined all the organic layers and dried using MgSO$_4$. After removal of solvent the crude product was obtained as pale white solid (80%) which was used without further purification. ^{1}H NMR (400 MHz, CDCl$_3$): δ 10.20 (bs, 1H); 7.31-7.33 (m, 2H); 7.08 (dd, 1H); 3.55 (s, 2H). ^{13}C NMR (100 MHz, CDCl$_3$): δ 176.13, 130.26, 129.76, 126.85, 126.66, 38.02.

Compound 3.13:[6] To an ether solution (80 ml) of 3.12 (8.0 g, 2.6 mmol) SOCl$_2$ (1.40 ml, 18.4 mmol) was added and the reaction mixture was refluxed for additional 6 hours at 80 °C. Then excess SOCl$_2$ was removed and the reaction mixture was redissolved in dichloroethane (80 ml) and slowly added to a solution of AlCl$_3$ in dichloroethane (80 ml)

at 0 ^{0}C over 2 hours. The reaction mixture was refluxed for 24 hours. After cooling to r.t. the reaction mixture was poured in to a mixture of ice (100 g) and concentrated HCl (200 ml). The aqueous phase was extracted using DCM (3 x 200 ml) and the combined organic phases were dried using $MgSO_4$. Then concentrated and the resulted crude product was purified using column chromatography (silica gel,hexane/DCM (1/4)) to give compound 3.13 as a pale brown solid (55 %).%). ^{1}H NMR (400 MHz, CD_2Cl_2): δ 7.95 (d, 1H); 7.05 (d, 1H); 4.12 (s, 2H). ^{13}C NMR (100 MHz, CD_2Cl_2): δ 190.70; 163.61; 142.36; 132.60; 123.42; 46.17.

Compound 3.14:[6] To a solution of MeOH/DCM (40 ml; 1:1 v:v) compound **3.13** (1.60 g, 10.24 mmol) was added followed by $NaBH_4$ (0.40 g, 10.24 mmol) at 0 ^{o}C. After complete addition the solution was stirred at room temperature for additional 3 hours. Then the resulted reaction mixture was diluted with DCM (200 ml) and poured slowly to an ice cold 1 N HCl (200 ml) solution and stirred at room temperature. for 30 min. Then the organic layer was separated and washed with H_2O. Then dried using $MgSO_4$. Then concentrated and the resulted crude product was purified using column chromatography (silica gel, DCM) to give compound **3.14** as a white solid (80 %).^{1}H NMR (400 MHz, CD_2Cl_2): δ 7.41 (d, 2H), 7.29 (d, 2H). ^{13}C NMR (100 MHz, CD_2Cl_2): δ 140.04, 127.97, 119.90.

Compound 3.15:[6] This was prepared by following the same procedure as the compound **2.9**. After column, **3-15** was obtained as a colorless oil (74%). ^{1}H NMR (400 MHz, CD_2Cl_2): δ 7.24 (s, 2H), 1.58 (m, 12H), 1.34 (m, 12 H), 1.14 (m, 12H), 0.90 (m, 18H). ^{13}C NMR (100 MHz, CDCl3): δ 147.83, 140.36, 126.45, 29.19, 27.51, 13.89, 11.11.
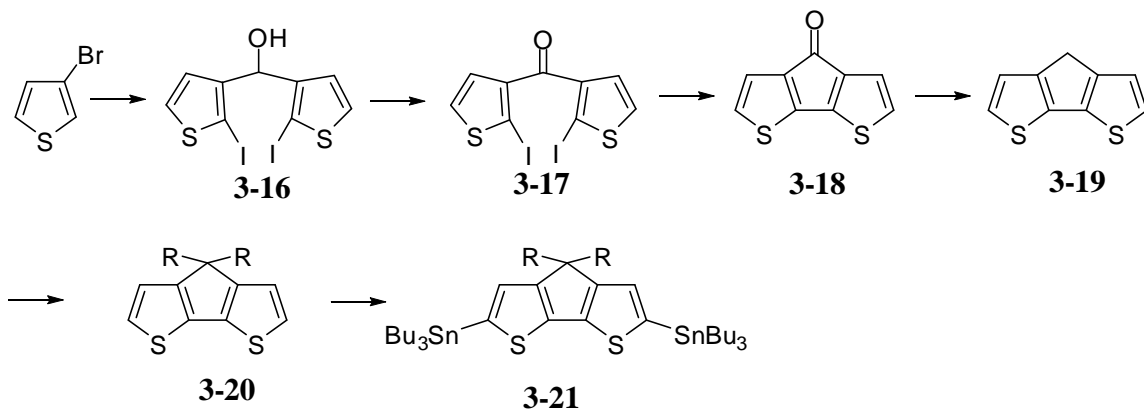
R: *n*-octyl **(a)**
R: 2-ethylhexyl **(b)**

Compound 3.16:[6,7] To an ether solution of 3-bromothiophene (3.26g, 20 mmol), n-BuLi (2.5M in hexane) (8 ml, 20 mmol) was added dropwise at -78 °C and stirred additional 4 hours. To this added a solution of thiophene-3-carbaldehyde (2.24 g, 20 mmol) in ether (30 ml) via a syringe. Then the reaction mixture was stirred at – 78 °C for additional 30 min and then warmed to room temperature and stirred for another 30 min. After cooling to -78 °C, n-BuLi (2.5 M in hexane) (16 ml, 40 mmol) was added. The reaction was stirred at -78 °C for additional 2 hours and then warmed to room temperature and continue stirring for additional 2 hours. After coling to – 78 °C, a solution of I_2 (15.99 g, 63.0 mmol) in ether (80 ml) was added dropwise. The reaction was warmed to room temperature and added a solution of 10% (w/w) aqueous Na_2SO_3 (50 ml) under vigorous stirring and the aqueous layer was acidified using 10% (w/w) aqueous HI solution till the pH is ~5. Then the ether layer was separated and washed using H_2O until neutral, and then dried over $MgSO_4$. Then concentrated and the resulted crude product was purified using column chromatography (silica gel, hexane/DCM 3:7) to give compound **3.16** as a white solid (80 %).^{1}H NMR (400 MHz, CDCl₃): δ 7.42 (d, 2H), 6.91 (d, 2H), 5.75 (d, 2H), 2.24 (d, 1H). ^{13}C NMR (100 MHz, CDCl₃): δ 146.52, 131.21, 126.76, 75.52, 71.46.

Compound 3.17:[6,7] To a solution of compound **3.16** (8.96 g, 20.0 mmol) in DCM (100 ml) , PCC (6.46 g, 30.0 mmol) was added as one portion at room temperature. Then stirred 12 hours at room temperature. Then the reaction mixture was filtered and washed using DCM several times. The resulted filterate was concentrated and purified by column column chromatography (silica gel, DCM) to obtain yellow solid which was further purified by recrystallization using MeOH to obtain yellow solid. (92%) ^{1}H NMR (400 MHz, CDCl$_3$): δ 7.45 (d, 2H), 7.04(d, 2H). ^{13}CNMR (100 MHz, CDCl$_3$): δ 185.32, 143.01, 131.44, 129.21, 81.14.

Compound 3.18:[6,7] To the compound **3.17** (2.23 g, 5 mmol) in DMF (20 ml) copper powder (0.96 g, 15 mmol) was added in one portion and the reaction mixture was refluxed for 20 h. After cooling to room temperature the reaction mixture was filtered using ether and ether layer was extracted 3 times using H$_2$O. Then the organic layer was washed with brine and dried over MgSO$_4$. Then concentrated and purified by column chromatography (silica gel, hexane/DCM (2/3)) to obtained compound 3.18 as a purple solid (92%) ^{1}H NMR (400 MHz, CDCl$_3$): δ 7.02 (d, 2H), 6.97 (d, 2H). ^{13}C NMR (100 MHz, CDCl$_3$): δ 182.52, 49.07, 142.31, 127.09, 121.65.

Compound 3.19:[6,7] To the compound **3.18** (0.25 g, 1.3 mmol) , finely ground KOH (0.25 g, 4.46 mmol), ethylene glycol (5 ml) and hydrazine hydrate (100%, 0.5 ml) were added and the reaction flask was heated to 180 ^{o}C and stirred for 12 hrs. Then cool down to room temperature. The resulted brown mixture was diluted with H$_2$O and extracted using DCM. All the organic layers were combined and washed with brine and dried over MgSO$_4$. Then concentrated and purified by column chromatography (silica gel, hexane) to obtained compound **3.19** as a white solid (70%) ^{1}H NMR (400 MHz, CDCl$_3$): δ 7.20

(d, 2H), 7.11 (d, 2H), 3.55 (s, 2H). ^{13}C NMR (100 MHz, CDCl$_3$): δ 149.82, 138.79, 124.61, 123.10, 31.95.

Compound 3.20a:[6,7] To compound **3.19** (1.0 g, 5.60 mmol) DMSO (30 ml) was added. Then *n*-octylbromide (2.2 g, 11.2 mmol) and KI was added followed by finely ground KOH (1.0 g) at 0 ^{o}C. Then the reaction mixture was stirred in room temperature for 12 hrs. Then H$_2$O (30 ml) was added at 0 ^{o}C. The reaction mixture was extracted with ether . All the organic layers were combined and washed with brine and dried over MgSO$_4$. Then concentrated and purified by column chromatography (silica gel, hexane) to obtained compound **3.20a** as a yellow oil (85%) ^{1}H NMR (400 MHz, CDCl$_3$): δ 7.17 (d, 2H), 6.96 (d, 2H), 1.83 (m, 4H), 1.58 (m, 20H), 0.92 (m, 4H), 0.84 (t, 6H). ^{13}C NMR (100 MHz, CDCl$_3$): δ 158.34, 136.65, 124.61, 121.85, 53.45, 37.94, 32.03, 30.25, 29.57, 29.47, 24.74, 22.85, 14.32.

Compound 3.20b: [7]This was prepared and isolated as a pale yellow liquid using the same procedure as compound **3.20a** but using 2-ethylhexyl bromide. yellow oil (90% yield). ^{1}H NMR (400 MHz, CD$_2$Cl$_2$): δ 7.08 (d, 2H), 6.91 (d, 2H), 3.43(m,2H),1.84(m, 4H), 0.97-0.83 (m, 19H), 0.73(t, 6H), 0.56 (t, 6H).

Compound 3.21a:[7] It was prepared by following the same procedure as compound **2.9**. **3.21a** was obtained as a pale yellow oil (92%). ^{1}H NMR (400 MHz, CDCl$_3$): δ 6.87 (s, 2H), 1.78 (m, 4H), 1.56 (m, 12H), 1.33 (m, 12H), 1.1 (m, 32H), 0.87 (m, 28H). ^{13}C NMR (100 MHz, CDCl$_3$): δ 160.48, 142.50, 136.03, 129.93, 52.26, 38.02, 32.08, 30.31, 29.62, 29.49, 29.23, 27.45, 24.87, 22.86, 14.32, 13.91, 11.11.

Compound 3.21b:[7] This was prepared and isolated as a pale yellow liquid using the same procedure as compound **3.21a**.Pale yellow oil (90% yield). ^{1}H NMR (400 MHz,

CD$_2$Cl$_2$):δ6.87(s,2H),1.83(br,s,4H),1.54(br,12H)1.30(br,12H),1.08-0.87(br,m,48H) ,0.72(t,6H), 0.54 (t,6H)

3.22   **3.23**

3.24   **3.25**   **3.26**

3.27   **3.28**   **3.29**
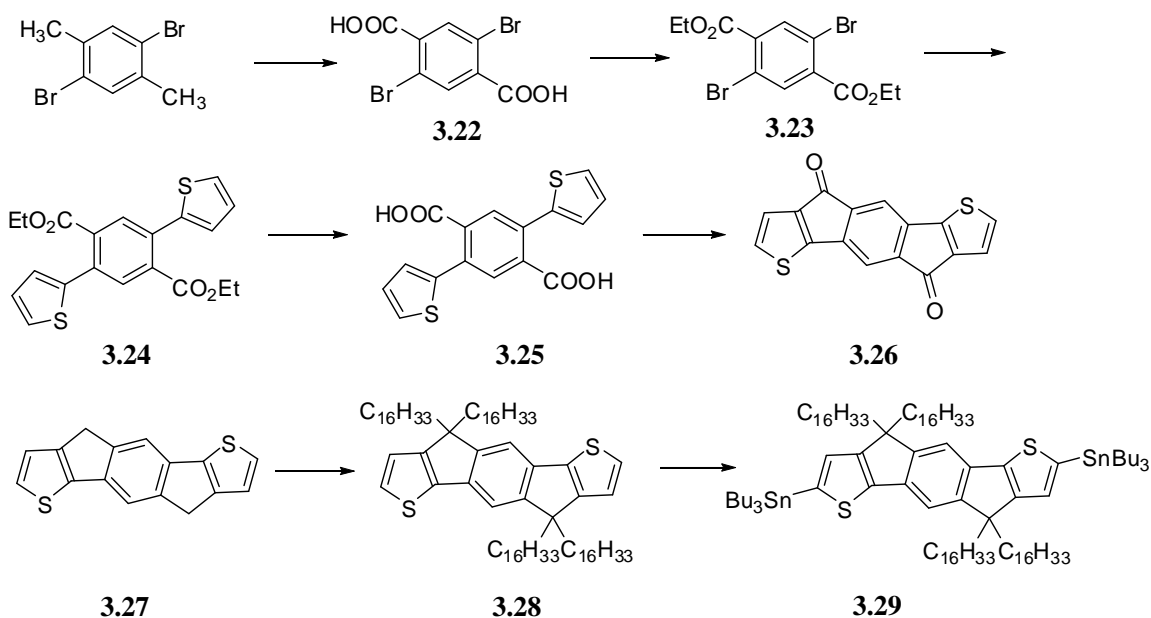
Compound 3.22:[8] 2,5-Dibromo-p-xylene (15 g, 0.057 mol) in pyridine (166 ml) was refluxed for 90 °C for 30 min:. To this added hot aqueous solution of KMnO$_4$ (40.5 g KMnO$_4$ in 110 ml of H2O and heated to 100 ^{0}C) over a period of 1 hour. After complete addition could see purple color solution. Refluxed this mixture for 120 °C overnight. Then cool down to room temperature. Could not see purple color. Completely turned in to brown color. The reaction mixture was filtered and residue was washed with hot H$_2$O and EtOAc. Then extracted the aqueous layer 3 times using EtOAc. The organic layer give unreacted starting material 2,5-Dibromo-p-xylene. Brownish color aqueous layer filtered through celite and obtain clear yellow solution. This was acidified with 3N HCl till the pH come to ~ 1. This resulted white solid was collected and the resulted filterate was again extracted 3 times using EtOAc. After removing solvent under reduced pressure obtained a white solid. Combined both these white solids and suspended it in 110 ml water. To this added 8 g of KOH. This solution

was heated to 90 $^{\circ}$C for 30 min: and then added an aq. Solution of KMnO$_4$ (22 grams in 300 ml) slowly over 40 min. Stirred 1 hour at 90 $^{\circ}$C. Then cool down to room temperature and added 10 ml of methanol. The resulted reaction mixture was filtered through celite and the resulted filterate was acidified again using 3M HCl till the pH reach to 1. Collected the white solid. Filterate also further extracted 3 times with EtOAc and concentrated to get some more white solid. Obtain 70% of the desired crude acid as a white solid.

Compound 3.23:[9,10] Compound **3.22** (10 g, 0.031 mol) was dissolved in EtOH (200 ml) and add conc. H$_2$SO$_4$ 20 ml. Then refluxed the reaction mixture for 2 days at 100 ^{0}C. After 2 days checked TLC and seem to be still some starting material is remaining (hex:EtOAc 1:1). Added another 20 ml of conc H$_2$SO$_4$ and 200 ml of EtOH with some molecular sieves. Refluxed again at 100 ^{0}C for another 1 day. Then washed the reaction mixture using DCM several times and collected the organic layer. This was dried over MgSO$_4$. After removal of solvent, the crude product was obtain as white color solid.(80%) ^{1}H NMR (400 MHz, CDCl$_3$): δ 6.89 (s, 2H), 1.80 (m, 4H), 1.56 (m, 12H), 1.33 (m, 12H), 1.1 (m, 32H), 0.89 (m, 28H).

Compound 3.24: Compound **3.23**(6.9044 g, 0.0182 mol) was dissolved in dry THF(30 ml) and added dropwise Pd(PPh$_3$)$_4$ in dry THF(10 ml) which was freshly prepared using Pd$_2$(dba)$_3$ and PPh$_3$; Pd loading is 5%. To this flask then added 2-tributylstannane thiophene and bubble N$_2$ for 15 min: Then refluxed at 80 ^{0}C overnight. After cooling to room temperature the reaction mixture was diluted with H$_2$O (40 mL) and extracted with DCM (3 x 20 mL). The combined organic phase was washed with brine (2 x 20 mL) and

dried over MgSO$_4$. After removal of solvent, the crude product was obtained and used without further purification (75%)

Compound 3.25:[11] Compound **3.24** (7.14 g, 0.0185 mol) was dissolved in 400 ml of bulk ethanol and to this added aq solution of NaOH (10 g of NaOH in H$_2$O). This mixture was refluxed overnight at 90 ^{o}C. Then concentrated and added 12 N HCl till become acidic. The resulted precipitate was collected by filteration and washed several times using water to get white color solid. (71%)^{1}H NMR (400 MHz, DMSO): δ 13.45 (s, 2H), 7.72(s, 2H), 7.70 (dd, 2H), 7.29 (dd, 2H), 7.16 (m, 2H)

Compound 3.26:[11] Compound **3.25** (2.0g, 0.0061 mol) was added to dry DCM 100 ml. Then added oxalyl chloride (2.08 ml, 4eq). To this mixture anhydrous DMF (0.94 ml) was added drop wise at room temperature. Stirred the mixture overnight at room temperature. Then concentrated it by bubbling N$_2$ and then dried it to obtain the crude acyl chloride as yellow color solid. This solid was again dissolved in dry DCM (80 ml) and added to a suspension of anhy AlCl$_3$(4g) in 120 ml of dry DCM at 0 ^{0}C. Then warm down to rt and stirred overnight. The resulted reaction mixture carefully poured into an ice cold 10% HCl solution (150 ml). Form a blue color precipitate and it was collected by filtration and further washed by using 2M HCl solution (100 ml). Then again washed using H$_2$O and acetone. Then dried in vacuum and obtain blue color solid. (79%) IR 1703 cm^{-1}

Compound 3.27:[11] To this blue color solid of compound **3.26** (1.21 g, 0.00411 mol) hydracine hydrate (100%) [hydrazine 64%] 4.38 ml (90.40 mmol) was added followed by KOH in 50 ml of diethylene glycol. Then under N$_2$ refluxed for 24 hours at 180 ^{0}C. Then

cool down and poured in to ice cold 12 N HCl. The resulted precipitate was collected and dried under vacuum. Obtain compound **3.27** as a pale brown solid (71%).

Compound 3.28:[11] Compound **3.27** (0.66 g, 0.0025 mol) was dissolved in dry DMSO (15 ml).To this added freshly prepared t-BuONa (5 grams of Na+ t-BuOH 5 ml and dissolved in 10 ml dry DMSO). The mixture was refluxed at 80 ^{0}C for 1 hour. To this added $C_{16}H_{33}Br$ 4.5 ml drop by drop at 80 ^{0}C. Kept refluxing further 05 hours. Then the mixture was poured in to ice water. The resulted precipitate was collected and washed with water and methanol. The crude product was purified via column using hexane as the eluent to give compound **3.28** as yellowish white solid (45%).^{1}H NMR (400 MHz, CD_2Cl_2): δ 7.27-7.26 (m,4H), 6.96(s,2H), 1.96(m,4H), 1.84(m,4H), 1.08-1.24 (m,104H), 0.87(m,20H)

Compound 3.29:[4] This was prepared and isolated as a pale yellow liquid using the same procedure as compound **2.9a**. Pale yellow oil (90% yield). ^{1}H NMR (400 MHz, CD_2Cl_2): δ6.93(s,2H),1.92(m,4H),1.83(m,4H),1.59(m,12H),1.36(m,12H),1.23(m,116H),0.89(m,40 H)^{13}CNMR(100MHz,$CDCl_3$):157.37,153.68,147.89,139.42,135.49,129.62,113.62,52.76, 39.06,31.75,29.93,29.53,29.19,28.64,27.04,24.08,22.51,13.92,13.49,10.71(**Note:**some peaks in[13]C NMR spectrum overlap).

General Procedure for Stille Polymerization:

To an air free flask containing the two monomers (0.2 mmol each) was added a mixture of $Pd_2(dba)_3$ and tri(o-tolyl)-phosphine (1:8 molar ratio between $Pd_2(dba)_3$ and tri(o-tolyl)-phosphine: 0.03% Pd loading) under inert atmosphere. After 3 pump/purge cycles of reduced pressure and refilling with N_2, anhydrous, degassed THF (4 ml) was added via syringe and the vessel was sealed and its contents stirred vigorously in an 80 °C bath for

48 hours. After cooling to room temperature, the reaction mixture was dripped to a 100 ml vigorously stirred methanol solution containing 5 ml of 12 N HCl. After stirred for 4 hours, the solid was collected by centrifugation. The solid polymer was dried and subjected to sequential soxhlet extraction. Unless until stated the common sequential solvents were methanol, acetone, hexane and chloroform. After soxhlet extraction the polymer solution was concentrated, re-precipitated into 100 ml methanol, collected by centrifugation and dried under reduced pressure.

3-**P1**
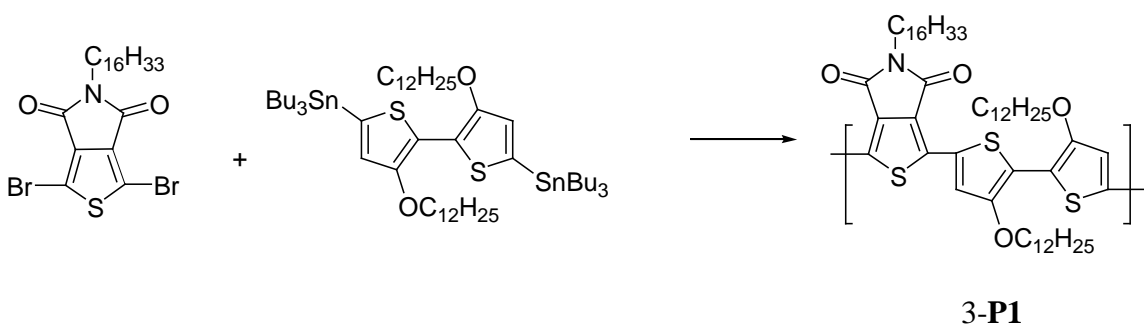
3-P1: Yield 93%. This was prepared following the general procedure for polymerization and purified by sequential soxhlet extraction using methanol, acetone, hexane and chloroform as solvents. After dried in vacuum polymer **3-P1** was obtained as dark blue solid. Mn: 28 kDa, PDI: 1.32 ^{1}H NMR (400 MHz, 130 ^{0}C, $C_2D_2Cl_4$): δ 8.08(s,2H), 4.38(s,br,4H), 3.76(s,br,2H), 2.08(m,br,4H), 1.36(m, br, 64H), 0.94(s, br, 9H)

3-P2
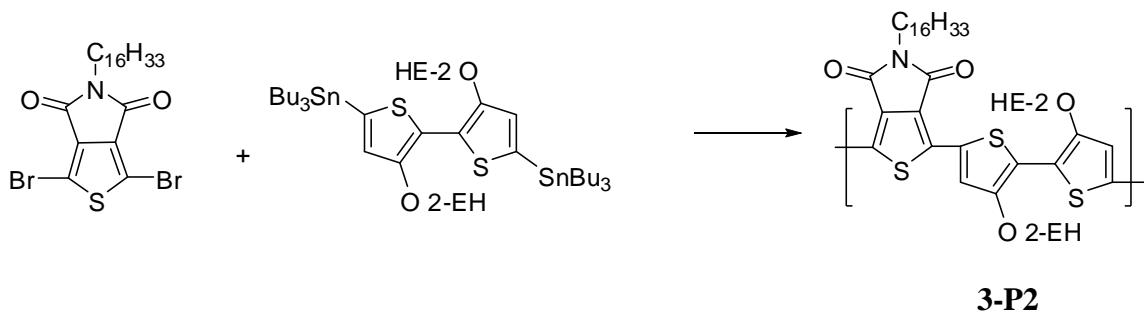
3-P2: Yield 79%. This was prepared following the general procedure for polymerization and purified by sequential soxhlet extraction using methanol, acetone, hexane and

chloroform as solvents. After dried in vacuum polymer **3-P2** was obtained as dark blue solid. Mn: 21 kDa, PDI: 2.5[1]HNMR (400 MHz, 130 ^{0}C, C$_2$D$_2$Cl$_4$): δ 8.11(s,2H),4.30(br,4H),3.74(br,2H),   2.04(br,2H),1.73-1.45(br,m,46H),1.06(br,t,15H).

3-P3
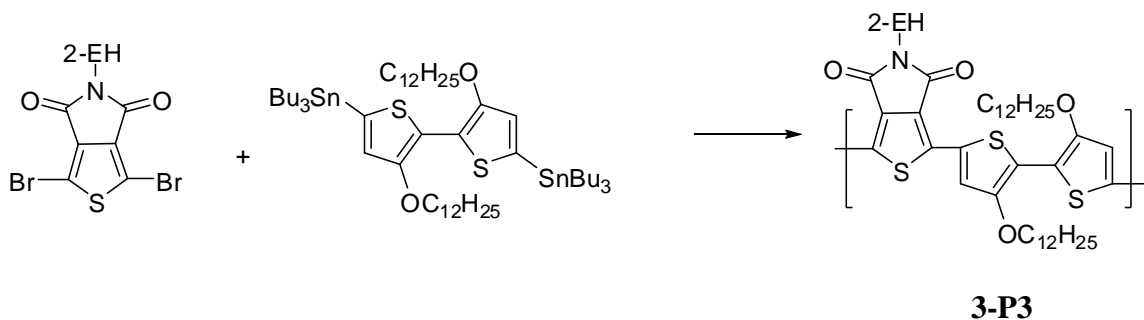
3-P3: Yield 96%. This was prepared following the general procedure for polymerization and purified by sequential soxhlet extraction using methanol, acetone, hexane and chloroform as solvents. After dried in vacuum polymer **3-P3** was obtained as dark blue solid. Mn: 21 kDa, PDI:2.5[1]H NMR (400 MHz, 130 ^{0}C, C$_2$D$_2$Cl$_4$): δ 8.06(s,br,2H),4.38(br,4H),3.68(br,2H), 2.11 (br,4H), 1.43(br,43H), 1.05-0.95(br,12H)

3-P4
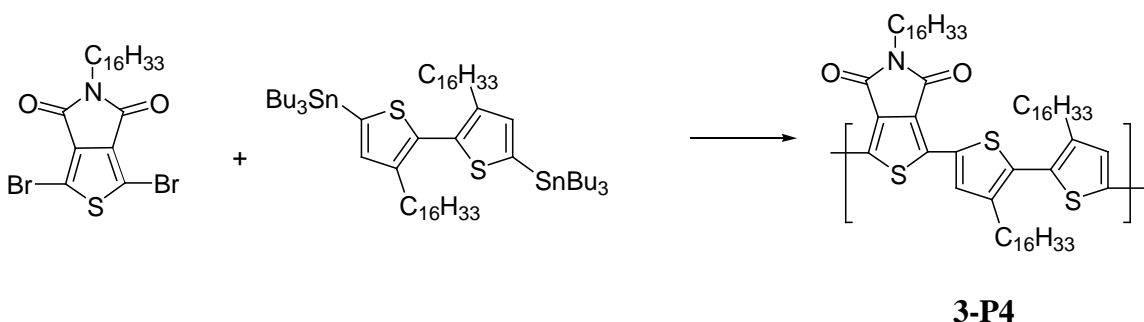
3-P4: Yield 85%. This was prepared following the general procedure for polymerization and purified by sequential soxhlet extraction using methanol, acetone and hexane as solvents. After dried in vacuum **3-P4** was obtain as brown color solid. Mn: 14 kDa, PDI: 1.41. ^{1}H NMR (400 MHz, 130 ^{0}C, C$_2$D$_2$Cl$_4$): δ 7.97(s,2H), 3.72(s,br,2H), 2.70(s,br,4H), 1.73(m, 6H), 1.34(m, br, 78H), 0.95(s, br, 9H)

3-P5
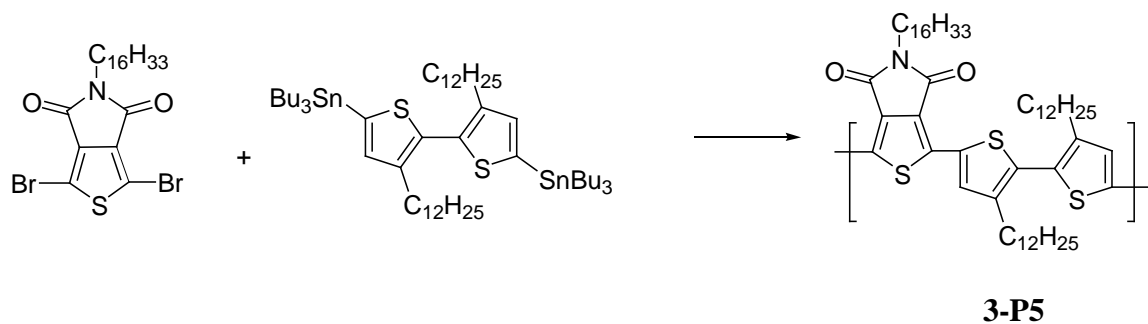
3-P5: Yield 92%. This was prepared following the general procedure for polymerization and purified by sequential soxhlet extraction using methanol, acetone and hexane as the solvents. After dried in vacuum **3-P5** was obtained as brown color solid.92%) Mn:13 kDa, PDI: 1.54. ^{1}H NMR (400 MHz, 130 ^{0}C, $C_2D_2Cl_4$): δ 7.98(s,2H), 3.74(s,br,2H), 2.68(s,br,4H), 1.73(m,br,10H), 1.36(m, br, 58H), 0.94(s, br, 9H)

3-P6
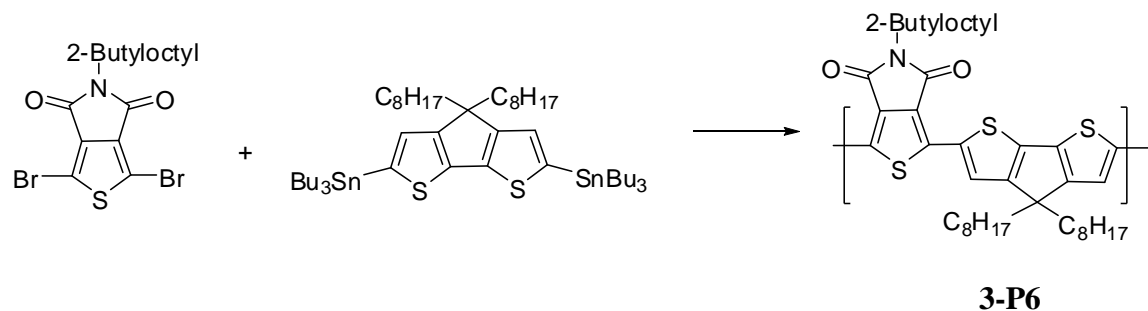
3-P6: Yield 89%. This was prepared following the general procedure for polymerization and purified by sequential soxhlet extraction using methanol, acetone , hexane and chloroform as the solvents. After dried in vacuum **3-P6** was obtained as brown color solid.89%) Mn:33 kDa, PDI: 1.6. ^{1}H NMR (400 MHz, 130 ^{0}C, $C_2D_2Cl_4$): δ 7.96(br,s,2H),3.68(br,s,2H),2.06(br,s,4H),1.45-1.30(br,m,41),0.93(br,m,12H)
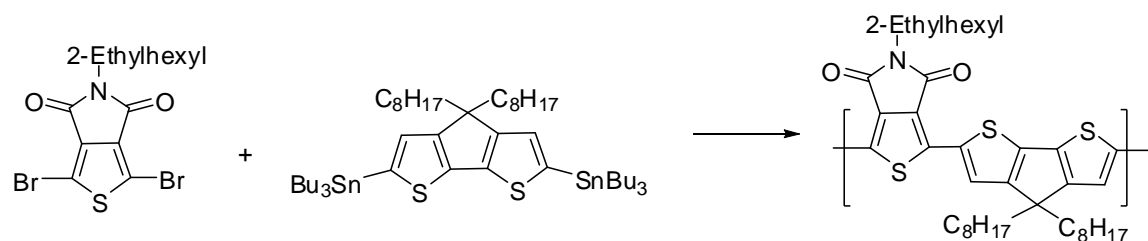
3-P7: Yield 93%. This was prepared following the general procedure for polymerization and purified by sequential soxhlet extraction using methanol, acetone , hexane and chloroform as the solvents. After dried in vacuum polymer **3-P7** was obtained as brown color solid.89%) Mn:29 kDa, PDI: 2.7. ^{1}H NMR (400 MHz, 130 ^{0}C, $C_2D_2Cl_4$): δ 7.96(br,s,2H), 3.70(br,s,2H), 2.05(br,4H), 1.45-1.30(br,m,34H), 1.06-0.93(br,m,12H)
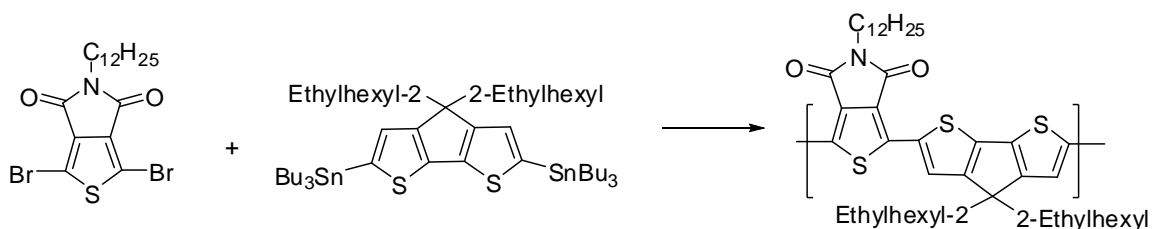
3-P8

3-P8: Yield 83%. This was prepared following the general procedure for polymerization and purified by sequential soxhlet extraction using methanol, acetone , hexane and chloroform as the solvents. After dried in vacuum polymer **3-P8** was obtained as brown color solid.89%) Mn:16 kDa, PDI: 1.53.
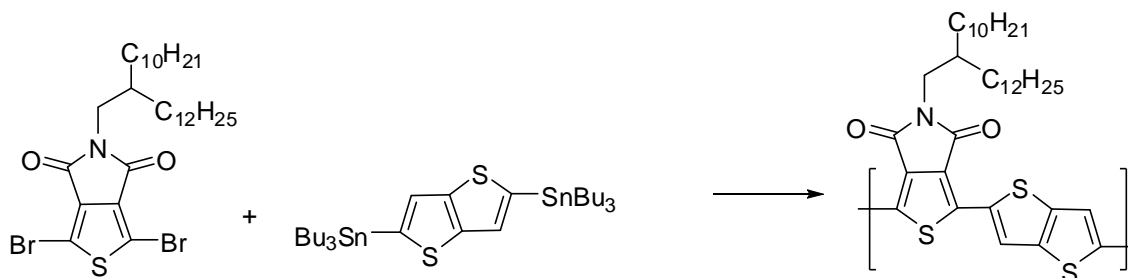
3-P9

3-P9: Yield 72%. This was prepared following the general procedure for polymerization and purified by sequential soxhlet extraction using methanol, acetone, hexane,chloroform and chlorobenzene as solvents. After dried in vacuum polymer **3-P9** obtained as deep

blue solid. Molecular weight was not available due to the low solubility in THF. ^{1}H NMR

(400 MHz, $C_2D_2Cl_4$, 130 ºC): δ 7.33(br,2H), 1.43(br very,42H),0.98(br,6H)
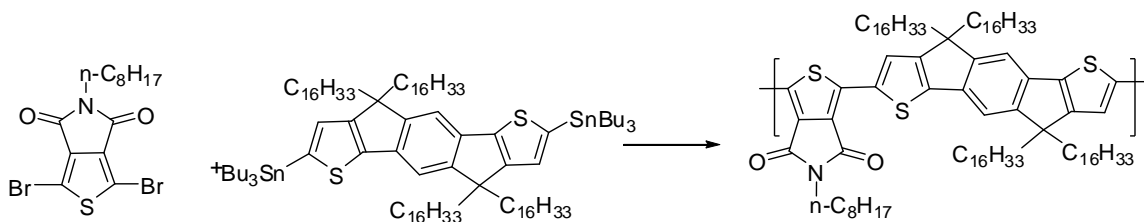
3-P10

3-P10: Yield 76%. This was prepared following the general procedure for polymerization

and purified by sequential soxhlet extraction using methanol, acetone, hexane,chloroform

as the solvents. After dried in vacuum polymer **3-P10** obtained as deep blue solid. Mn:15

kDa, PDI: 1.69.   ^{1}H NMR (400 MHz, $C_2D_2Cl_4$, 130 ºC): δ 7.53(br,s,2H),

3.72(br,s,2H),2.08(br,s,8H), 1.45-1.29(br,m,123),0.89(br,16H)

6.3 Synthesis section of chapter 04

4.0

4.1

4.2   a. n-dodecyl
         b. 2-ethylhexyl
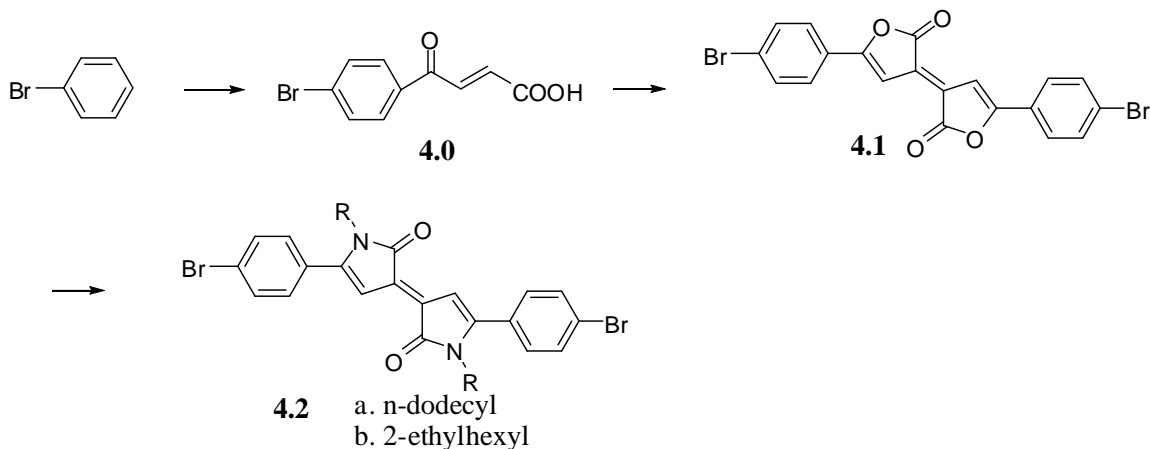
Compound 4.0:[12] In a 2 neck round-bottom flask equipped with a water-cooled condenser, 10 g (0.102 mol) of maleic anhydride was dissolved in 200 ml of dry DCM by continuous stirring. After cooling to 0 °C anhydrous $AlCl_3$ (1.2 eq, 16.32g, 0.122 mol) was added portion wise, followed by dropwise addition of bromobenzene (1.0 eq, 10.71 ml, 0.102 mol), during which the yellow suspension turned to orange then red-brown. After stirring 30 min at 0 °C, the reaction mixture was allowed to slowly warm to RT and stirred overnight, before cautiously quenching at 0 °C with 200 ml of 1M HCl. The organic layer was separated, the aqueous layer further extracted 3 times using DCM, and the combined organic layers were then washed with water, brine and dried over MgSO4. After concentration, the residue was suspended in hexanes and sonicated 30 min, then filtered and dried to give the target yellow solid, which was used without further purification. (90% yield, 23.41g). ^{1}H NMR (400MHz,*d*-DMSO) δ: 7.88 (d,2H, J=8.56 Hz), 7.79 (d,1H, J=15.54 Hz), 7.67 (d,2H, J=8.55 Hz), 6.67 (d,2H, J=15.54 Hz) ^{13}C NMR (100MHz, CDCl3) δ: 128.36,130.75, 132.12, 133.46, 135.21, 135.69, 166.37, 188.64

Compound 4.1: Compound **4.0** (10 g, 0.039 mol, 1eq), anhydrous CuCl (1.425 g, 0.0144 mol,0.37 eq), ammonium chloride (1.5405 g, 0.029 mol, 0.75 eq) and 35 ml of glacial

acetic acid were combined under N_2 in a 500 ml vacuum flask with rotary valve and the mixture sparged with N_2 for 15 min. The vessel was sealed and heated at 140 °C for 2 hours, then the resulting maroonish color suspension was cooled to RT and concentrated under reduced pressure. Filtered the resulting solid using copious amount of water. Then washed it using ethanol and finally with ether. The resulting reddish brown solid was recrystallized from glacial acetic acid and used without further purification (65% yield, 6.032 g) .

Compound4.2a: To compound **4.1** (2 g, 0.0042 mol) in a 2-neck round bottom flask fitted with a reflux condenser and magnetic stir bar was added glacial acetic acid (25 ml) and the whole sparged with N_2 for 15 min. n-$C_{12}H_{25}NH_2$ (3.08 g, 0.0168 mol, 4 eq) was added and the vessel heated in a 140 ^{0}C bath for 2hrs, followed by concentration of the bluish suspension under reduced pressure. The residue was redissolved in DCM and extracted 3 times with H_2O then brine. The organic layer was dried over $MgSO_4$, concentrated under reduced pressure, and the residue purified by column chromatography (silica gel 1:1 hexane:dichloromethane) to yield a blue powder. (0.68 g, 20%) ^{1}H NMR (400MHz, $CDCl_3$) δ: 7.57(d,4H), 7.36(d,4H), 6.86(s,2H), 3.62(t,4H), 1.39 (broad t, 4H), 1.22-1.13 (broad m, 40H), 0.85 (t,3H) ^{13}C NMR (100MHz, CDCl3) δ: 171.35, 151.96, 132.42, 130.42, 129.19, 124.43, 103.68, 41.21, 32.12, 29.27, 29.82, 26.79, 22.90, 14.38 (**Note:** some peaks in^{13}C NMR spectrum overlap).

Compound 4.2b: This was prepared similar to the above compound **4.2a** using compound **4.1** (1.5 g, 0.0032 mol) but using 2-ethyl hexyl amine (4eq) as the amine portion.(15%)^{1}H NMR(400MHz,$CDCl_3$)δ:0.67(t,6H),0.77(t,6H),1.03(b,20H),1.30(b,2H),

3.58(m,4H),6.85(s,2H),7.36(d,4H),7.56(d,4H).^{13}CNMR(100MHz,CDCl3)δ:10.62,14.17,2

3.01,23.87 , 28.53 ,30.48,38.71, 4.54,103.86,124.31,129.23,130.75,132.24,152.04,171.36.

4.3   **4.4**   **4.5**

4.6   **4.7**
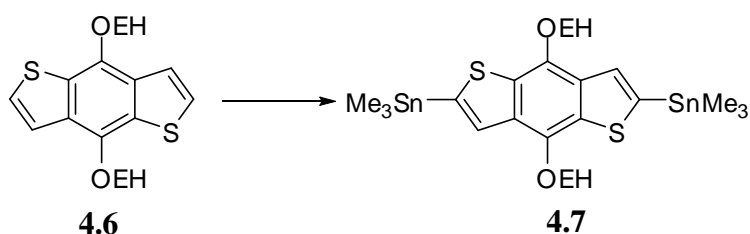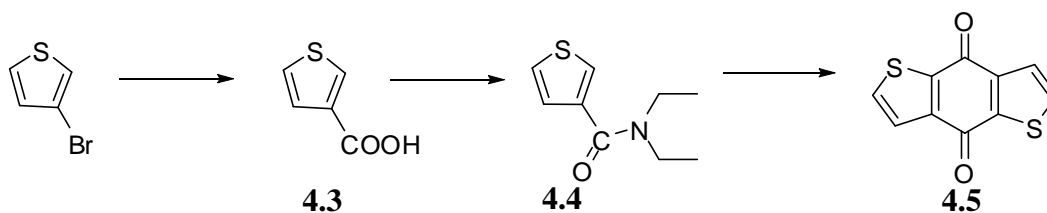
Compound 4.3:[13] n-BuLi (51 ml, 0.127 mol) was added dropwise   to the 3-
bromothiophene (10 ml, 0.106 mol) solution in dry ether (150 ml) at -78 $^{\circ}$C. Then stirred
30 min at -78 $^{\circ}$C. Then quickly poured this white color suspension to a flask containing
finely powdered dry ice and stirred vigorously for 2 hours. Then added slowly 1M HCl
150 ml. Then concentrated and extracted 3 times using EtOAc. The organic layer was
dried using MgSO$_4$ and concentrated under reduced pressure. Compound 4.3 was
obtained as a pale brown solid. (35%)

Compound 4.4:[14] To a suspension of compound **4.3** (1.6298 g, 0.0127 mol) in dry
chloroform (10 ml) SOCl$_2$ (3.23 ml, 0.04445 mol) was added drop wise and then heated
to 70 ^{0}C for 3 hrs. The suspension dissolved completely and formed yellow-brown clear
solution. Then cool down to room temperature and bubble N$_2$ to remove all the solvent.
Formed green color solid. To this solid then added 8 ml of dry DCM and then cool down
to 0 $^{\circ}$C. Then added dried diethyl amine (4.28 ml, 3.3 eq) drop wise. This form a brown

color suspension. Stirred at room temperature for overnight. Then added H_2O and extracted 3 time using DCM. Dried the organic layer using $MgSO_4$ and concentrated the organic layer using reduced pressure. Obtain brown color oil. Used this crude product for the next step without further purification. The crude product can purify via column using EtOAc as the eluent to give compound **4.4** as faint yellow oil.(70%) ^{1}H NMR (400MHz, CDCl$_3$) δ: 7.29(dd,1H), 7.13(dd,1H), 7.00(dd,1H), 3.29(br,s), 1.010(6H,s). ^{13}CNMR(100MHz,CDCl3)δ:166.25,137.20,126.56,125.48,124.71,42.93,39.45,14.18, 12.70.

Compound 4.5:[15] Compound **4.4** (2.876 g,0.0157 mol) was dissolved in dry ether 20 ml. To this added freshly prepared LDA in ether (0.0173 mol) at -78 ^{o}C dropwise. Then kept 10 min at -78 ^{o}C. Then warm down to room temperature. The yellow color reaction mixture turned to brown color. After 15 min could see pale white suspension. This was stirred overnight at room temperature. To this added ice H_2O. Formed light green precipitate. The precipitate was suspended on methanol and sonicated. Then filtered again and collected the olive green solid. (73%) ^{1}H NMR (400MHz, CDCl$_3$) δ: 7.63(d,1H), 7.66(d,1H)

Compound 4.6:[16] Zn dust(1.44 g, 3.0 eq) was added to compound **4.5** (0.00734 mol,1.61 g) in 30 ml of degassed water. To this NaOH (5.87 g,20eq) was added and the resulted green suspension was refluxed for 1 hour at 100 ^{o}C. While refluxing this turn to reddish brown color. After 1 hour cool down to room temperature. Then added (*n*-Bu)$_4$NBr (23.66 mg, 0.01 eq) followed by 2-ethylhexyl bromide. Then again refluxed at 100 ^{0}C overnight. Could see greenish brown color. Then cool down to room temperature and diluted with DCM. Dried the organic layer using $MgSO_4$ and concentrated to obtain the

crude product as yellow color oil. This was purified via column using hexans:DCM 9:1 mixture and after concentration finally obtain yellow color oil.(65%) ^{1}HNMR(400MHz,CDCl$_3$)δ:7.48(d,2H),7.37(d,2H),4.20(d,4H),1.82(m,2H),1.73-1.53(m,8H),1.41(m,8H),1.03(t,6H),0.96(t,6H)^{13}CNMR(100MHz,CDCl3)δ:144.86 ,131.69 ,130.15,126.10,120.44,76.20, 40.89,30.69, 29.43,24.08,23.34,14.36,11.53

Compound 4.7:[16,17] Compound **4.6** (0.9079 g, 0.00203 mol) was dissolved in dry THF (30 ml) and cool down to -78 ^{o}C. To this added n-BuLi drop wise (2.03 ml, 2.5 eq) The pale yellow solution turn to red orange color. Stirred 1 hour at -78 ^{o}C. Then warm down to room temperature. Could see pale tannish color. Kept in room temperature for 30 min. Then cool down to -78° C. Then added Me$_3$SnCl(1.0M solution in hexane) 6.09 ml (3.0 eq) as one portion. Stirred overnight. Can see clear yellow solution. The reaction mixture was quenched with water and extracted using ether 3 times. Remove all the solvent under reduced pressure. The resulted yellowish solid was recrystalized using isopropanol. (92%)^{1}H NMR(400MHz,CDCl$_3$)δ:7.49(s,2H),4.17(d,4H),1.79-1.57(m,10H),1.38(m,8H), 1.00 (t,6H) ,0.92(t,6H),0.42(s,18H)^{13}CNMR(100MHz,CDCl3)δ:143.47,140.59, 134.07 ,133.11, 128.19 ,40.90,30.76,29.47,24.13,23.41,14.43,11.59

4.5   4.8   4.9   4.10
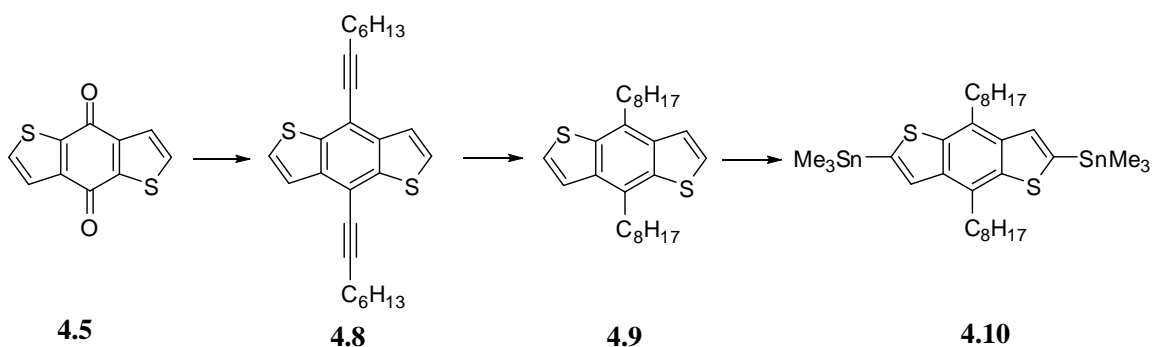
Compound 4.8:[17] To a solution of 1-octyne (1.485 g, 0.0135 mol) in dry THF was added (6ml , 0.012 mol) i-PrMgCl (2M in THF) dropwise at rt. Then the reaction mixture was

refluxed at 60 $^{\circ}$C for 100 min. and then cool down to room temperature. Then added compound **4.5** (0.5g, 0.00227 mol) to this solution. Immidiately turn to dark blue color. Again refluxed at 60 $^{\circ}$C and kept 1 hour. Then cool down and added $SnCl_2.2H_2O$ (4.2 g, 8.15 eq) in 10% HCl (8 ml) dropwise. When adding $SnCl_2.2H_2O$ solution, reaction mixture turned to red color. Then again refluxed overnight at 65 ^{0}C. Then cool down to room temperature and diluted with water. This was extracted with hexane three times. The organic phase was dried using $MgSO_4$ and concentrated under reduced pressure. The compound was purified using column chromatography using hex:DCM 3:1 as the elutent to obtained red color solid.(77%) ^{1}HNMR(400MHz,CDCl$_3$)δ :7.55(d,2H) ,7.48(d,2H) ,2.61(t,4H),1.71 (m, 4H) ,1.53(m,4H),1.35(m,8H),0.91(t,6H)

Compound 4.9:[17] Compound **4.8** (0.498 g,0.00122 mol) was dissolved in bulk THF (94 ml) and bubble N_2 for 15 min. Added Pd/C(10% wt) as one portion. Then bubble H_2 for 5 minutes using H_2 balloon and kept under H_2 atmosphere using a H_2 balloon at room temperature. After 20 min filter the reaction mixture through celite and further washed with DCM. Remove all the solvents using reduced pressure. The crude compound was purified using a column chromatography using hexane as the elutent to obtained compound **4.9** as white color solid.(87%)^{1}HNMR(400MHz,CDCl$_3$)δ:7.45-7.44(d,2H),7.43-7.41(d,2H),3.15(t,4H) ,1.78(m,4H),1.44(m,4H),1.24(m,16H),0.85(6H)

Compound 4.10: It was prepared by following the same procedure as compound **4.7**. Obtain white color solid (90%).

General Procedure for Stille Polymerization:

To an air free flask containing the two monomers (0.2 mmol each) was added a mixture of $Pd_2(dba)_3$ and tri(o-tolyl)-phosphine (1:8 molar ratio between $Pd_2(dba)_3$ and tri(o-tolyl)- phosphine: 0.03% Pd loading) under inert atmosphere. After 3 pump/purge cycles of reduced pressure and refilling with N_2, anhydrous, degassed THF (4 ml) was added via syringe and the vessel was sealed and its contents stirred vigorously in an 80 °C bath for 48 hours. After cooling to room temperature, the reaction mixture was dripped into 100 ml vigorously stirred methanol. After stirring for 4 hours, the solid was collected by centrifugation. The solid polymer was dried and subjected to sequential soxhlet extraction with methanol, acetone, hexane, and chloroform. After soxhlet extraction the polymer solution was concentrated (~15 ml) re-precipitated into 100 ml methanol, collected by centrifugation and dried under reduced pressure. Low solubility in THF prevented molecular weight determinations.

4-P1: Yield 83%. This was prepared following the general procedure for polymerization and purified by sequential soxhlet extraction using methanol, acetone, hexane, chloroform as solvents. After dried in vacuum polymer **4-P1** was obtained as deep blue solid. Molecular weight was not available due to the low solubility in THF. ^{1}H NMR (400 MHz, $C_2D_2Cl_4$, 90 °C): δ 0.94(b,s,12.44H),1.28-1.48(broad m,62.25H), 1.96(b,s, 6.07H), 3.27 (b,s,4.40H), 3.78(b,s,4H), 7.06(s,1.62H), 7.50-7.06(br,d,4.59H), 7.81-7.92(br,d,5.24H)

4-P2: Yield 84%. This was prepared following the general procedure for polymerization and purified by sequential soxhlet extraction using methanol, acetone, hexane, chloroform as solvents. After dried in vacuum polymer **4-P2** was obtained as deep blue

solid. Molecular weight was not available due to the low solubility in THF. ^{1}H NMR (400

MHz, C$_2$D$_2$Cl$_4$, 90 °C): δ 0.91(broad s,6H),1.05(b,6H), 1.15(b,6H), 1.29(b,44H), 1.52(b,12H), 1.96 (b,2H), 3.79(b,4H),4.36(b,4H), 7.08(s,2H), 7.67(b,4H), 7.85(d,4H)

4-P3: Yield 82%. This was prepared following the general procedure for polymerization and purified by sequential soxhlet extraction using methanol, acetone, hexane, chloroform as solvents. After dried in vacuum polymer **4-P3** was obtained as deep blue solid. Molecular weight was not available due to the low solubility in THF. ^{1}H NMR (400

MHz, C$_2$D$_2$Cl$_4$, 90 °C): δ 0.82(b,6H),0.88(b,6H), 0.96(b,6H), 1.38(b,40H), 1.98(b,2H), 3.26(b,4H), 3.75(b,4H), 7.07(s,2H), 7.65(b,4H), 7.82(s,2H), 7.92(b,4H)

4-P4: Yield 82%. This was prepared following the general procedure for polymerization and purified by sequential soxhlet extraction using methanol, acetone, hexane, chloroform as solvents. After dried in vacuum polymer **4-P4** was obtained as deep blue solid. Molecular weight was not available due to the low solubility in THF. ^{1}H NMR (400

MHz, C$_2$D$_2$Cl$_4$, 90 °C): δ 0.79-0.84(b,12H), 1.02(b,6.35H), 1.17(b,20.54H) 1.47(broad m,14.23H), 1.71(b,m,7.80H), 1.94(b,m,2.28H), 3.73(br,m,3.48H),4.33(b,s,4H), 7.04(s,1.77H), 7.63(b,3.40H), 7.63(br,3.40H), 7.85-7.80(br,d,5.24H)

4-P5: Yield 74%. This was prepared following the general procedure for polymerization and purified by sequential soxhlet extraction using methanol, acetone, hexane, chloroform as solvents. After dried in vacuum polymer 4-P5 was obtained as deep blue solid. Molecular weight was not available due to the low solubility in THF. ^{1}H NMR (400

MHz, C$_2$D$_2$Cl$_4$, 90 °C): δ 0.88(b,11.9H), 1.26(b,60H), 1.61-1.51(b,8H) 2.04-1.85(broad m,5.95H), 3.73(b,s,3.55H), 7.03(s,1.86H), 7.35(b,s,2.77H), 7.573(b,s,3.73H), 7.36(b,s,3.93H)

4-P6: Yield 48%. This was prepared following the general procedure for polymerization and purified by sequential soxhlet extraction using methanol, acetone, hexane, chloroform as solvents. After dried in vacuum polymer **4-P6** was obtained as deep blue solid. Molecular weight was not available due to the low solubility in THF. ^{1}H NMR (400 MHz, $C_2D_2Cl_4$, 90 °C): δ 0.91(br,18.18H), 1.6-1.28(b,m,118.17H),2.06-1.88(b,m,12H),3.75(broad m,t,4.08H), 7.05(s,1.85H), 7.38(br,s,5.93H), 7.78-7.60(br,d,4.25 H)

6.5 Electrochemistry measurements

DPV curves for Chapter 2: Polymer films (1mg/ml in Chlorobenzene) in tetra-n-butylammonium hexafluorophosphate solution (0.1 M in dry acetonitrile), 295 K, Scan rate = 50 mV. s^{-1} Corrected for Fc/Fc$^{+.}$

2-P6

HOMO= 4.8+0.14
4.94eV

2-P7

HOMO= 4.8+0.25
5.05eV

2-P8

HOMO= 4.8+0.28
5.08eV

2-P9

HOMO= 4.8+0.30
5.1eV
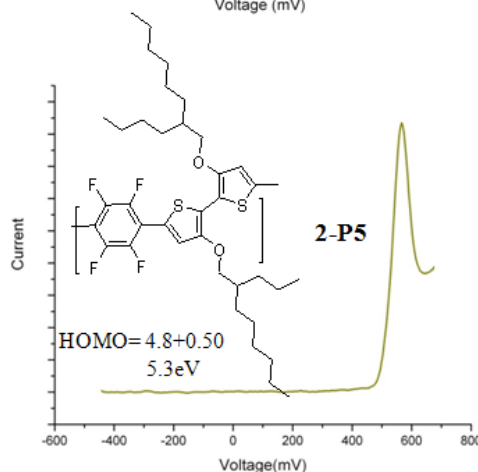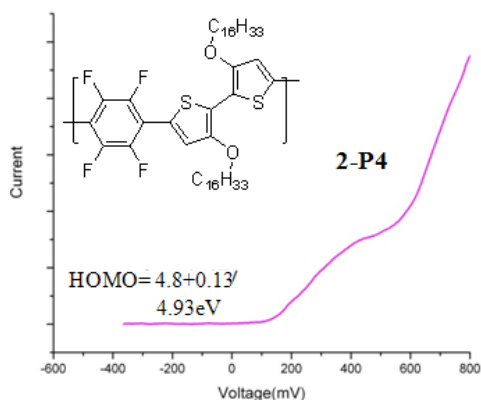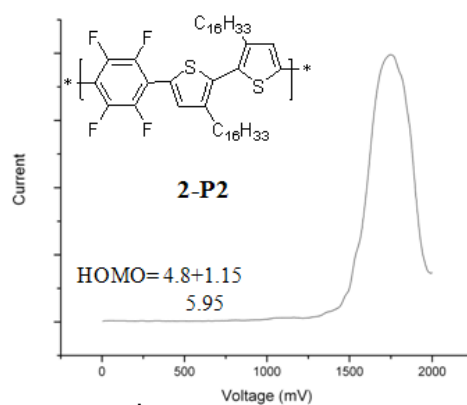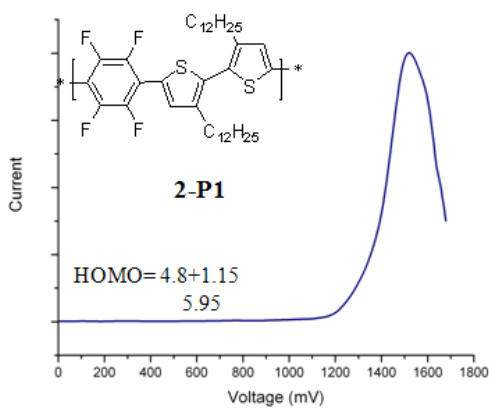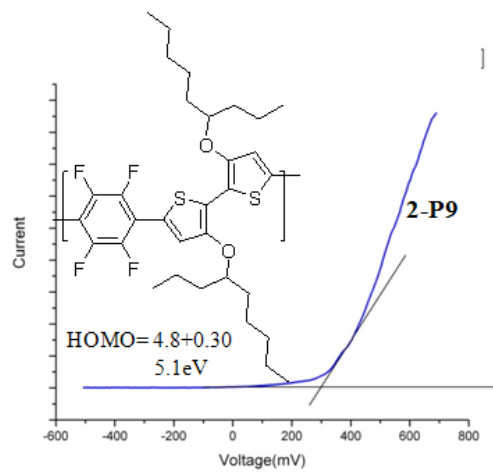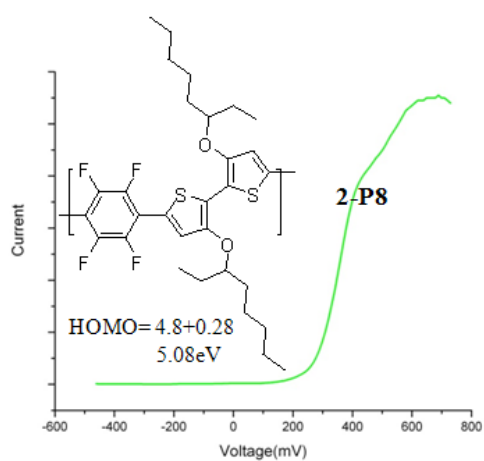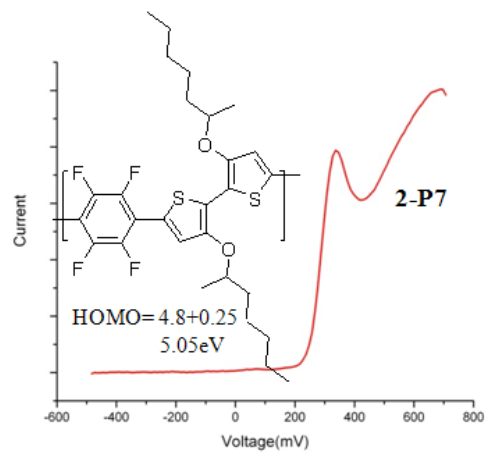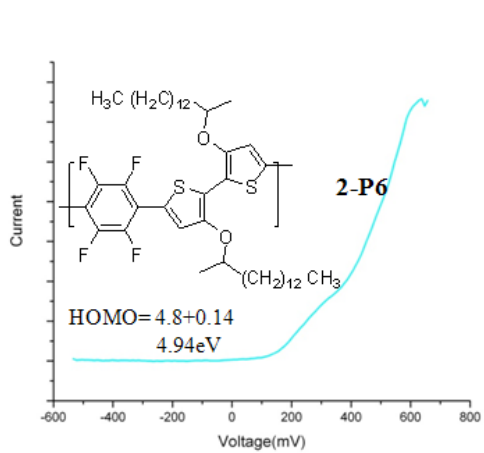
DPV curves for Chapter 3: Polymer films (1mg/ml in Chlorobenzene) in tetra-n-butylammonium hexafluorophosphate solution (0.1 M in dry acetonitrile), 295 K, Scan rate = 50 mV. s^{-1} Corrected for Fc/Fc$^{+.}$
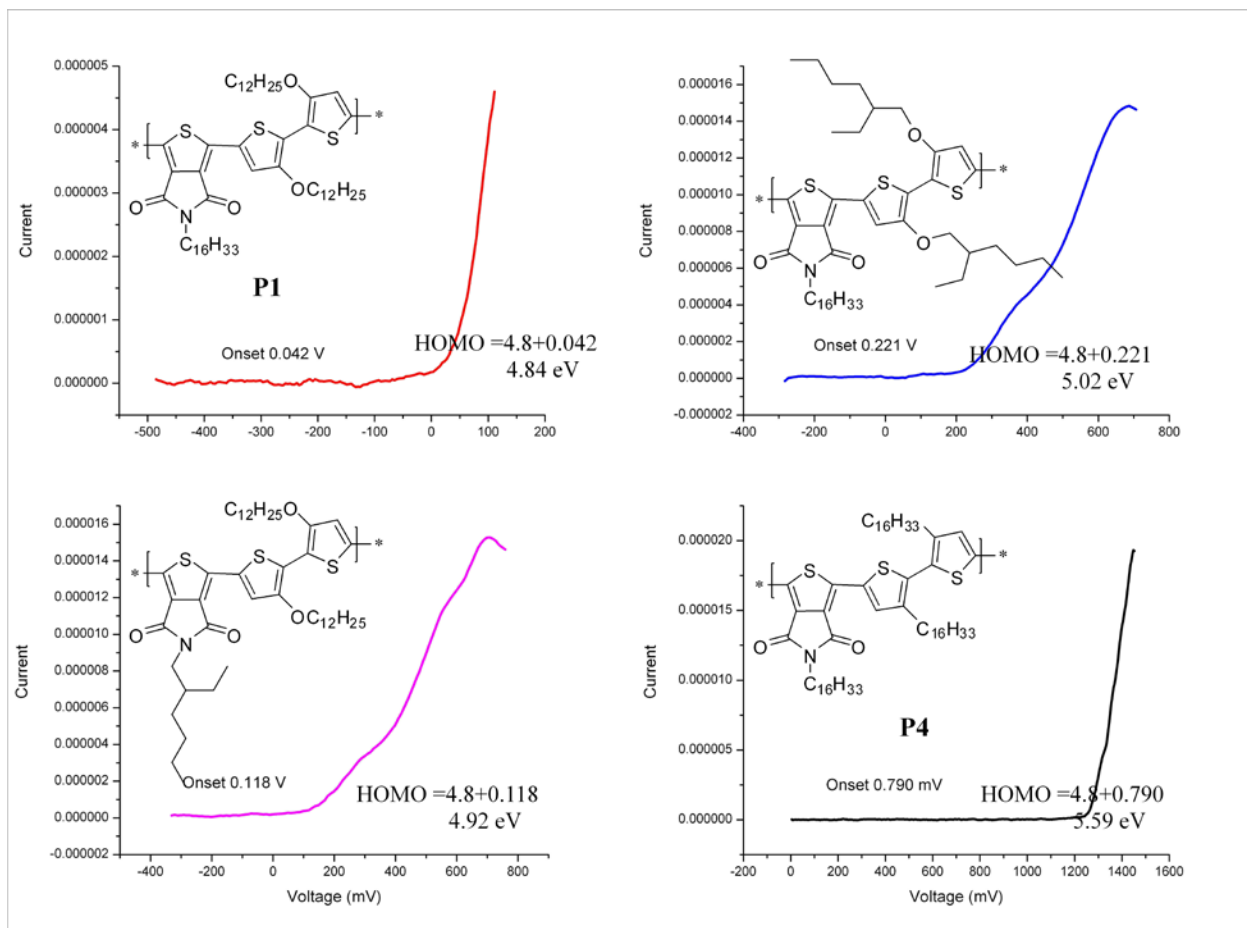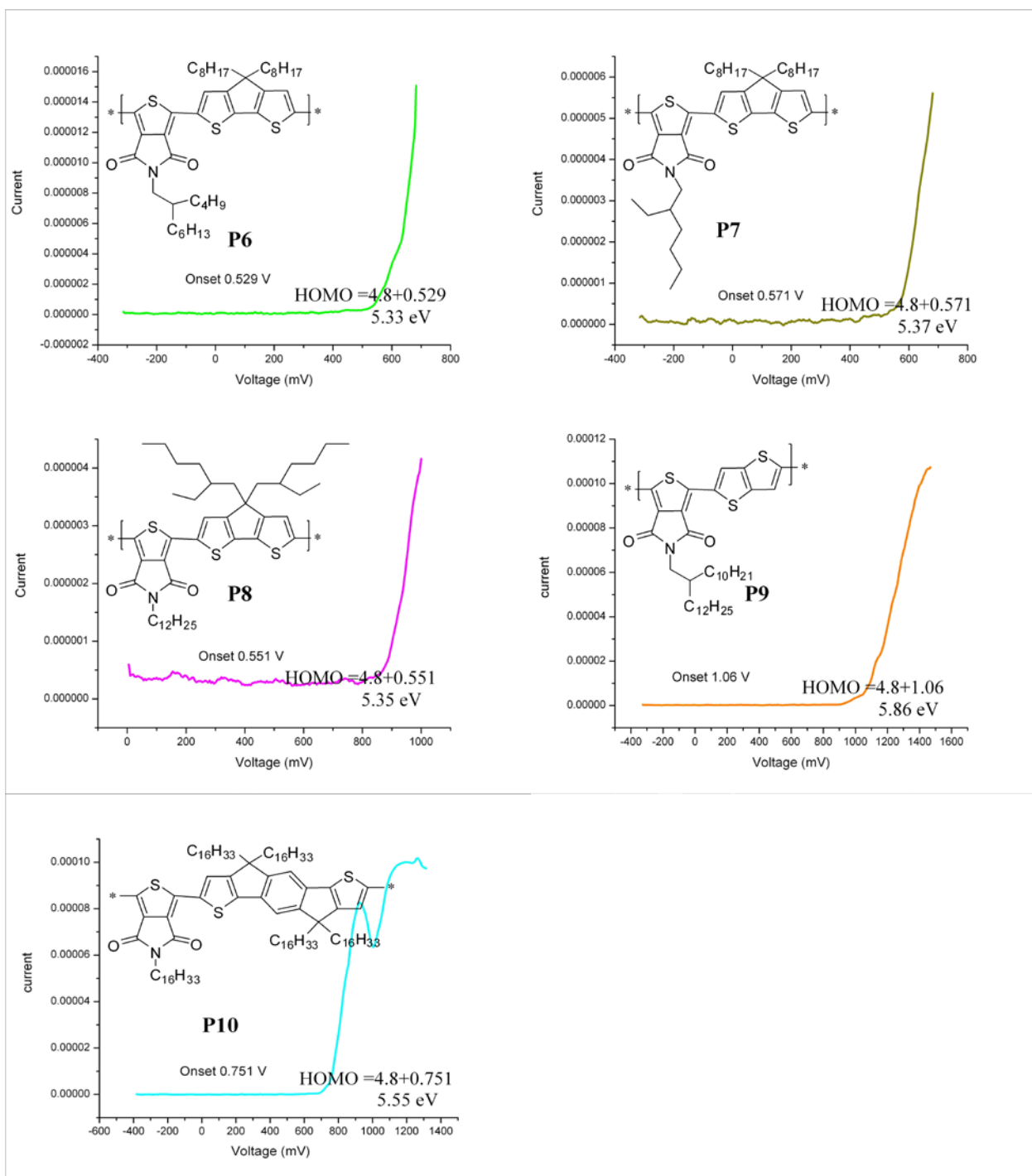
DPV curves for Chapter 4: Polymer films (1mg/ml in Chlorobenzene) in tetra-n-butylammonium hexafluorophosphate solution (0.1 M in dry acetonitrile), 295 K, Scan rate = 50 mV. s^{-1} Corrected for Fc/Fc$^{+.}$
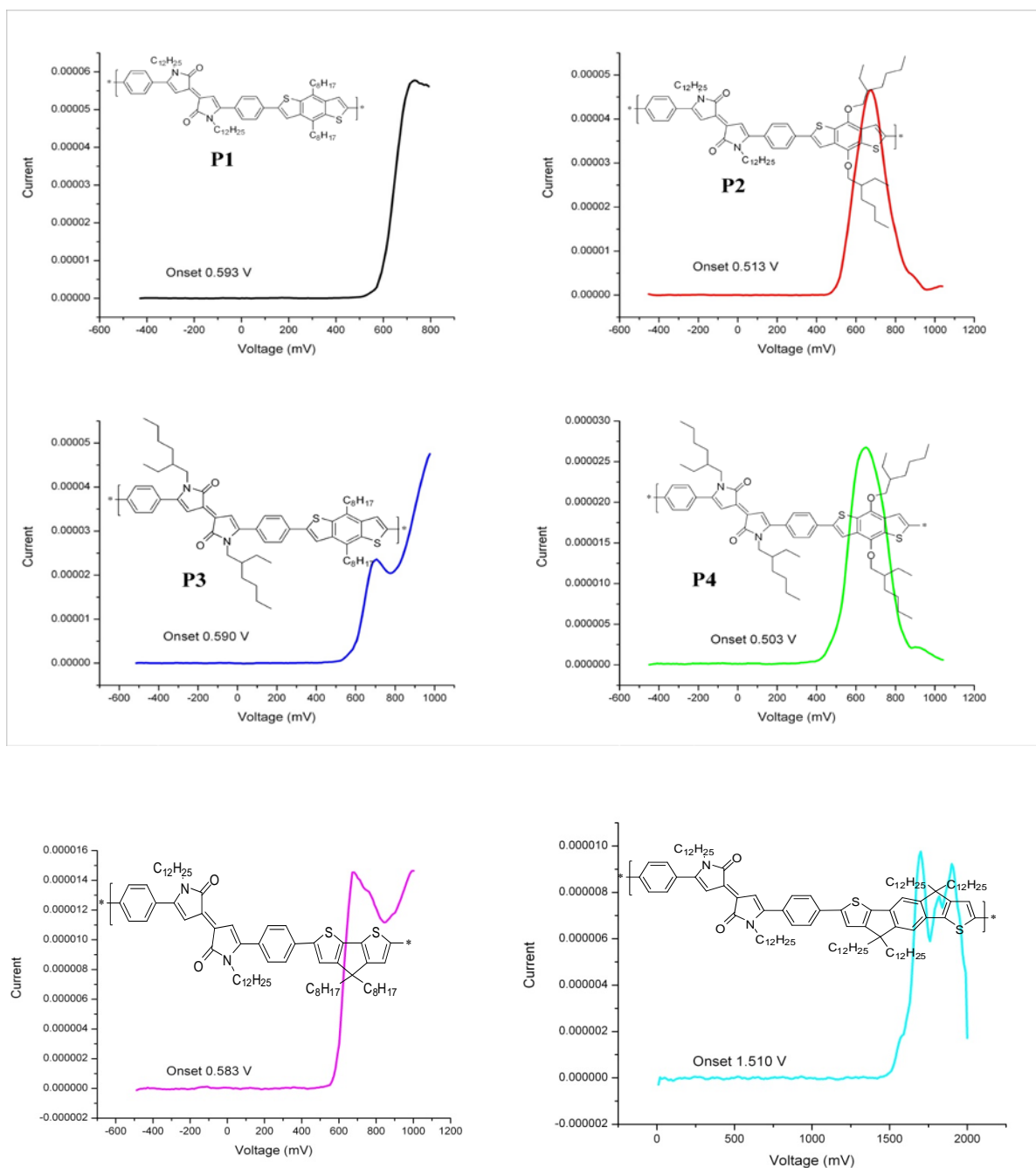
NMR Spectra for Chapter 2.
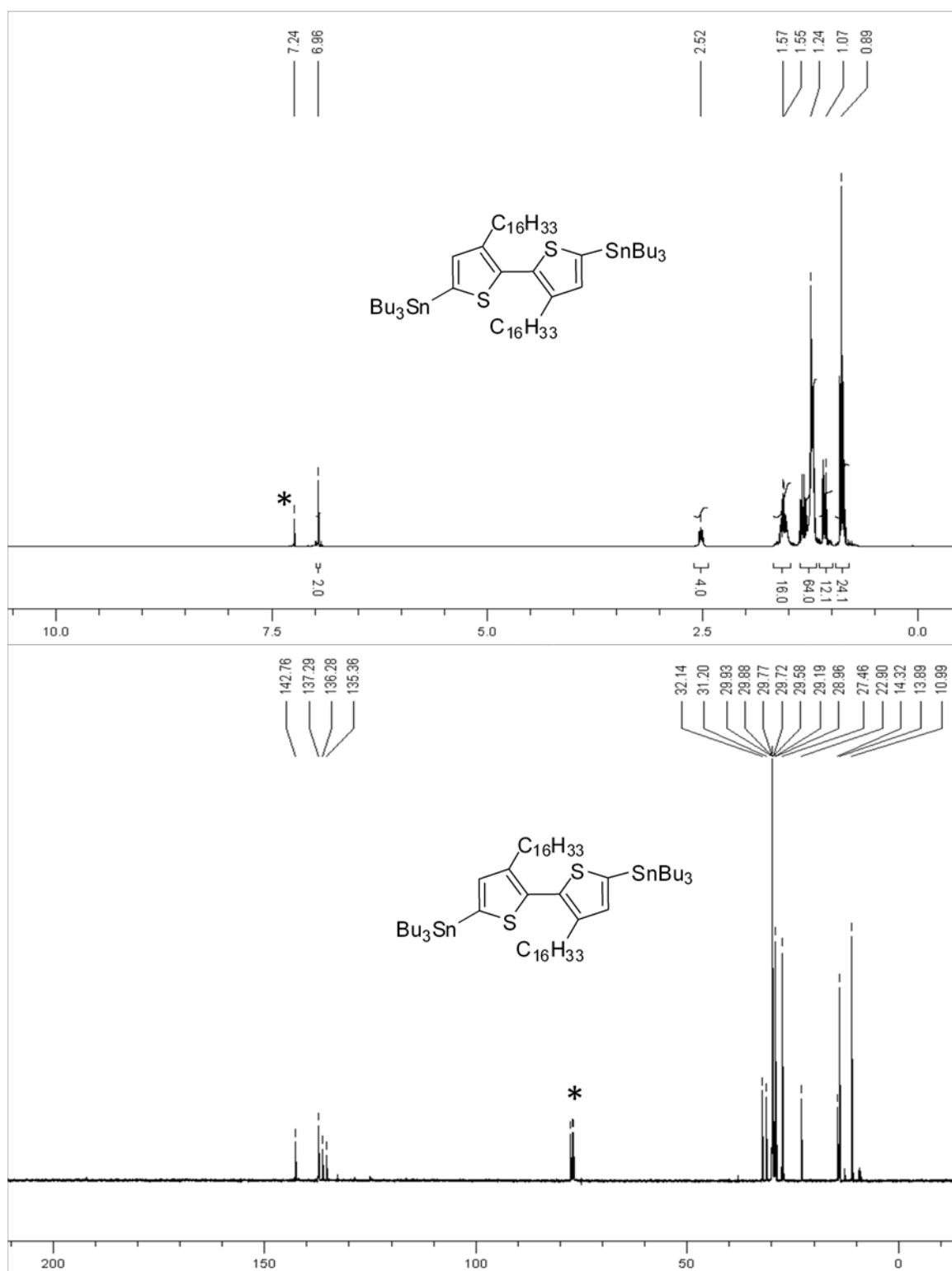
Figure: 6.1: ^{1}H (top) and ^{13}C (bottom) NMR spectra (CDCl$_3$, r.t.) of compound **2.4b** (*solvent).
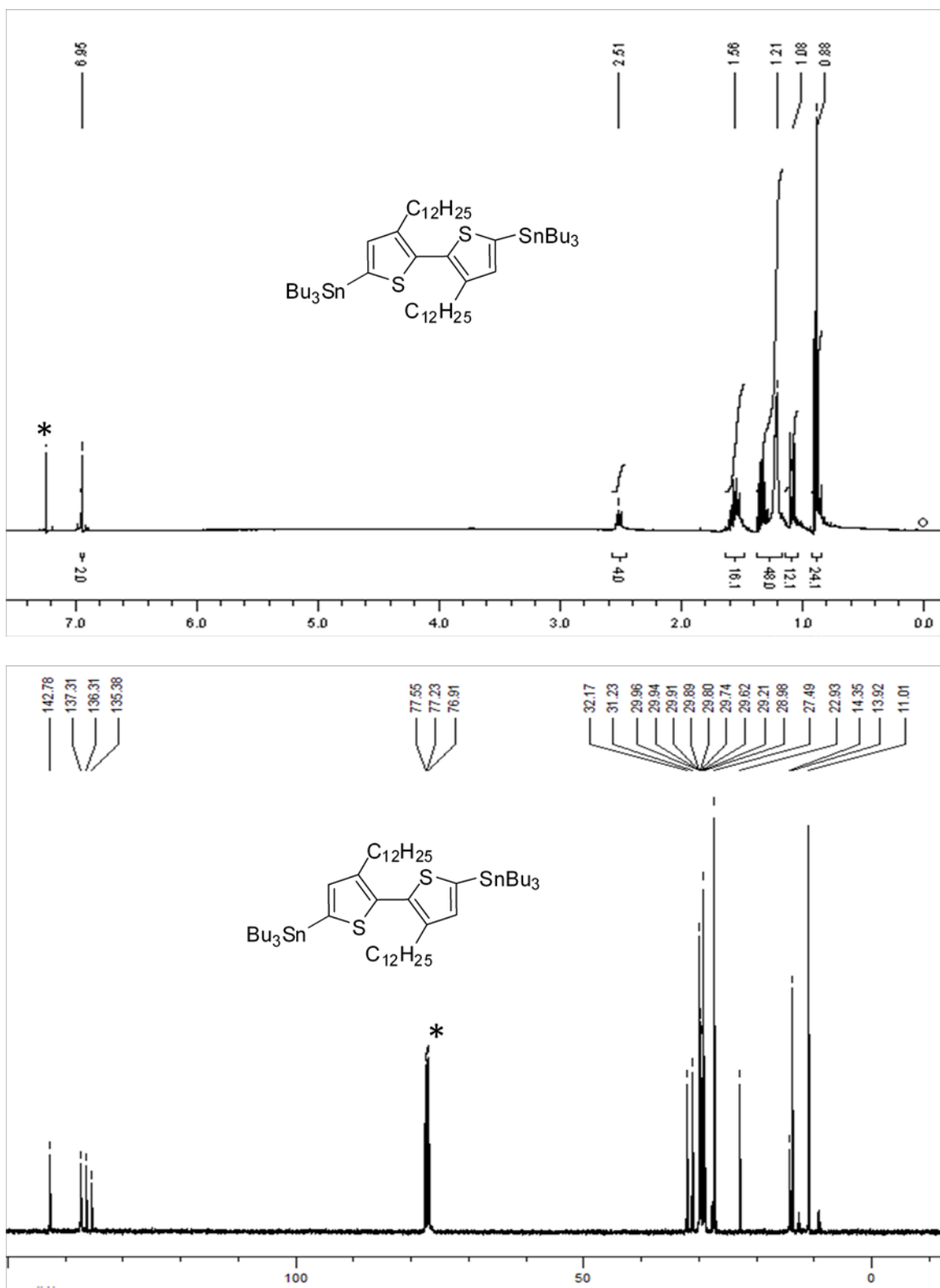
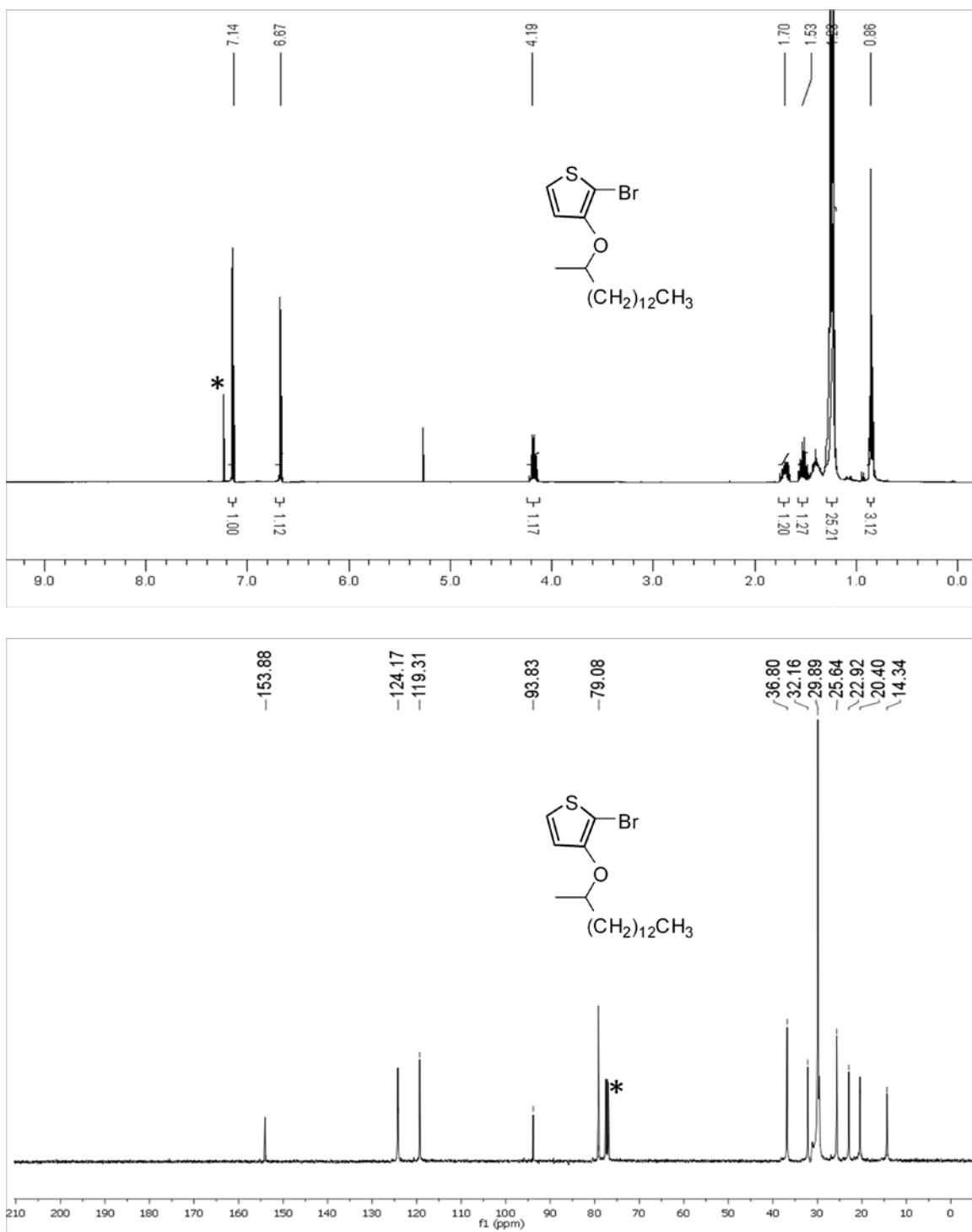**Figure 6.2:** ^{1}H (top) and ^{13}C (bottom) NMR spectra (CDCl$_3$, r.t.) of compound **2.4a** (*solvent).
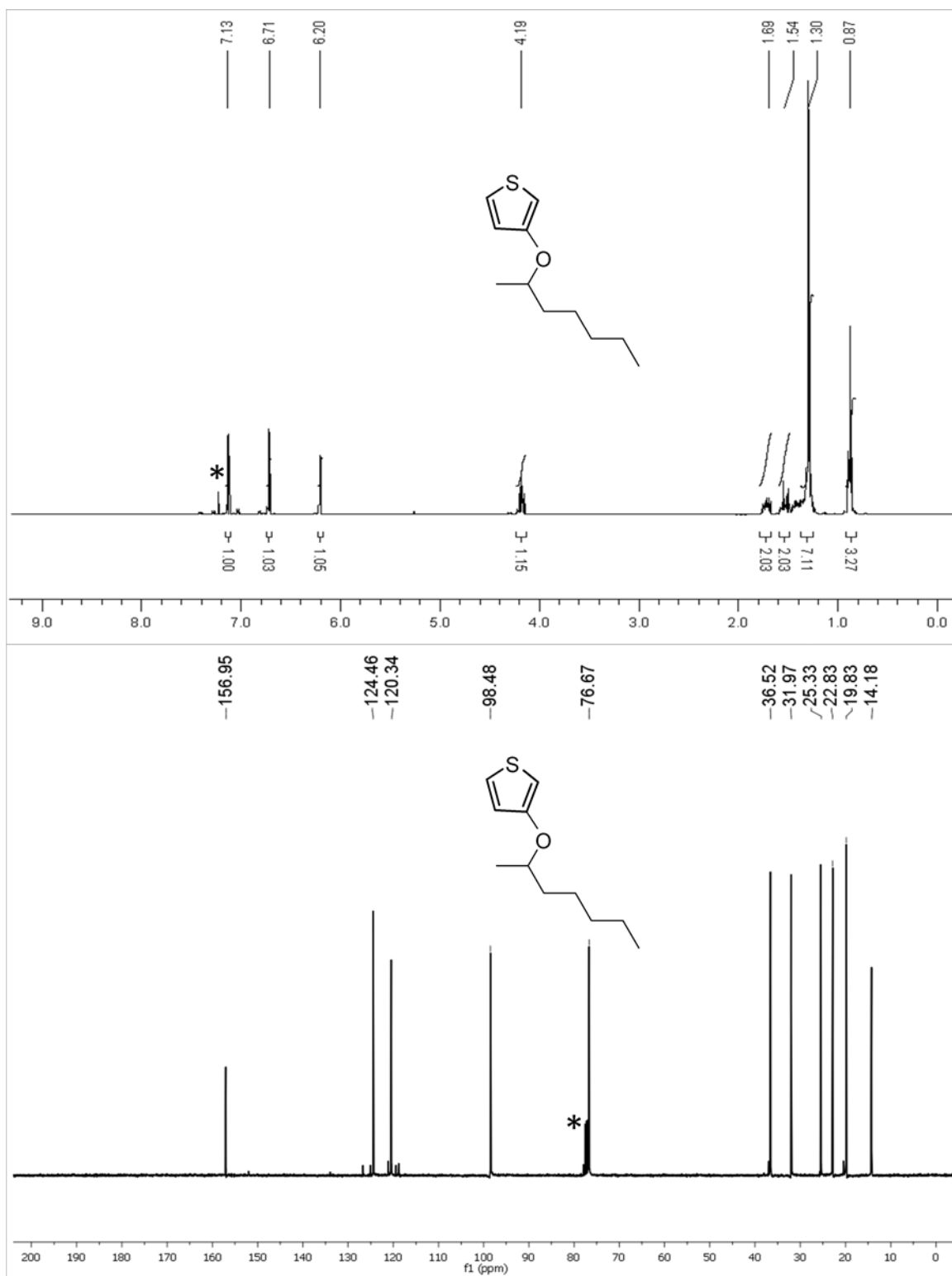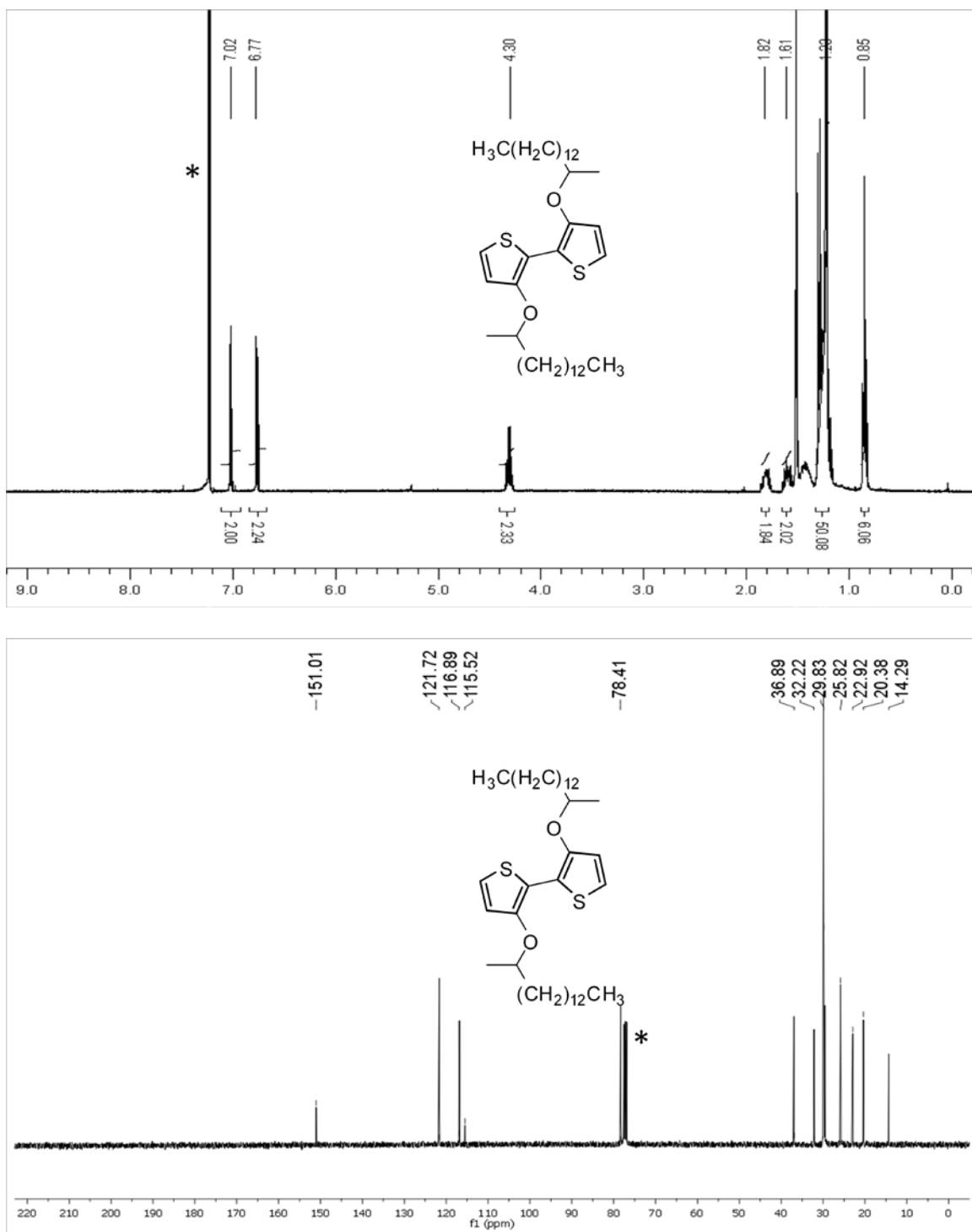
Figure 6.3: ^1H (top) and ^{13}C (bottom) NMR spectra (CDCl$_3$, r.t.) of compound **2.6a** (*solvent).
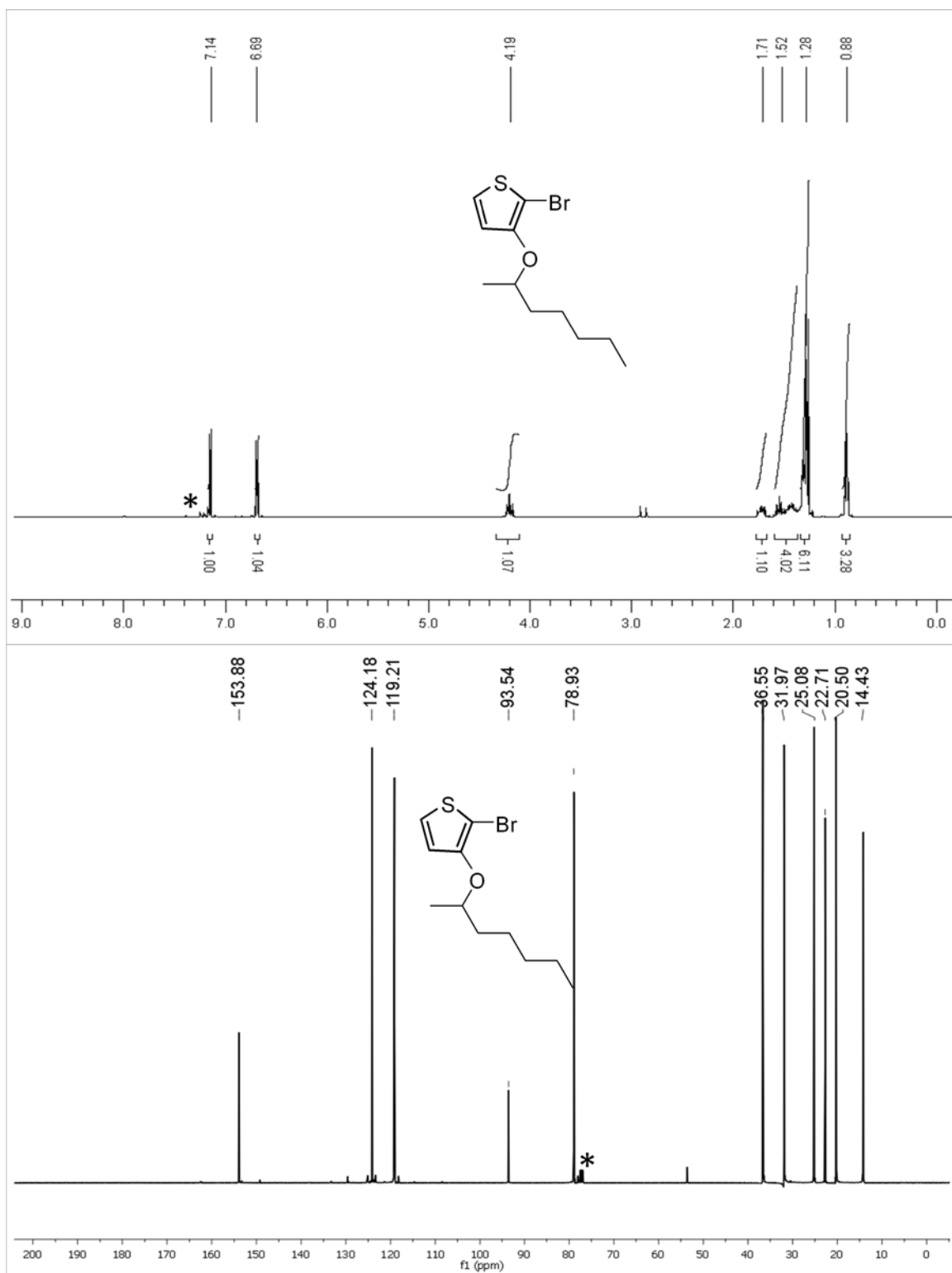
Figure 6.4: ^{1}H (top) and ^{13}C (bottom) NMR spectra (CDCl$_3$, r.t.) of compound **2.7a** (*solvent).
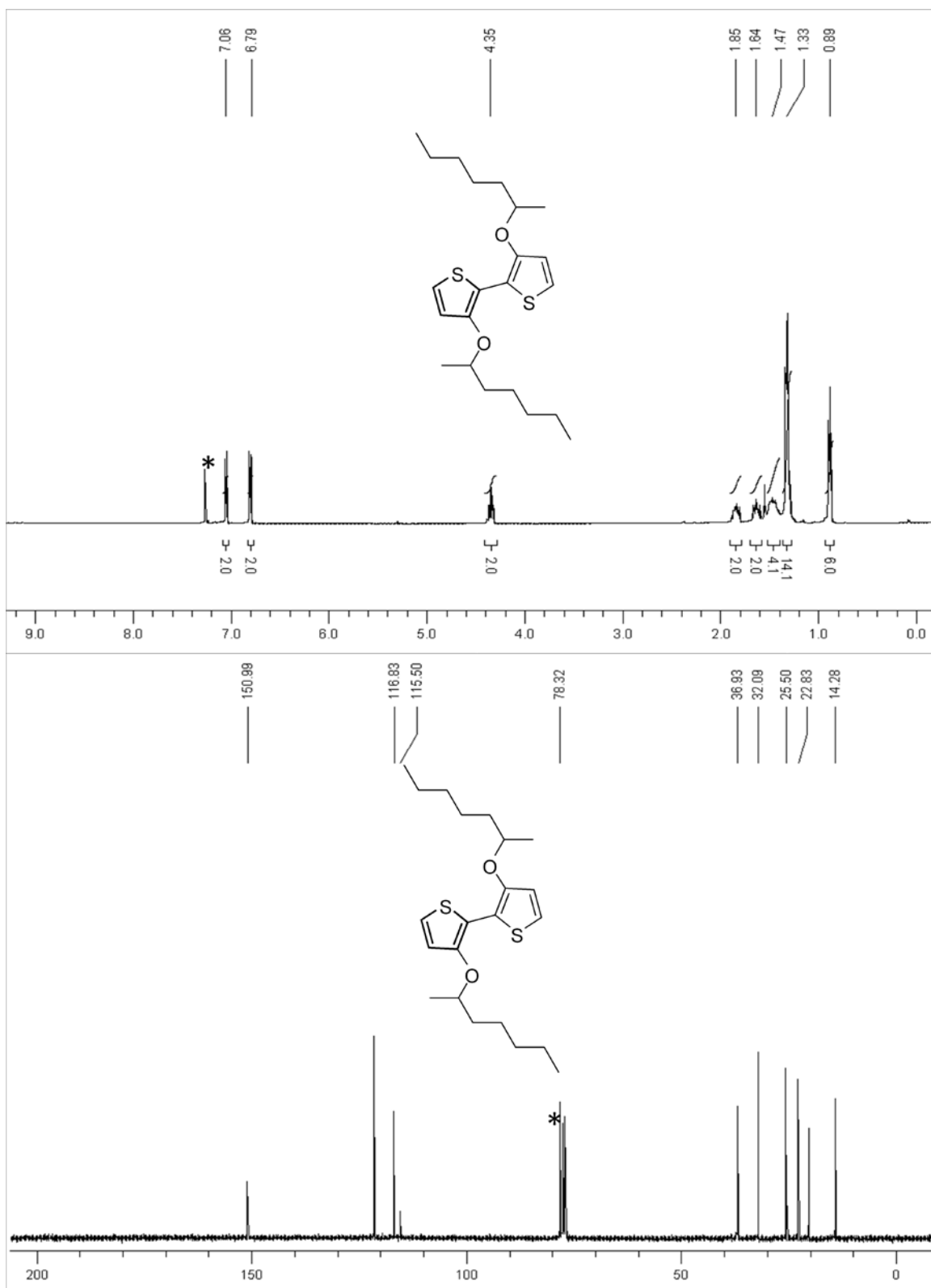
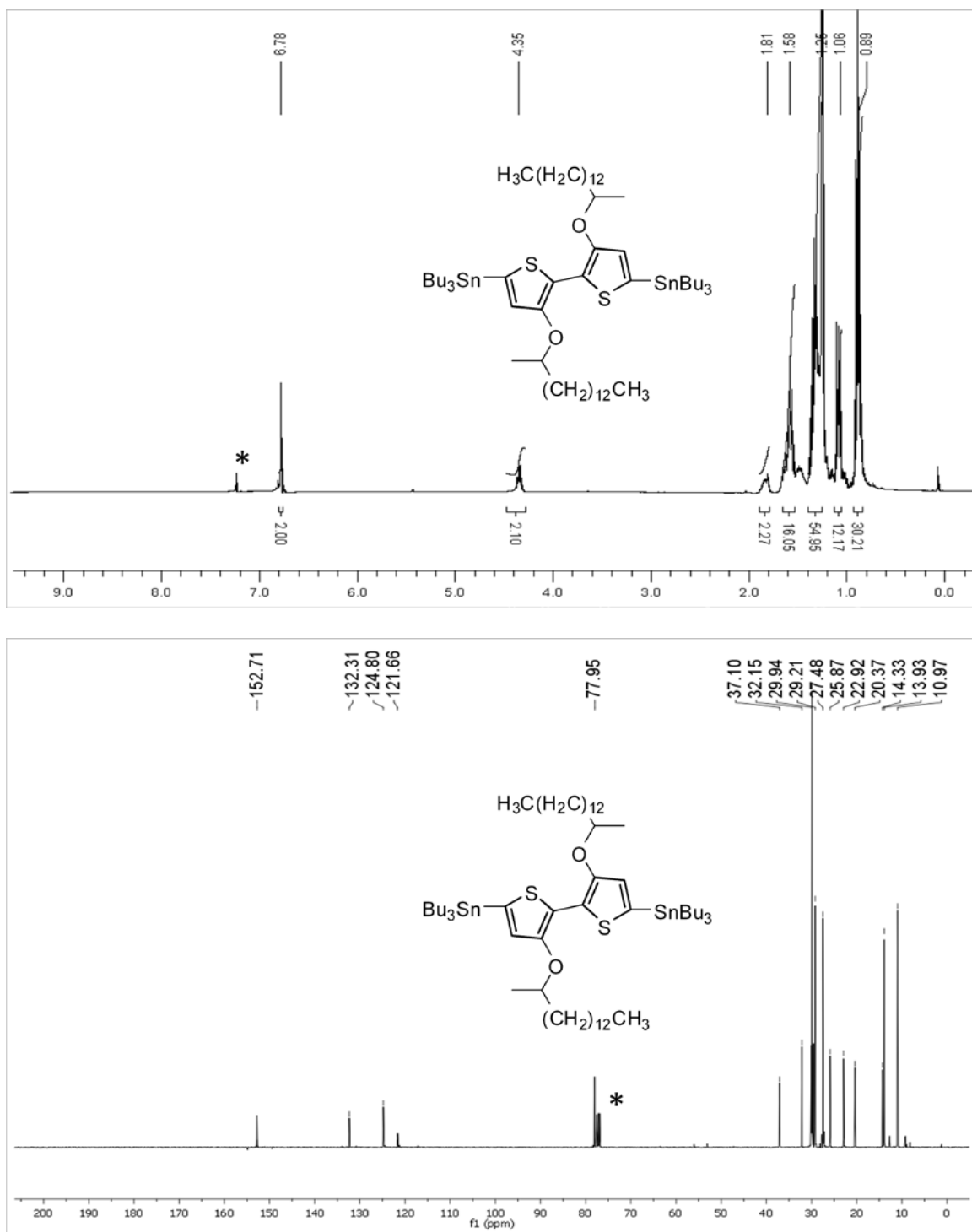**Figure 6.5:** ^{1}H (top) and ^{13}C (bottom) NMR spectra (CDCl$_3$, r.t.) of compound **2.8a** (*solvent).
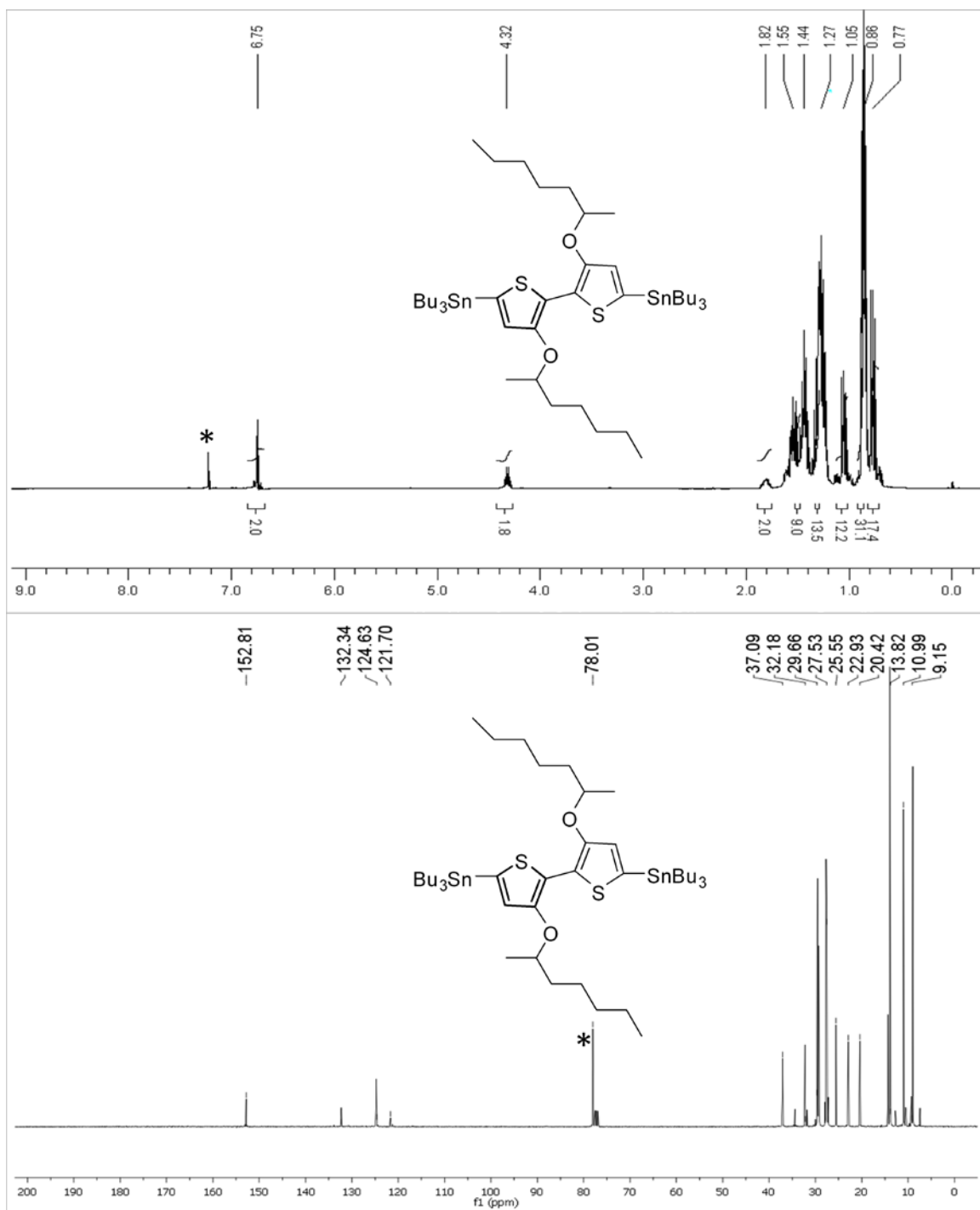
Figure 6.6: ^{1}H (top) and ^{13}C (bottom) NMR spectra (CDCl$_3$, r.t.) of compound **2.9a** (*solvent).
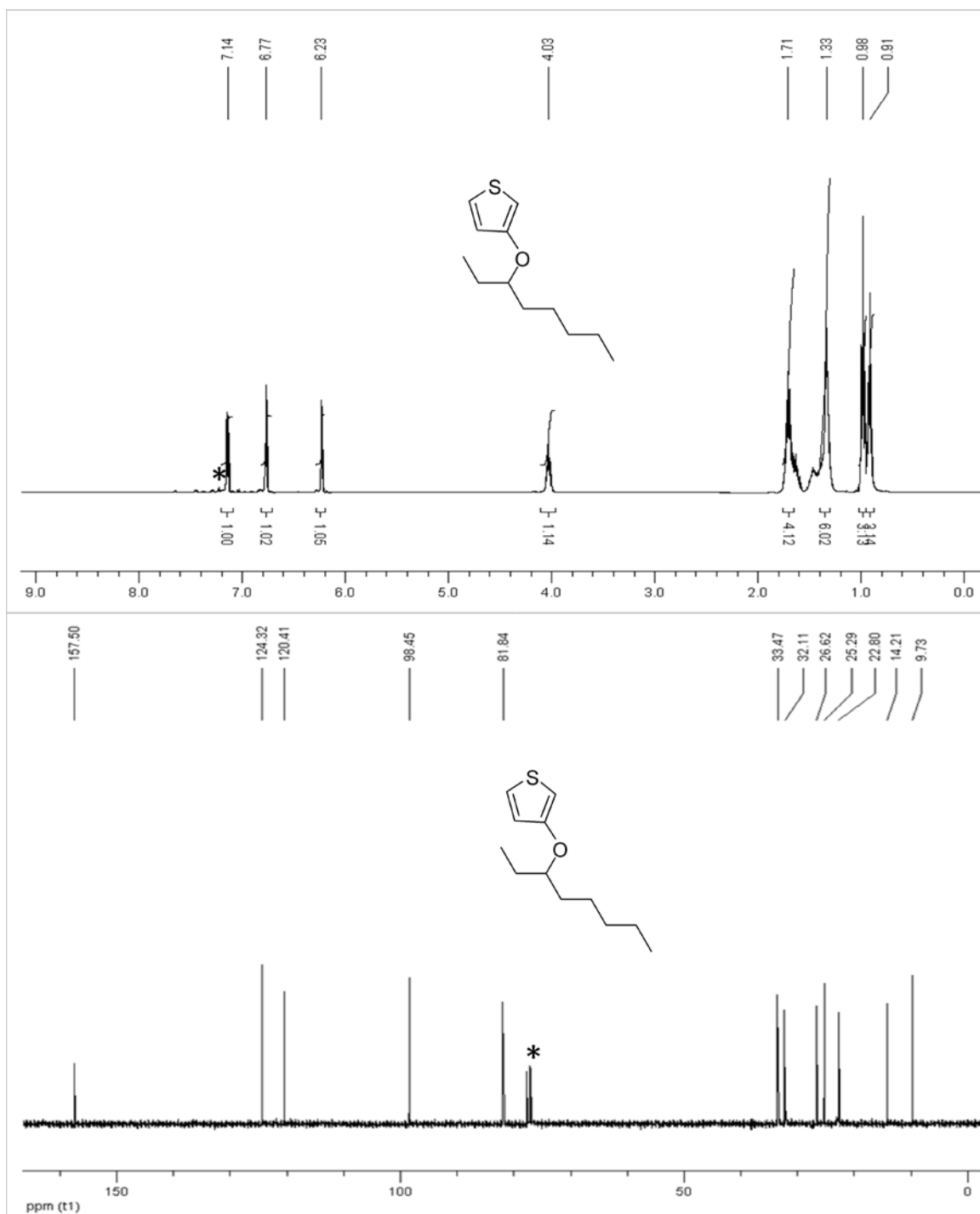
Figure 6.7: ^{1}H (top) and ^{13}C (bottom) NMR spectra (CDCl₃, r.t.) of compound **2.6b**(*solvent).
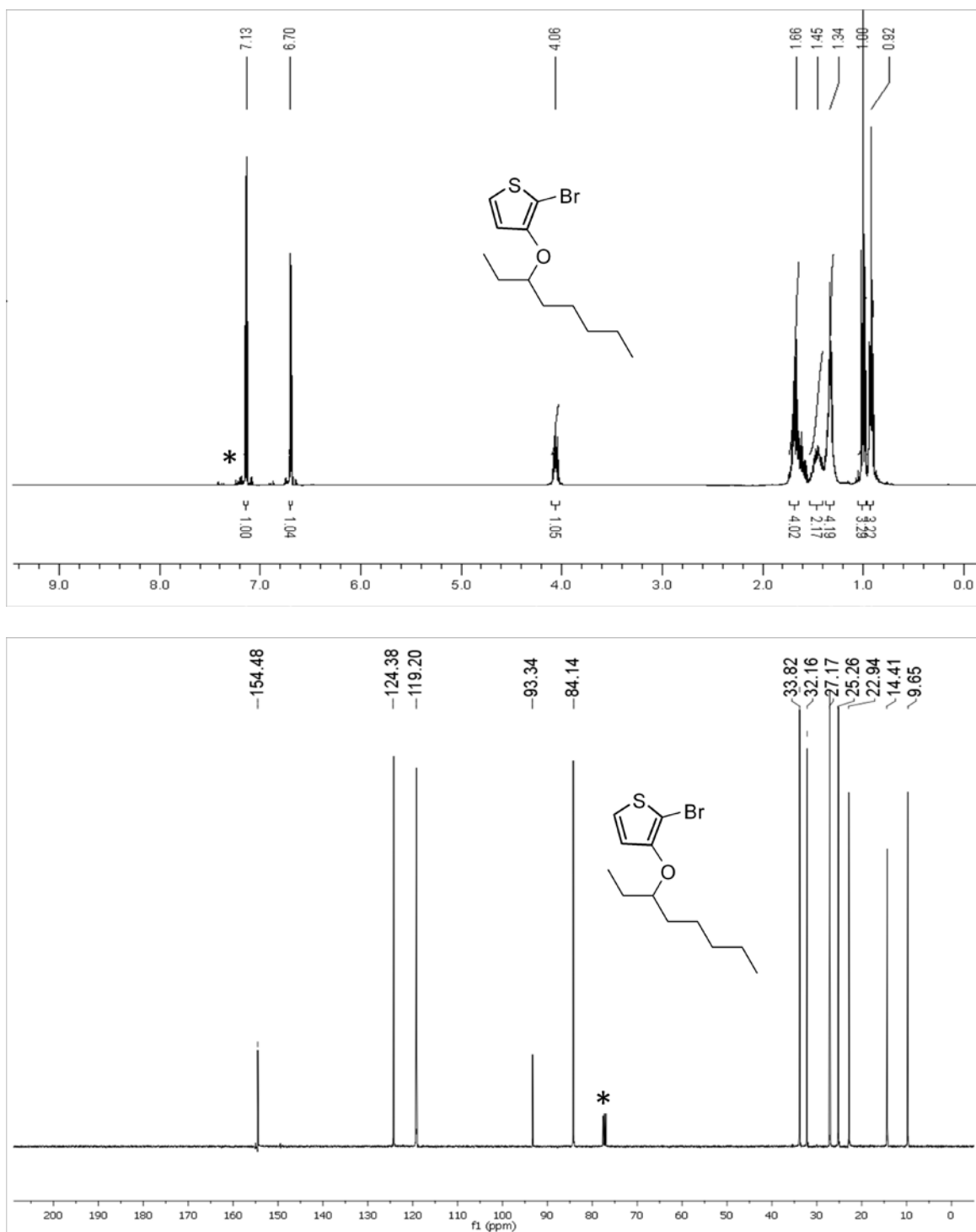
Figure 6.8: ^{1}H (top) and ^{13}C (bottom) NMR spectra (CDCl$_3$, r.t.) of compound **2.7b** (*solvent).
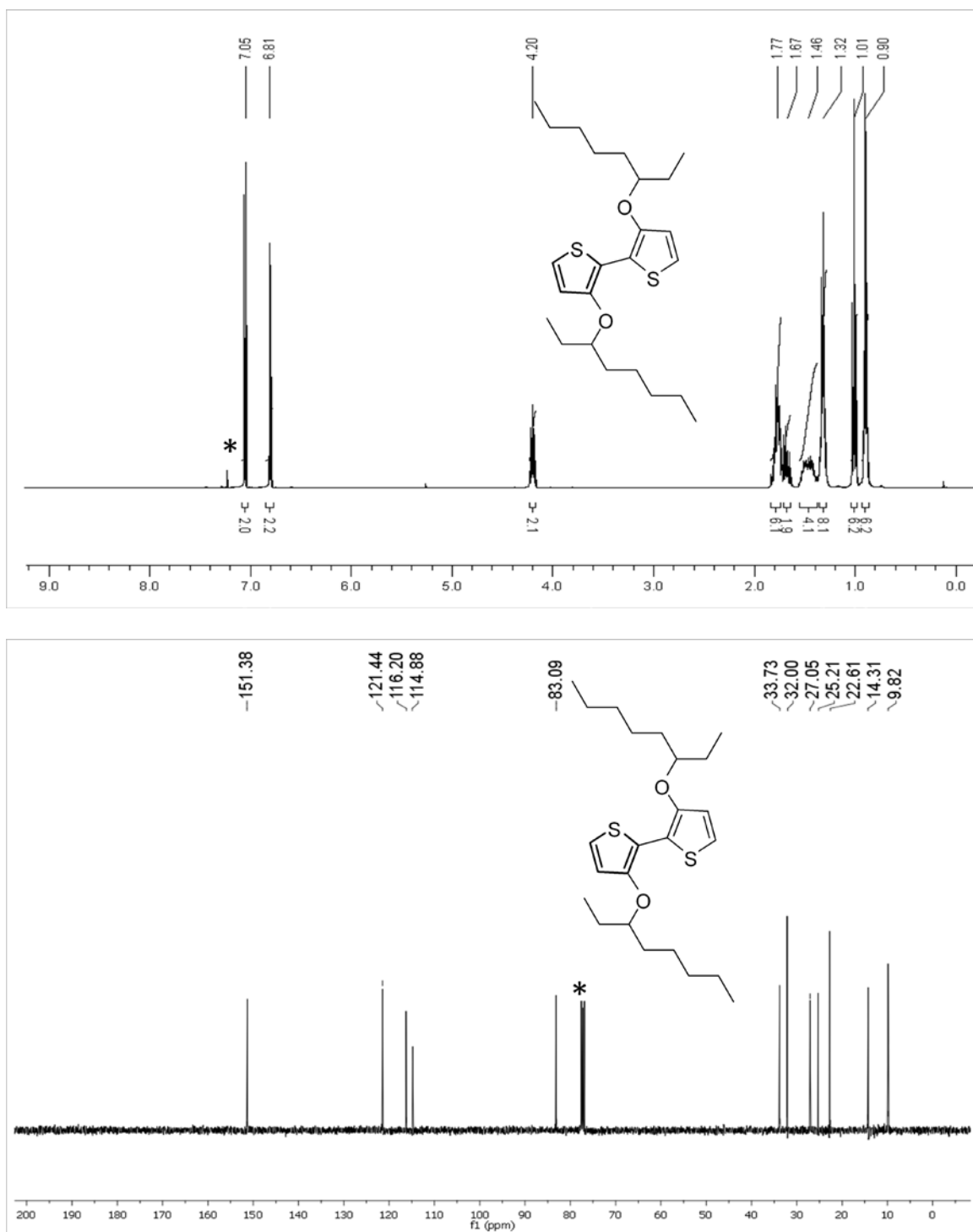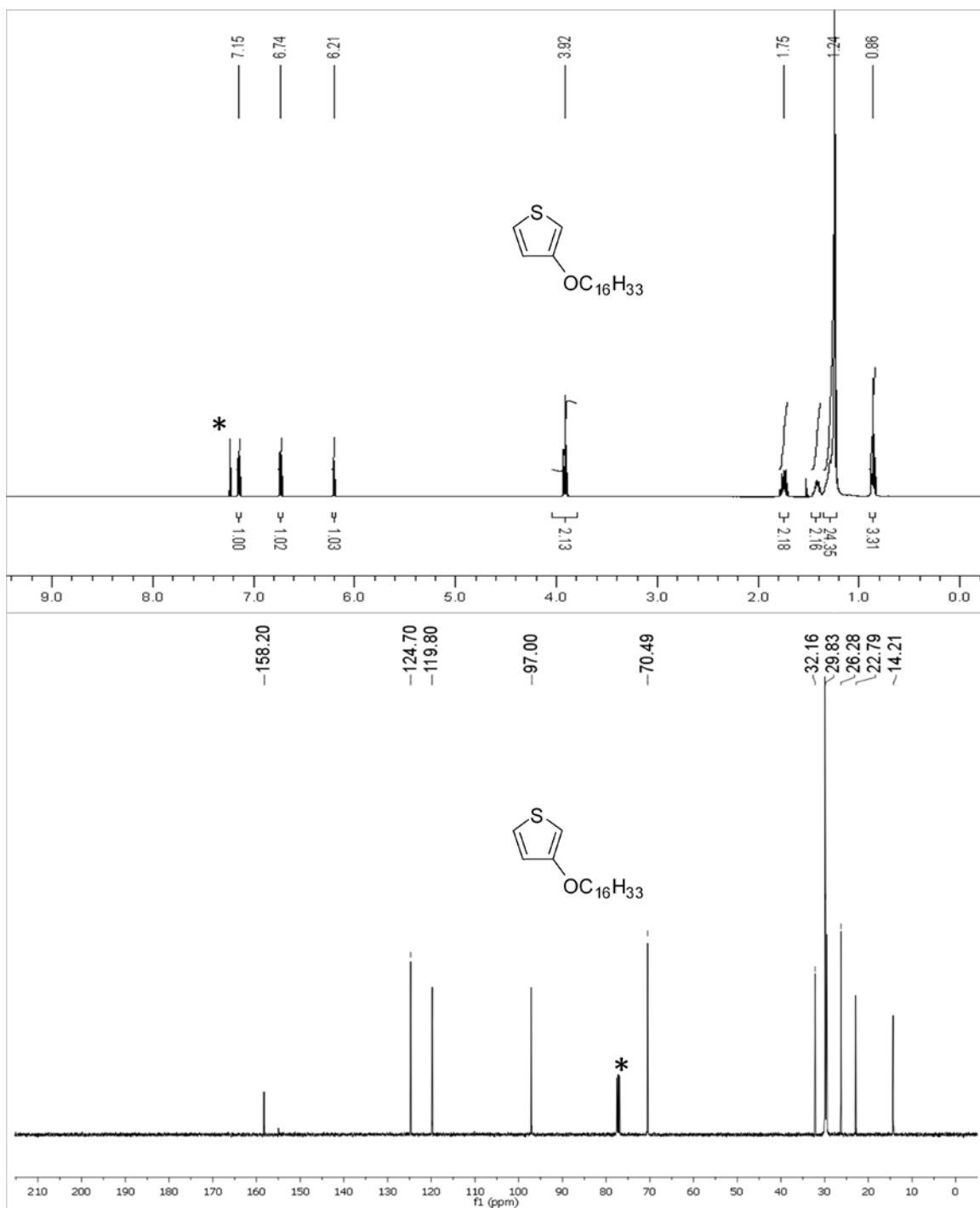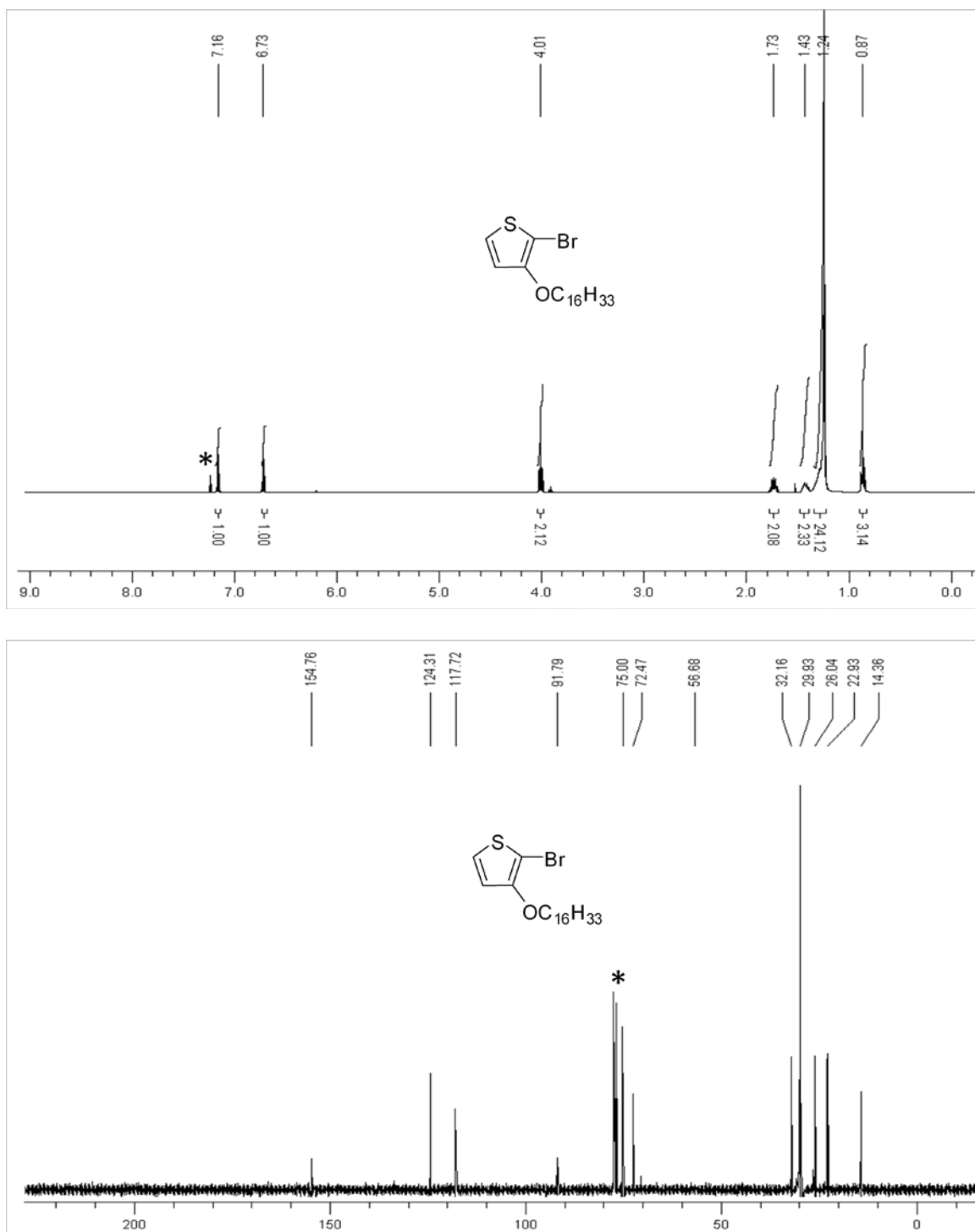
Figure 6.9: ^{1}H (top) and ^{13}C (bottom) NMR spectra (CDCl$_3$, r.t.) of compound **2.8b** (*solvent)
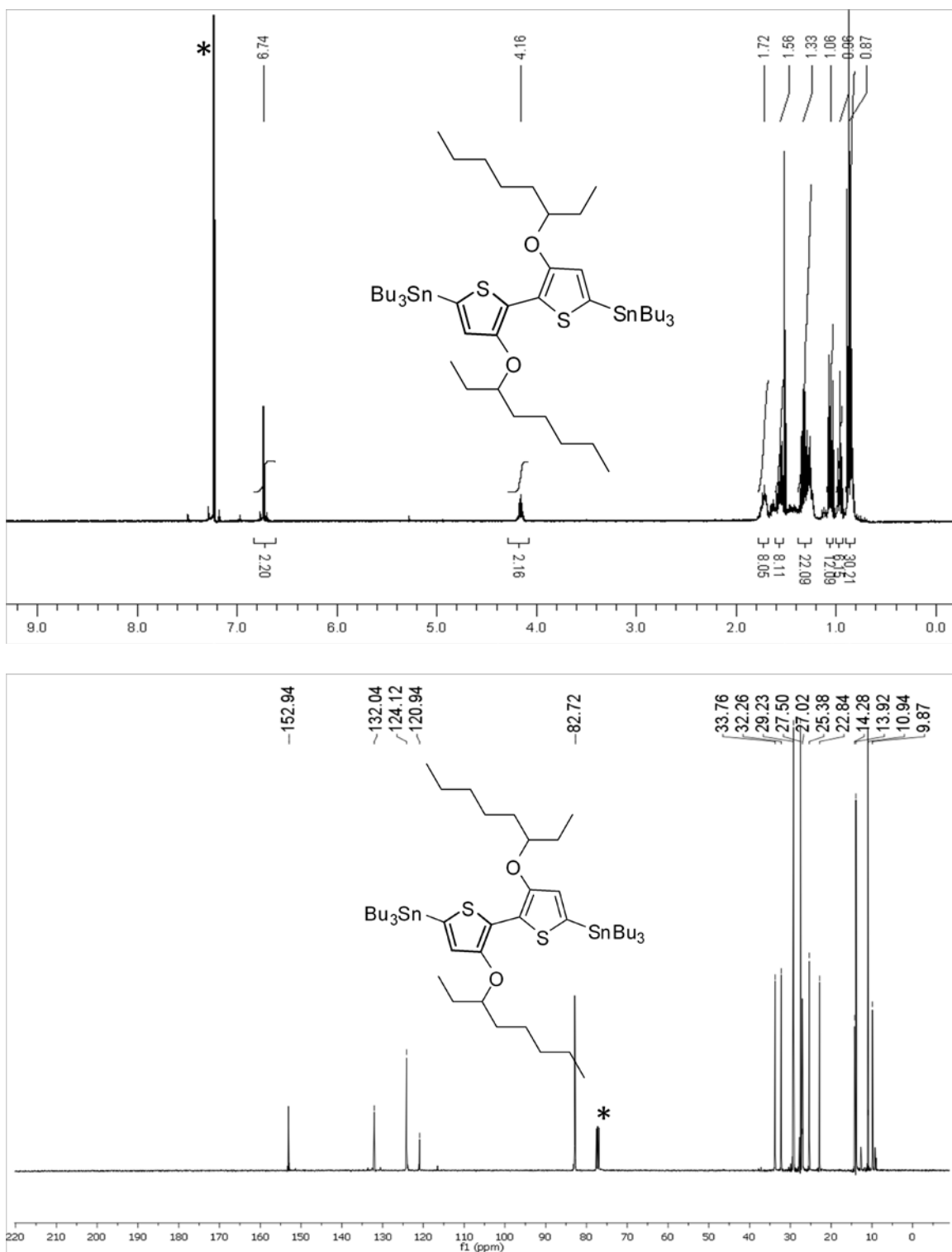
Figure 6.10: ^{1}H (top) and ^{13}C (bottom) NMR spectra (CDCl$_3$, r.t.) of compound **2.9b** (*solvent).
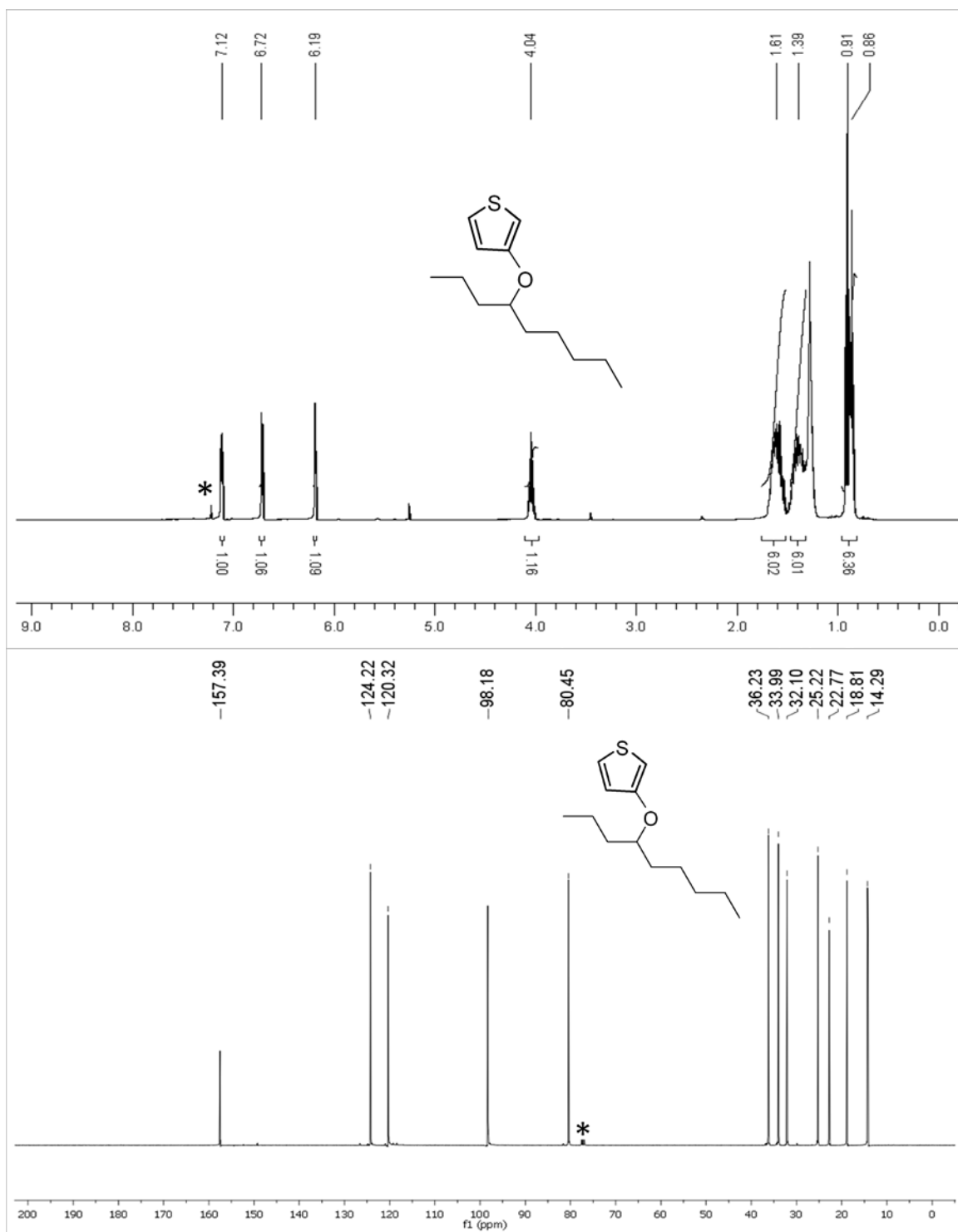
Figure 6.11: ^{1}H (top) and ^{13}C (bottom) NMR spectra (CDCl$_3$, r.t.) of compound **2.6c** (*solvent).
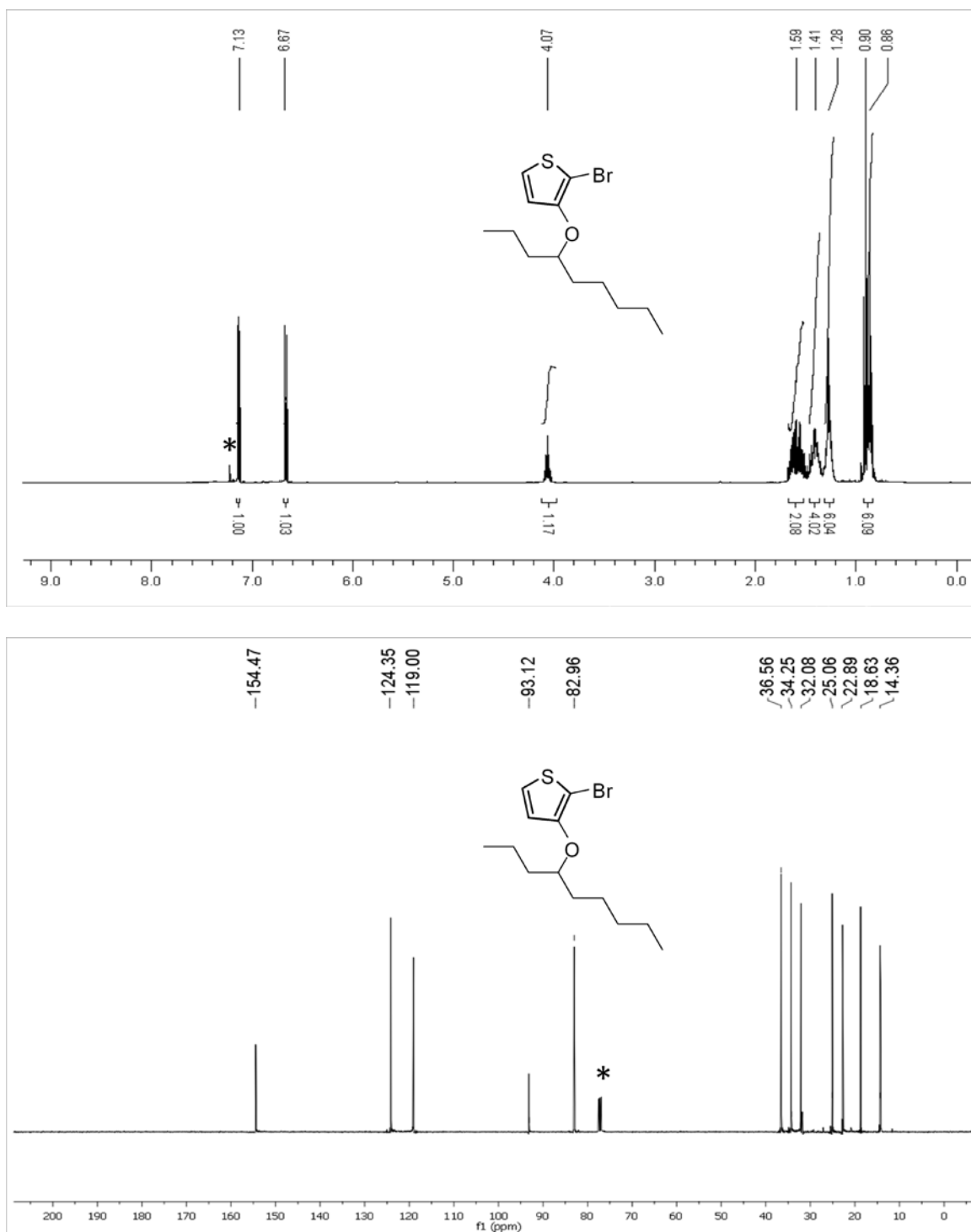
Figure 6.12: ^{1}H (top) and ^{13}C (bottom) NMR spectra (CDCl$_3$, r.t.) of compound **2.7c** (*solvent).
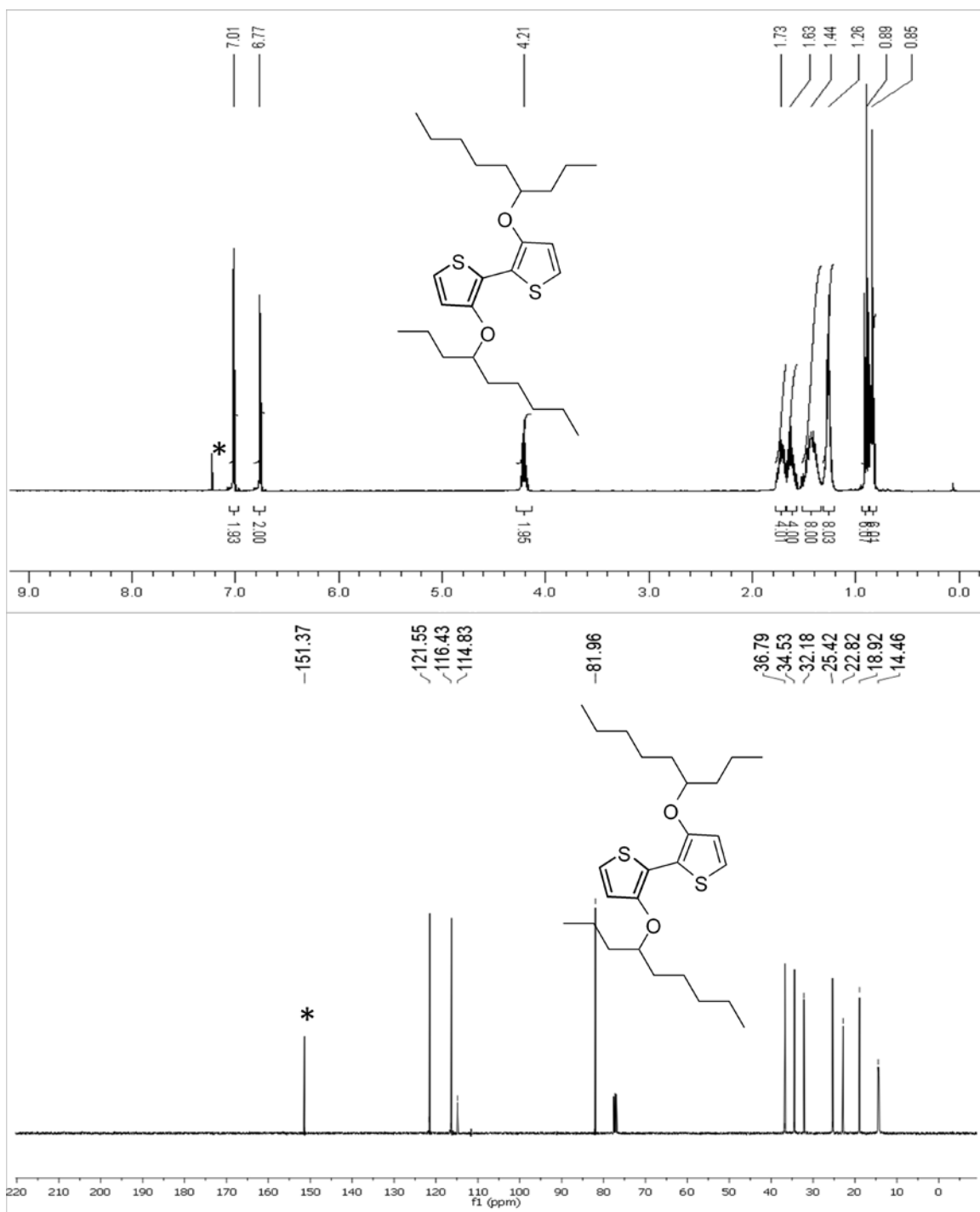
Figure 6.13: ^{1}H (top) and ^{13}C (bottom) NMR spectra (CDCl$_3$, r.t.) of compound **2.8c**(*solvent).
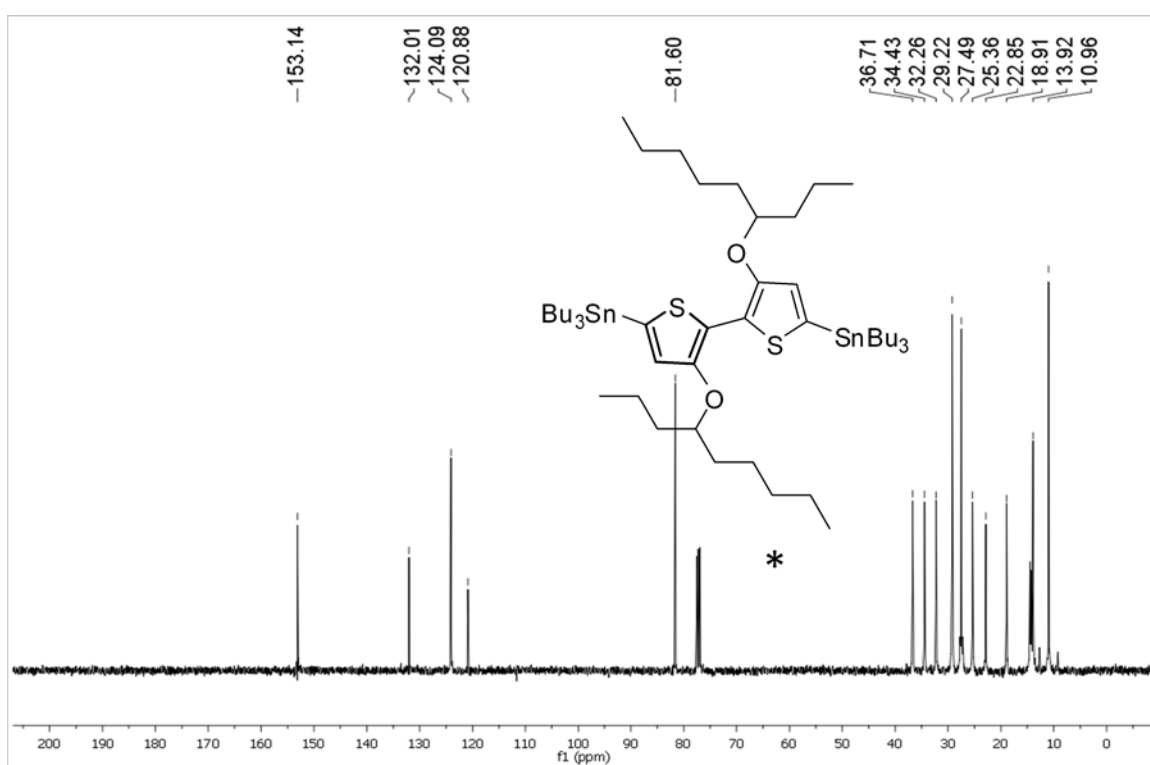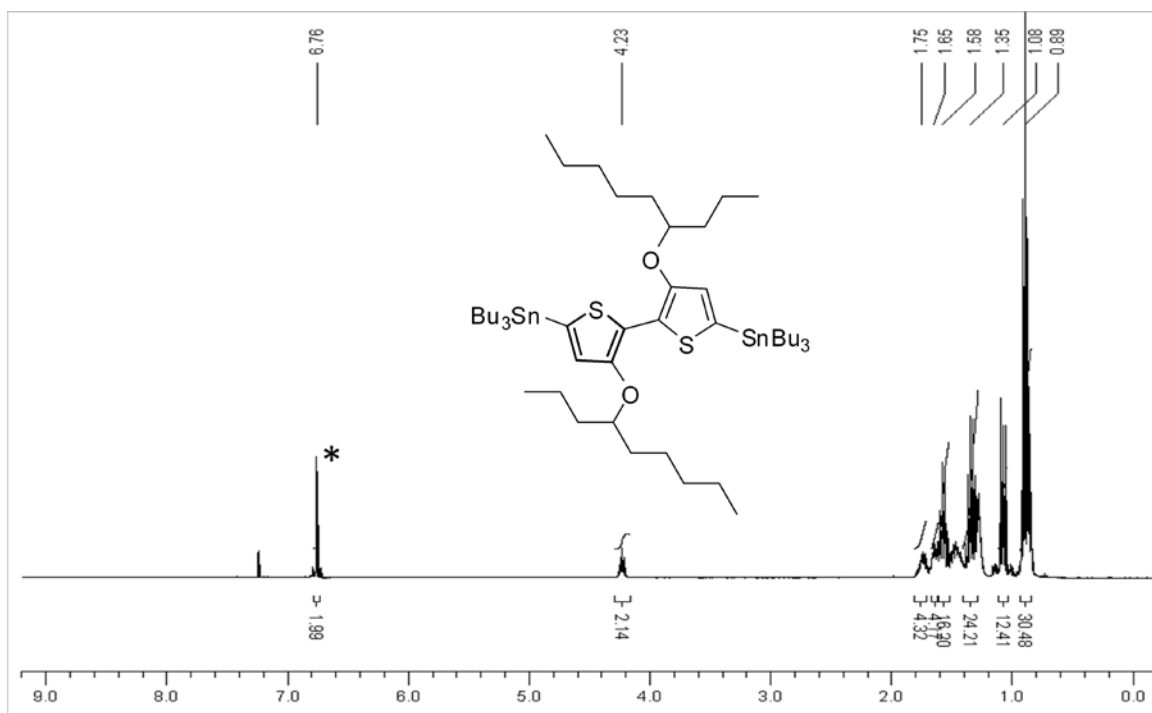
Figure 6.14: ^{1}H (top) and ^{13}C (bottom) NMR spectra (CDCl$_3$, r.t.) of compound **2.9c**(*solvent).
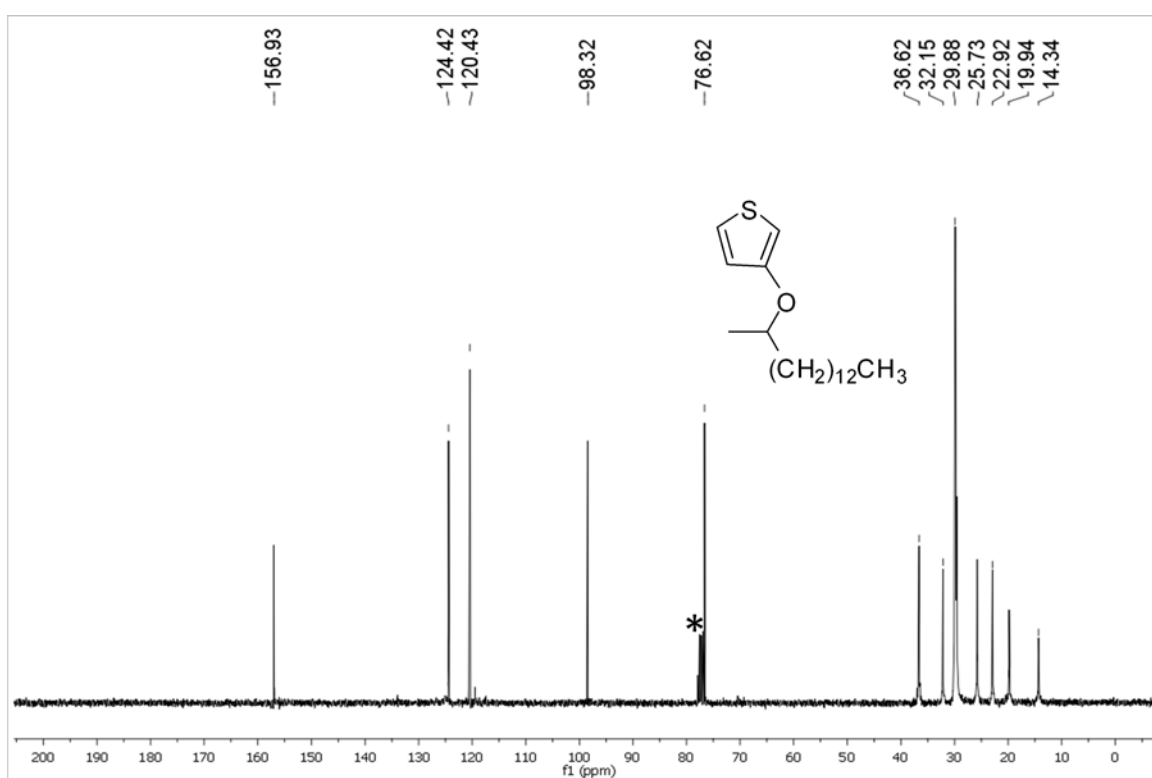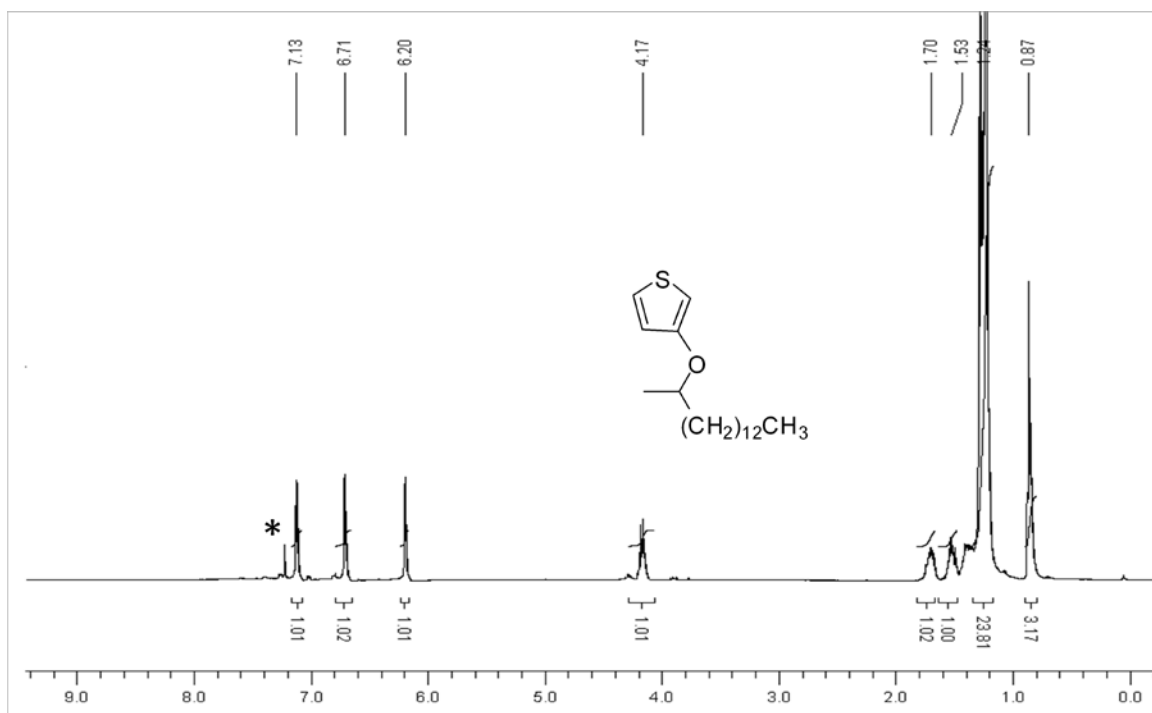
Figure 6.15: ^1H (top) and ^{13}C (bottom) NMR spectra (CDCl$_3$, r.t.) of compound **2.6d**(*solvent).
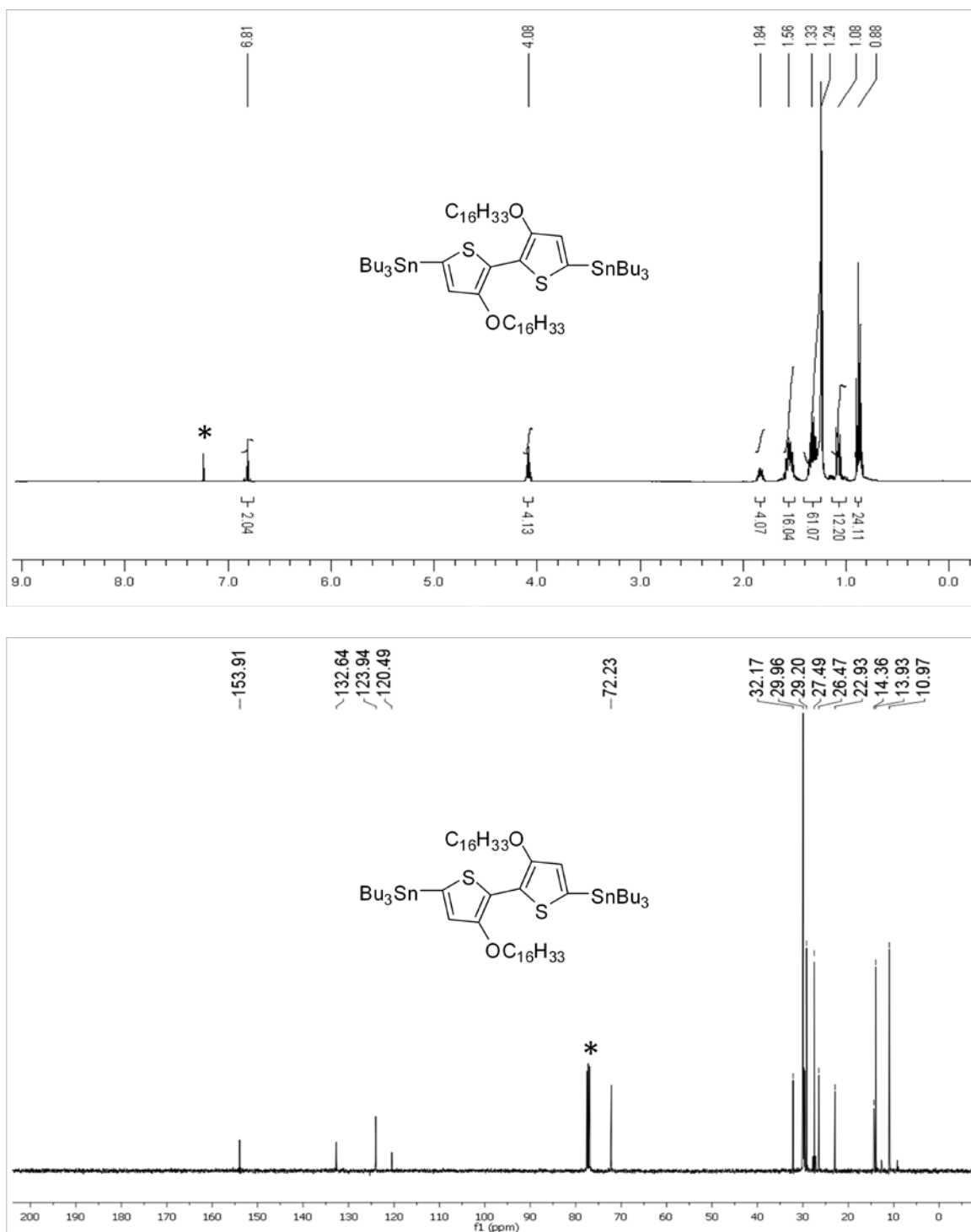
Figure 6.16: ^1H (top) and ^{13}C (bottom) NMR spectra (CDCl$_3$, r.t.) of compound **2.7d** (*solvent).
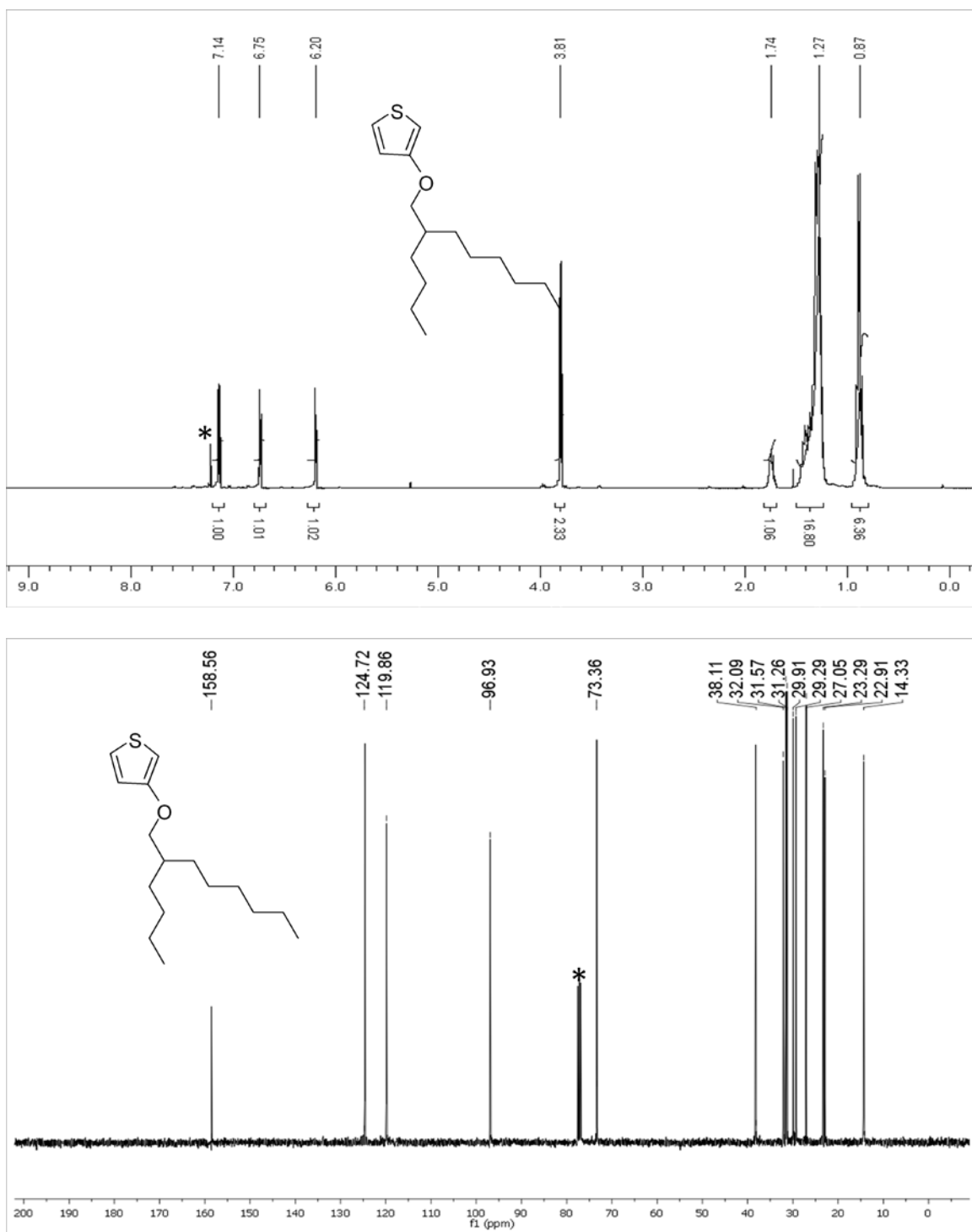
Figure 6.17: ^{1}H (top) and ^{13}C (bottom) NMR spectra (CDCl$_3$, r.t.) of compound **2.8d** (*solvent).

Figure 6.18: ^{1}H (top) and ^{13}C (bottom) NMR spectra (CDCl$_3$, r.t.) of compound **2.9d** (*solvent).

Figure 6.19: ^{1}H (top) and ^{13}C (bottom) NMR spectra (CDCl$_3$, r.t.) of compound **2.6e**(*solvent).

Figure 6.20: ^{1}H (top) and ^{13}C (bottom) NMR spectra (CDCl$_3$, r.t.) of compound **2.7e** (*solvent).
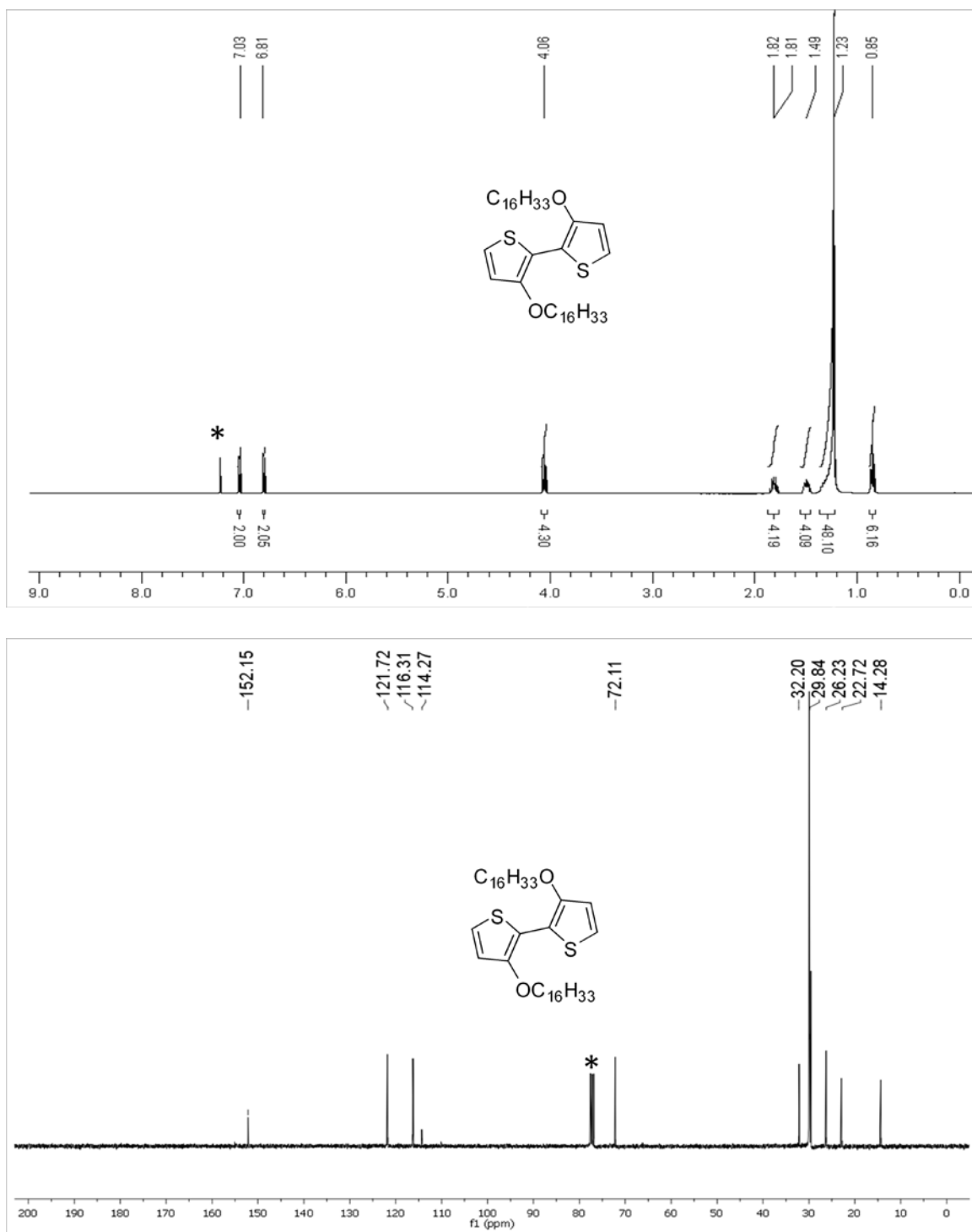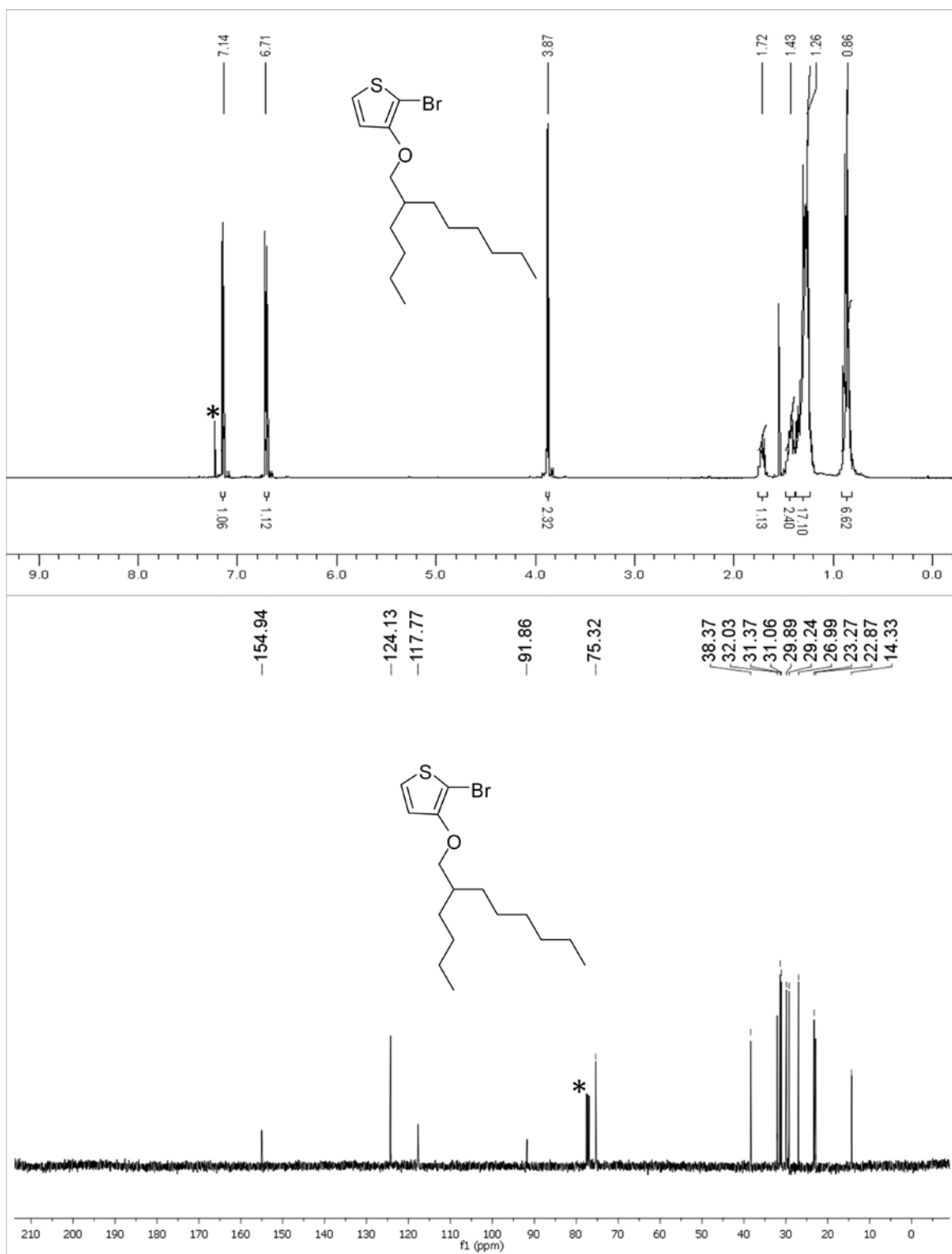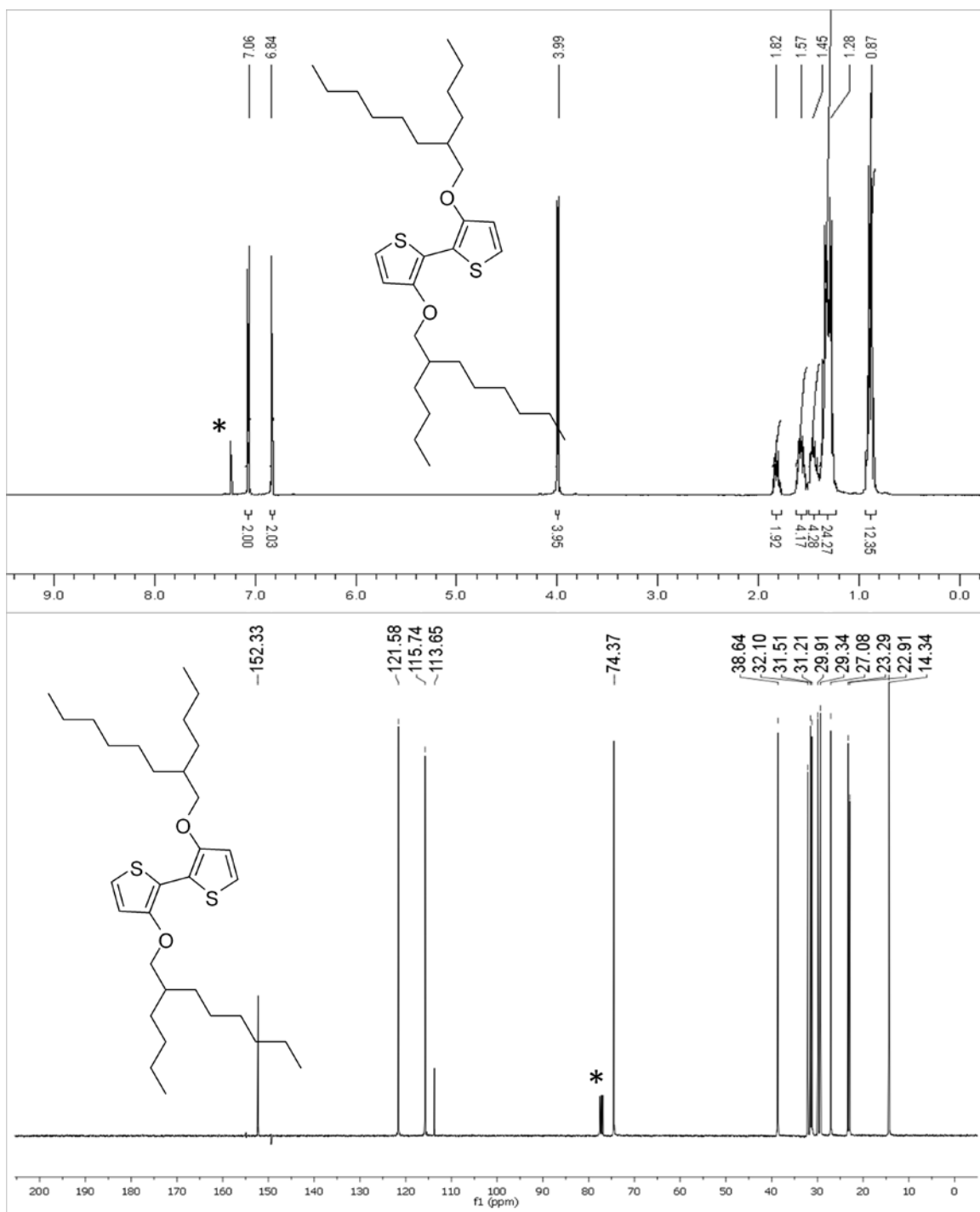
Figure 6.21: ^{1}H (top) and ^{13}C (bottom) NMR spectra (CDCl$_3$, r.t.) of compound **2.8e**(*solvent).

195

Figure 6.22: ¹H (top) and ¹³C (bottom) NMR spectra (CDCl₃, r.t.) of compound **2.9e**(*solvent).

Figure 6.23: ^{1}H (top) and ^{13}C (bottom) NMR spectra (CDCl$_3$, r.t.) of compound **2.6f**(*solvent).

Figure 6.24: ^{1}H (top) and ^{13}C (bottom) NMR spectra (CDCl$_3$, r.t.) of compound **2.7f**(*solvent).

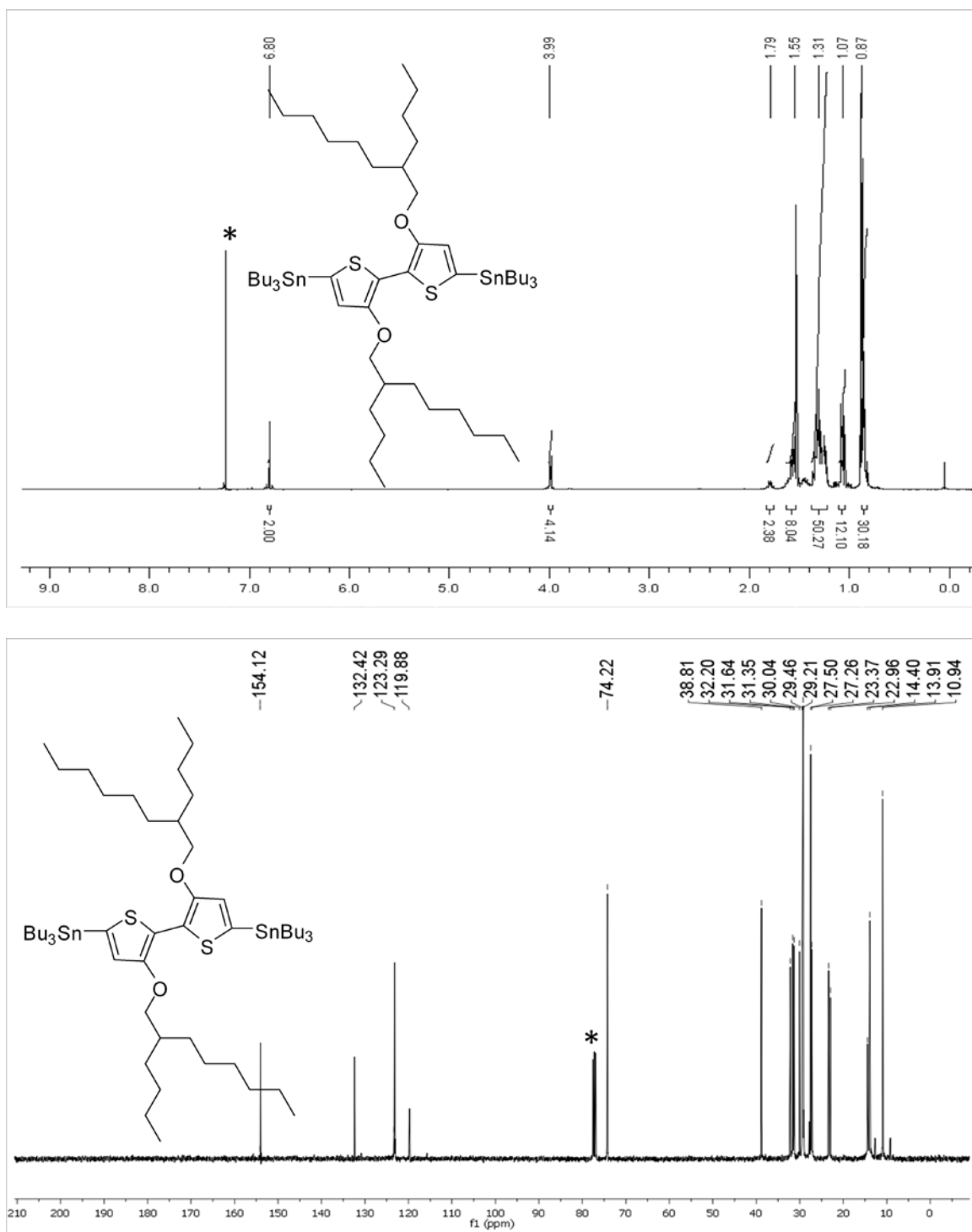**Figure 6.25:** ^{1}H (top) and ^{13}C (bottom) NMR spectra (CDCl$_3$, r.t.) of compound **2.8f** (*solvent).

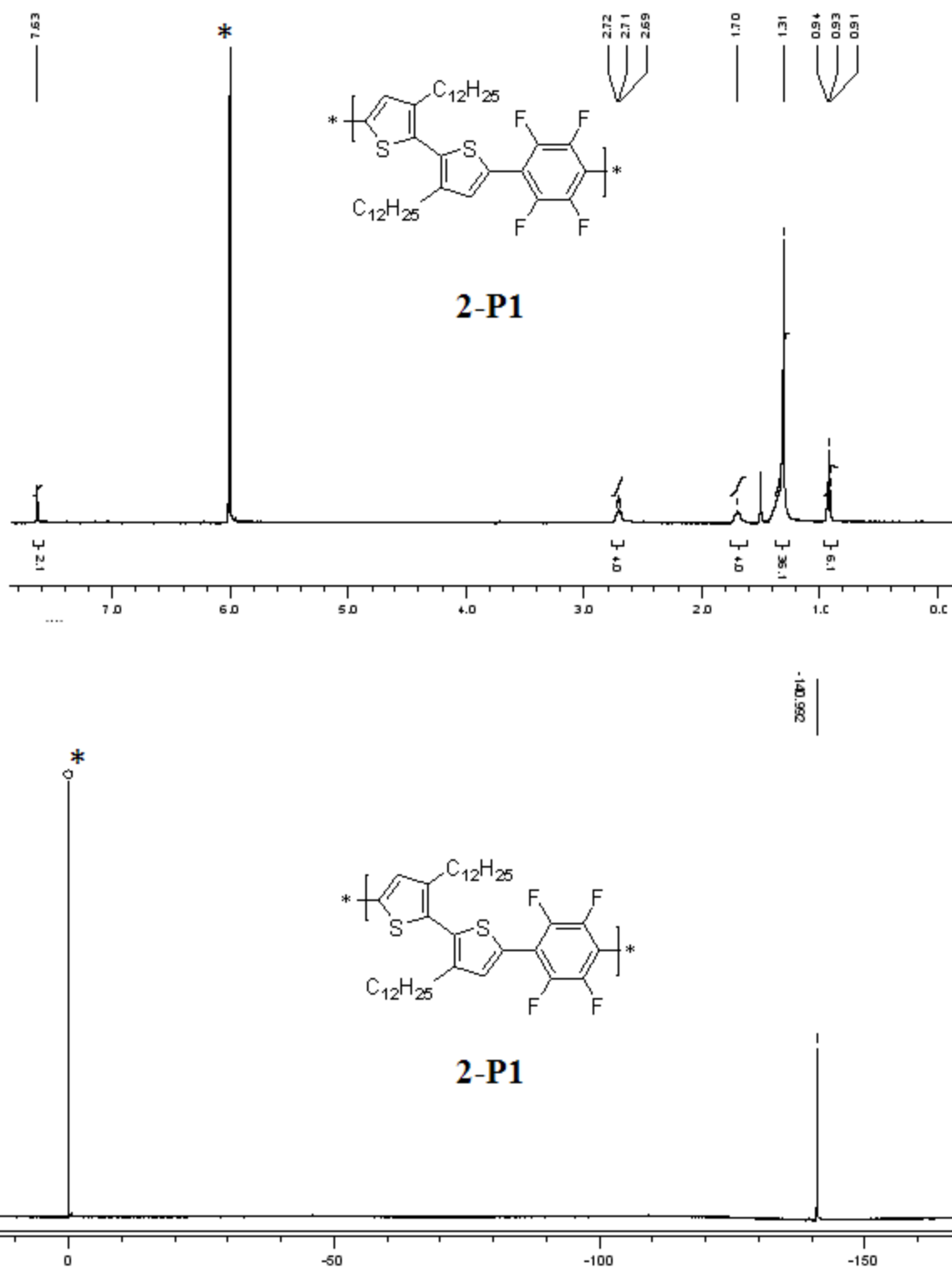**Figure 6.26:** ^{1}H (top) and ^{13}C (bottom) NMR spectra (CDCl$_3$, r.t.) of compound **2.9f** (*solvent).

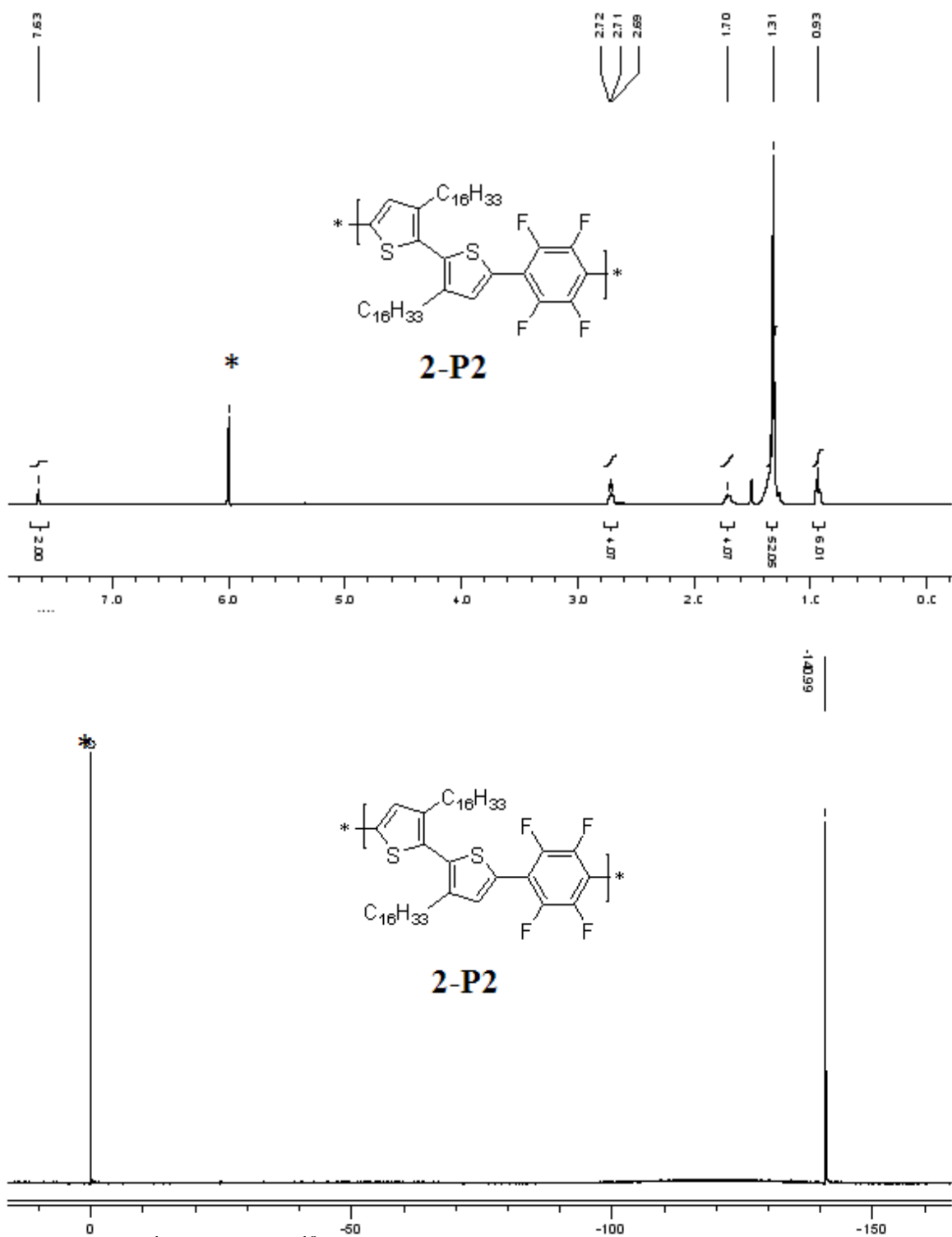**Figure 6.27:** ^1H (top) and ^{19}F (bottom) NMR spectra ($C_2D_2Cl_4$, 90 ℃) of Polymer **2-P1**(*solvent).

Figure 6.28: ^{1}H (top) and ^{19}F (bottom) NMR spectra (C$_2$D$_2$Cl$_4$, 90 ℃) of Polymer **2-P2**(*solvent).

.
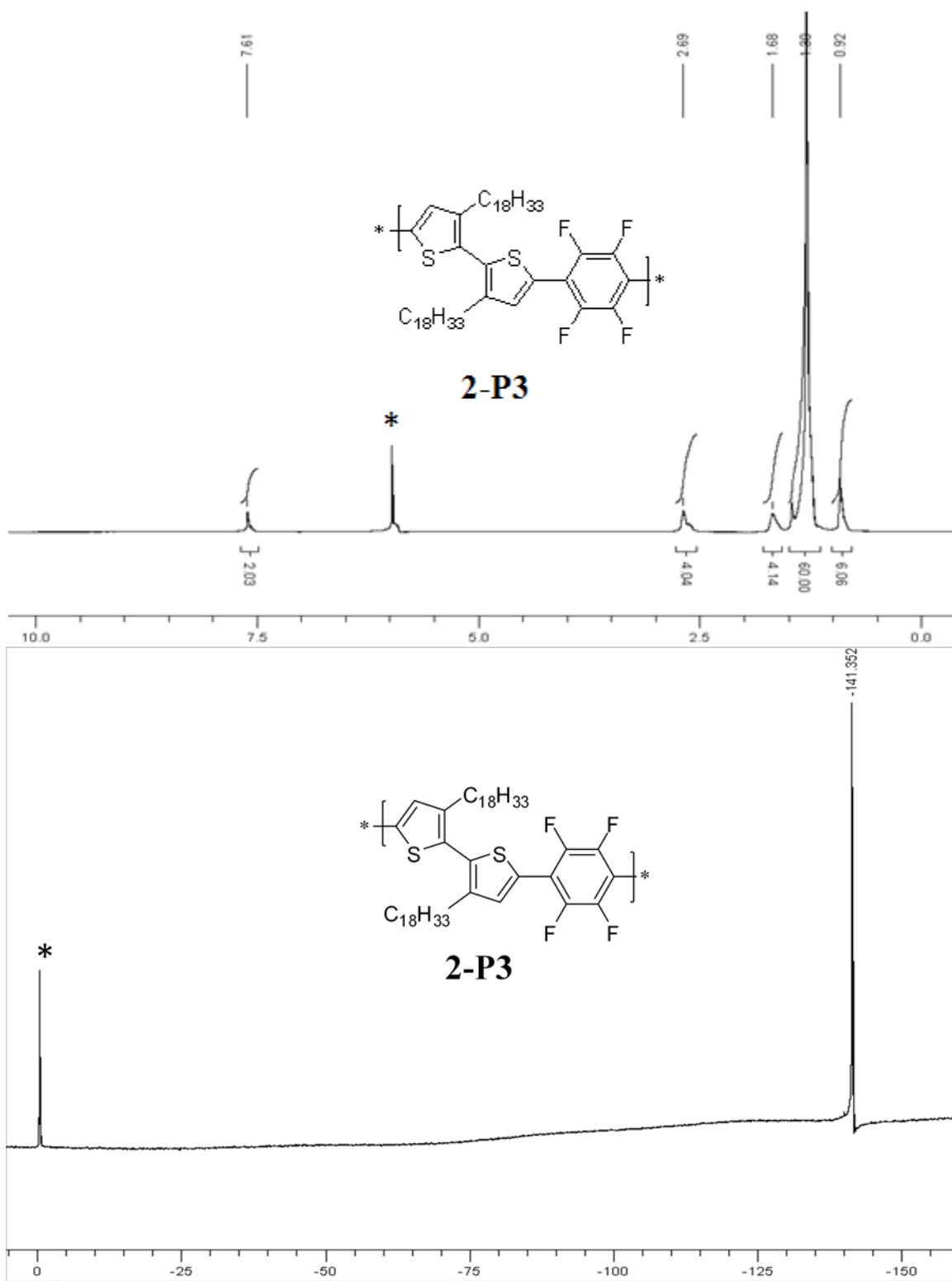
Figure 6.29: ^{1}H (top) and ^{19}F (bottom) NMR spectra (C$_2$D$_2$Cl$_4$, 90 °C) of Polymer **2-P3**(*solvent).

.
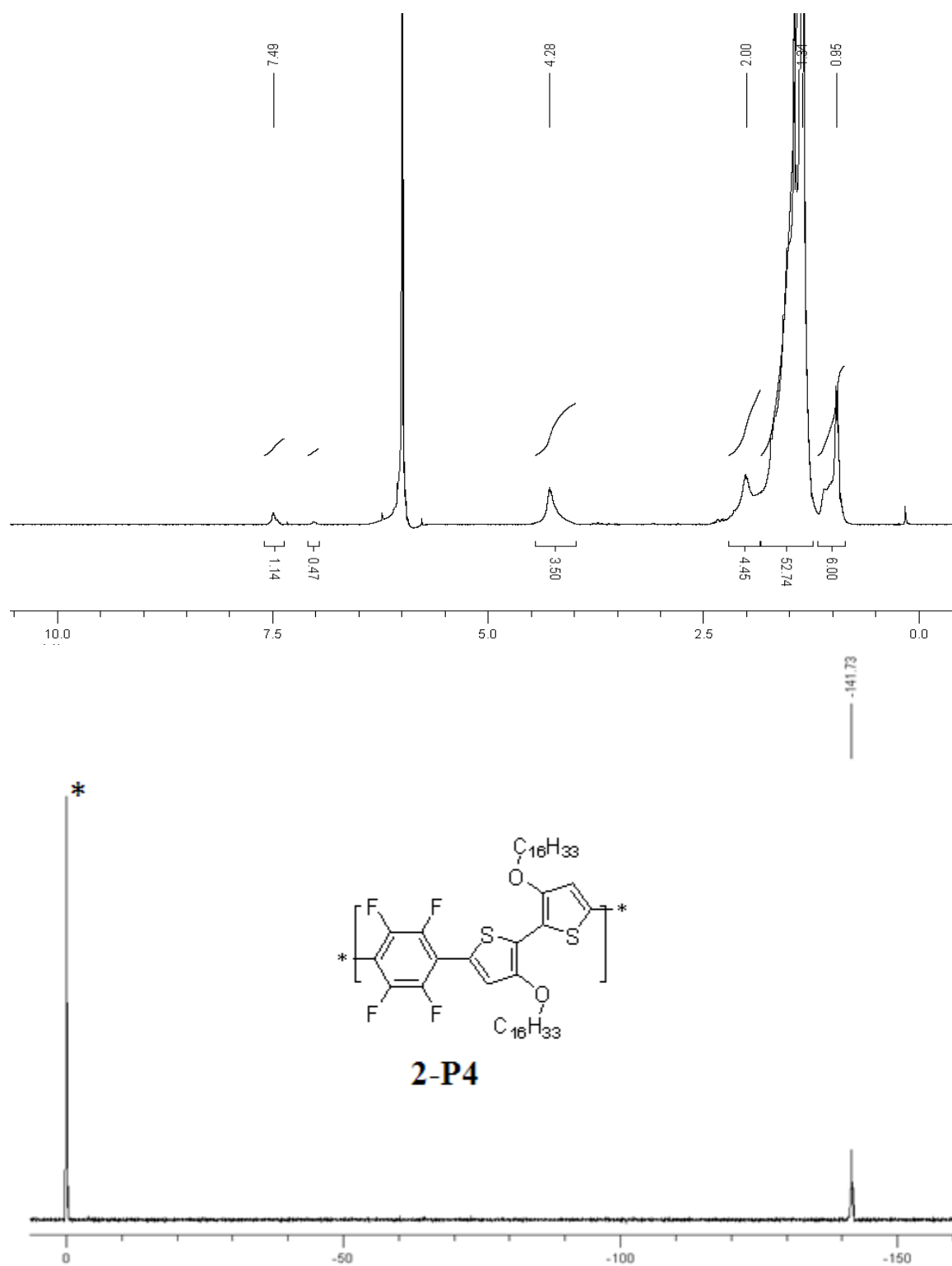
Figure 6.30: ^{1}H (top) and ^{19}F (bottom) NMR spectra (C$_2$D$_2$Cl$_4$, 90 °C) of Polymer **2-P4**(*solvent).
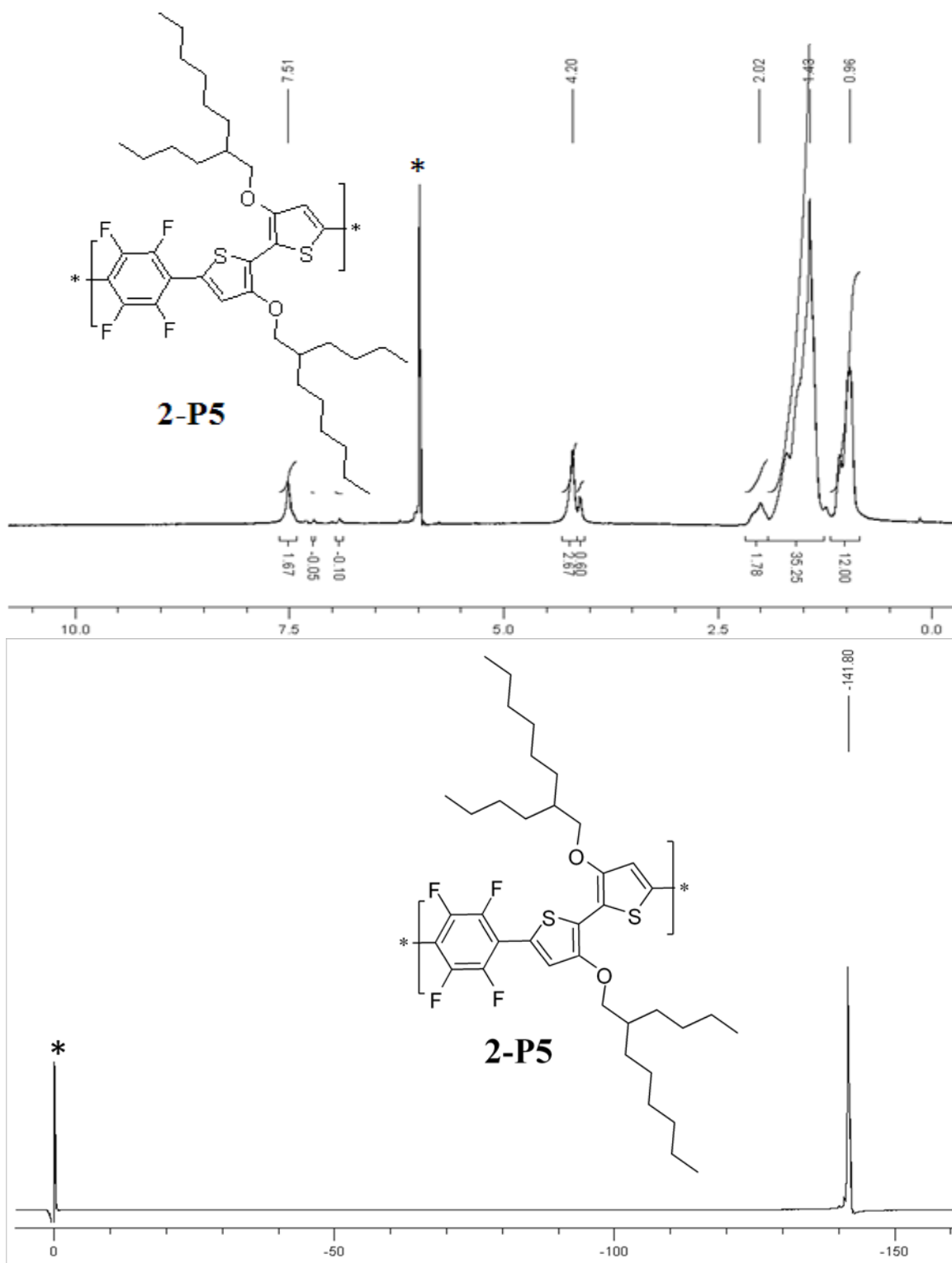
Figure 6.31: ^{1}H (top) and ^{19}F (bottom) NMR spectra (C$_2$D$_2$Cl$_4$, 90 °C) of Polymer **2-P5**(*solvent).
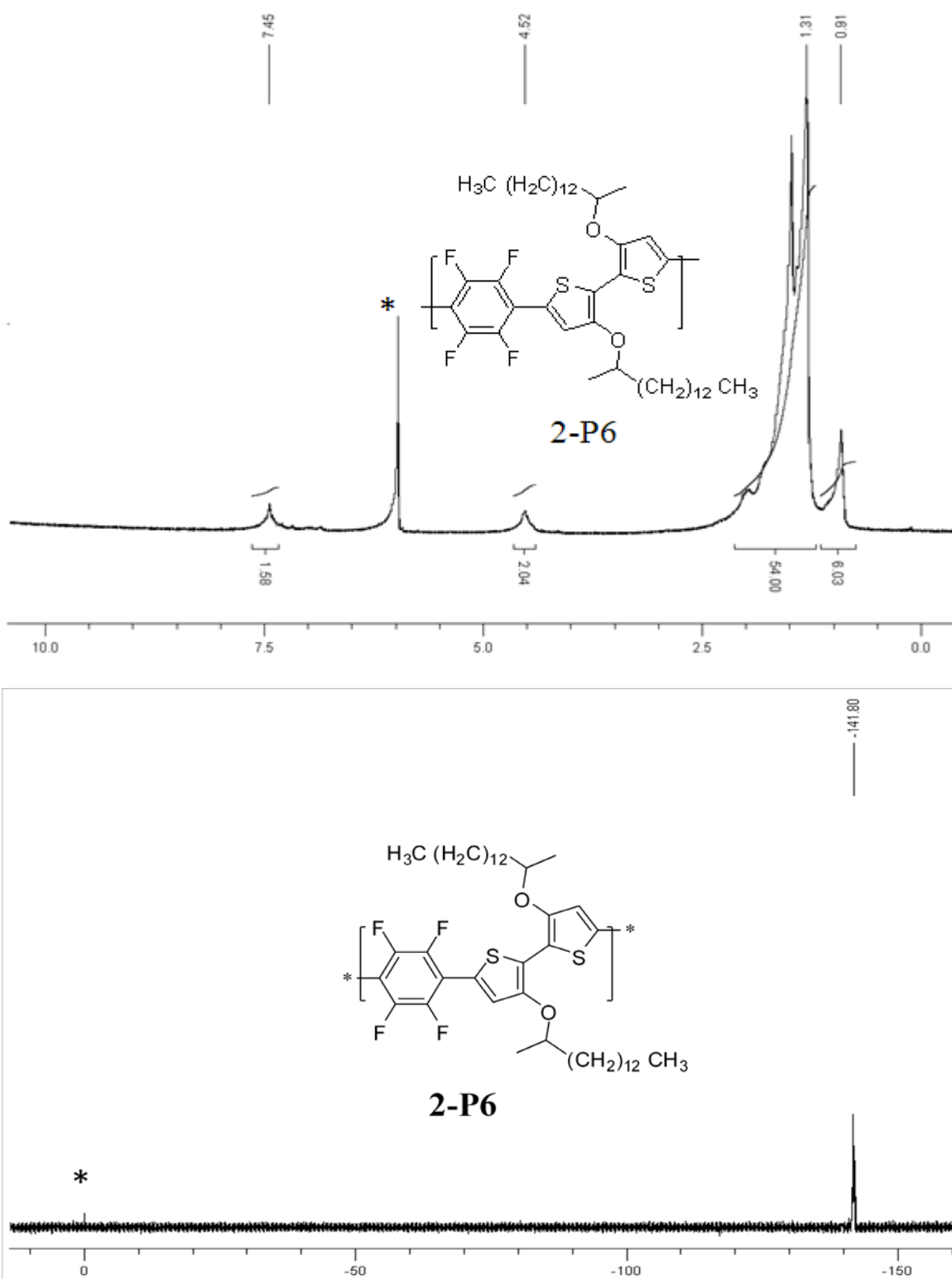
Figure 6.32: ¹H (top) and ¹⁹F (bottom) NMR spectra (C₂D₂Cl₄, 90 ℃) of Polymer **2-P6**(*solvent).
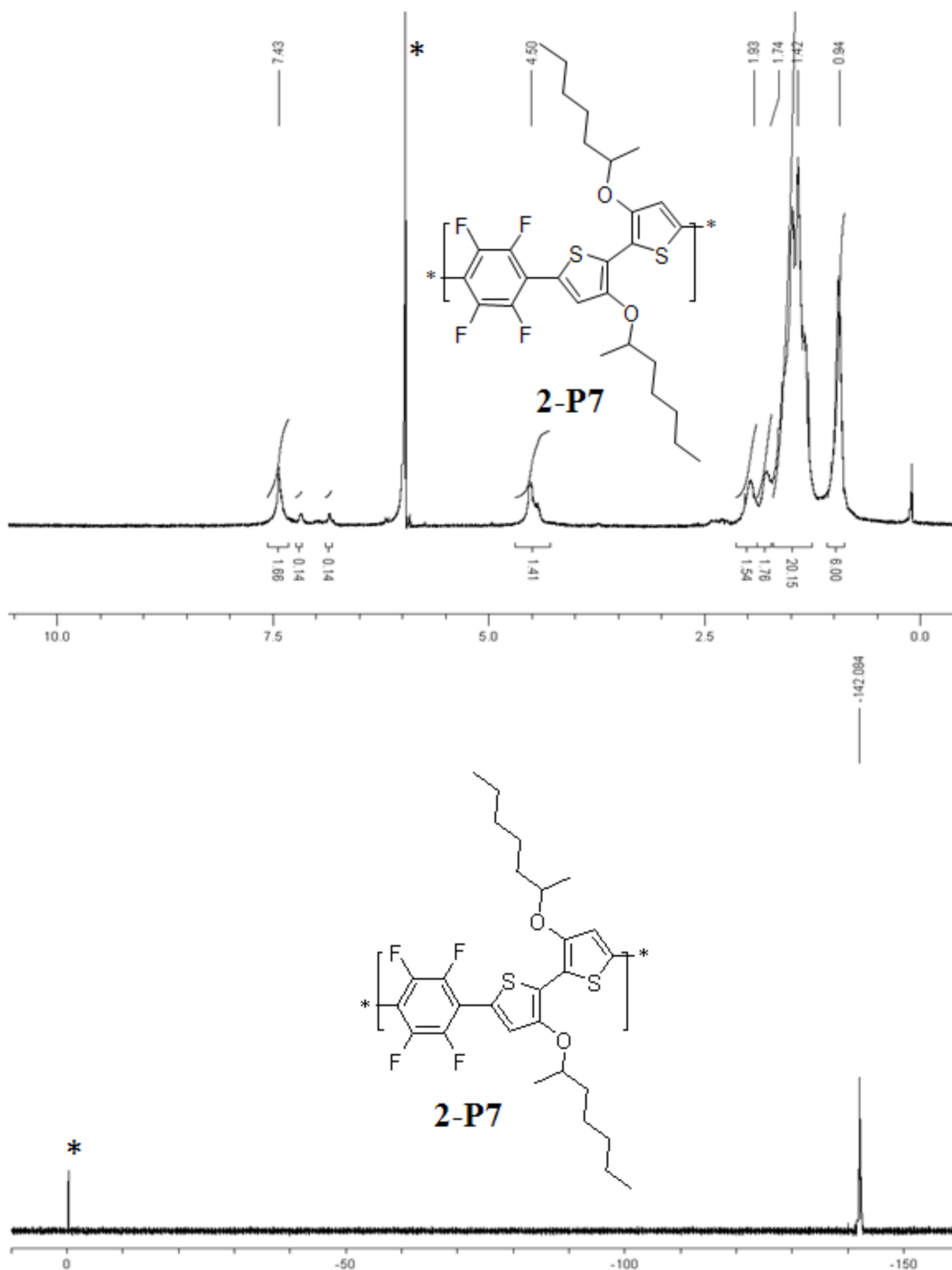
Figure 6.33: ^{1}H (top) and ^{19}F (bottom) NMR spectra ($C_2D_2Cl_4$, 90 ℃) of Polymer **2-P7**(*solvent).
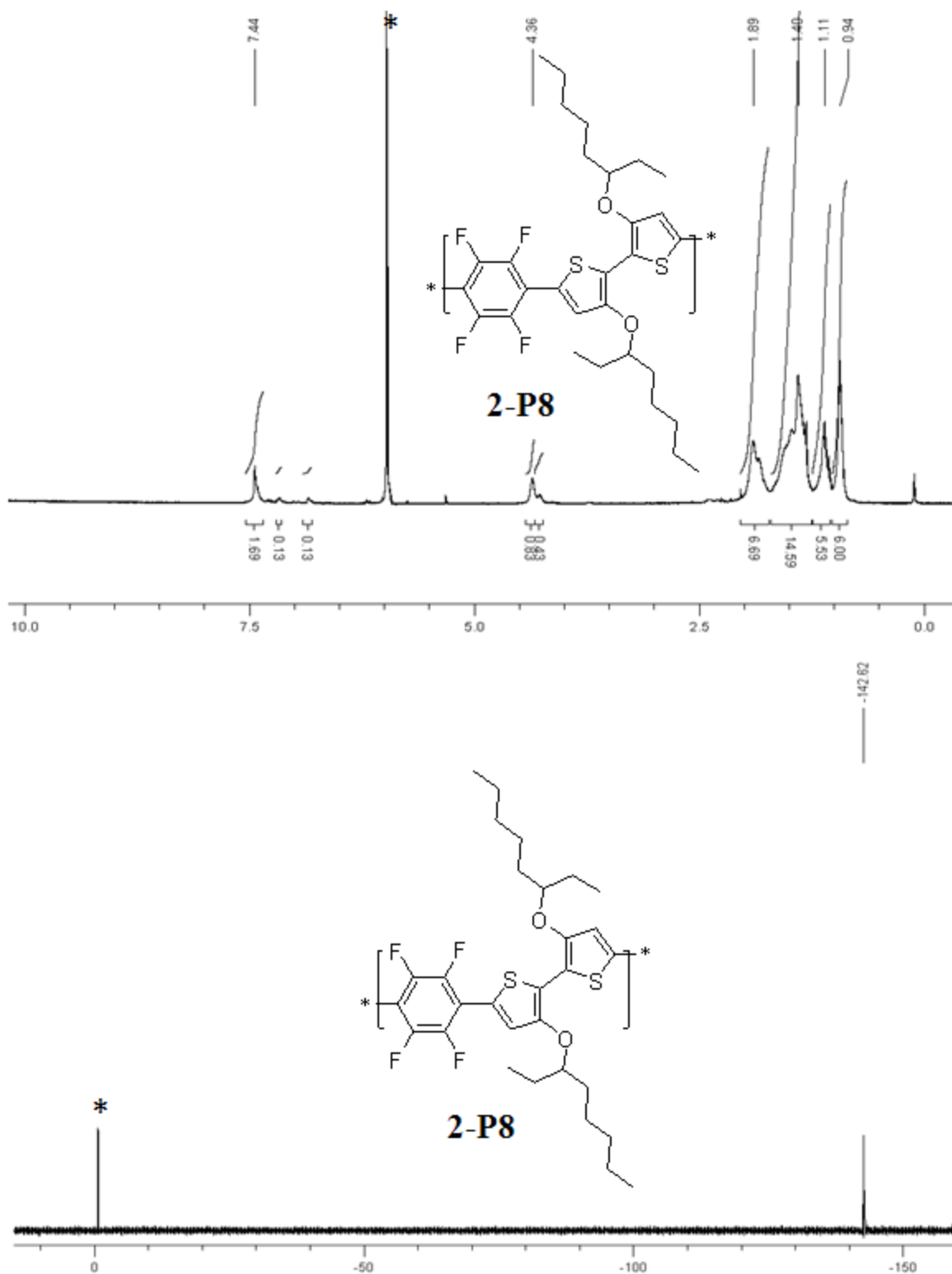
Figure 6.34: ^1H (top) and ^{19}F (bottom) NMR spectra (C$_2$D$_2$Cl$_4$, 90 °C) of Polymer **2-P8**(*solvent).
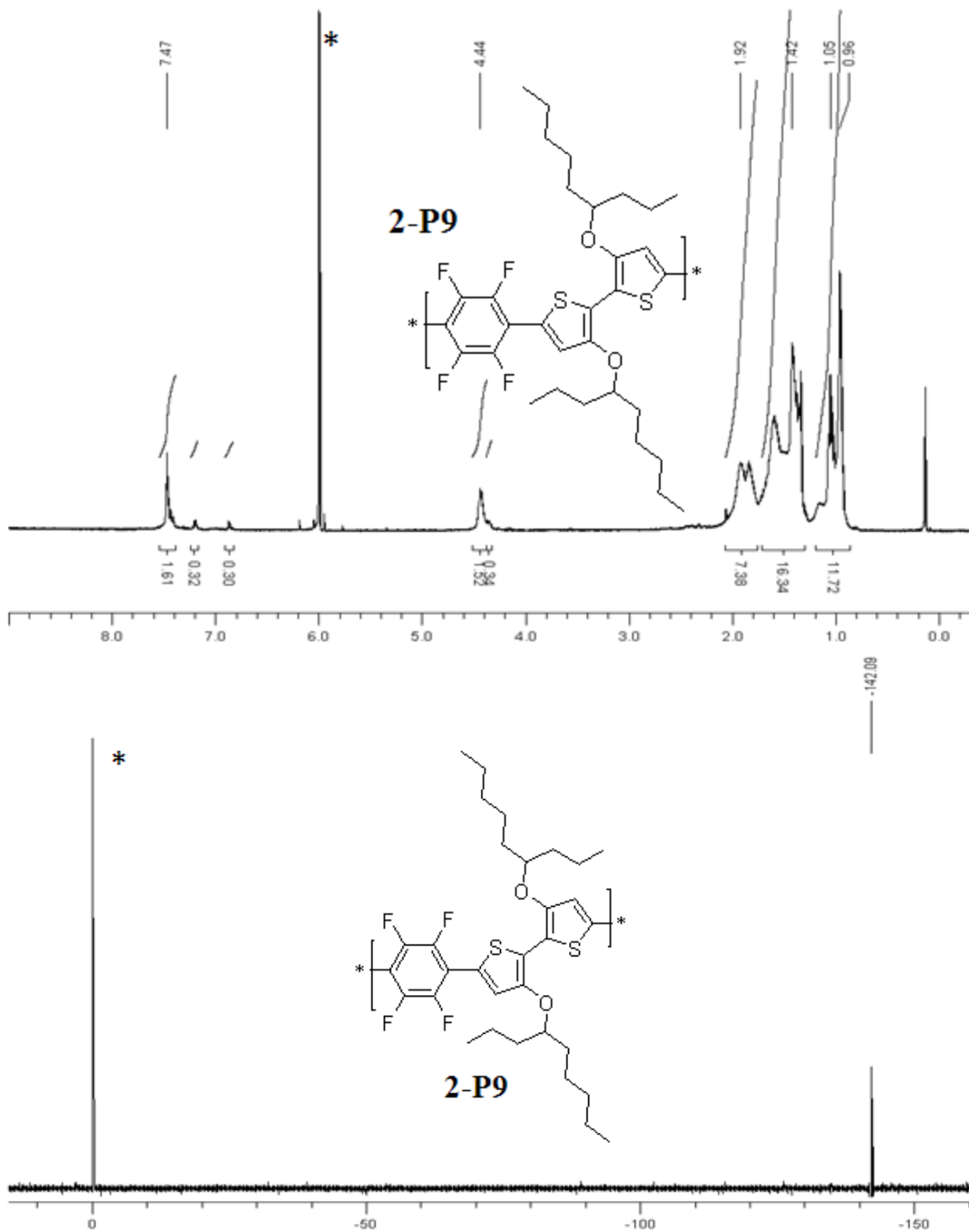
Figure 6.35: ^{1}H (top) and ^{19}F (bottom) NMR spectra (C$_2$D$_2$Cl$_4$, 90 °C) of Polymer **2-P9**(*solvent).

Figure 6.35: ^{1}H (top) and ^{13}C (bottom) NMR spectra (CDCl$_3$, r.t.) of compound **3.2**(*solvent).
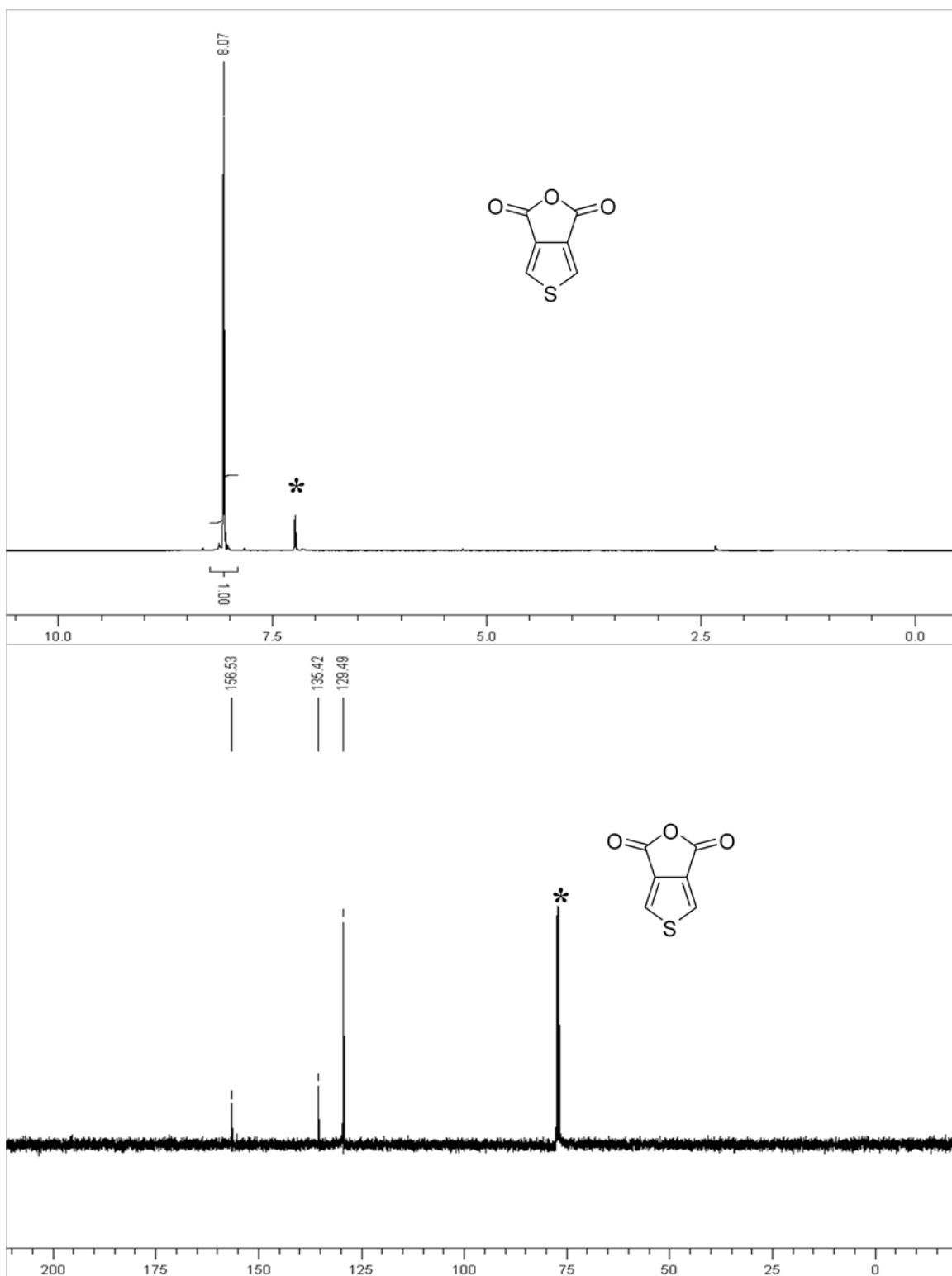
Figure 6.36: ^{1}H (top) and ^{13}C (bottom) NMR spectra (CDCl$_3$, r.t.) of compound 3.4 (*solvent).
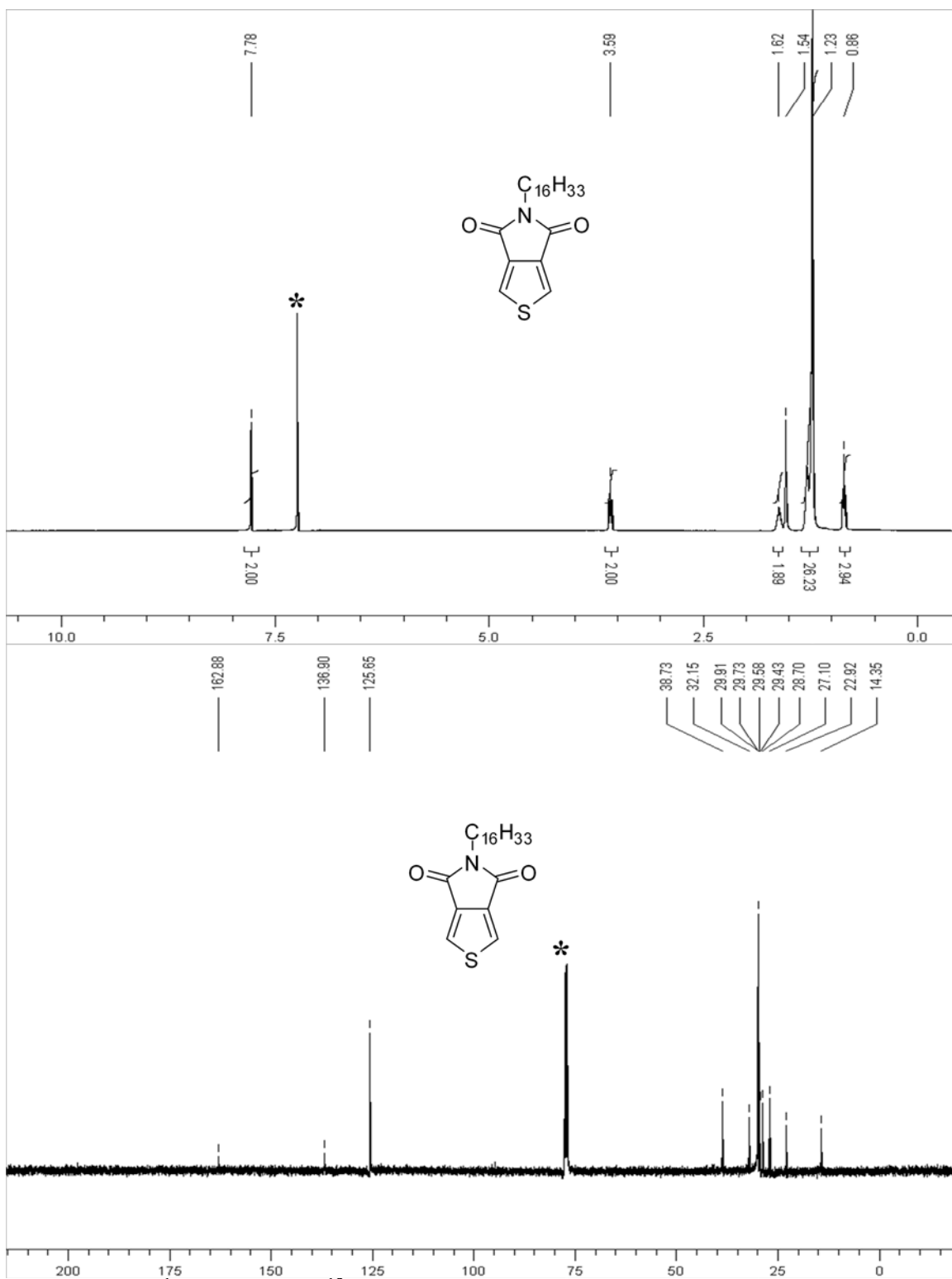
Figure 6.37: ^1H (top) and ^{13}C (bottom) NMR spectra (CDCl$_3$, r.t.) of compound **3.8**(*solvent).

Figure 6.38: ^{1}H (top) and ^{13}C (bottom) NMR spectra (CDCl$_3$, r.t.) of compound **3.9** (*solvent).

Figure 6.39: ^{1}H (top) and ^{13}C (bottom) NMR spectra (CDCl$_3$, r.t.) of compound (*solvent).

Figure 6.40: ^{1}H (top) and ^{13}C (bottom) NMR spectra (CDCl$_3$, r.t.) of compound **3.10**(*solvent).
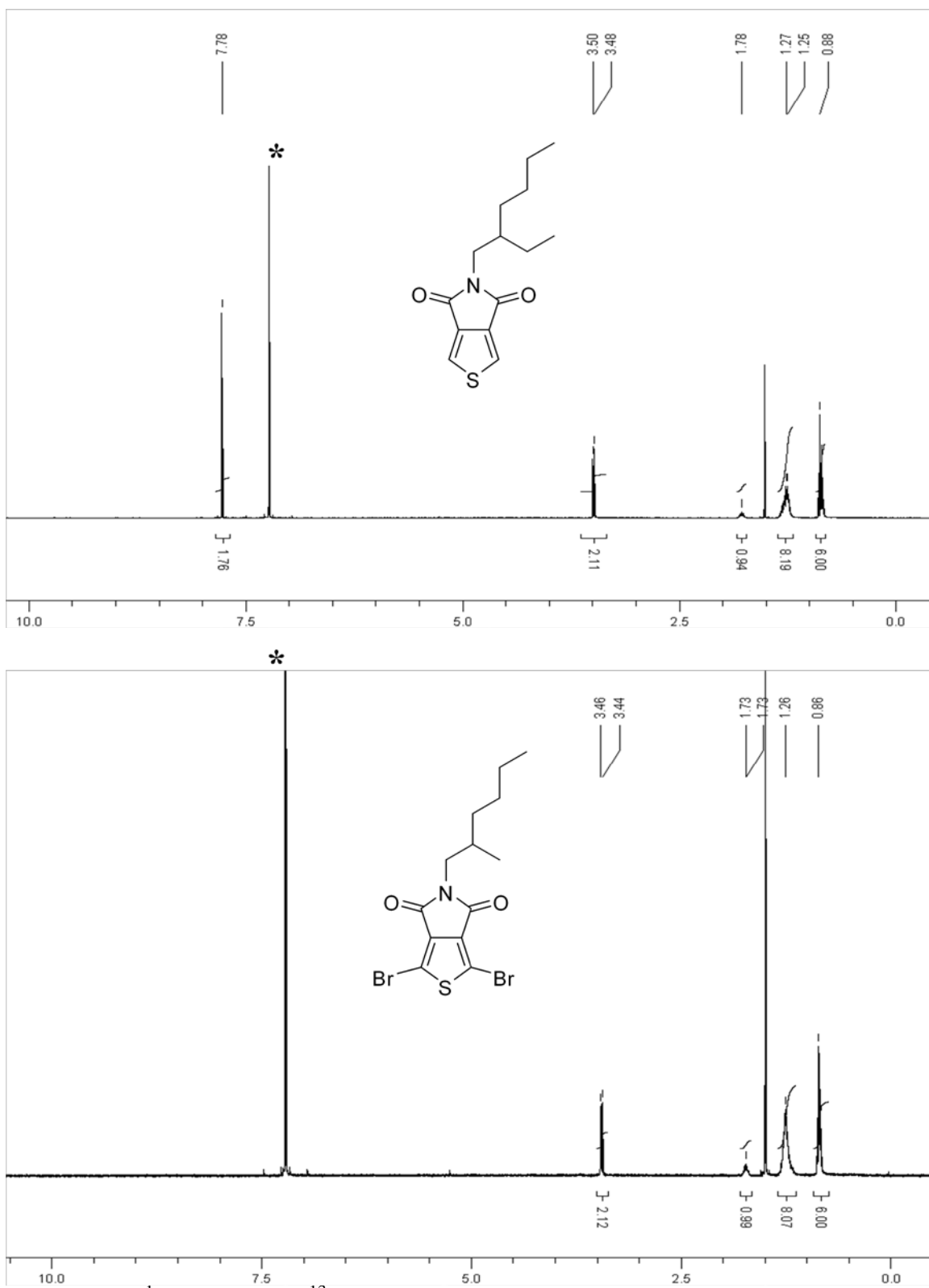
Figure 6.41: ^1H (top) and ^{13}C (bottom) NMR spectra (CDCl$_3$, r.t.) of compound **3.11**(*solvent).
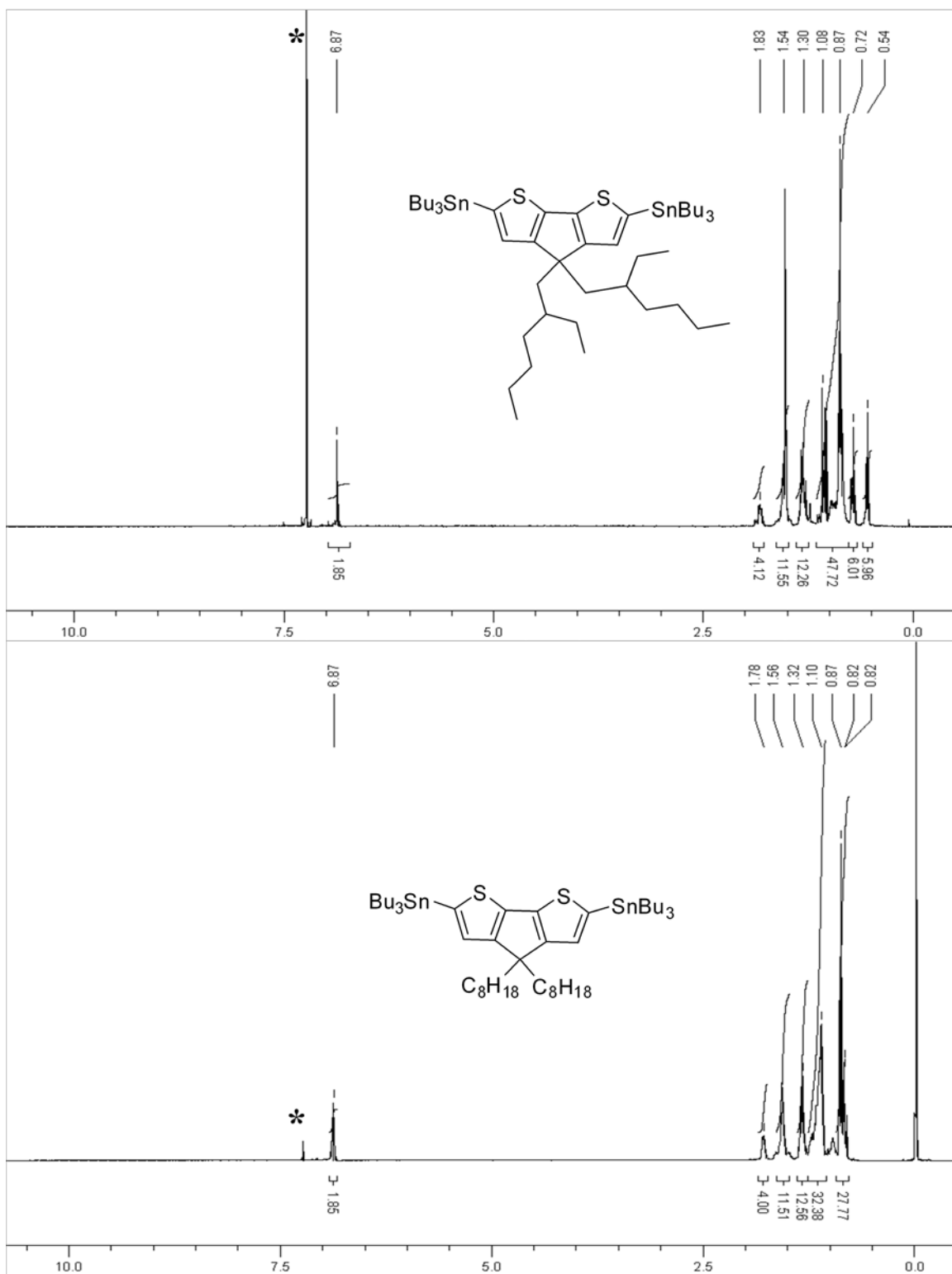
Figure 6.42:^{1}H NMR spectra 3.21b (top) 3.21 a (bottom)(CDCl$_3$, r.t.) (*solvent).
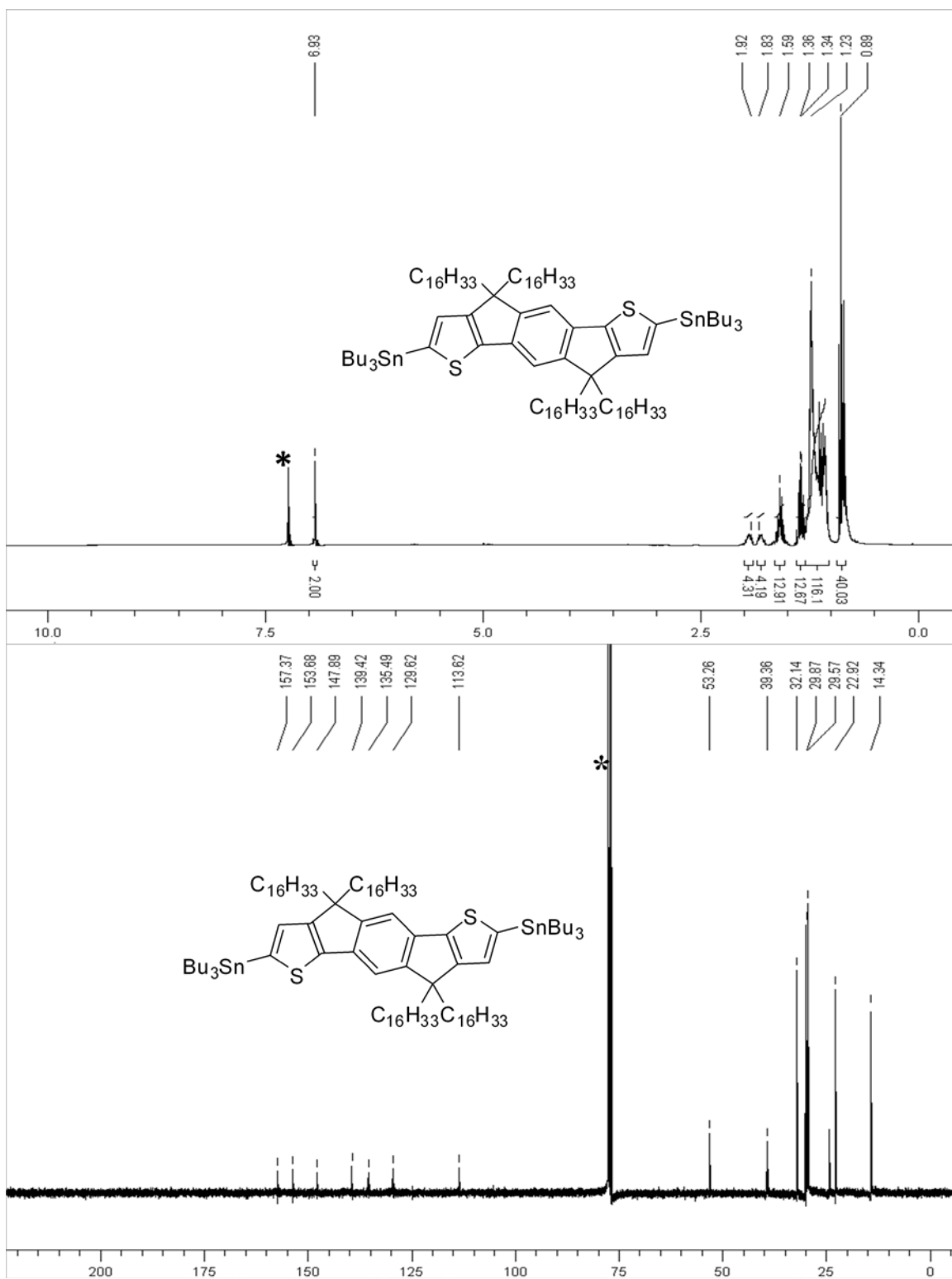
Figure 6.43: ^{1}H (top) and ^{13}C (bottom) NMR spectra (CDCl$_3$, r.t.) of compound **3.29** (*solvent).
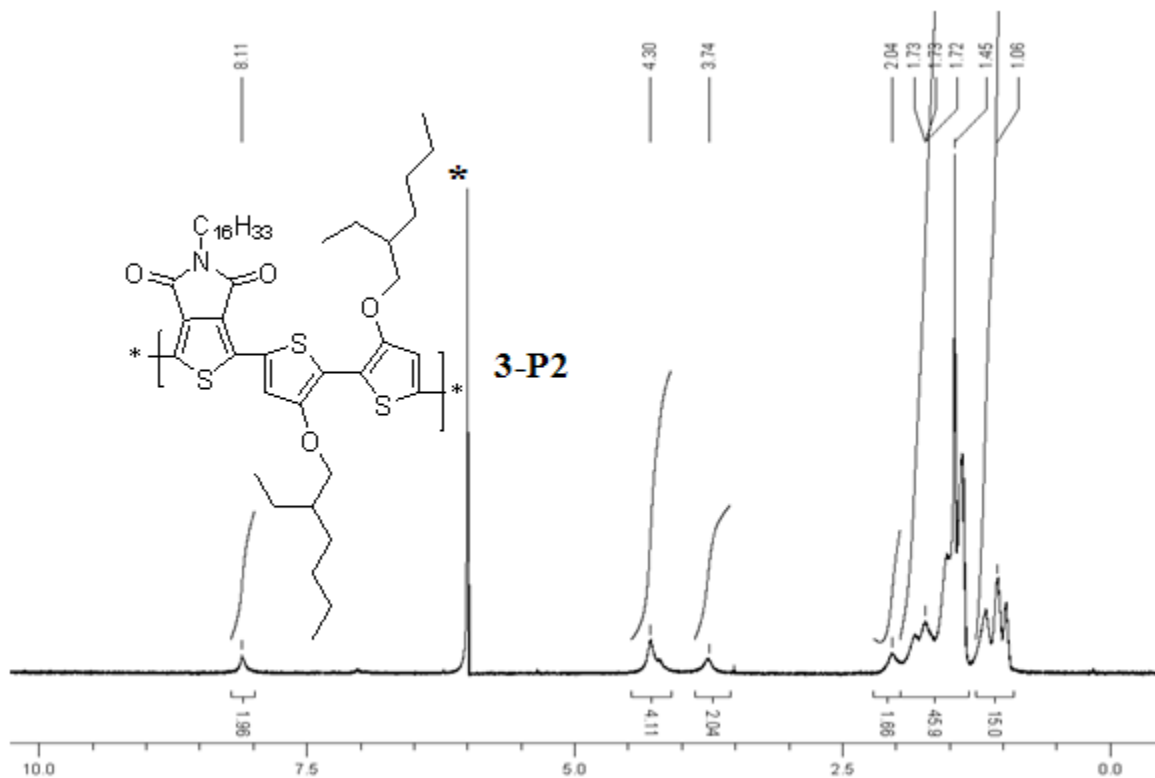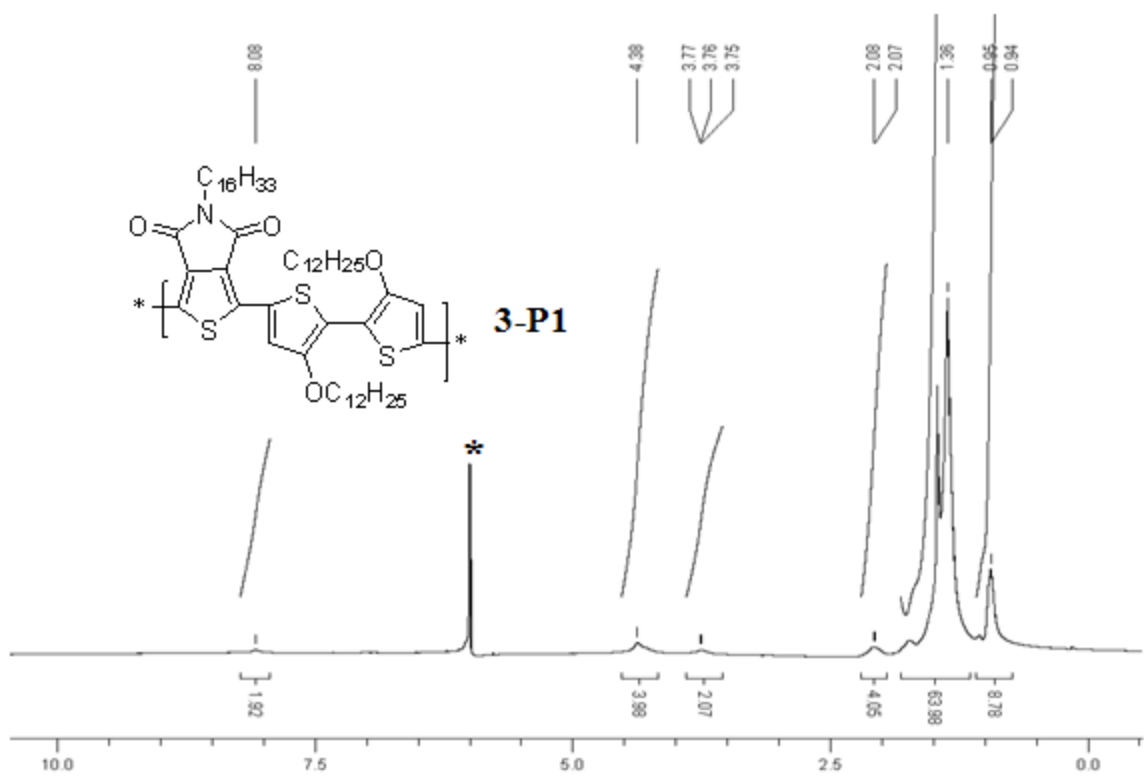
Figure 6.44 ^{1}H NMR spectra of polymer **3-P1** (top) and **3-P2** (bottom) (C$_2$D$_2$Cl$_4$, 130 ^{0}C) of compound (*solvent).
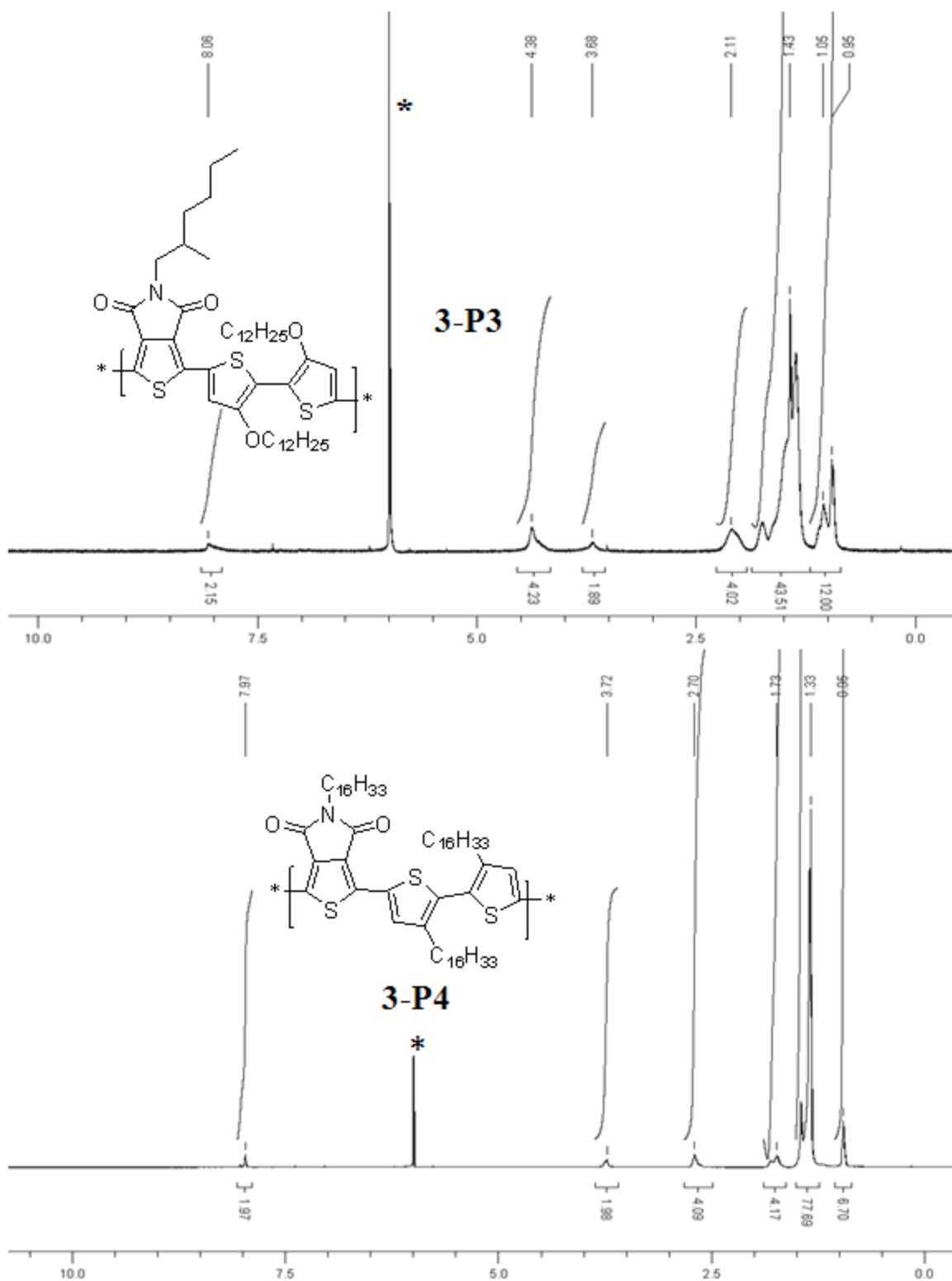
Figure 6.45 ^{1}H NMR spectra of polymer **3-P3** (top) and **3-P4** (bottom) (C$_2$D$_2$Cl$_4$, 130 ^{0}C) of compound (*solvent).
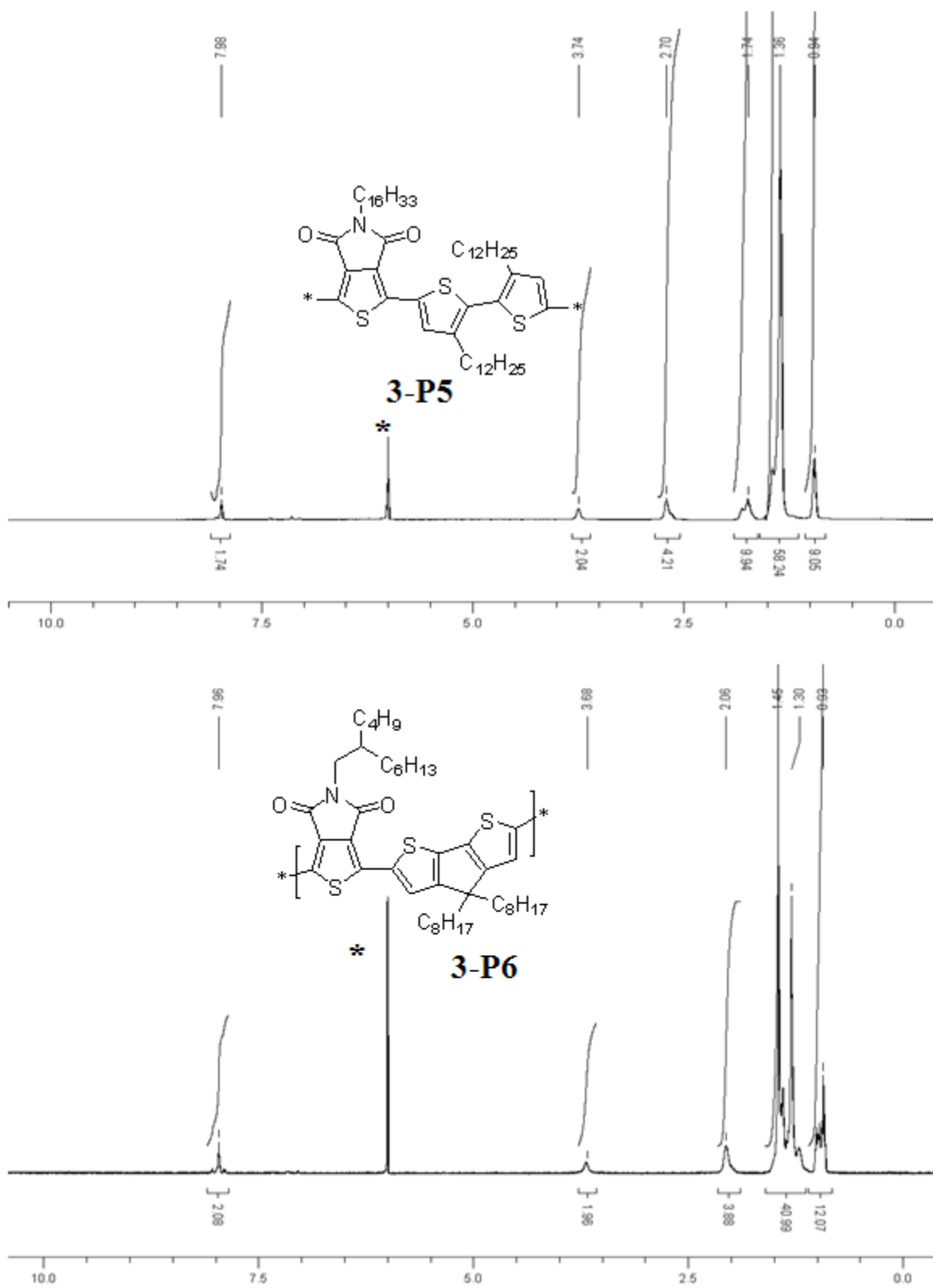
Figure 6.46 ^{1}H NMR spectra of polymer **3-P5** (top) and **3-P6** (bottom) ($C_2D_2Cl_4$, 130 ^{0}C) of compound (*solvent).
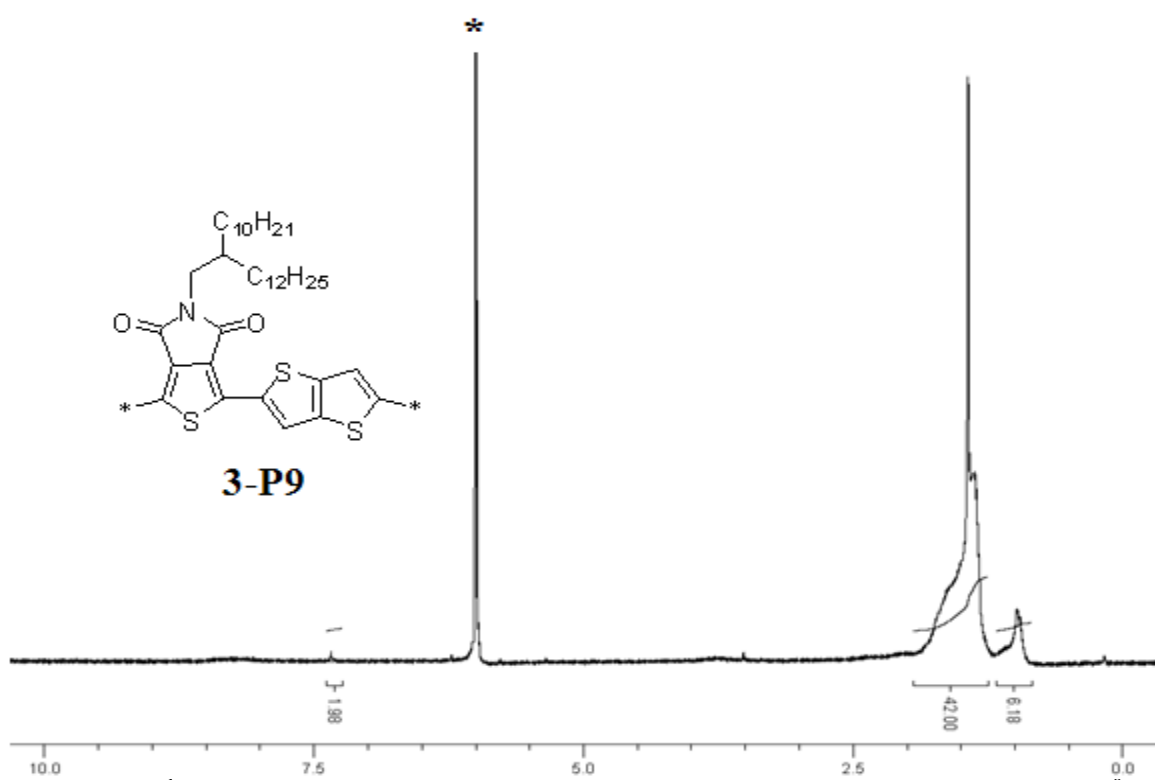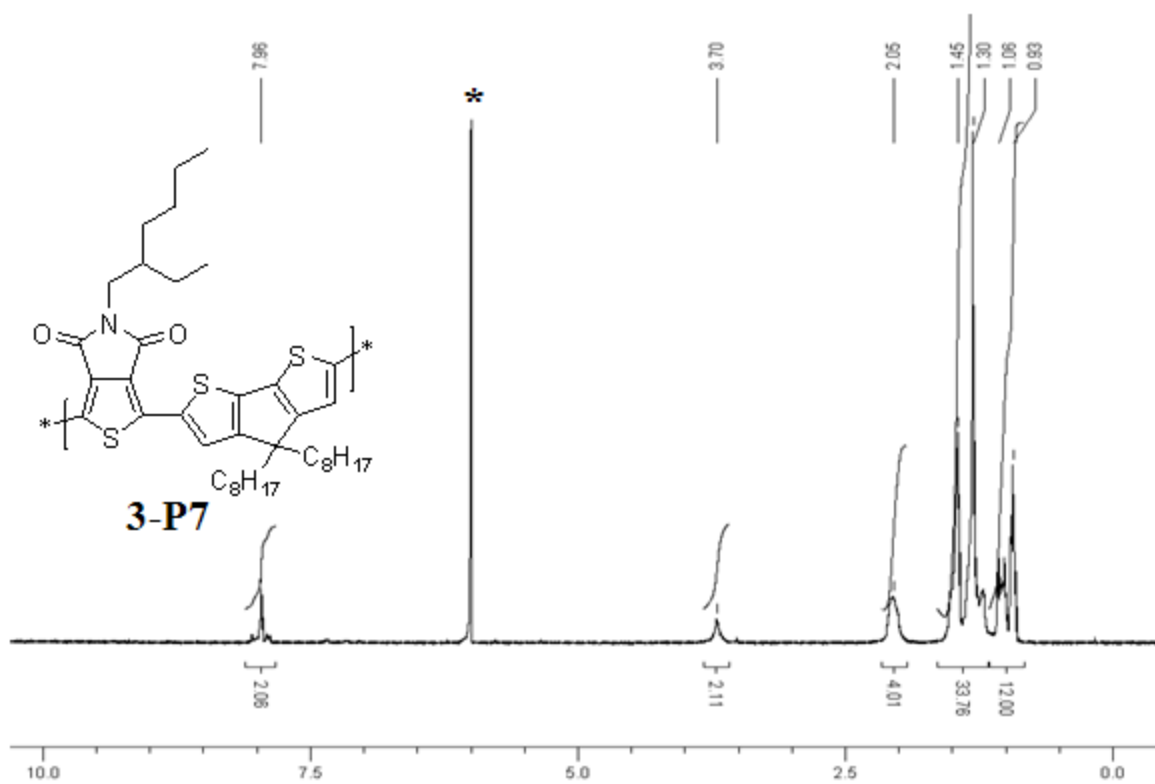
Figure 6.47 ^{1}H NMR spectra of polymer **3-P7** (top) and **3-P6** (bottom) (C$_2$D$_2$Cl$_4$, 130 ^{0}C) of compound (*solvent).

NMR spectra for Chapter 4
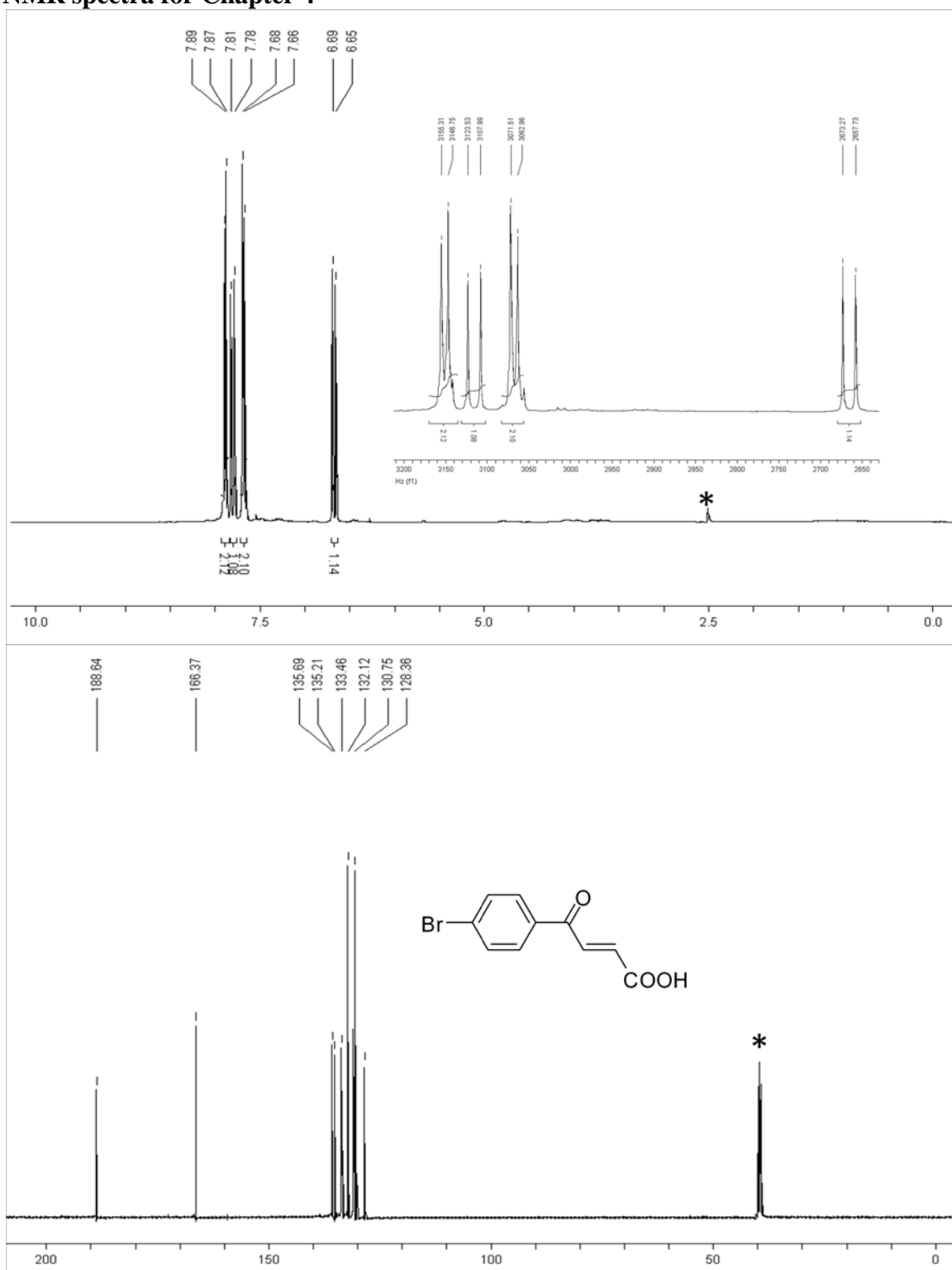
Figure 6.48 ^{1}H (top) and ^{13}C (bottom) NMR spectra (DMSO, r.t.) of compound **4.0**(*solvent).
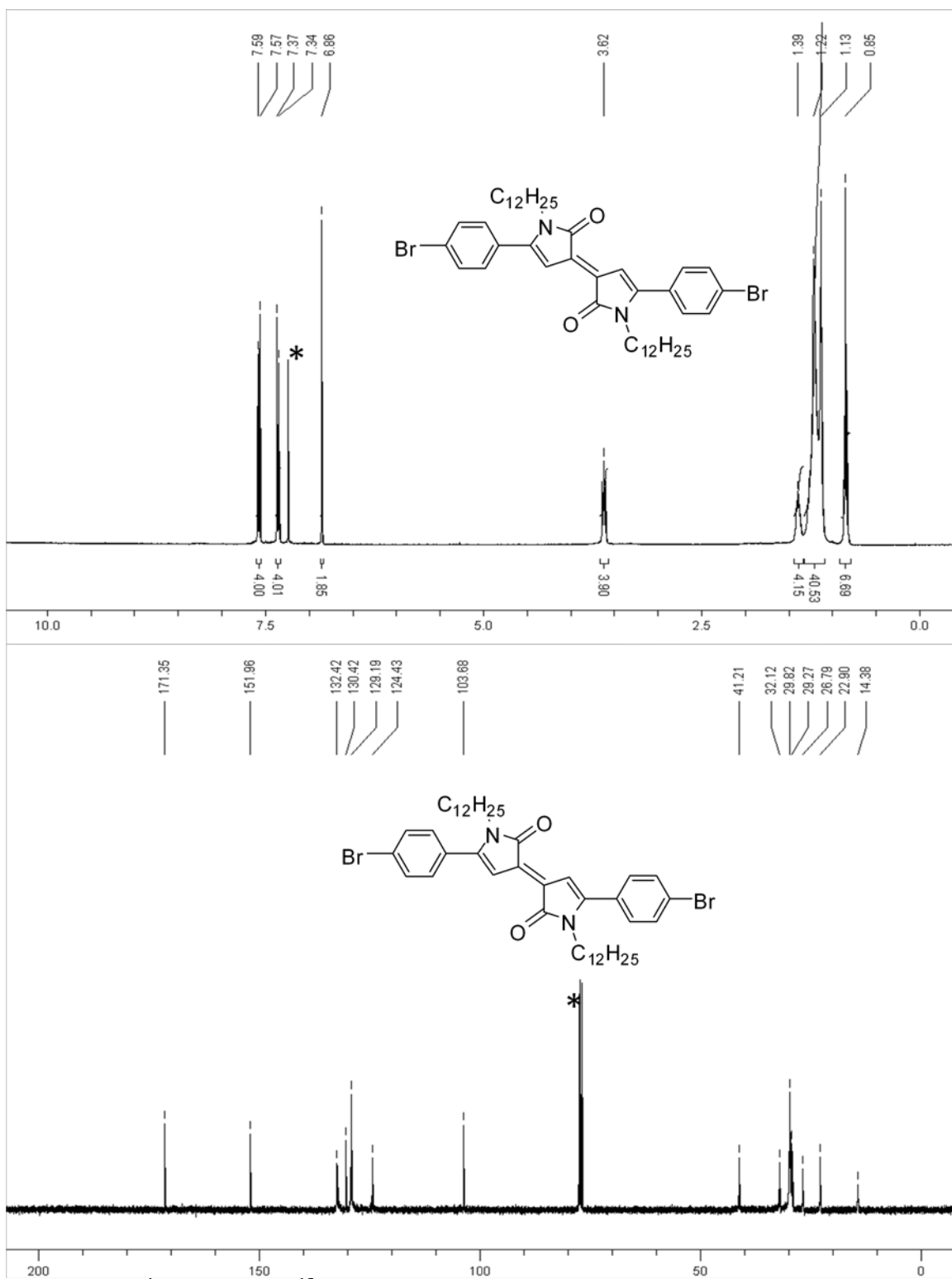
Figure 6.49 ^{1}H (top) and ^{13}C (bottom) NMR spectra (CDCl$_3$, r.t.) of compound **4.2a** (*solvent).
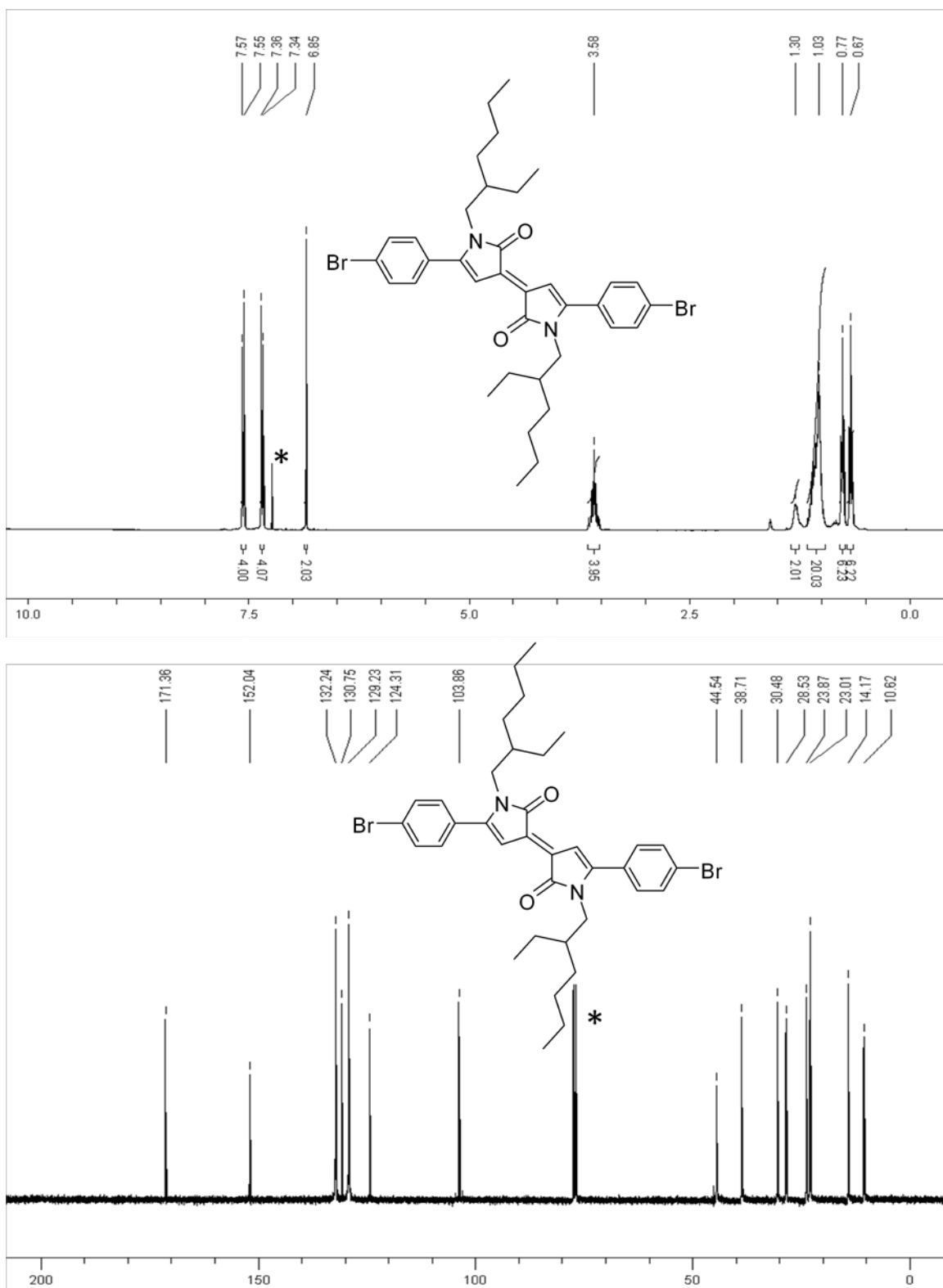
Figure 6.50 ^{1}H (top) and ^{13}C (bottom) NMR spectra (CDCl$_3$, r.t.) of compound **4.2b** (*solvent).
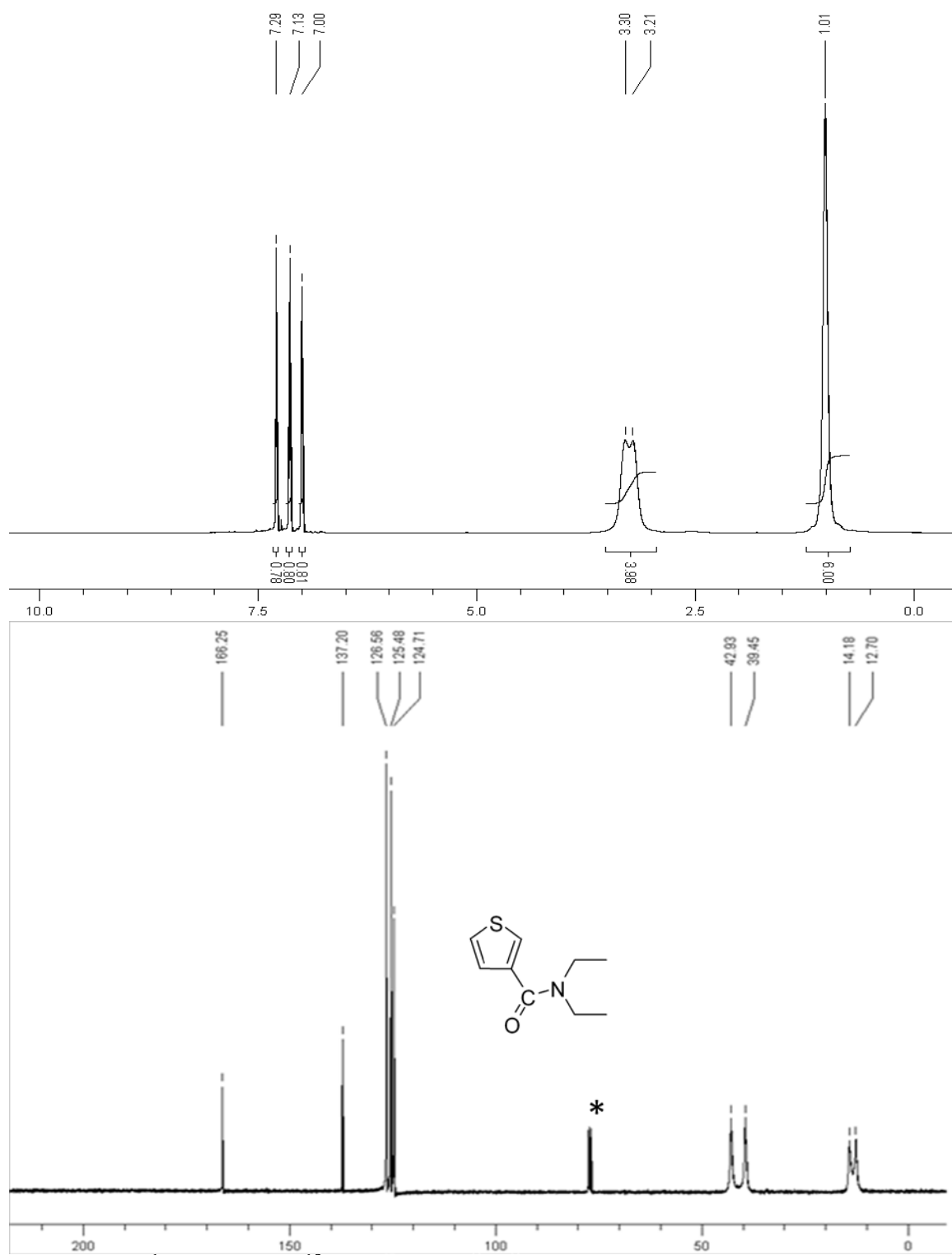
Figure 6.51 ^{1}H (top) and ^{13}C (bottom) NMR spectra (CDCl$_3$, r.t.) of compound **4.4** (*solvent).

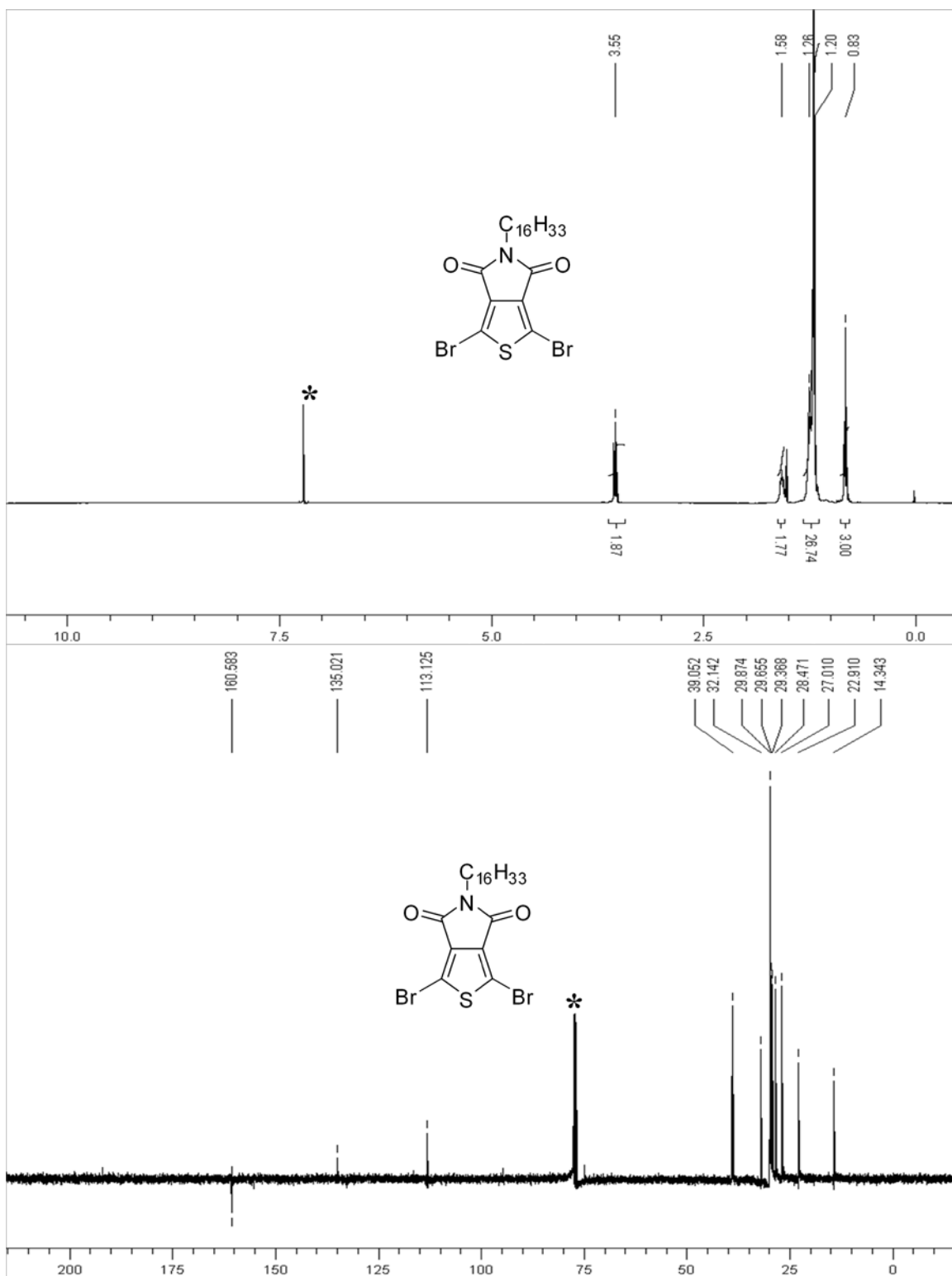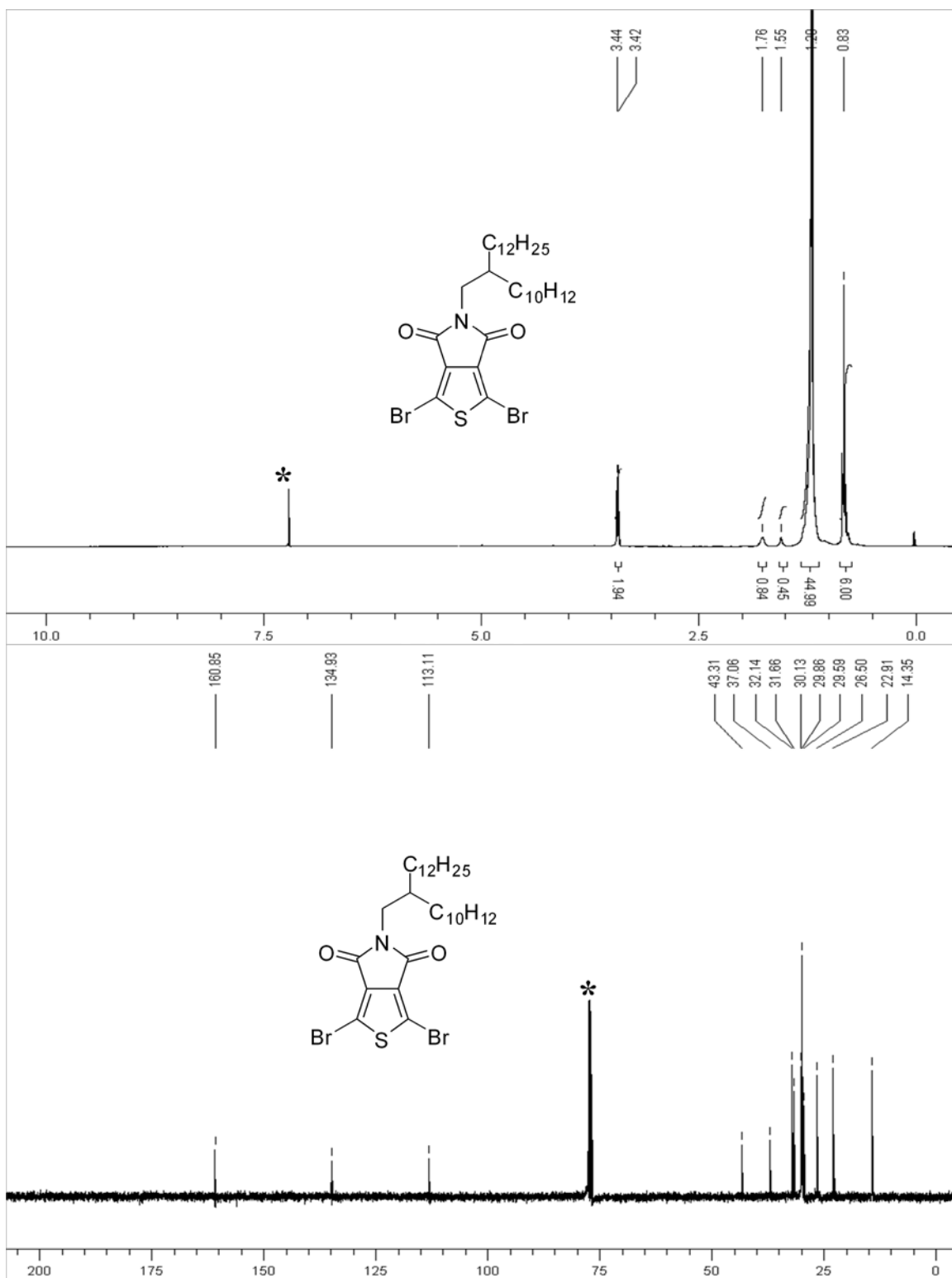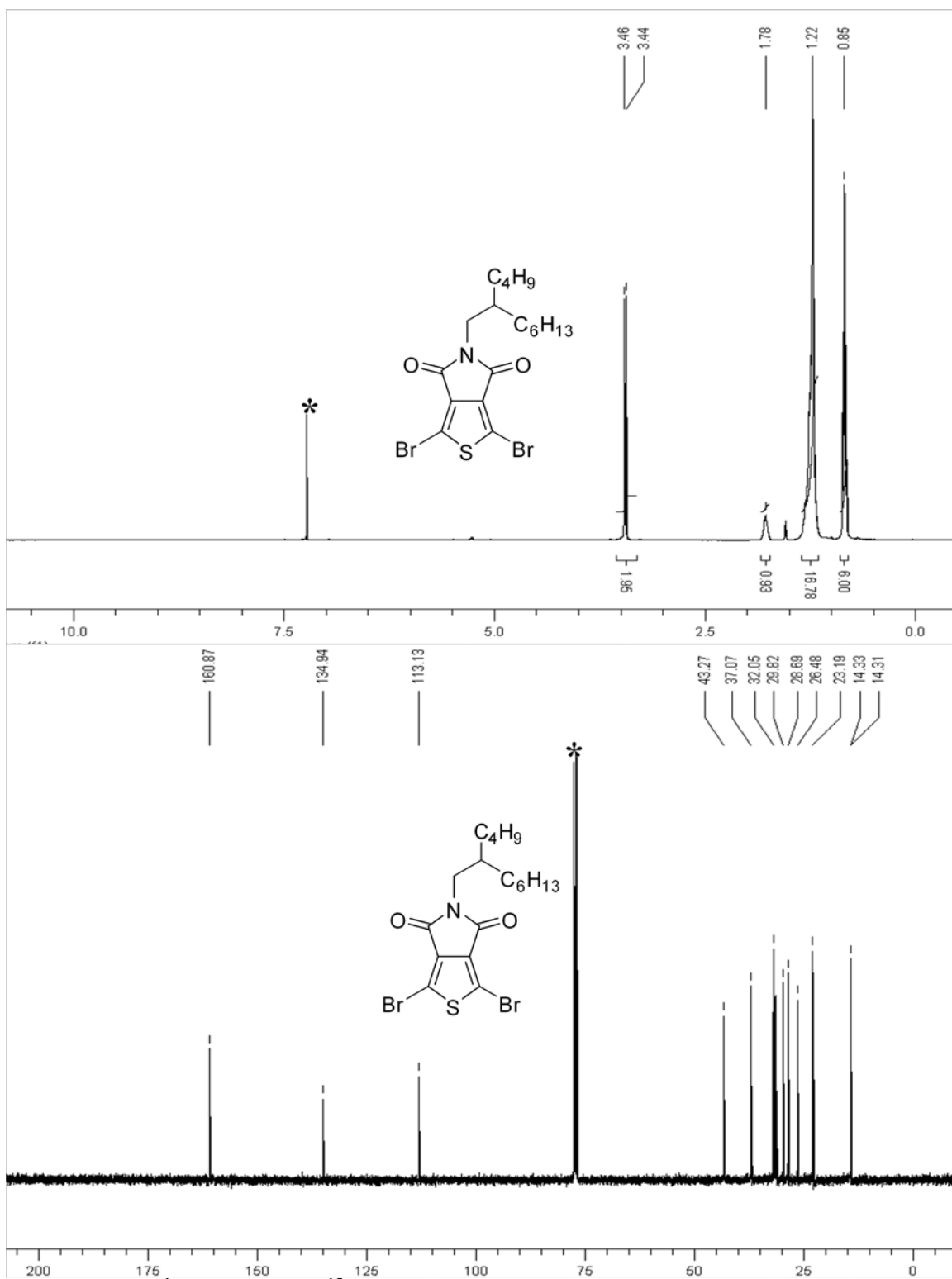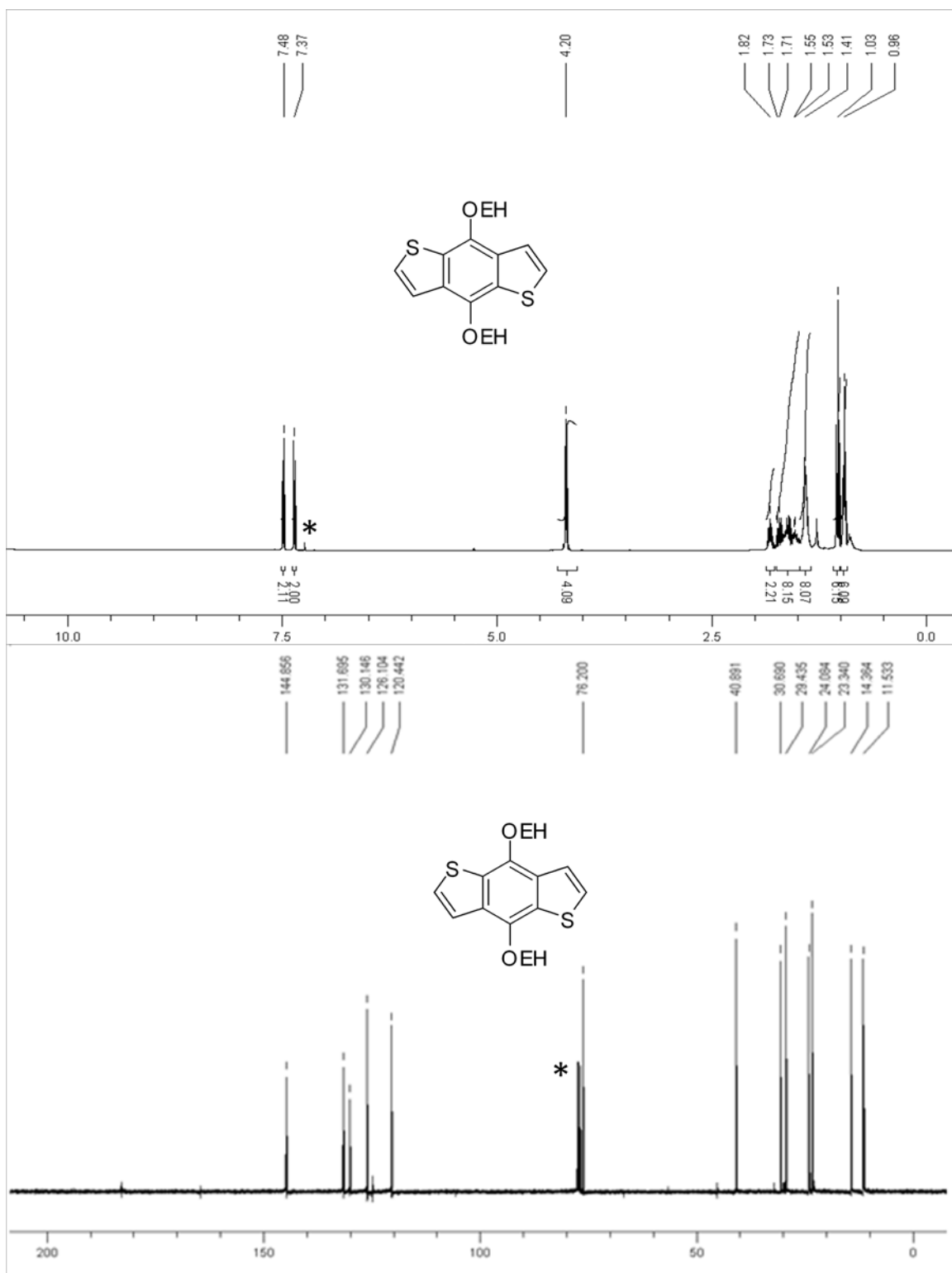**Figure 6.52** ^{1}H (top) and ^{13}C (bottom) NMR spectra (CDCl₃, r.t.) of compound **4.6** (*solvent).
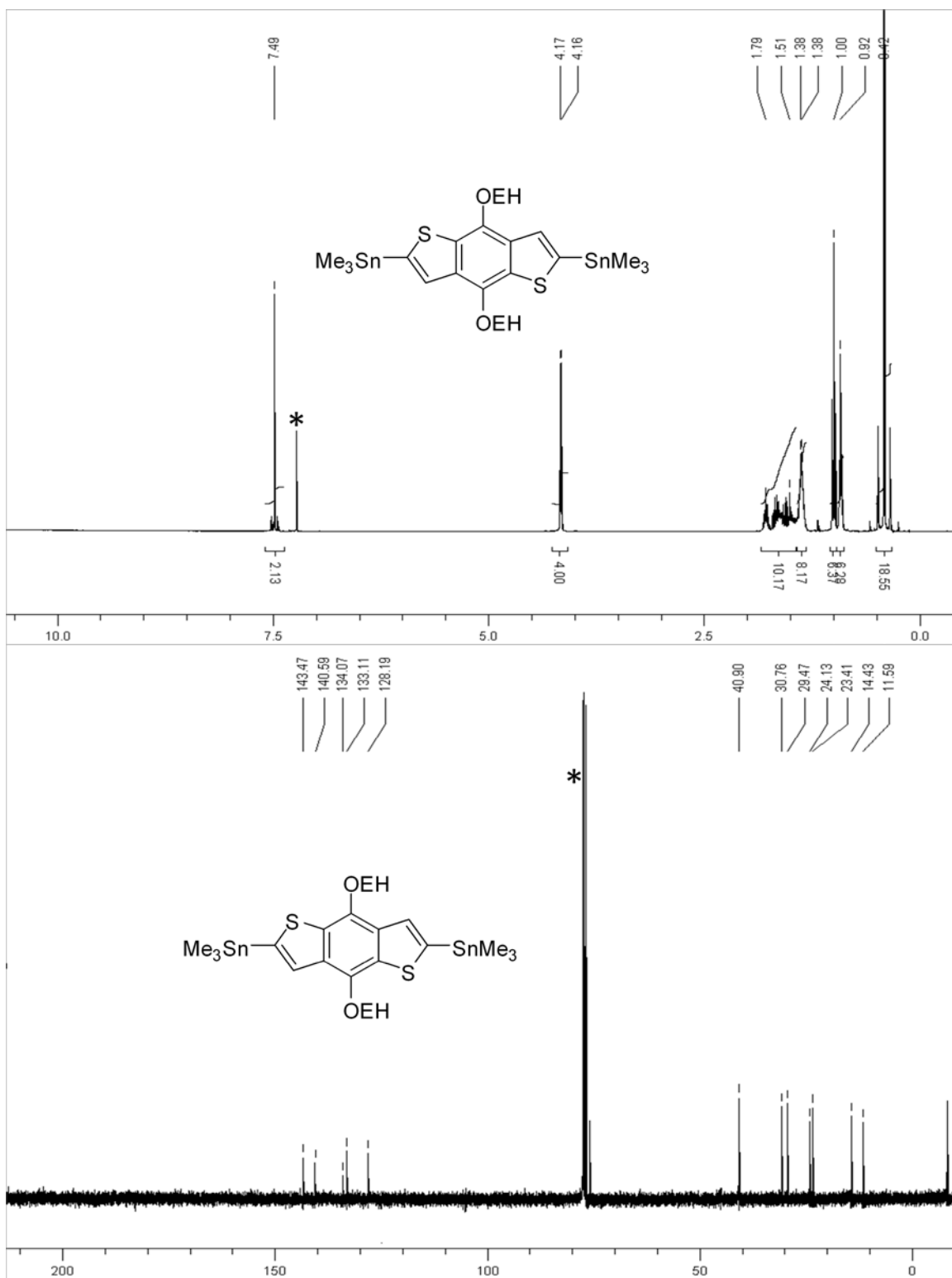
Figure 6.53 ^{1}H (top) and ^{13}C (bottom) NMR spectra (CDCl$_3$, r.t.) of compound

4.7(*solvent).
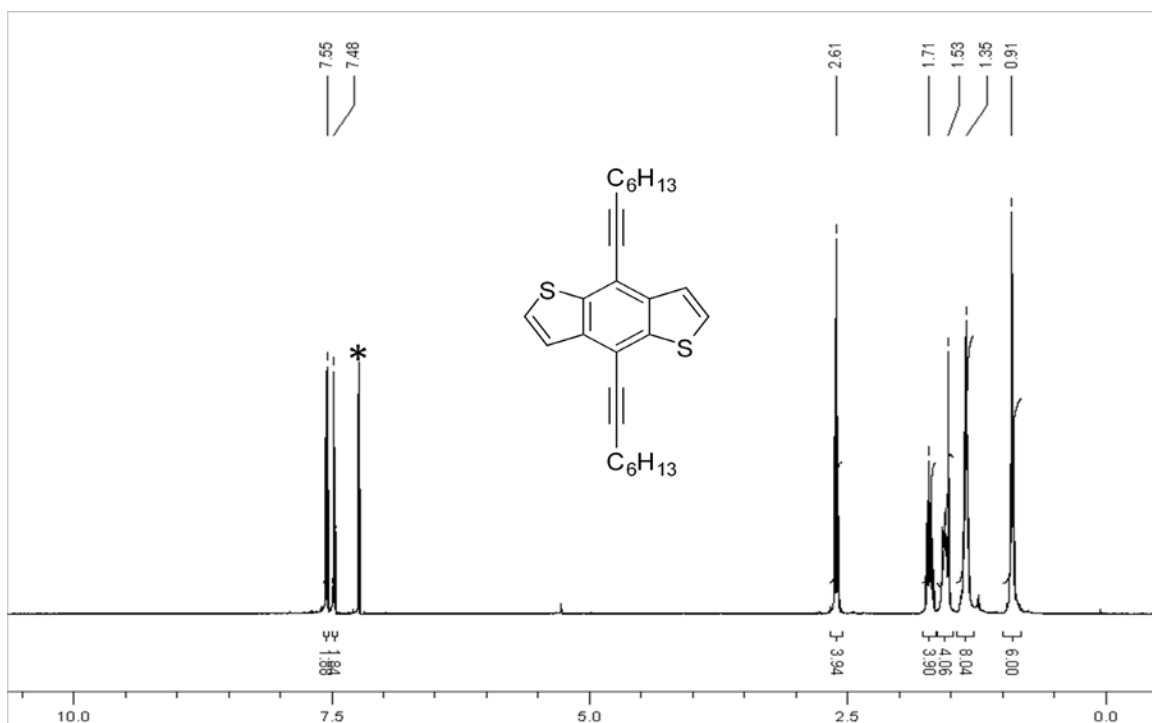
Figure 6.54 ^{1}H (top) and ^{13}C (bottom) NMR spectra (CDCl$_3$, r.t.) of compound **4.8** (*solvent).
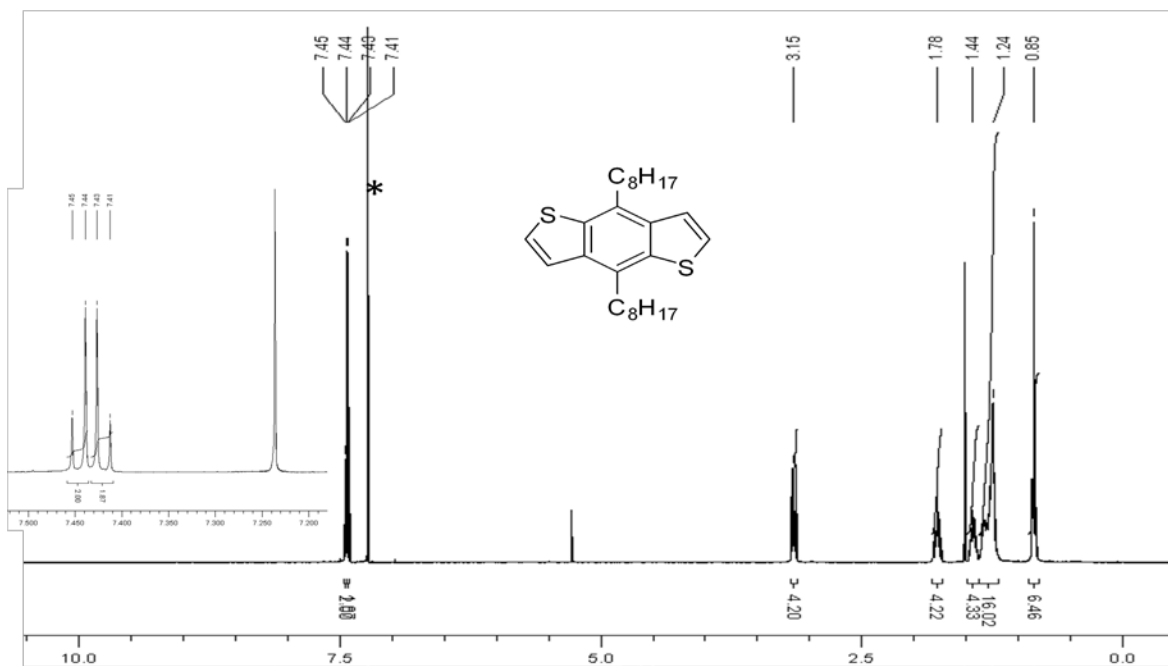
Figure 6.55 ^{1}H (top) and ^{13}C (bottom) NMR spectra (CDCl$_3$, r.t.) of compound **4.9**(*solvent).
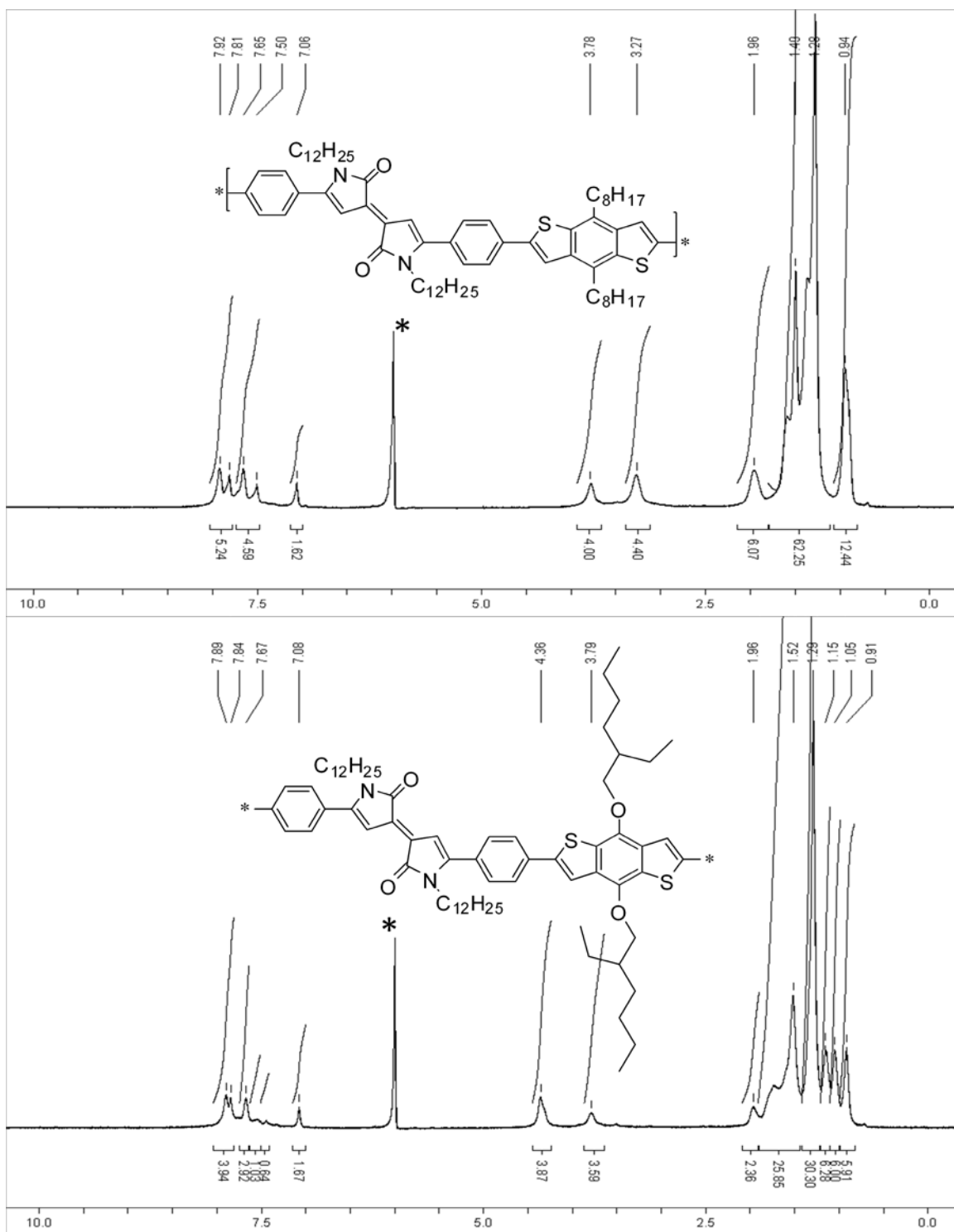
Figure 6.56 ^{1}H NMR spectra of polymer **4-P1** (top) and **4-P2** (bottom) (C$_2$D$_2$Cl$_4$, 90 ^{0}C) of compound (*solvent).
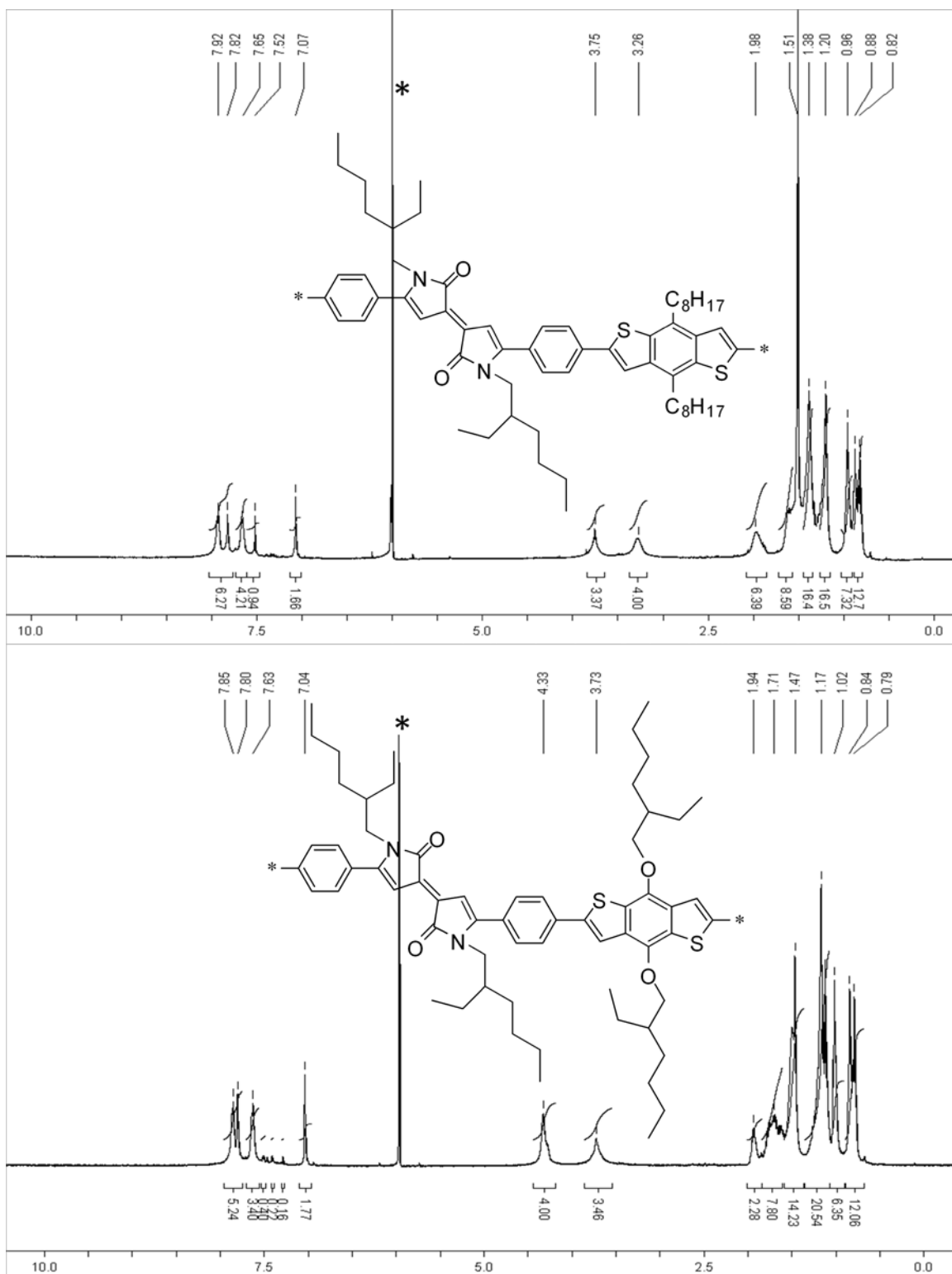
Figure 6.57 ^{1}H NMR spectra of polymer **4-P3** (top) and **4-P4** (bottom) (C$_2$D$_2$Cl$_4$, 90 ^{0}C) of compound (*solvent).
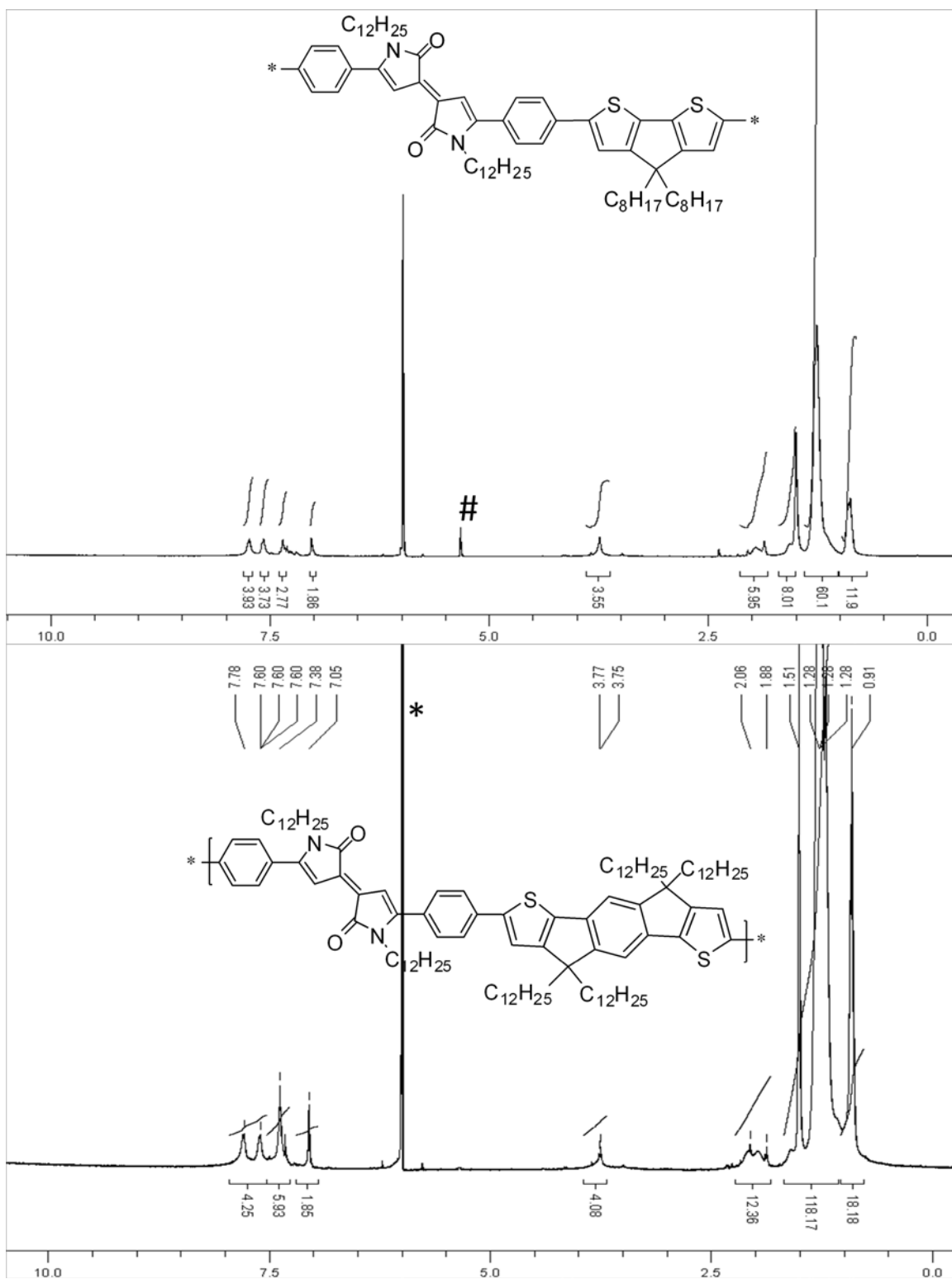
Figure 6.58 ^{1}H NMR spectra of polymer **4-P5** (top) and **4-P6** (bottom) (C$_2$D$_2$Cl$_4$, 90 ^{0}C) of compound (*solvent).

List of abbreviations

D-A	Donor-Acceptor
D	Donor
A	Acceptor
TFB	Tetrafluorobenzene
TPD	Thiophene-imide
PD	Pechmann Dye
BDT	Benzodithiophene
HOMO	Highest occupied molecular orbitals
LUMO	Lowest occupied molecular orbitals
FMO	Frontier molecular orbitals
OSC	Organic solar cell
OLED	Organic light-emitting diodes
OTFT	Organic thin film transistor
OFET	Organic field effect transistors
PVD	Photovoltaic device
ECD	Electronic chromism device
RF-ID	Radio-frequency identification
PCE	Power conversion efficiency
BLA	Bond length alternation
PSC	Polymer solar cell
V_{oc}	Open circuit voltage
OPV	Organic Photovoltaic
CPDT	Cyclopentadithiophene
IDT	Indacenodithiophene
PH	Phthalimide
II	Isoindigo
DPP	diketopyrrole [3,4-c]pyrrole-1,4-Dione
CV	Cyclic voltammetry
DPV	Differential-pulse voltammetry

PMMA	Poly(methylmethacrylate)
V_{sd}	Source-drain voltage
V_{gs}	Gate voltage
V_t	Threshold voltage
DSC	Differential scanning calorimetry
DFT	Density functional theory
PLE	Photoluminescence excitation
PL	Photoluminescence
THF	Tetrahydrofuran
UPS	Ultra-violet photoelectron spectroscopy
J_{sc}	Short circuit current
NIR	Near infrared

References:

(1)   Shirakawa, H.; Louis, E. J.; MacDiarmid, A. G.; Chiang, C. K.; Heeger, A. J. *Journal of the Chemical Society, Chemical Communications* **1977**, 578.
(2)   Ringsdorf, H. *Angewandte Chemie (International ed. in English)* **2004**, *43*, 1064.
(3)   Friend, R. H.; Gymer, R. W.; Holmes, A. B.; Burroughes, J. H.; Marks, R. N.; Taliani, C.; Bradley, D. D. C.; Dos Santos, D. A.; Bredas, J. L.; Logdlund, M.; Salaneck, W. R. *Nature (London)* **1999**, *397*, 121.
(4)   Zaumseil, J.; Sirringhaus, H. *Chemical Reviews (Washington, DC, United States)* **2007**, *107*, 1296.
(5)   Guenes, S.; Neugebauer, H.; Sariciftci, N. S. *Chemical Reviews (Washington, DC, United States)* **2007**, *107*, 1324.
(6)   Argun, A. A.; Aubert, P.-H.; Thompson, B. C.; Schwendeman, I.; Gaupp, C. L.; Hwang, J.; Pinto, N. J.; Tanner, D. B.; MacDiarmid, A. G.; Reynolds, J. R. *Chemistry of Materials* **2004**, *16*, 4401.
(7)   Thomas Samuel, W., 3rd; Joly Guy, D.; Swager Timothy, M. *Chemical reviews* **2007**, *107*, 1339.
(8)   Rotzoll, R.; Mohapatra, S.; Olariu, V.; Wenz, R.; Grigas, M.; Dimmler, K.; Shchekin, O.; Dodabalapur, A. *Applied Physics Letters* **2006**, *88*, 123502/1.
(9)   Katz, H. E. *Chemistry of Materials* **2004**, *16*, 4748.
(10)   Allard, S.; Forster, M.; Souharce, B.; Thiem, H.; Scherf, U. *Angewandte Chemie, International Edition* **2008**, *47*, 4070.
(11)   Dimitrakopoulos, C. D.; Malenfant, P. R. L. *Advanced Materials (Weinheim, Germany)* **2002**, *14*, 99.
(12)   Kraft, A.; Grimsdale, A. C.; Holmes, A. B. *Angewandte Chemie, International Edition* **1998**, *37*, 403.
(13)   Anthony John, E. *Chemical reviews* **2006**, *106*, 5028.
(14)   Coakley, K. M.; McGehee, M. D. *Chemistry of Materials* **2004**, *16*, 4533.
(15)   Chen, H.-Y.; Hou, J.; Zhang, S.; Liang, Y.; Yang, G.; Yang, Y.; Yu, L.; Wu, Y.; Li, G. *Nature Photonics* **2009**, *3*, 649.
(16)   Liang, Y.; Wu, Y.; Feng, D.; Tsai, S.-T.; Son, H.-J.; Li, G.; Yu, L. *Journal of the American Chemical Society* **2009**, *131*, 56.
(17)   de Leeuw, D. M.; Simenon, M. M. J.; Brown, A. R.; Einerhand, R. E. F. *Synthetic Metals* **1997**, *87*, 53.
(18)   Letizia, J. A.; Cronin, S.; Ortiz, R. P.; Facchetti, A.; Ratner, M. A.; Marks, T. J. *Chemistry--A European Journal* **2010**, *16*, 1911.
(19)   Zhan, X.; Facchetti, A.; Barlow, S.; Marks, T. J.; Ratner, M. A.; Wasielewski, M. R.; Marder, S. R. *Advanced Materials (Weinheim, Germany)* **2011**, *23*, 268.
(20)   Oh, J. H.; Sun, Y.-S.; Schmidt, R.; Toney, M. F.; Nordlund, D.; Konemann, M.; Wurthner, F.; Bao, Z. *Chemistry of Materials* **2009**, *21*, 5508.
(21)   Jones, B. A.; Facchetti, A.; Wasielewski, M. R.; Marks, T. J. *Journal of the American Chemical Society* **2007**, *129*, 15259.
(22)   Thompson, B. C.; Kim, Y.-G.; McCarley, T. D.; Reynolds, J. R. *Journal of the American Chemical Society* **2006**, *128*, 12714.
(23)   Roncali, J. *Macromolecular Rapid Communications* **2007**, *28*, 1761.
(24)   Roncali, J. *Chemical Reviews (Washington, D. C.)* **1997**, *97*, 173.

(25)   Hou, J.; Tan, Z. a.; Yan, Y.; He, Y.; Yang, C.; Li, Y. *Journal of the American Chemical Society* **2006**, *128*, 4911.

(26)   Li, Y.; Zou, Y. *Advanced Materials (Weinheim, Germany)* **2008**, *20*, 2952.

(27)   Hou, J.; Yang, C.; He, C.; Li, Y. *Chemical Communications (Cambridge, United Kingdom)* **2006**, 871.

(28)   Wudl, F.; Kobayashi, M.; Heeger, A. J. *Journal of Organic Chemistry* **1984**, *49*, 3382.

(29)   Akoudad, S.; Roncali, J. *Chemical Communications (Cambridge)* **1998**, 2081.

(30)   Zhang, Q. T.; Tour, J. M. *Journal of the American Chemical Society* **1998**, *120*, 5355.

(31)   Zhang, X.-R.; Richter, L. J.; DeLongchamp, D. M.; Kline, R. J.; Hammond, M. R.; McCulloch, I.; Heeney, M.; Ashraf, R. S.; Smith, J. N.; Anthopoulos, T. D.; Schroeder, B.; Geerts, Y. H.; Fischer, D. A.; Toney, M. F. *Journal of the American Chemical Society* **2011**, *133*, 15073.

(32)   Biniek, L.; Fall, S.; Chochos, C. L.; Anokhin, D. V.; Ivanov, D. A.; Leclerc, N.; Leveque, P.; Heiser, T. *Macromolecules (Washington, DC, United States)* **2010**, *43*, 9779.

(33)   Zhang, Z.-G.; Wang, J. *Journal of Materials Chemistry* **2012**, *22*, 4178.

(34)   Chen, M.-H.; Hou, J.; Hong, Z.; Yang, G.; Sista, S.; Chen, L.-M.; Yang, Y. *Advanced Materials (Weinheim, Germany)* **2009**, *21*, 4238.

(35)   Blouin, N.; Michaud, A.; Leclerc, M. *Advanced Materials (Weinheim, Germany)* **2007**, *19*, 2295.

(36)   Seo, J. H.; Gutacker, A.; Sun, Y.; Wu, H.; Huang, F.; Cao, Y.; Scherf, U.; Heeger, A. J.; Bazan, G. C. *Journal of the American Chemical Society* **2011**, *133*, 8416.

(37)   Muehlbacher, D.; Scharber, M.; Morana, M.; Zhu, Z.; Waller, D.; Gaudiana, R.; Brabec, C. *Advanced Materials (Weinheim, Germany)* **2006**, *18*, 2884.

(38)   Zhang, S.; Guo, Y.; Fan, H.; Liu, Y.; Chen, H.-Y.; Yang, G.; Zhan, X.; Liu, Y.; Li, Y.; Yang, Y. *Journal of Polymer Science, Part A: Polymer Chemistry* **2009**, *47*, 5498.

(39)   Yue, W.; Zhao, Y.; Shao, S.; Tian, H.; Xie, Z.; Geng, Y.; Wang, F. *Journal of Materials Chemistry* **2009**, *19*, 2199.

(40)   Zhu, Z.; Waller, D.; Gaudiana, R.; Morana, M.; Muehlbacher, D.; Scharber, M.; Brabec, C. *Macromolecules (Washington, DC, United States)* **2007**, *40*, 1981.

(41)   Coppo, P.; Turner, M. L. *Journal of Materials Chemistry* **2005**, *15*, 1123.

(42)   Peet, J.; Kim, J. Y.; Coates, N. E.; Ma, W. L.; Moses, D.; Heeger, A. J.; Bazan, G. C. *Nature Materials* **2007**, *6*, 497.

(43)   Amb, C. M.; Chen, S.; Graham, K. R.; Subbiah, J.; Small, C. E.; So, F.; Reynolds, J. R. *Journal of the American Chemical Society* **2011**, *133*, 10062.

(44)   Chu, T.-Y.; Lu, J.; Beaupre, S.; Zhang, Y.; Pouliot, J.-R.; Wakim, S.; Zhou, J.; Leclerc, M.; Li, Z.; Ding, J.; Tao, Y. *Journal of the American Chemical Society* **2011**, *133*, 4250.

(45)   Liang, Y.; Feng, D.; Wu, Y.; Tsai, S.-T.; Li, G.; Ray, C.; Yu, L. *Journal of the American Chemical Society* **2009**, *131*, 7792.

(46)   Zhang, W.; Smith, J.; Watkins, S. E.; Gysel, R.; McGehee, M.; Salleo, A.; Kirkpatrick, J.; Ashraf, S.; Anthopoulos, T.; Heeney, M.; McCulloch, I. *Journal of the American Chemical Society* **2010**, *132*, 11437.

(47) Chen, Y.-C.; Yu, C.-Y.; Fan, Y.-L.; Hung, L.-I.; Chen, C.-P.; Ting, C. *Chemical Communications (Cambridge, United Kingdom)* **2010**, *46*, 6503.

(48) Donaghey, J. E.; Ashraf, R. S.; Kim, Y.; Huang, Z. G.; Nielsen, C. B.; Zhang, W.; Schroeder, B.; Grenier, C. R. G.; Brown, C. T.; D'Angelo, P.; Smith, J.; Watkins, S.; Song, K.; Anthopoulos, T. D.; Durrant, J. R.; Williams, C. K.; McCulloch, I. *Journal of Materials Chemistry* **2011**, *21*, 18744.

(49) Zeng, G.; Chua, S.-J.; Huang, W. *Thin Solid Films* **2002**, *417*, 194.

(50) Ong, K.-H.; Lim, S.-L.; Tan, H.-S.; Wong, H.-K.; Li, J.; Ma, Z.; Moh Lionel, C. H.; Lim, S.-H.; de Mello John, C.; Chen, Z.-K. *Advanced materials (Deerfield Beach, Fla.)* **2011**, *23*, 1409.

(51) Huo, L.; Guo, X.; Zhang, S.; Li, Y.; Hou, J. *Macromolecules (Washington, DC, United States)* **2011**, *44*, 4035.

(52) Shi, Q.; Fan, H.; Liu, Y.; Hu, W.; Li, Y.; Zhan, X. *Journal of Physical Chemistry C* **2010**, *114*, 16843.

(53) Zhang, M.; Guo, X.; Li, Y. *Advanced Energy Materials* **2011**, *1*, 557.

(54) Wang, E.; Hou, L.; Wang, Z.; Hellstroem, S.; Zhang, F.; Inganaes, O.; Andersson, M. R. *Advanced Materials (Weinheim, Germany)* **2010**, *22*, 5240.

(55) Zhang, J.; Cai, W.; Huang, F.; Wang, E.; Zhong, C.; Liu, S.; Wang, M.; Duan, C.; Yang, T.; Cao, Y. *Macromolecules (Washington, DC, United States)* **2011**, *44*, 894.

(56) Mondal, R.; Ko, S.; Norton, J. E.; Miyaki, N.; Becerril, H. A.; Verploegen, E.; Toney, M. F.; Bredas, J.-L.; McGehee, M. D.; Bao, Z. *Journal of Materials Chemistry* **2009**, *19*, 7195.

(57) Zhou, E.; Cong, J.; Yamakawa, S.; Wei, Q.; Nakamura, M.; Tajima, K.; Yang, C.; Hashimoto, K. *Macromolecules (Washington, DC, United States)* **2010**, *43*, 2873.

(58) Li, K.-C.; Huang, J.-H.; Hsu, Y.-C.; Huang, P.-J.; Chu, C.-W.; Lin, J.-T. s.; Ho, K.-C.; Wei, K.-H.; Lin, H.-C. *Macromolecules (Washington, DC, United States)* **2009**, *42*, 3681.

(59) Zhang, M.; Fan, H.; Guo, X.; He, Y.; Zhang, Z.; Min, J.; Zhang, J.; Zhao, G.; Zhan, X.; Li, Y. *Macromolecules (Washington, DC, United States)* **2010**, *43*, 5706.

(60) Shi, Q.; Fan, H.; Liu, Y.; Chen, J.; Ma, L.; Hu, W.; Shuai, Z.; Li, Y.; Zhan, X. *Macromolecules (Washington, DC, United States)* **2011**, *44*, 4230.

(61) Ahmed, E.; Kim, F. S.; Xin, H.; Jenekhe, S. A. *Macromolecules (Washington, DC, United States)* **2009**, *42*, 8615.

(62) Peng, B.; Najari, A.; Liu, B.; Berrouard, P.; Gendron, D.; He, Y.; Zhou, K.; Zou, Y.; Leclerc, M. *Macromolecular Chemistry and Physics* **2010**, *211*, 2026.

(63) Price Samuel, C.; Stuart Andrew, C.; Yang, L.; Zhou, H.; You, W. *J Am Chem Soc* **2011**, *133*, 4625.

(64) Li, Z.; Ding, J.; Song, N.; Lu, J.; Tao, Y. *Journal of the American Chemical Society* **2010**, *132*, 13160.

(65) Ding, J.; Li, Z.; Cui, Z.; Robertson, G. P.; Song, N.; Du, X.; Scoles, L. *Journal of Polymer Science, Part A: Polymer Chemistry* **2011**, *49*, 3374.

(66) Wang, M.; Hu, X.; Liu, P.; Li, W.; Gong, X.; Huang, F.; Cao, Y. *Journal of the American Chemical Society* **2011**, *133*, 9638.

(67)   Guo, X.; Kim, F. S.; Jenekhe, S. A.; Watson, M. D. *Journal of the American Chemical Society* **2009**, *131*, 7206.

(68)   Guo, X.; Ortiz, R. P.; Zheng, Y.; Kim, M.-G.; Zhang, S.; Hu, Y.; Lu, G.; Facchetti, A.; Marks, T. J. *Journal of the American Chemical Society* **2011**, *133*, 13685.

(69)   Guo, X.; Xin, H.; Kim, F. S.; Liyanage, A. D. T.; Jenekhe, S. A.; Watson, M. D. *Macromolecules (Washington, DC, United States)* **2011**, *44*, 269.

(70)   Guo, X.; Ortiz, R. P.; Zheng, Y.; Hu, Y.; Noh, Y.-Y.; Baeg, K.-J.; Facchetti, A.; Marks, T. J. *Journal of the American Chemical Society* **2011**, *133*, 1405.

(71)   Guo, X.; Watson, M. D. *Organic Letters* **2008**, *10*, 5333.

(72)   Wang, E.; Ma, Z.; Zhang, Z.; Vandewal, K.; Henriksson, P.; Inganas, O.; Zhang, F.; Andersson, M. R. *Journal of the American Chemical Society* **2011**, *133*, 14244.

(73)   Mei, J.; Graham, K. R.; Stalder, R.; Reynolds, J. R. *Organic Letters* **2010**, *12*, 660.

(74)   Wienk, M. M.; Turbiez, M.; Gilot, J.; Janssen, R. A. J. *Advanced Materials (Weinheim, Germany)* **2008**, *20*, 2556.

(75)   Cho, S.; Lee, J.; Tong, M.; Seo, J. H.; Yang, C. *Advanced Functional Materials* **2011**, *21*, 1910.

(76)   Cui, C.; Fan, H.; Guo, X.; Zhang, M.; He, Y.; Zhan, X.; Li, Y. *Polymer Chemistry* **2012**, *3*, 99.

(77)   Liang, Y.; Xu, Z.; Xia, J.; Tsai, S.-T.; Wu, Y.; Li, G.; Ray, C.; Yu, L. *Advanced Materials (Weinheim, Germany)* **2010**, *22*, E135.

(78)   Sabouraud, G.; Sadki, S.; Brodie, N. *Chemical Society Reviews* **2000**, *29*, 283.

(79)   Waltman, R. J.; Bargon, J. *Canadian Journal of Chemistry* **1986**, *64*, 76.

(80)   Toshima, N.; Hara, S. *Progress in Polymer Science* **1995**, *20*, 155.

(81)   Cheng, Y.-J.; Luh, T.-Y. *Journal of Organometallic Chemistry* **2004**, *689*, 4137.

(82)   Tamao, K.; Sumitani, K.; Kumada, M. *J. Amer. Chem. Soc.* **1972**, *94*, 4374.

(83)   Echavarren, A. M.; Stille, J. K. *Journal of the American Chemical Society* **1987**, *109*, 5478.

(84)   Miyaura, N.; Suzuki, A. *Chemical Reviews (Washington, D. C.)* **1995**, *95*, 2457.

(85)   Sonogashira, K. *Journal of Organometallic Chemistry* **2002**, *653*, 46.

(86)   Yamamoto, T.; Morita, A.; Miyazaki, Y.; Maruyama, T.; Wakayama, H.; Zhou, Z. H.; Nakamura, Y.; Kanbara, T.; Sasaki, S.; Kubota, K. *Macromolecules* **1992**, *25*, 1214.

(87)   Maryanoff, B. E.; Reitz, A. B. *Chem. Rev.* **1989**, *89*, 863.

(88)   Bao, Z.; Chan, W.; Yu, L. *Chemistry of Materials* **1993**, *5*, 2.

(89)   Bao, Z.; Chan, W. K.; Yu, L. *Journal of the American Chemical Society* **1995**, *117*, 12426.

(90)   Espinet, P.; Echavarren Antonio, M. *Angewandte Chemie (International ed. in English)* **2004**, *43*, 4704.

(91)   Hoeben, F. J. M.; Jonkheijm, P.; Meijer, E. W.; Schenning, A. P. H. J. *Chemical Reviews (Washington, DC, United States)* **2005**, *105*, 1491.

(92)   Murphy, A. R.; Frechet, J. M. J. *Chemical Reviews (Washington, DC, United States)* **2007**, *107*, 1066.

(93)   Bronstein, H.; Chen, Z.; Ashraf, R. S.; Zhang, W.; Du, J.; Durrant, J. R.; Shakya Tuladhar, P.; Song, K.; Watkins, S. E.; Geerts, Y.; Wienk, M. M.; Janssen, R. A. J.; Anthopoulos, T.; Sirringhaus, H.; Heeney, M.; McCulloch, I. *Journal of the American Chemical Society* **2011**, *133*, 3272.

(94)   Subramaniyan, S.; Xin, H.; Kim, F. S.; Shoaee, S.; Durrant, J. R.; Jenekhe, S. A. *Advanced Energy Materials* **2011**, *1*, 854.

(95)   Kline, R. J.; McGehee, M. D.; Kadnikova, E. N.; Liu, J.; Frechet, J. M. J. *Advanced Materials (Weinheim, Germany)* **2003**, *15*, 1519.

(96)   Newman, C. R.; Frisbie, C. D.; da Silva Filho, D. A.; Bredas, J.-L.; Ewbank, P. C.; Mann, K. R. *Chemistry of Materials* **2004**, *16*, 4436.

(97)   Sariciftci, N. S.; Smilowitz, L.; Heeger, A. J.; Wudl, F. *Science (Washington, DC, United States)* **1992**, *258*, 1474.

(98)   Thompson, B. C.; Frechet, J. M. J. *Angewandte Chemie, International Edition* **2008**, *47*, 58.

(99)   Li, G.; Zhu, R.; Yang, Y. *Nature Photonics* **2012**, *6*, 153.

(100)   Hoppe, H.; Glatzel, T.; Niggemann, M.; Hinsch, A.; Lux-Steiner, M. C.; Sariciftci, N. S. *Nano Letters* **2005**, *5*, 269.

(101)   Chan, S.-H.; Hsiao, Y.-S.; Hung, L.-I.; Hwang, G.-W.; Chen, H.-L.; Ting, C.; Chen, C.-P. *Macromolecules (Washington, DC, United States)* **2010**, *43*, 3399.

(102)   Lee Jae, K.; Ma Wan, L.; Brabec Christoph, J.; Yuen, J.; Moon Ji, S.; Kim Jin, Y.; Lee, K.; Bazan Guillermo, C.; Heeger Alan, J. *J Am Chem Soc* **2008**, *130*, 3619.

(103)   Lee, J. K.; Ma, W. L.; Brabec, C. J.; Yuen, J.; Moon, J. S.; Kim, J. Y.; Lee, K.; Bazan, G. C.; Heeger, A. J. *Journal of the American Chemical Society* **2008**, *130*, 3619.

(104)   Yao, Y.; Hou, J.; Xu, Z.; Li, G.; Yang, Y. *Advanced Functional Materials* **2008**, *18*, 1783.

(105)   Zheng, G.-Z.; Meshitsuka, G.; Ishizu, A. *Journal of Polymer Science, Part B: Polymer Physics* **1995**, *33*, 2211.

(106)   Dittmer, J. J.; Marseglia, E. A.; Friend, R. H. *Advanced Materials (Weinheim, Germany)* **2000**, *12*, 1270.

(107)   Pearson, A.; Wang, T.; Jones, R.; Lidzey, D.; Staniec, P.; Hopkinson, P.; Donald, A. *Macromolecules (Washington, DC, United States)* **2012**, *45*, 1499.

(108)   Dickey, K. C.; Anthony, J. E.; Loo, Y.-L. *Advanced Materials (Weinheim, Germany)* **2006**, *18*, 1721.

(109)   Miller, S.; Fanchini, G.; Lin, Y.-Y.; Li, C.; Chen, C.-W.; Su, W.-F.; Chhowalla, M. *Journal of Materials Chemistry* **2008**, *18*, 306.

(110)   Bull, T. A.; Pingree, L. S. C.; Jenekhe, S. A.; Ginger, D. S.; Luscombe, C. K. *ACS Nano* **2009**, *3*, 627.

(111)   Huang, J.-H.; Li, K.-C.; Chien, F.-C.; Hsiao, Y.-S.; Kekuda, D.; Chen, P.; Lin, H.-C.; Ho, K.-C.; Chu, C.-W. *Journal of Physical Chemistry C* **2010**, *114*, 9062.

(112)   Woo, C. H.; Thompson, B. C.; Kim, B. J.; Toney, M. F.; Frechet, J. M. J. *Journal of the American Chemical Society* **2008**, *130*, 16324.

(113)   Piliego, C.; Holcombe, T. W.; Douglas, J. D.; Woo, C. H.; Beaujuge, P. M.; Frechet, J. M. J. *Journal of the American Chemical Society* **2010**, *132*, 7595.

(114)   Sirringhaus, H. *Advanced Materials (Weinheim, Germany)* **2005**, *17*, 2411.

(115)   Park, Y. D.; Kim, D. H.; Jang, Y.; Cho, J. H.; Hwang, M.; Lee, H. S.; Lim, J. A.; Cho, K. *Organic Electronics* **2006**, *7*, 514.

(116)   Tsao, H.-N.; Cho, D. M.; Park, I.-S.; Hansen, M. R.; Mavrinskiy, A.; Yoon, D.-Y.; Graf, R.; Pisula, W.; Spiess, H. W.; Muellen, K. *Journal of the American Chemical Society* **2011**, *133*, 2605.

(117)   Chen, H.; Guo, Y.; Yu, G.; Zhao, Y.; Zhang, J.; Gao, D.; Liu, H.; Liu, Y. *Advanced Materials (Weinheim, Germany)*, Ahead of Print.

(118)   Chen, Z.; Lee Mi, J.; Shahid Ashraf, R.; Gu, Y.; Albert-Seifried, S.; Meedom Nielsen, M.; Schroeder, B.; Anthopoulos Thomas, D.; Heeney, M.; McCulloch, I.; Sirringhaus, H. *Advanced materials (Deerfield Beach, Fla.)* **2012**, *24*, 647.

(119)   Small, C. E.; Chen, S.; Subbiah, J.; Amb, C. M.; Tsang, S.-W.; Lai, T.-H.; Reynolds, J. R.; So, F. *Nature Photonics* **2012**, *6*, 115.

(120)   Anthony, J. E.; Brooks, J. S.; Eaton, D. L.; Parkin, S. R. *Journal of the American Chemical Society* **2001**, *123*, 9482.

(121)   Anthony, J. E.; Eaton, D. L.; Parkin, S. R. *Organic Letters* **2002**, *4*, 15.

(122)   Adam, D.; Schuhmacher, P.; Simmerer, J.; Haeussling, L.; Siemensmeyer, K.; Etzbach, K. H.; Ringsdorf, H.; Haarer, D. *Nature (London, United Kingdom)* **1994**, *371*, 141.

(123)   Iino, H.; Hanna, J.-i.; Haarer, D. *Physical Review B: Condensed Matter and Materials Physics* **2005**, *72*, 193203/1.

(124)   Wu, J.; Watson, M. D.; Zhang, L.; Wang, Z.; Muellen, K. *Journal of the American Chemical Society* **2004**, *126*, 177.

(125)   Szarko, J. M.; Guo, J.-C.; Liang, Y.-Y.; Lee, B.-D.; Rolczynski, B. S.; Strzalka, J.; Xu, T.; Loser, S.; Marks, T. J.; Yu, L.-P.; Chen, L.-X. *Advanced Materials (Weinheim, Germany)* **2010**, *22*, 5468.

(126)   Wang, E.; Hou, L.; Wang, Z.; Ma, Z.; Hellstrom, S.; Zhuang, W.; Zhang, F.; Inganas, O.; Andersson, M. R. *Macromolecules (Washington, DC, United States)* **2011**, *44*, 2067.

(127)   Li, Z.; Zhang, Y.; Tsang, S.-W.; Du, X.-M.; Zhou, J.-Y.; Tao, Y.; Ding, J.-F. *Journal of Physical Chemistry C* **2011**, *115*, 18002.

(128)   Boudouris, B. W.; Ho, V.; Jimison, L. H.; Toney, M. F.; Salleo, A.; Segalman, R. A. *Macromolecules (Washington, DC, United States)* **2011**, *44*, 6653.

(129)   Yang, L.; Zhou, H.; You, W. *Journal of Physical Chemistry C* **2010**, *114*, 16793.

(130)   Bronstein, H.; Leem, D. S.; Hamilton, R.; Woebkenberg, P.; King, S.; Zhang, W.; Ashraf, R. S.; Heeney, M.; Anthopoulos, T. D.; de Mello, J.; McCulloch, I. *Macromolecules (Washington, DC, United States)* **2011**, *44*, 6649.

(131)   Holcombe, T. W.; Norton, J. E.; Rivnay, J.; Woo, C. H.; Goris, L.; Piliego, C.; Griffini, G.; Sellinger, A.; Bredas, J.-L.; Salleo, A.; Frechet, J. M. J. *Journal of the American Chemical Society* **2011**, *133*, 12106.

(132)   Yiu, A. T.; Beaujuge, P. M.; Lee, O. P.; Woo, C. H.; Toney, M. F.; Frechet, J. M. J. *Journal of the American Chemical Society* **2012**, *134*, 2180.

(133)   Ko, S.; Hoke, E. T.; Pandey, L.; Hong, S.; Mondal, R.; Risko, C.; Yi, Y.; Noriega, R.; McGehee, M. D.; Bredas, J.-L.; Salleo, A.; Bao, Z. *Journal of the American Chemical Society* **2012**, *134*, 5222.

(134)   Johns, J. E.; Muller, E. A.; Frechet, J. M. J.; Harris, C. B. *Journal of the American Chemical Society* **2010**, *132*, 15720.

(135) Yamamoto, T.; Sanechika, K.; Yamamoto, A. *Journal of Polymer Science, Polymer Letters Edition* **1980**, *18*, 9.

(136) McCullough, R. D.; Lowe, R. D. *Journal of the Chemical Society, Chemical Communications* **1992**, 70.

(137) Loewe, R. S.; Khersonsky, S. M.; McCullough, R. D. *Advanced Materials (Weinheim, Germany)* **1999**, *11*, 250.

(138) Chen, T. A.; Rieke, R. D. *Journal of the American Chemical Society* **1992**, *114*, 10087.

(139) Kline, R. J.; DeLongchamp, D. M.; Fischer, D. A.; Lin, E. K.; Richter, L. J.; Chabinyc, M. L.; Toney, M. F.; Heeney, M.; McCulloch, I. *Macromolecules (Washington, DC, United States)* **2007**, *40*, 7960.

(140) Ong, B. S.; Wu, Y.; Liu, P.; Gardner, S. *Journal of the American Chemical Society* **2004**, *126*, 3378.

(141) McCulloch, I.; Heeney, M.; Bailey, C.; Genevicius, K.; MacDonald, I.; Shkunov, M.; Sparrowe, D.; Tierney, S.; Wagner, R.; Zhang, W.; Chabinyc, M. L.; Kline, R. J.; McGehee, M. D.; Toney, M. F. *Nature Materials* **2006**, *5*, 328.

(142) Wang, Y.; Watson, M. D. *Macromolecules (Washington, DC, United States)* **2008**, *41*, 8643.

(143) Sainova, D.; Janietz, S.; Asawapirom, U.; Romaner, L.; Zojer, E.; Koch, N.; Vollmer, A. *Chemistry of Materials* **2007**, *19*, 1472.

(144) Crouch, D. J.; Skabara, P. J.; Lohr, J. E.; McDouall, J. J. W.; Heeney, M.; McCulloch, I.; Sparrowe, D.; Shkunov, M.; Coles, S. J.; Horton, P. N.; Hursthouse, M. B. *Chemistry of Materials* **2005**, *17*, 6567.

(145) Barbarella, G.; Zambianchi, M.; Antolini, L.; Ostoja, P.; Maccagnani, P.; Bongini, A.; Marseglia, E. A.; Tedesco, E.; Gigli, G.; Cingolani, R. *Journal of the American Chemical Society* **1999**, *121*, 8920.

(146) Pomerantz, M. *Tetrahedron Letters* **2003**, *44*, 1563.

(147) Irvin, J. A.; Schwendeman, I.; Lee, Y.; Abboud, K. A.; Reynolds, J. R. *Journal of Polymer Science, Part A: Polymer Chemistry* **2001**, *39*, 2164.

(148) McCulloch, I.; Bailey, C.; Giles, M.; Heeney, M.; Love, I.; Shkunov, M.; Sparrowe, D.; Tierney, S. *Chemistry of Materials* **2005**, *17*, 1381.

(149) Liu, J.; Zhang, R.; Sauve, G.; Kowalewski, T.; McCullough, R. D. *Journal of the American Chemical Society* **2008**, *130*, 13167.

(150) Cho, D. M.; Parkin, S. R.; Watson, M. D. *Organic Letters* **2005**, *7*, 1067.

(151) Dutta, T.; Woody, K. B.; Parkin, S. R.; Watson, M. D.; Gierschner, J. *Journal of the American Chemical Society* **2009**, *131*, 17321.

(152) Zhang, Z.-B.; Fujiki, M. *Polymer Journal (Tokyo, Japan)* **2001**, *33*, 597.

(153) Dreuw, A.; Weisman, J. L.; Head-Gordon, M. *Journal of Chemical Physics* **2003**, *119*, 2943.

(154) Dierksen, M.; Grimme, S. *Journal of Physical Chemistry A* **2004**, *108*, 10225.

(155) Milian Medina, B.; Wasserberg, D.; Meskers, S. C. J.; Mena-Osteritz, E.; Bauerle, P.; Gierschner, J. *Journal of Physical Chemistry A* **2008**, *112*, 13282.

(156) Gierschner, J.; Cornil, J.; Egelhaaf, H.-J. *Advanced Materials (Weinheim, Germany)* **2007**, *19*, 173.

(157) Gierschner, J.; Mack, H.-G.; Luer, L.; Oelkrug, D. *Journal of Chemical Physics* **2002**, *116*, 8596.

(158) Gierschner, J.; Mack, H. G.; Egelhaaf, H. J.; Schweizer, S.; Doser, B.; Oelkrug, D. *Synthetic Metals* **2003**, *138*, 311.

(159) Halkyard, C. E.; Rampey, M. E.; Kloppenburg, L.; Studer-Martinez, S. L.; Bunz, U. H. F. *Macromolecules* **1998**, *31*, 8655.

(160) Schubert, M.; Dolfen, D.; Frisch, J.; Roland, S.; Steyrleuthner, R.; Stiller, B.; Chen, Z.; Scherf, U.; Koch, N.; Facchetti, A.; Neher, D. *Advanced Energy Materials* **2012**, *2*, 369.

(161) Xie, Y.; Bao, Y.; Du, J.; Jiang, C.; Qiao, Q. *Physical Chemistry Chemical Physics* **2012**, *14*, 10168.

(162) Shepherd, W. E. B.; Platt, A. D.; Hofer, D.; Ostroverkhova, O.; Loth, M.; Anthony, J. E. *Applied Physics Letters* **2010**, *97*, 163303/1.

(163) Weitz, R. T.; Amsharov, K.; Zschieschang, U.; Barrena Villas, E.; Goswami, D. K.; Burghard, M.; Dosch, H.; Jansen, M.; Kern, K.; Klauk, H. *Journal of the American Chemical Society* **2008**, *130*, 4637.

(164) Tatemichi, S.; Ichikawa, M.; Koyama, T.; Taniguchi, Y. *Applied Physics Letters* **2006**, *89*, 112108/1.

(165) Yao, J. H.; Chi, C.; Wu, J.; Loh, K.-P. *Chemistry--A European Journal* **2009**, *15*, 9299.

(166) Rak, S. F.; Jozefiak, T. H.; Miller, L. L. *Journal of Organic Chemistry* **1990**, *55*, 4794.

(167) Usta, H.; Kim, C.; Wang, Z.; Lu, S.; Huang, H.; Facchetti, A.; Marks, T. J. *Journal of Materials Chemistry* **2012**, *22*, 4459.

(168) Katz, H. E.; Lovinger, A. J.; Johnson, J.; Kloc, C.; Slegrist, T.; Li, W.; Lin, Y. Y.; Dodabalapur, A. *Nature (London)* **2000**, *404*, 478.

(169) Guo, X.; Kim, F. S.; Seger, M. J.; Jenekhe, S. A.; Watson, M. D. *Chemistry of Materials* **2012**, *24*, 1434.

(170) Guo, X.-G.; Watson, M. D. *Macromolecules (Washington, DC, United States)* **2011**, *44*, 6711.

(171) Delgado, M. C. R.; Kim, E.-G.; da Silva Filho Demetrio, A.; Bredas, J.-L. *J Am Chem Soc* **2010**, *132*, 3375.

(172) Huang, C.; Barlow, S.; Marder, S. R. *Journal of Organic Chemistry* **2011**, *76*, 2386.

(173) Yagai, S.; Usui, M.; Seki, T.; Murayama, H.; Kikkawa, Y.; Uemura, S.; Karatsu, T.; Kitamura, A.; Asano, A.; Seki, S. *Journal of the American Chemical Society* **2012**, *134*, 7983.

(174) Yan, H.; Chen, Z.; Zheng, Y.; Newman, C.; Quinn, J. R.; Dotz, F.; Kastler, M.; Facchetti, A. *Nature (London, United Kingdom)* **2009**, *457*, 679.

(175) Letizia, J. A.; Salata, M. R.; Tribout, C. M.; Facchetti, A.; Ratner, M. A.; Marks, T. J. *Journal of the American Chemical Society* **2008**, *130*, 9679.

(176) Zhan, X.; Tan, Z. a.; Domercq, B.; An, Z.; Zhang, X.; Barlow, S.; Li, Y.; Zhu, D.; Kippelen, B.; Marder, S. R. *Journal of the American Chemical Society* **2007**, *129*, 7246.

(177) Durban, M. M.; Kazarinoff, P. D.; Luscombe, C. K. *Macromolecules (Washington, DC, United States)* **2010**, *43*, 6348.

(178) Zhan, X.; Tan, Z. a.; Zhou, E.; Li, Y.; Misra, R.; Grant, A.; Domercq, B.; Zhang, X.-H.; An, Z.; Zhang, X.; Barlow, S.; Kippelen, B.; Marder, S. R. *Journal of Materials Chemistry* **2009**, *19*, 5794.

(179) Wurthner, F.; Ahmed, S.; Thalacker, C.; Debaerdemaeker, T. *Chemistry--A European Journal* **2002**, *8*, 4742.

(180) Wuerthner, F. *Chemical Communications (Cambridge, United Kingdom)* **2004**, 1564.

(181) Horowitz, G.; Kouki, F.; Spearman, P.; Fichou, D.; Nogues, C.; Pan, X.; Garnier, F. *Advanced Materials (Weinheim, Germany)* **1996**, *8*, 242.

(182) Malenfant, P. R. L.; Dimitrakopoulos, C. D.; Gelorme, J. D.; Kosbar, L. L.; Graham, T. O.; Curioni, A.; Andreoni, W. *Applied Physics Letters* **2002**, *80*, 2517.

(183) Chen, Z.; Zheng, Y.; Yan, H.; Facchetti, A. *Journal of the American Chemical Society* **2009**, *131*, 8.

(184) Wurthner, F.; Stepanenko, V.; Chen, Z.; Saha-Moller Chantu, R.; Kocher, N.; Stalke, D. *The Journal of organic chemistry* **2004**, *69*, 7933.

(185) Laquindanum, J. G.; Katz, H. E.; Dodabalapur, A.; Lovinger, A. J. *Journal of the American Chemical Society* **1996**, *118*, 11331.

(186) See, K. C.; Landis, C.; Sarjeant, A.; Katz, H. E. *Chemistry of Materials* **2008**, *20*, 3609.

(187) Aneziris, C. G.; Dudczig, S.; Gerlach, N.; Berek, H.; Veres, D. *Advanced Engineering Materials* **2010**, *12*, 478.

(188) Xin, H.; Guo, X.; Ren, G.; Watson, M. D.; Jenekhe, S. A. *Advanced Energy Materials* **2012**, *2*, 575.

(189) Nielsen, C. B.; Bjornholm, T. *Organic Letters* **2004**, *6*, 3381.

(190) Zou, Y.; Najari, A.; Berrouard, P.; Beaupre, S.; Reda Aich, B.; Tao, Y.; Leclerc, M. *Journal of the American Chemical Society* **2010**, *132*, 5330.

(191) Pan, H.; Wu, Y.; Li, Y.; Liu, P.; Ong, B. S.; Zhu, S.; Xu, G. *Advanced Functional Materials* **2007**, *17*, 3574.

(192) Li, J.; Qin, F.; Li, C. M.; Bao, Q.; Chan-Park, M. B.; Zhang, W.; Qin, J.; Ong, B. S. *Chemistry of Materials* **2008**, *20*, 2057.

(193) Hao, Z.; Iqbal, A. *Chemical Society Reviews* **1997**, *26*, 203.

(194) Anthony, J. E. *Angewandte Chemie, International Edition* **2008**, *47*, 452.

(195) Langhals, H. *Helvetica Chimica Acta* **2005**, *88*, 1309.

(196) Greene, M. *High Performance Pigments* **2002**, 249.

(197) Toutchkine, A.; Nguyen, D.-V.; Hahn, K. M. *Organic Letters* **2007**, *9*, 2775.

(198) Chen, C.-C.; Dou, L.; Zhu, R.; Chung, C.-H.; Song, T.-B.; Zheng, Y. B.; Hawks, S.; Li, G.; Weiss, P. S.; Yang, Y. *ACS Nano* **2012**, *6*, 7185.

(199) Walter, M. G.; Rudine, A. B.; Wamser, C. C. *Journal of Porphyrins and Phthalocyanines* **2010**, *14*, 759.

(200) Hoppe, H.; Sariciftci, N. S. *Journal of Materials Research* **2004**, *19*, 1924.

(201) Meyer, T.; Ogermann, D.; Pankrath, A.; Kleinermanns, K.; Mueller, T. J. J. *Journal of Organic Chemistry* **2012**, *77*, 3704.

(202) Kronenberg, N. M.; Deppisch, M.; Wuerthner, F.; Lademann, H. W. A.; Deing, K.; Meerholz, K. *Chemical Communications (Cambridge, United Kingdom)* **2008**, 6489.

(203) Choi, H.; Paek, S.; Song, J.; Kim, C.; Cho, N.; Ko, J. *Chemical Communications (Cambridge, United Kingdom)* **2011**, *47*, 5509.

(204) Piyakulawat, P.; Keawprajak, A.; Wlosnewski, J.; Forster, M.; Asawapirom, U. *Synthetic Metals* **2011**, *161*, 1238.

(205) Bijleveld, J. C.; Zoombelt, A. P.; Mathijssen, S. G. J.; Wienk, M. M.; Turbiez, M.; de Leeuw, D. M.; Janssen, R. A. J. *Journal of the American Chemical Society* **2009**, *131*, 16616.

(206) Bundgaard, E.; Krebs, F. C. *Solar Energy Materials & Solar Cells* **2007**, *91*, 954.

(207) Li, Y.; Sonar, P.; Singh, S. P.; Soh, M. S.; van Meurs, M.; Tan, J. *Journal of the American Chemical Society* **2011**, *133*, 2198.

(208) Li, Y.; Singh, S. P.; Sonar, P. *Advanced Materials (Weinheim, Germany)* **2010**, *22*, 4862.

(209) Walker, B.; Tamayo, A. B.; Dang, X.-D.; Zalar, P.; Seo, J. H.; Garcia, A.; Tantiwiwat, M.; Nguyen, T.-Q. *Advanced Functional Materials* **2009**, *19*, 3063.

(210) Zhang, G.; Fu, Y.; Xie, Z.; Zhang, Q. *Macromolecules (Washington, DC, United States)* **2011**, *44*, 1414.

(211) Stalder, R.; Mei, J.; Reynolds, J. R. *Macromolecules (Washington, DC, United States)* **2010**, *43*, 8348.

(212) Bogert, M. T.; Ritter, J. J. *Journal of the American Chemical Society* **1924**, *46*, 2871.

(213) Klingsberg, E. *Chemical Reviews (Washington, DC, United States)* **1954**, *54*, 59.

(214) Norsten, T. B.; Kantchev, E. A. B.; Sullivan, M. B. *Organic Letters* **2010**, *12*, 4816.

(215) Kantchev, E. A. B.; Norsten, T. B.; Tan, M. L. Y.; Ng, J. J. Y.; Sullivan, M. B. *Chemistry--A European Journal* **2012**, *18*, 695.

(216) Silver, J.; Ahmet, M. T.; Bowden, K.; Miller, J. R.; Rahmat, S.; Reynolds, A.; Bashall, A.; McPartlin, M.; Trotter, J. *Journal of Materials Chemistry* **1994**, *4*, 1201.

(217) Susumu, K.; Fisher, J. A. N.; Zheng, J.; Beratan, D. N.; Yodh, A. G.; Therien, M. J. *Journal of Physical Chemistry A* **2011**, *115*, 5525.

(218) Albota, M.; Beljonne, D.; Bredas, J.-L.; Ehrlich, J. E.; Fu, J.-Y.; Heikal, A. A.; Hess, S. E.; Kogej, T.; Levin, M. D.; Marder, S. R.; McCord-Maughon, D.; Perry, J. W.; Rockel, H.; Rumi, M.; Subramaniam, G.; Webb, W. W.; Wu, X.-L.; Xu, C. *Science (Washington, D. C.)* **1998**, *281*, 1653.

(219) He, G. S.; Tan, L.-S.; Zheng, Q.; Prasad, P. N. *Chemical Reviews (Washington, DC, United States)* **2008**, *108*, 1245.

(220) Entwistle, C. D.; Collings, J. C.; Steffen, A.; Palsson, L.-O.; Beeby, A.; Albesa-Jove, D.; Burke, J. M.; Batsanov, A. S.; Howard, J. A. K.; Mosely, J. A.; Poon, S.-Y.; Wong, W.-Y.; Ibersiene, F.; Fathallah, S.; Boucekkine, A.; Halet, J.-F.; Marder, T. B. *Journal of Materials Chemistry* **2009**, *19*, 7532.

(221) Fang, C. S.; Bergmann, W. *Journal of Organic Chemistry* **1951**, *16*, 1231.

(222) Cornil, J.; Gueli, I.; Dkhissi, A.; Sancho-Garcia, J. C.; Hennebicq, E.; Calbert, J. P.; Lemaur, V.; Beljonne, D.; Bredas, J. L. *Journal of Chemical Physics* **2003**, *118*, 6615.

(223) Karsten, B. P.; Viani, L.; Gierschner, J.; Cornil, J.; Janssen, R. A. J. *Journal of Physical Chemistry A* **2008**, *112*, 10764.

(224) Gadisa, A.; Mammo, W.; Andersson, L. M.; Admassie, S.; Zhang, F.; Andersson, M. R.; Inganaes, O. *Advanced Functional Materials* **2007**, *17*, 3836.

(225) Jespersen, K. G.; Beenken, W. J. D.; Zaushitsyn, Y.; Yartsev, A.; Andersson, M.; Pullerits, T.; Sundstrom, V. *Journal of Chemical Physics* **2004**, *121*, 12613.

(226) Ma, Z.; Wang, E.; Jarvid, M. E.; Henriksson, P.; Inganaes, O.; Zhang, F.; Andersson, M. R. *Journal of Materials Chemistry* **2012**, *22*, 2306.

(227) Liu, B.; Zou, Y.; Peng, B.; Zhao, B.; Huang, K.; He, Y.; Pan, C. *Polymer Chemistry* **2011**, *2*, 1156.

(228) Stalder, R.; Grand, C.; Subbiah, J.; So, F.; Reynolds, J. R. *Polymer Chemistry* **2012**, *3*, 89.

(229) Khor, E.; Ng, S. C.; Li, H. C.; Chai, S. *Heterocycles* **1991**, *32*, 1805.

(230) Lu, G.; Usta, H.; Risko, C.; Wang, L.; Facchetti, A.; Ratner, M. A.; Marks, T. J. *Journal of the American Chemical Society* **2008**, *130*, 7670.

(231) Keegstra, M. A.; Peters, T. H. A.; Brandsma, L. *Tetrahedron* **1992**, *48*, 3633.

(232) Leriche, P.; Raimundo, J.-M.; Turbiez, M.; Monroche, V.; Allain, M.; Sauvage, F.-X.; Roncali, J.; Frere, P.; Skabara, P. J. *Journal of Materials Chemistry* **2003**, *13*, 1324.

(233) Yao, Y.; Tour, J. M. *Macromolecules* **1999**, *32*, 2455.

(234) Chen, C.-P.; Chan, S.-H.; Chao, T.-C.; Ting, C.; Ko, B.-T. *Journal of the American Chemical Society* **2008**, *130*, 12828.

(235) Wong, K.-T.; Chao, T.-C.; Chi, L.-C.; Chu, Y.-Y.; Balaiah, A.; Chiu, S.-F.; Liu, Y.-H.; Wang, Y. *Organic Letters* **2006**, *8*, 5033.

(236) MacDowell, D. W. H.; Springsteen, A. W. *Journal of Organic Chemistry* **1976**, *41*, 3046.

(237) Michaelides, M. R.; Hong, Y.; DiDomenico, S., Jr.; Bayburt, E. K.; Asin, K. E.; Britton, D. R.; Lin, C. W.; Shiosaki, K. *Journal of Medicinal Chemistry* **1997**, *40*, 1585.

(238) Beimling, P.; Kobmehl, G. *Chemische Berichte* **1986**, *119*, 3198.

(239) Zhang, G.; Fu, Y.; Zhang, Q.; Xie, Z. *Chemical Communications (Cambridge, United Kingdom)* **2010**, *46*, 4997.

(240) Herbst, W.; Hunger, K. Industrial Organic Pigments (Second Completely Revised Edition); Weinheim, 1997

Vita

PERSONAL INFORMATION

Name	Arawwawala Don Thilanga Liyanage
Place of Birth	Colombo, Sri Lanka
Nationality	Sri Lankan

EDUCATION

2007-2012	Ph.D Candidate (Organic Chemistry)	Univ. of Kentucky, Lexington
2002-2006	B.Sc. Chemistry with First class upper division	Univ. of Colombo, Sri Lanka

INDUSTRIAL EXPERIENCE

2012 Jul-2012 Oct	Intern	Vindico NanoBio Technology, Inc Lexington, KY

TEACHING EXPERIENCE

2006-2007   Teaching Assistant, University of Colombo, Sri Lanka (Assisted Undergraduate Practical Classes in Organic, Inorganic and Physical Chemistry and conducted Chemistry tutorial classes for the second year Chemistry students).

2007-2010   Teaching Assistant for Organic Chemistry Lab courses. University of Kentucky, Lexington. (First and second semester and advanced, totally ~07 semesters. CHE 231, 233 and 533).

PROFESSIONAL AFFLIATIONS

• Member of Sri Lanka Association for the Advancement of Science (SLAAS).
• Member of the American Chemical Society.
• Member of the Materials Research Society.

PRESENTATIONS

• Liyanage, A.D.; Watson, M.D; B. "Optimization of opto-electronic properties in conjugated donor-acceptor co-polymers via steric bulk side chain regulation", 64th

Southeastern Regional Meeting of the American Chemical Society (SERMACS), Raleigh, North Carolina 2012. (Oral)

• Liyanage, A.D.; Watson, M.D. "Organic Conjugated Polymers: Synthesis and Structure-Property Studies" Kentucky Academic of Science (KAS) annual meeting 2009. (Oral)

PUBLICATIONS

• Guo, X; Hao, X; Kim, F. S; **Liyanage, A.D.T**; Jenekhe, S. A.; Watson, M. D. "Thieno[3,4-*c*]pyrrole-4,6-dione-based donor−acceptor conjugated polymers for Solar Cells**"** *Macromolecules.* **2011,** *44***,** 269.

• **Liyanage, A.D.T;** Watson, M. D. "Optimization of donor-acceptor conjugated polymer opto-electronic properties via side-chain steric bulk" *in preparation.*

• **Liyanage, A.D.T;** Watson, M. D. "Donor-acceptor conjugated polymers with broad bimodal absorption profiles based on a novel acceptor" *in preparation.*